FS SONNE
FAHRTBERICHT SO142
CRUISE REPORT SO142

HULA

INTERDISCIPLINARY INVESTIGATIONS ON THE TIMING OF THE HAWAII-EMPEROR BEND AND THE ORIGIN OF LITHOSPHERIC ANOMALIES ALONG THE MUSICIAN SEAMONT CHAIN

MIDWAY - HONOLULU
MAY 30 - JUNE 28, 1999

Edited by
Ernst R. Flueh, John O´Connor,
Jason Phipps Morgan, and Jochen Wagner
with contributions of cruise participants

GEOMAR
Forschungszentrum
für marine Geowissenschaften
der Christian-Albrechts-Universität
zu Kiel

KIEL 1999

GEOMAR REPORT 90

GEOMAR
Research Center
for Marine Geosciences
Christian Albrechts University
in Kiel

Redaktion dieses Reports:
Ernst R. Flueh, John O´Connor, Jason Phipps Morgan und Jochen Wagner

GEOMAR REPORT
ISSN 0936 - 5788

GEOMAR
Forschungszentrum
für marine Geowissenschaften
Wischhofstr. 1-3
D - 24148 Kiel
Tel. (0431) 600-2555, 600-2505

Editors of this issue:
Ernst R. Flueh, John O´Connor, Jason Phipps Morgan, and Jochen Wagner

GEOMAR REPORT
ISSN 0936 - 5788

GEOMAR
Research Center
for Marine Geosciences
Wischhofstr. 1-3
D - 24148 Kiel
Tel. (49) 431 / 600-2555, 600-2505

TABLE OF CONTENTS

1.1 ZUSAMMENFASSUNG

Die SONNE Fahrt SO142 HULA II (Interdisziplinäre Untersuchungen zur zeitlichen Einordnung des **H**awaii-Emperor Knicks und zum **U**rsprung von **L**ithosphären **A**nomalien an der Musician Seamount Kette) führte vom 30. Mai bis zum 27. Juni 1999 in das Gebiet der Musician Seamounts nördlich Hawaiis. Neben den geowissenschaftlichen Untersuchungen war ein biologisches Arbeitsprogramm zur Bioluminizenz von Tiefseefischen ein Bestandteil der Fahrt.

Im Bereich der Musician Seamounts wurden zwei Arbeitsgebiete ausgewählt, der Italienische Rücken im Norden und der Bach Rücken im Süden. Beide Rücken wurden mit Hydroakustik und Magnetik detailliert kartiert, durch zahlreiche Dredgezüge (insgesamt 13) intensiv beprobt und zur Untersuchung der Krustenstruktur wurden weitwinkelseismische Profile senkrecht zu den Rückenachsen vermessen.

Die detaillierten bathymetrischen Untersuchungen ergaben deutliche Unterschiede in den beiden bis zu 3000 m hohen Rücken. Der im Norden gelegene Italienische Rücken besteht aus mehreren en-echelon versetzten Segmenten, während der Bach Rücken weitaus homogener und gleichförmiger aufgebaut ist. Einzelne Seamounts zeigen ausgeprägte magnetische Anomalien von bis zu 400 nT. Entlang von drei langen und einem kürzeren seismischen Weitwinkelprofil wurden insgesamt 47 Ozeanboden Hydrophone (OBH) ausgebracht und nahezu 600 Profilkilometer mit zwei großen Airguns überschossen. Alle Geräte konnten erfolgreich geborgen werden, und die registrierten seismischen Daten sind von hervorragender Qualität. Es wurden Reichweiten von bis zu 150 km erzielt; auf allen Profilen kann die Krustenstruktur von der umgebenden, ungestörten ozeanischen Kruste und den Rücken gut bestimmt werden. Erste Analysen zeigen, daß die Musician Seamounts im wesentlichen durch effusiven Vulkanismus mit nur einem untergeordneten Anteil von Underplating gekennzeichnet sind.

Während aller dreizehn Dredge Stationen konnten Gesteinsproben erfolgreich geborgen werden. Fünf Stationen lagen längs des Italienischen Rückens im Norden. Eine Dredge entlang der Murray Fracture Zone erbrachte Gesteinsproben, die für spätere Altersuntersuchungen des Meeresbodens der Musician Kette geeignet sind. Sieben Dredgen wurden längs des Bach Rückens durchgeführt, eine letzte wurde am östlichen Ende des Beethoven Rückens ausgeführt. Obwohl die meisten Proben mit einer Schicht MnOx umgeben waren, enthielten doch alle Dredgen einige Gesteine, die sich potentiell für eine hochpräzise Altersbestimmung eignen. Die Proben wurden für die Preparation von Mikorproben, Altersbestimmungen, geochemischen Analysen, und das eventuelle Extrahieren von Gläsern, soweit dies möglich sein wird, in dünne Sektionen unterteilt. Außerdem wurden MnOx und andere eventuelle hydrothermale Krusten systematisch untersucht. Weitere Untersuchungen werden petrographische Analysen dünner Sektionen sowie die Bestimmung von Spurenelementen beinhalten. Ein weiterer Schwerpunkt liegt auf der radiometrischen Altersbestimmung mit der 40Ar/39Ar Methode. Die hochdetaillierte Altersbestimmung der einzelnen Musician Seamount Rücken sowie deren geochemische Veränderungen mit der Zeit stellen ein Hauptuntersuchungsziel dar. Dabei sollen zwei Fragen beantwortet werden:

(1): wurden die Rücken als einzelne Strukturen längs vulkanischer Achsen erzeugt oder

(2): wurde ihre Entstehung durch die Mischung von Plume- und Spreizungsachsenmaterial, die an den westlichen und östlichen Enden der Rücken entstanden, beeinflußt.

Zur Untersuchung der Biolumineszenz und der Anpassungsstrategien des visuellen Systems wurden 21 Trawls aus Tiefen zwischen 500 und 1500m (tagsüber) bzw. 200 und 800 m (nachts) durchgeführt. Dabei kam als Netz ein RMT 8+1 sowie ein spezielles "closing cod -end" zum Einsatz. Der darin enthaltene thermisch isolierte Zylinder kann mit Hilfe einer Zeituhr verschlossen werden und ermöglicht damit einen optimalen Erhaltungszustand der Tiere, wenn sie an Bord kommen. Viele Exemplare überlebten sogar bis zu mehreren Stunden.
Die Fänge erbrachten eine überaus reichliche Ausbeute von fast 50 verschiedenen Fischarten, 20 Crustaceen- und 15 Cephalopden-Arten. Darunter befanden sich zu etwa 2/3 Spezies, welche eine circumglobale Verbreitung haben und daher eindeutig zu identifizieren waren. Bei den übrigen Exemplaren müssen erst weitere Analysen zeigen, ob es sich um bisher noch nicht beschriebene Arten handelt, da Fänge im Bereich der Musician Seamounts zuvor noch nicht durchgeführt wurden.

Die Arbeiten an Bord konzentrierten sich zunächst auf die spektrale Analyse der Biolumineszenzsignale der überlebenden Tiere. Darüber hinaus wurde in großem Umfang Material gesammelt und für die weitere Untersuchung in den Heimatlabors präpariert und konserviert. Von besonderem Interesse sind dabei Proben der Sehpigmente einiger Stomiiden, deren Fähigkeit zur Wahrnehmung des von ihnen erzeugten Lichts im Bereich jenseits von 600nm mit Hilfe dieses Materials weiter analysiert werden kann. Weiterhin konnten an Bord eine Reihe von Experimenten an lebendem Retina- bzw. Hirngewebe durchgeführt werden. Dabei sollte der bisher ungeklärte Prozeß der Außengliederneuerung in Netzhäuten mit multiplen Stäbchenschichten (wie sie für die meisten Tiefseefische typisch sind) durch Aufnahme von Lucifer Yellow studiert werden. Durch selektive Markierung der Projektionsneurone der Retina und des Bulbus olfactorius und deren Projektionsareale im Gehirn mit Hilfe von Dextranen und DiI soll schließlich die relative Bedeutung dieser beiden Sinnessysteme quantifiziert werden.

1.2 SUMMARY

Sonne Cruise SO142 HULA II was dedicated to the study of the Musician's Seamount Province north of Hawaii. The cruise left Midway on May 30, and arrived in Honolulu on June 27, 1999. In addition to the geologicial studies of this volcanic province, an ancillary biological field program studied the bioluminescence of deep sea marine life.

Two regions of the Musicians seamount province were selected for intensive study: the Italian Ridge in the Northern Musicians (i.e. North of the Murray Fracture Zone which bisects this province), and the Bach Ridge in the south. Swath bathymetry and magnetic anomaly maps were made for both elongate ridges, and they were also intensively dredged (13 dredge stations.) To determine the deep crustal structure beneath these ridges, four wide-angle seismic profiles were collected orthogonal to the strike of each ridge.

The detailed bathymetric maps show striking differences between the two 3000m high, 300+km long volcanic elongate ridges. The northern Italian Ridge is composed of an en-echelon series of elongate 'seamounts' that strike at an oblique angle to the overall ridge trend, while the southern Bach Ridge is more linear and uniform along-strike. Some of their along-strike seamounts display significant magnetic anomalies up to 400 nT. Forty-seven ocean bottom hydrophones were deployed along four profiles, and almost 600 km of wide-angle seismic data were collected. All instruments were successfully recovered. The seismic data appears to be of high quality, with mantle phase arrivals seen to offsets of 150 km. On each profile, the crustal structure associated with the ridge can be distinguished from that of the surrounding and underlying oceanic crust. Our preliminary analysis implies that the volcanic elongate ridges in the Musicians seamount province are mainly built through effusive volcanism, with only a minor contribution from magmatic underplating within and beneath the underlying oceanic crust.

All thirteen dredge stations recovered rocks that appear to be suitable for future dating and geochemical analysis. Five of these stations were on the Italian Ridge in the north. Dredging of the Murray Fracture Zone during transit to Bach Ridge sampled rocks suitable for establishing the age of the seafloor on which the Musician Chain was built. Another seven dredges were completed along Bach Ridge, while a final dredge station was located at the eastern end Beethoven Ridge. Although rocks recovered were very altered and usually coated with a thick layer of MnOx, all dredges contained at least some rocks that are potentially suitable for high precision age dating. Representative rock pieces were cut from these samples for thin and microprobe section preparation, age dating, geochemical analyses, and further processing to extract glass (if applicable). In addition, MnOx and possible hydrothermal crusts were systematically sampled. Further studies will involve petrographic examination of thin sections, analyses of phenocryst and groundmass phases using the electron microprobe, determination of major and trace element geochemistry by X-ray fluorescence spectrometry or inductively coupled plasma mass spectrometry, and radiometric dating by the 40Ar/39Ar incremental heating technique. The key objectives of such work are to obtain high precision ages for each Musician Chain seamount and ridge and to establish any changes in geochemistry with time. These data will allow us to address two key questions; (1) were the Musician Chain elongated ridges created quickly as single lines of volcanism and (2) did their creation involve mixing

between plume and spreading-axis materials originating from the western and eastern sides of these ridges.

For the study of bioluminescence and related adaptation strategies of visual systems in the mesopleagic fauna we performed 21 trawls at depths between 500 - 1,500m during daytime and 200 – 800 m at night. Each trawl used the SOC RMT 8+1 fishing gear equipped with a closing cod end, a thermally isolated container, and a timer controlled closing device to isolate samples during their retrieval through shallow warm water. We succeeded in retrieving a great number of animals in optimal condition for further analysis of visual physiology and anatomy. Many specimens survived for several hours after being brought on board.

The trawls yielded a rich catch of almost 50 different species of deep-sea fish, 20 species of decapod crustaceans and 15 species of cephalopods. Among these were about two thirds with a circumglobal distribution which could therefore clearly be identified. The unambiguous identification of the remainig specimens must await further analysis and comparison with type specimens before it can be accurately determined whether novel species have been found, as the fauna of the Musician seamount area has not been sampled previously.

Work on board concentrated mainly on the spectral analysis of the bioluminescent signals in surviving animals as well as large scale collection and preparation of material for further analysis at home. Of particular interest are rare probes of visual pigments of some stomiid fishes who are capable of perceiving light in the far red which they produce themselves. Some experiments were also performed on living retinal and brain tissue. In order to study the process of outer segment renewal in multiple bank retinae the fluorescent dye Lucifer Yellow was included into the culture medium for uptake into newly formed discs. Other labelled tracer molecules (dextranes, DiI) were used to stain the projection neurons in the retina and the olfactory bulb and to reveal their projection area in the brain; this approach allows us to determine the relative importance of these two sensory systems.

2. INTRODUCTION
2.1 AIMS OF THE PROJECT
(THE HULA SCIENCE TEAM)

The primary goal of the geological components of the HULA2 field program is to study a new type of hotspot-related magmatism that is particularly well-expressed in the Musicians seamount province north of the Hawaiian Islands. Our planned field program was to take us to a region of the worlds ocean that has been extremely poorly sampled for deepwater sea life. Because of this, a biological sampling component was also added to the campaign with 4 days of ship-time devoted to deep-water trawling with the Southhampton Rectangular Midwater Trawl ($8m^2$) with closing cod end. Specific biologic aims are to study the photobiology (visual physiology and bioluminescence) of midwater Pacific fauna to complement and extend previous Atlantic studies. Biologic aspects of this project will be detailed in a separate section of the project report (section 2.4). The next sections will discuss the geological aims of the project and present background for this part of the field program.

The HULA2 field program conducted a geophysical, geochronological, and geochemical investigation of a new type of hotspot-related magmatism whose large-scale impact only became evident with the recent global gravity and 'predicted topography' maps based on dense global satellite altimetric coverage [e.g. Smith and Sandwell, 1996]. The Musicians seamount province [see Figure 2.1.1] is a type-example of this class of feature. When this seamount province was created between ~75-95 Ma [Pringle, 1992], the Pacific Plate was moving NNW (azimuth ~320), and the N-S striking Pacific-Farallon axis was less than ~800 km to the east of the 'Euterpe' hotspot. (Euterpe is one of the muses of musicians.) Several long (up to 500 km-long), E-W-striking ridges formed between the hotspot and Pacific-Farallon spreading axis, nearly, but not exactly parallel to the relative motion direction recorded by nearby fracture zones.

The Musicians area is one of the best regions to study this newly realized class of hotspot-related volcanism. The basic reason is that the Muscians records a relatively rare example when the absolute motion direction of the Pacific Plate (as shown by the ~320° trend of the Musician seamounts) is at a high angle to the relative motion of Pacific-Farallon spreading (as shown by the ~80° trend of the fracture zones). Because of this, the hotspot-ridge interaction is relatively immune to 'overprinting' by hotspot-ridge induced volcanism occurring at a later time, resulting in a very clear signal of this interaction. In addition, the chain of seamounts on the western edge of the Musicians seamount province has already been sampled and well-dated [Pringle, 1992]. This simple hotspot-like seamount chain was found to have an extremely straightforward age progression in comparison to the Hawaiian chain, perhaps because it is composed of small monogenentic volcanos. The fact that the western seamount chain in the Musicians province is already well-sampled and dated means that the geochemical and geochronological segments of our proposed study can focus on sampling and dating the elongate ridges themselves.

Little is known about what makes a volcanic elongate ridge (VER), and workers are still trying to even classify this type of morphologic feature. Off-axis en-echelon ridges have been found in some parts of the Pacific Basin (e.g. the 'Puka Puka' ridges west of the southern East Pacific Rise), and as noted in Figure 2.3.1, many other VERs are now evident in satellite altimetric data that are clearly related to past plume-ridge interactions. (These and other examples of hotspot-ridge interaction will be summarized in section 2.3) Many first-order questions about these ridges have yet to be answered. Are elongate ridges formed uniquely during the interaction of mantle plume and spreading ridge magmatism? Are many ridges

Fig.2.1.1 The Musicians Seamount Province. The Hawaiian Arch Volcanics Field North of Oahu is outlined with a black line.

fracture zones reactivated during hotspot magmatism? (This mechanism could be possible for about half the ridges which form parallel to relative-plate motion directions.) Are they pull-apart features filled with hotspot magmatism? Do they have a deep crustal structure? Can they form in intraplate regions away from spreading centers?

2.1.1 GEOPHYSICAL GOALS

To help answer these questions we performed the first geophysical study of these ridges. shooting several refraction lines to image the crustal and mantle structure of an volcanic elongate ridge (VER), and making detailed bathymetric and morphologic maps of several representative ridges.

Seismic profiles were shot across each of these ridges and their surrounding ocean crust. A key goal of these cross-sections is to determine whether the ridges are built largely by either magmatic underplating or by extrusive volcanism. Figure 2.2.1.1 shows that magmatic underplating near the Moho is predicted to produce thicker-than-normal ocean crust section of high-velocity seismic layer 3 beneath a volcanic ridge. (For example, magmatic underplating appears to be a prevalent constructional mechanism for the Ninetyeast Ridge in the Indian Ocean (SO131, Flueh et al., 1999a).). Alternatively, VERs made be largely made by extrusive volcanism, in which case they would be expected to have a much thicker-than-normal extrusive (slow-velocity) seismic layer 2. We can further test these seismic models by comparing the gravity-anomaly computed from a density-seismic velocity scaling relation with the observed gravity along each seismic profile. Joint inversion of seismic and gravity data will also be used to address whether either magmatic underplating or extrusive volcanism is the main cause of ridge relief. Preliminary seismic results are discussed in section 6.3.

A key swath-mapping goal of this study is to make Hydrosweep-based maps of two long VERs in both the northern and southern sections of the Musicians Province. (The Northern Musicians Province is defined to lie north of the Murray Fracture Zone.). The sample ridges are the Italian Ridge in the North (an elongate en-enchelon ridge comprised from W to E by the Verdi, Rossini, Puccini, Bizet*, and Donizetti seamounts), and the almost-as-long, but less en-echelon (i.e. more linear) Bach Ridge in the South. These swath-maps will be used to characterize the characteristic slopes of these features, and to search for evidence of normal faulting and constructional volcanism. Our preliminary results are discussed in section 6.1.

2.1.2 PETROLOGIC GOALS

The main petrologic goals of this project focussed on the elongate ridges in the Musicians seamount province and their relation to the nearby seamount chain to the west and spreading center to the east. We spent most of our effort on dredging two representative ridges to try to obtain a good relative chronology of these features with respect to the seamount chain and spreading center. Ar^{40}-Ar^{39} dating of these samples will be performed to obtain this chronology, which should help to determine how rapidly and coevally these elongate volcanic ridges formed. In addition these dredge rock samples will be measured for their trace and major element chemistry. This data will be used to try to relate their geochemistry to that of the nearby seamount and mid-ocean ridge magmatism. In addition, we took advantage of the fortuitious passage over a large scarp on the Murray Fracture Zone to dredge for a representative sample of mid-ocean ridge crust created at the neighboring spreading center during the time of formation of the northern elongate volcanic ridges. Finally, during our transit to Oahu we crossed the newly

Seismic Consequences of Lithospheric Underplating and Extrusive Volcanism

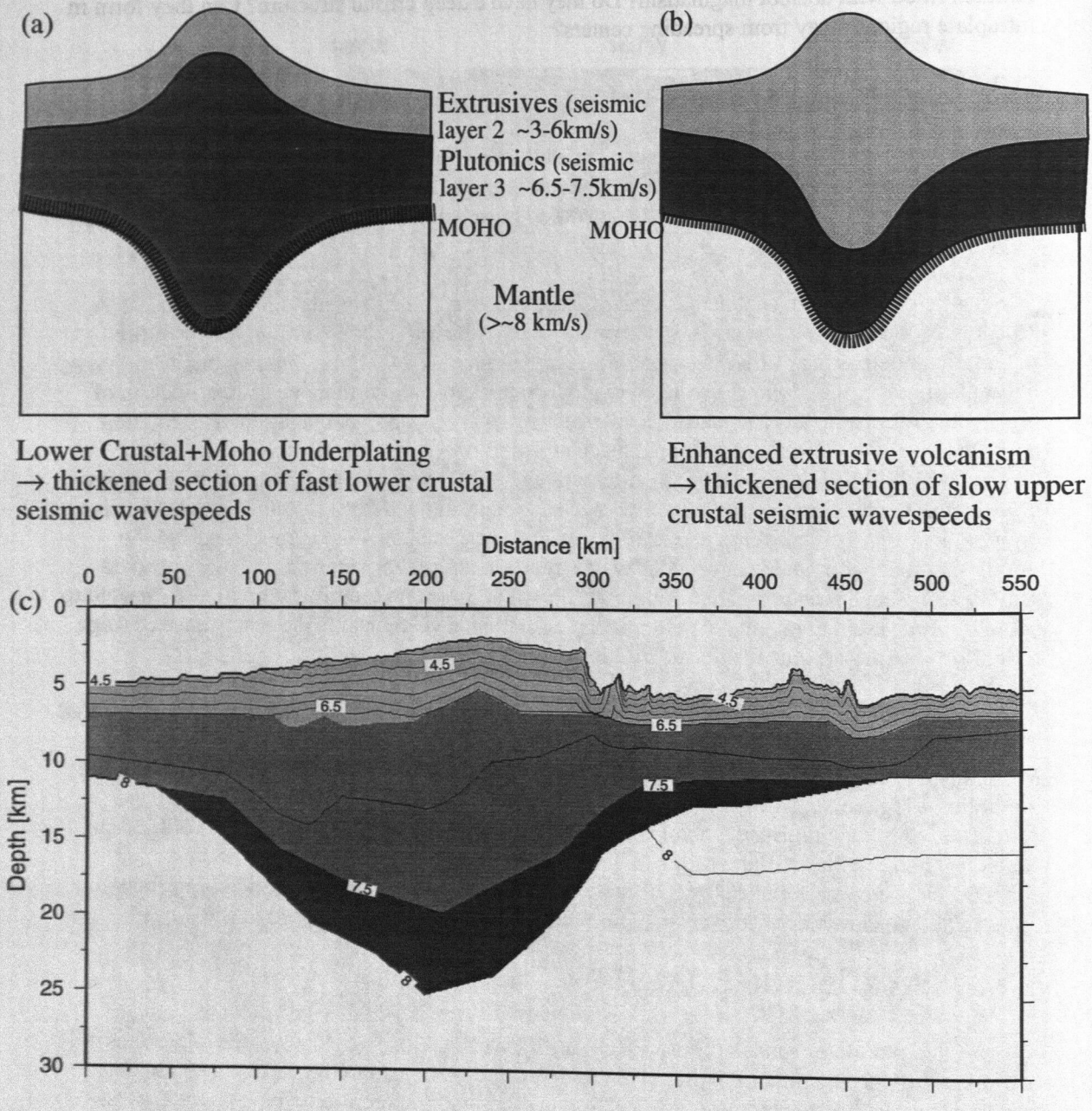

Fig. 2.1.1.1 (a) The crustal structure associated with topography created by magmatic underplating within the lower oceanic crust and Moho. Magmatic underplating typically results in the intrusion of high-seismic velocity gabbros and ultramafic cumulates, resulting in a much thicker 'seismic layer 3' than normal oceanic crust.
(b) The crustal structure associated with anomalous extrusive volcanism. Extrusive volcanism leads to a thickening of the less-dense and slow-seismic velocity extrusive section which leads to a relative thickening of 'seismic layer 2'.
(c) A recent seismic velocity cross-section of the Ninety-East Ridge near 17°S, 90°E. (from SO131) This is an example of magmatic underplating compensating the elevated topography. Seismic contours every 0.5 km/s. The lightest shading is for extrusive basalts (3.5-6.6 km.s). Intermediate shaded gabbros are from 6.6-7.2 km/s, and dark shaded underplated ultramafics have wave-speeds between 7.5-7.8 km/s. In this example, underplating has greatly thickened the gabbro section and also created a hyperfast crustal 'ultramafic' section above the Moho.

discovered Hawaiian Arch volcanic field (cf. Fig. 2.1.1). We performed a single video-rock grab traverse to obtain photographic coverage and rock samples of this extremely large and unusual volcanic field.

2.2 TECTONIC HISTORY
2.2.1 THE NORTH PACIFIC

The early tectonic history of the North Pacific is still not very well known (Atwater and Severinghouse, 1989). The main difficulty is that during the late Cretaceous, between ~115-85 Ma, the Earth's magnetic field did not reverse its polarity. Without magnetic stripes to provide a good clock for the seafloor age during this 'Cretaceous Quiet Zone', it is hard to unravel the multiple changes in the relative motions of the Pacific and its neighboring Kula and Farallon Plates that occurred during this time period. Most previous workers have placed these plate motion changes relatively early in the Cretaceous Quiet Zone (ca. ~110 Ma). For example, Mueller et al.'s (1997) seafloor age map shown in Figure 2.2.1.1 has a period of extremely rapid Pacific-Farallon spreading between 120-110 Ma followed by a stable opening speed at roughly 1/3 of the rapid rate between ~110-80 Ma. We believe that the age of the seafloor beneath the Musicians's Seamount Province is significantly younger than predicted by Mueller et al's (1997) map (~96 Ma vs. ~110 Ma), and that the major changes in Cretacous Pacific-Farallon motion occurred more recently than assumed by Mueller et al. (1997) or other previous workers. The following discussion is based on work begun while onboard the ship.

The history of the Musicians Seamount Province appears to place a single strong age constraint on the tectonic history of the Western Pacific. The following discussion is based on previous Ar^{40}-Ar^{39} age determinations of individual Musicians seamounts by Pringle (1992) and a newly adopted image-processing technique for the satellite altimetry-derived gravity field that particularly well emphasizes the detailed tectonic structures within fracture zones and other sediment-filled deeps. [The processing 'trick' is to take the gradient of the gravity field in a particular direction and then to plot only this gradient as an 'artificial lighting' on a perfectly gray background. This trick highlights coherent small-amplitude changes in the gravity gradient that are masked when shading on top of plots of the actual gravity values as a color or gray-shade value. The result is that we can now more clearly see structural features within satellite-based gravity maps, e.g., Figure 2.2.1.6. Our code for this is:

```
img2latlong $world_grav.img.7.2 –T1 –v6.2 –R$AREA –I2m –V –G$AA
grdgradient $AA –A350 –N –V –GtmpBB
grdhisteq tmpBB –N –V –GtmpCC
grdmath tmpCC -.4 x = $DD
#  (use fz.cpt == -500  160 160 160  +500  160 160 160 )
grdimage $AA –Jm.15 –R$AREA –I$DD –Cfz.cpt –K >fz.ps  ]
```

basis, the 'faster spreading rates' ended much later (~ 85 Ma) than implied by Mueller (whose very fast spreading ends at 110 Ma).

The Musicians are one of the oldest hotspot tracks on the Pacific Plate. Figure 2.2.1.4 shows a recent reconstruction of Pacific-hotspot motion for the past 120Ma. No Musician data went into this Figure 2.2.1.2 shows Pringle's (1992) Ar^{40}-Ar^{39} ages of the Musician seamounts. An age-distance plot of this data is given in Figure 2.2.1.3, showing that the Pacific Plate moved NNW over the Euterpe Hotspot at a rate of about 60 mm/yr. The oldest Musician seamount

Figure 2.2.1.1: Seafloor age map for the North Pacific compares both the age-map of Mueller et al. (1997) and our preferred reconstruction based on work done during this cruise. Our seafloor age estimates are shown by age-ticks along the N and S sides of the major fracture zones (black lines) while the Mueller et al (1997) ages are the white contour lines (My). In the Musicians region (Cret. Quiet Zone), these age-estimates differ by up to 15 Ma.

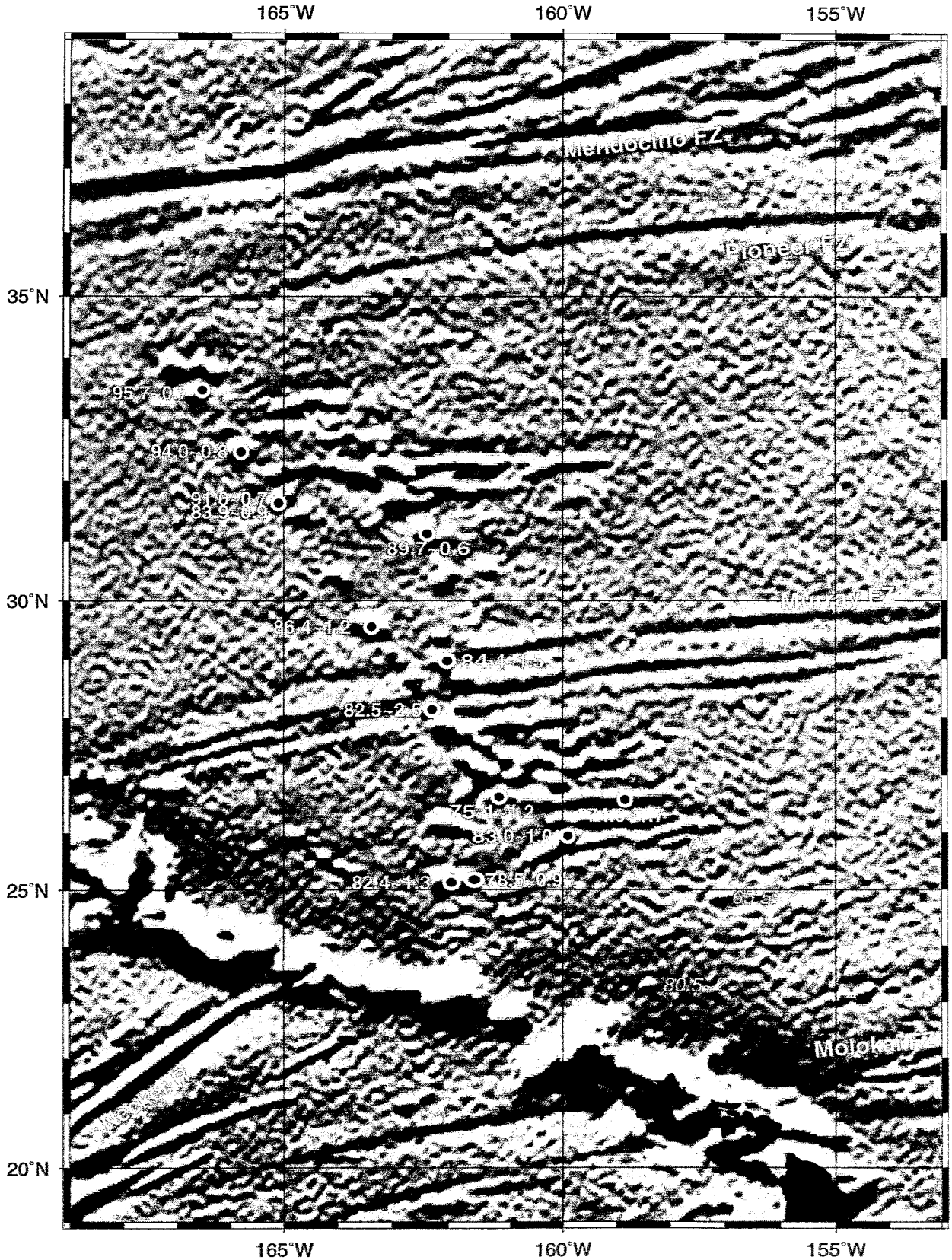

Figure 2.2.1.2: Known Ages Within the Musicians Seamount Province.

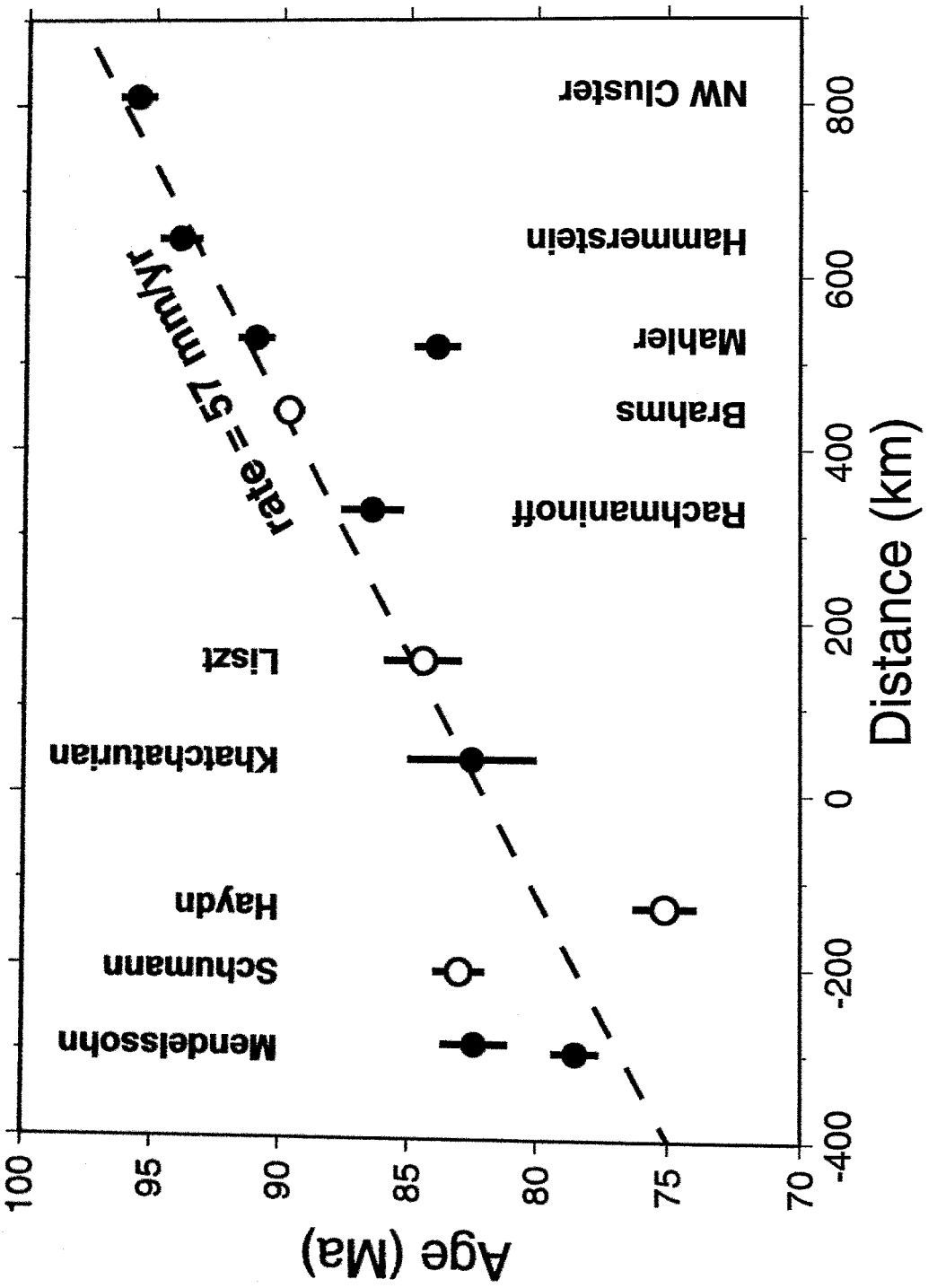

Figure 2.2.1.3: Age-speed relations along the Western seamount track in the Musicians Seamount Province (Ages from Pringle, 1992). Closed circles refer to seamounts along the western trail while open circles denote seamounts at the same latitude that lie to the east of the western trail of seamounts.

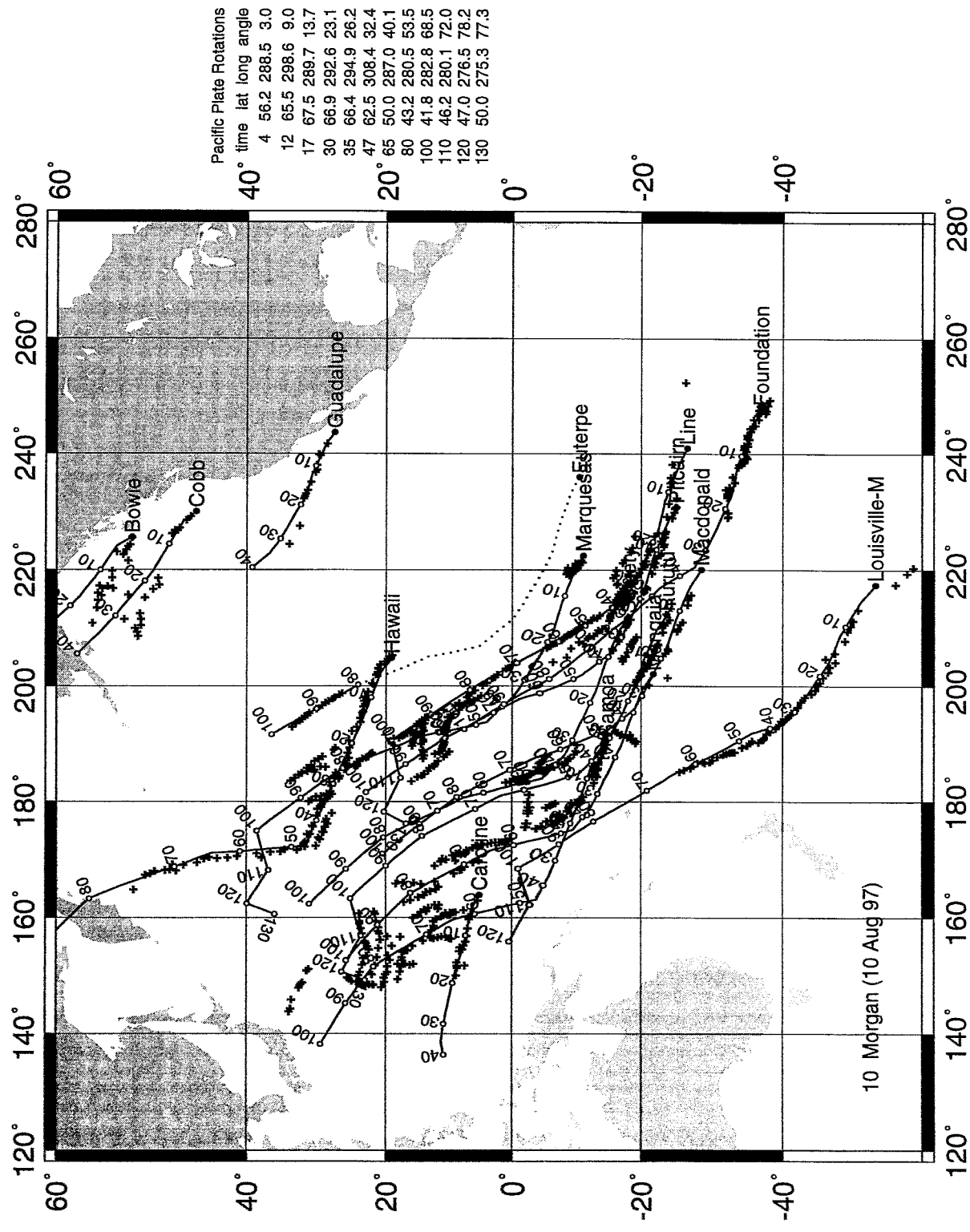

Figure 2.2.1.4: Hotspot tracks on the Pacific Plate (based on a reconstruction by W. J. Morgan) The table shows the Pacific-Hotspot Frame stage poles assumed in this reconstruction. In this reconsruction, hotspots are assumed to not move with respect to each other.

appears just south of the Pioneer Fracture Zone. We assume that the hotspot crossed the Pioneer Fracture Zone at ~ 96 Ma – i.e., prior to this time, Euterpe produced seamounts on the Farallon Plate, which is why no earlier trace is preserved on the Pacific Plate. We use this to constrain the age of the seafloor here as the 'Quiet Zone' precludes any magnetic anomaly constraints during this time interval. On this reconstruction, but to make the Musicians at their respective ages, there would have had to have been a hotspot source at about 10° S, where "Euterpe" is plotted on this figure.

Figure 2.2.1.5 shows a reconstruction of Pacific-Farallon plate motions based on the fracture zone trends highlighted in Figure 2.2.1.6. The Pioneer Fracture Zone is the trace of a relatively small-offset transform fault with roughly ~100 km offset that lies ~200 km south of the extremely large offset Mendocino Fracture Zone. We are fairly confident that the Pioneer Transform Fault had a small ridge-offset because it shows simple 'kinks' in response to changes in the direction of Pacific-Farallon spreading and the magnetic anomaly offsets are known for the eastern half of this fracture zone. Small-offset transforms can easily reorganize in response to changes in relative plate motions while large-offset transforms form large compressional ridges or 'extensional relay zones' that result in a staircase en-echelon pattern after a change in plate motion. For example, compare the traces of the small-offset Pioneer and Clarion FZs to that of the large-offset Mendocino and Murray FZs (Figure 2.2.1.5). Steve Cande noted this phenomena and suggested that one should use small-offset FZs to determine the times of changes in spreading direction. Therefore, we use the the Pioneer FZ (and the more southern Clarion FZ) to accurately determine the direction of motion between the Pacific and Farallon Plates.

Note that when the large left-offset fracture zones (Mendocino, Molokai) open up into many 'relays', the right-offset fracture zones (Murray, and to a lesser extent the Clarion) close-up, and vice-versa. Also coming out of this analysis is the observation that whereas before about 48 Ma (the time of the Emperor bend) all of the fracture zones can be fit by one set of rotation parameters; since that time the 'northern' (Surveyor, Mendocino, Pioneer) cannot be fit with the same rotation parameters as the 'southern' (Murray, Molokai, Clarion, and the Clipperton/ Galapagos/Marquesas, not shown in any figure here but used in the analysis). This implies that the 'Farallon' was one plate up until ~ 48 Ma, but at that time, coincidental with the Emperor bend, the Farallon split into two plates. The non-parallel trends of the Murray and Pioneer has long been an enigma that appears to be solved. Our rotation parameters to fit these fracture zones are given in Table 2.2.1.1.

Our model to explain the Musicians-Spreading Ridge interaction is shown in Figure 2.2.1.7. In this we show the hotspot track on the Pacific plate, showing its position at 96, 93, 90, 87, and 84 Ma. (These points are taken from the straight line fit shown in Figure 2.2.1.3.) Also shown in this figure are our seafloor isochrons. These are based on the assumption that the initiation of the track on the Pacific plate is the result of the Pioneer FZ crossing over the active hotspot – prior to this time the track was on the Farallon and not the Pacific plate. We then interpolate the seafloor ages between the 'known' 96 Ma crossing point and the 84 Ma 'oldest known' magnetic anomaly position. With heavy lines, we show the isochron at the same age as the nearby hotspot in the region nearest the hotspot. These 'heavy lines' step away from the hotspot, then jump back after the large age-offset of the Murray fracture zone. The elongate ridges have a similar pattern, they get longer and longer as the distance from hotspot to isochron-of-the-same-age increases, until abruptly they cease (as the distance from hotspot to ridge becomes too great for hotspot-ridge interaction). Note that the longest ridges cross over their respective isochrons, this is an error that could be corrected by fine tuning the isochron spreading rate. Our model offers

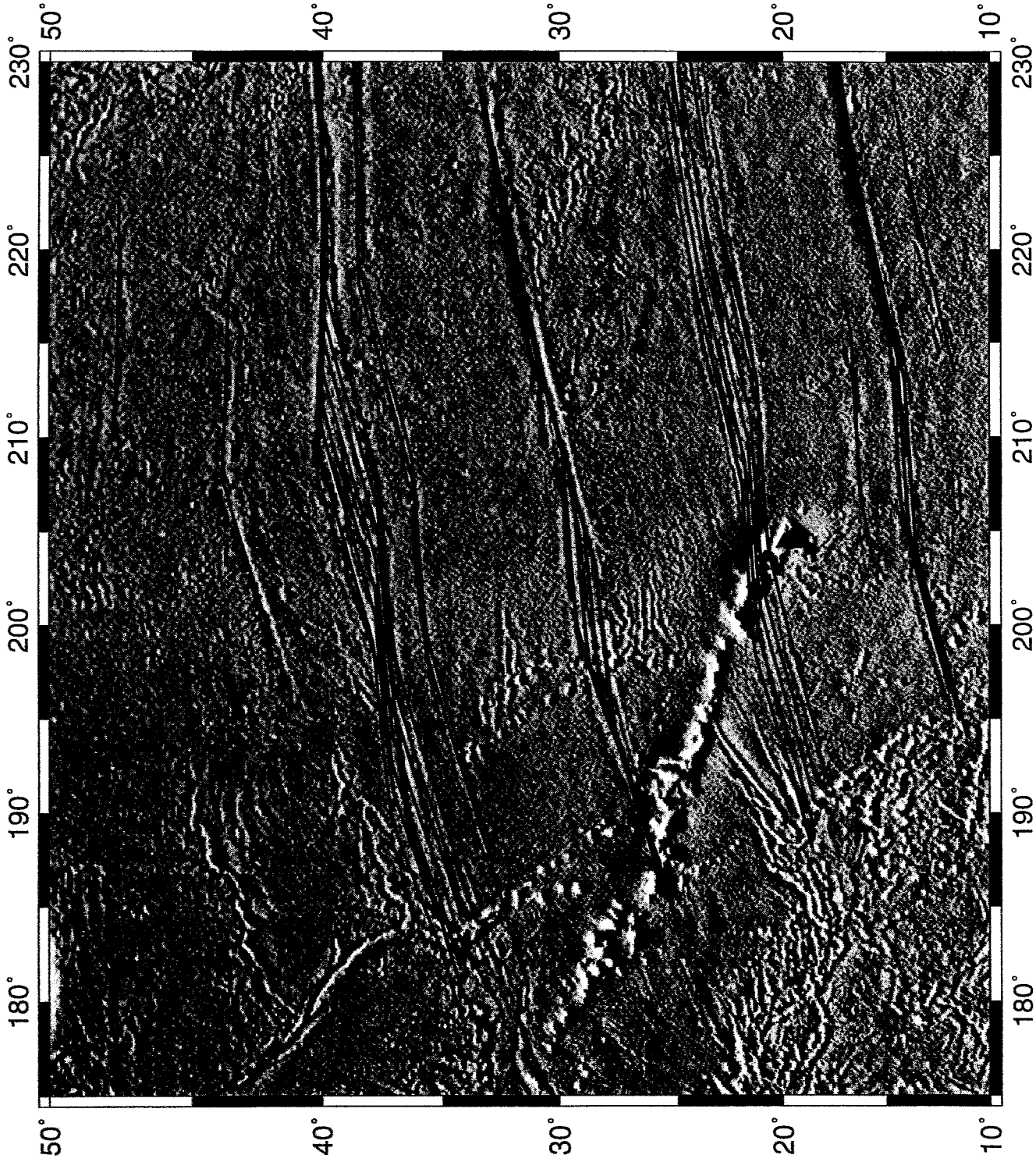

Figure 2.2.1.5: Modelled and observed fracture zone trends on the Pacific Plate, based on a reconstruction developed during this cruise. The background map is a shaded map of the gravity gradient illuminated from a direction of 350°. During changes in plate motion a long-offset tranform fault may split into several small segments, resulting in a 'Zed' pattern when the relative motion again changes to return to a similar direction.

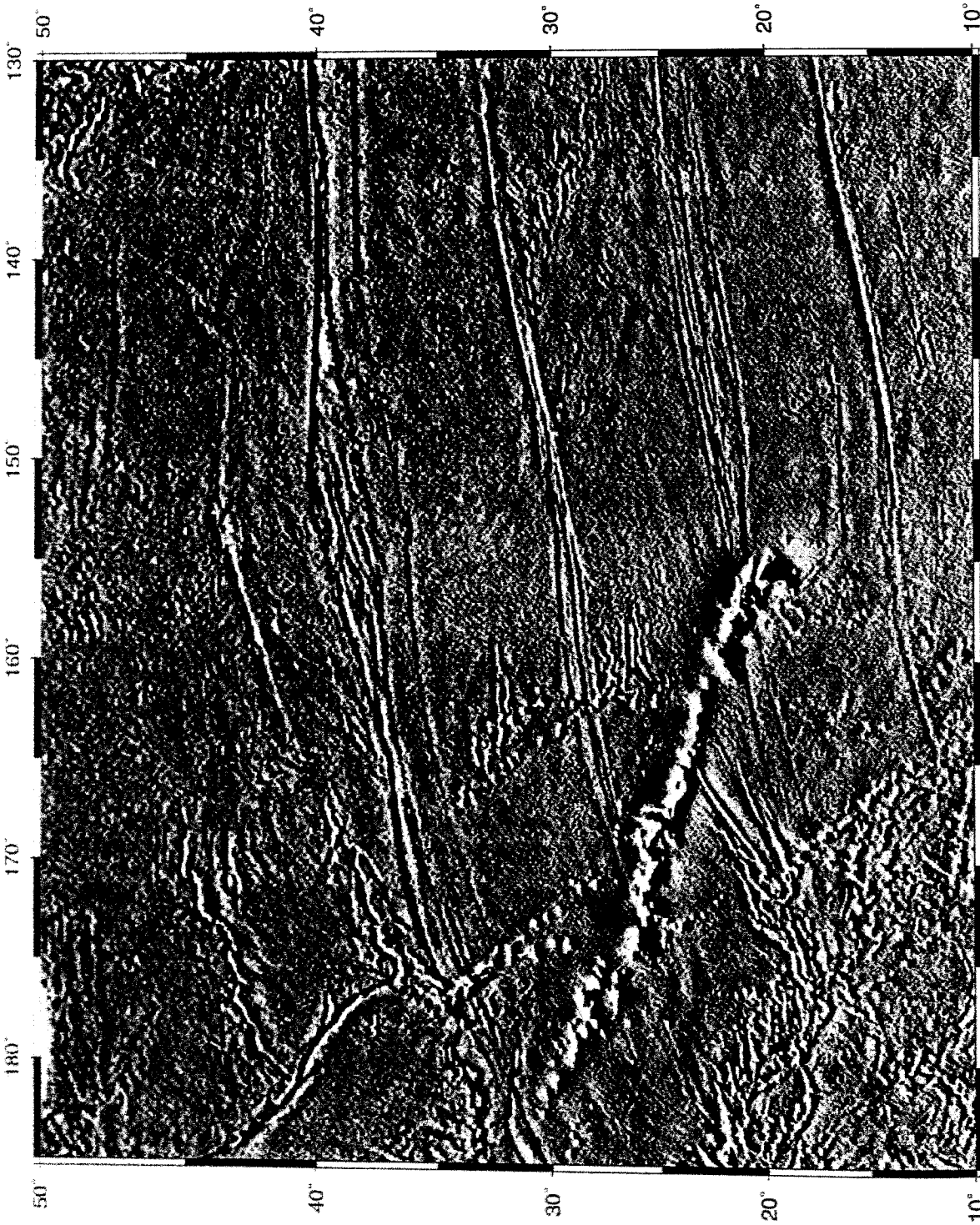

Figure 2.2.1.6: Observed fracture zone trends on the Pacific Plate. This is a plot of the gravity gradient inferred from satellite altimetry which is illuminated from an angle of 350°.

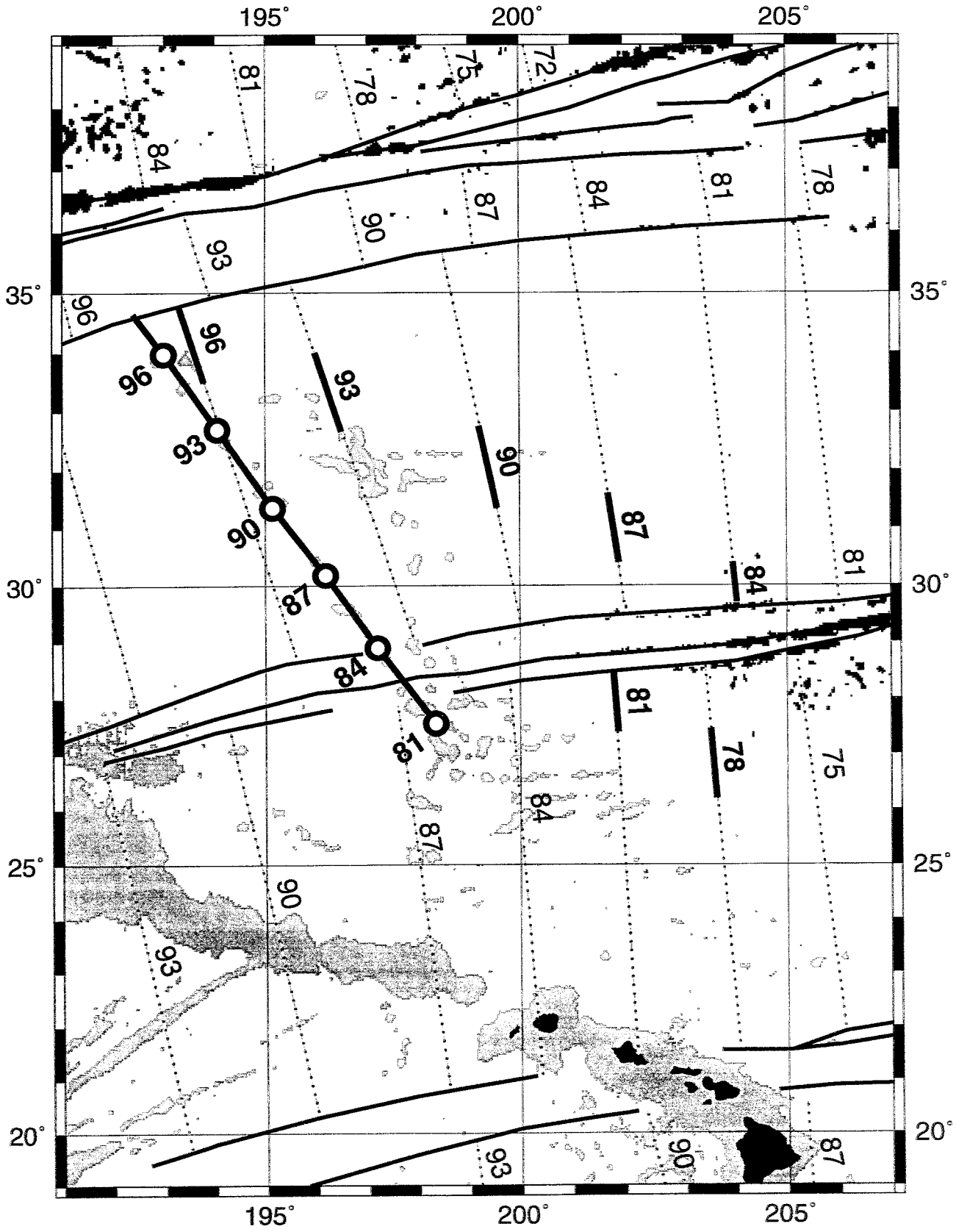

Figure 2.2.1.7: Reconstruction for seafloor ages and the hotspot track of the Euterpe Hotspot during the creation of the Musicians Seamount Province (reconstruction done during this field campaign).

no explanation as to why the Musician track appears to change direction just after crossing the Murray FZ (i.e., to include Chopin and Mendelssohn seamounts) except to note that the overall Pacific motion (Figure 2.2.1.4) has a change in direction at about 80 Ma (85 Ma would be equally precise given the uncertainty in the assignment of '80' for this change). However, it is curious that the nearest thing to 'kinks' in the fracture zone directions of the Pioneer and Murray occur at just the times the Musician track crosses these fracture zones.

Table 2.2.1.1 Relative Motion of the Pacific – Farallon Plates

Pacific – N. Farallon Stage Poles

time interval(Ma)		Lat(°N)	Long(°E)	Angle(°cw)
48	25	80.0	220.0	14.3
75	48	78.0	130.0	11.0
88	75	83.0	60.0	8.0
94	88	57.0	46.0	6.1
110	94	74.7	133.2	12.0

Pacific – S. Farallon Stage Poles

time interval(Ma)		Lat(°N)	Long(°E)	Angle(°cw)
48	25	73.5	80.0	9.0
75	48	78.0	130.0	11.0
88	75	83.0	60.0	8.0
94	88	57.0	46.0	6.1
110	94	74.7	133.2	12.0

Note: the exact times of the turning points are very uncertain, the poles and angles between these turning points are more certain. The 'Angle' is half of the total Pacific-Farallon opening.

Figure 2.2.1.8 is a velocity triangle for the Pacific– Farallon–Hotspot system. The directions and rates of the Pacific-Farallon relative motions are from our analysis of the position of the isochron at 96 Ma where the Musician track ends at the Pioneer FZ; the Pacific–Hotspot motion is from the data of Pringle (1992). The distance between the 96 Ma and 84 Ma isochrons implies a (full) spreading rate of the Pacific–Farallon of ~ 230 mm/yr – i.e., that it was a superfast spreading center. In this time interval, the hotspot track (Pacific–Hotspot) has a direction and rate of ~ 320°, 56 mm/yr and the Pacific-Farallon relative motion is ~ 240°, 230 mm/yr. Thus the ridge-crest moves away from the hotspot at a rate of 100 mm/yr. This can be seen in the lefthand side of Figure 2.2.1.8. By 84 Ma, the direction of spreading is more east-west and the spreading rate has decreased, both of these factors combine to reduce the rate that the ridge-crest moves away from the hotspot to about 50 mm/yr (see righthand side of this figure). Perhaps some difference in the character of the elongate ridges in the northern and southern Musicians is related to this speed difference.

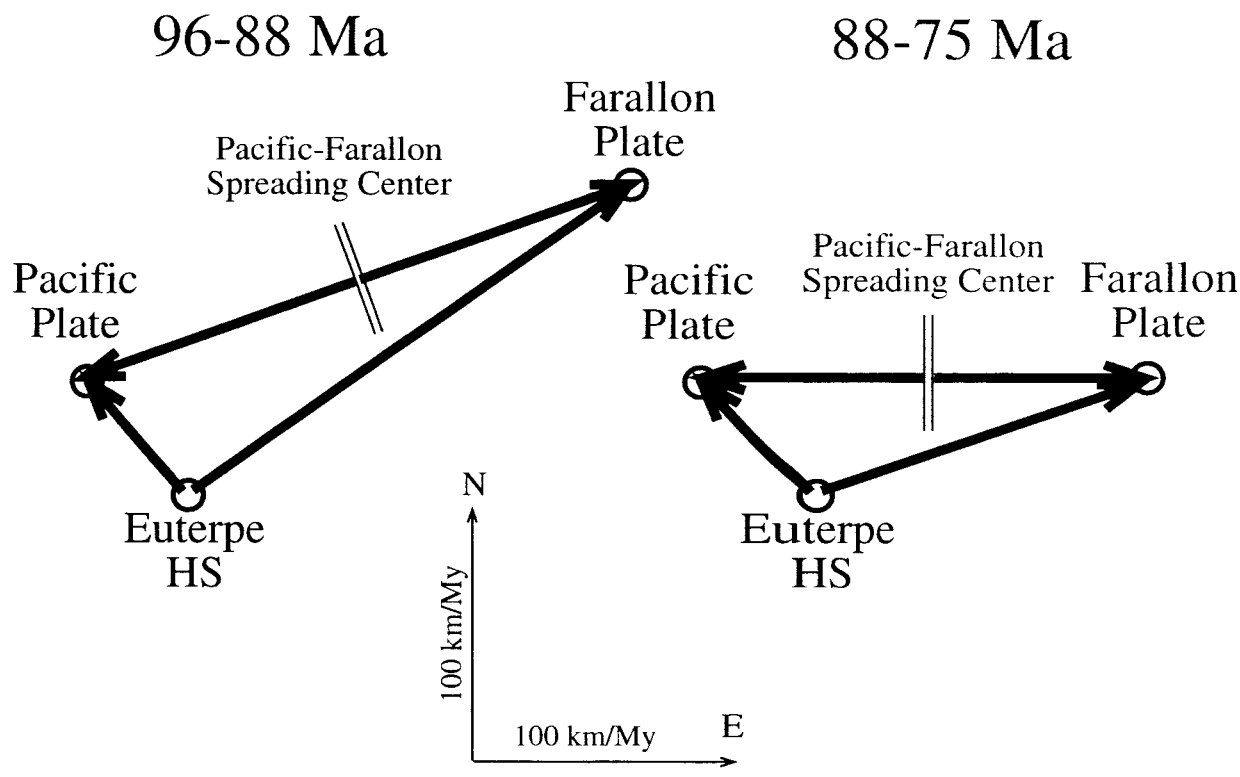

Figure 2.2.1.8: Relative and absolute Pacific and Farallon Plate velocities with respect to each other and the Euterpe Hotspot during the time of formation of the Musicians Seamount Province between ~96Ma and ~75Ma

2.2.2 THE MUSICIAN'S SEAMOUNT PROVINCE

2.2.2.1 REGIONAL GEOLOGY OF THE MUSICIANS

The 40-odd seamounts and elongate ridges of the musicians seamount province were first mapped with bathymetric profiles in the 1960s and 1970's. However, the pervasive volcanic elongate ridges (VERs) were not recognized until satillite altimetry-based gravity maps showed the connected nature of what had been previously mapped as isolated seamounts. Several distinct lineations due to the alignment of individual seamounts and volcanic ridges in a region of the North Pacific created on Cretaceous sea floor were previously recognized and studied (Pringle, 1992) (Fig. 2.2.1.2). Two distinct lines which are parallel to the northern Line Islands chain starting at about 36°N-196°W (just south of the Pioneer fracture zone) down to the vicinity of the Molokai fracture zone were identified. One is the NW-SE lineation made up of individual seamounts showing an age progression from 95 Ma (in the North) to 82 Ma (Khatchaturian seamount) (Pringle, 1992). The other more north-south lineation is not well constrained because of the scarcity of isolated volcanic edifices and their disruption by East-West trending VERs. The E-W VERs have an orientation that is nearly parallel to the traces of North Pacific major fracture zones. Each VER has several volcanic summits along its crest, and VERs may also be segmented into en echelon linear volcanos. A key question to be addressed in this study is whether the volcanic cones might have formed at the same time as the individual seamounts at the western boundary of the seamount province (cf. Fig. 2.1.1). The Musicians province is

bisected by the ENE-striking Murray Fracture zone, and renewed elongate volcanic ridge activity appears just south of the fracture zone. (where the seafloor age becomes younger and the seamounts appear to be built on younger seafloor.)

The seamounts have variable sizes and are found at depths of 2500 m and 4900 m. Previous work suggested that the Musician Seamounts never reached the surface of the sea floor (Campbell et al., 1980). However, some of the shallowest edifices (Mendelssohn and Rachmaninoff) might have erupted subaerially (Pringle, 1992). It is estimated from the seafloor cooling depth-age relation that the Musician seamount have subsided 3000 meters since they were formed. From our data, so far, we do not have supporting evidence for very shallow water (<500 m) and/or subaerial volcanism – i.e., no coraline or other shallow-water sediments, and vesiculated basalts but none that demands subaerial/very-shallow eruption.

2.2.2.2 THE VOLCANICS

Previous studies on the petrology and age dating were made on the volcanics collected mainly from the isolated seamounts forming the NW-SE lineation of the hotspot track (Fig. 2.2.2.2.1). The samples showed a compositional change from alkalic lavas (alkali basalt to trachytic rocks) to MORBs. These rocks are mainly on the alkali side of the compositional range defined from trace element geochemistry (ZrY > 4-8) (Pringle, 1992). Few dredge hauls (6 stations) were previously collected (HIG, Pringle, 1992, compilation) from the linear E-W trending Italian Ridge located in the northern area and called the Bizet seamount (2 dredges) and Donizetti seamount (1 dredge), In the southern Musicians, the Rameau (1 dredge, no age) and Bach ridges (2 dredges) were also previously sampled (Fig. 2.9). The volcanics from these ridges consist of a mixture of both alkalic lavas (alkali-basalts, trachybasalts, trachy-andesite and trachytes) and more depleted MORB (Zr/Y =2-4) type of volcanics. The silicic lavas (SiO_2> 54%, trachy-andesite, trachytes) are found on the Hammerstein and uncharted (33°29'N-166°32'W) seamounts along the NW-SE lineation. The isotopic data obtained from the area (Pringle, 1992) indicates that all samples analysed fall in the lower field of Sr ($^{87}Sr/^{86}Sr$=0.702844-0.704303) and Pb ($^{206}Pb/^{204}Pb$=15.57-15.64) isotopic ratios of the Lines Island volcanics. The Musician seamount lavas are generally similar to E-MORBs and alkali seamount magmatism (OIB Ocean Island Basalts types) (Zindler et al., 1984). It was suggested that the positive correlation between incompatible trace elements (Nb/Y and Zr/Y) and isotopic ratios (Nd and Sr) indicates a mixing trend between depleted EPR and enriched OIB type sources, but Pringle (1992) suggests that the Musician seamount volcanicism was influenced more by near ridge axial magmatism than by intraplate processes.

2.3 THE MORPHOLOGIC TRACES OF HOTSPOT-RIDGE INTERACTIONS

Hotspots (the surface melting expression of presumed underlying mantle plumes) have a long-known geochemical influence on the melt production and geochemistry of neighboring spreading centers. For example, the Iceland and Azores hotspots have a large effect on their neighboring sections of the mid-Atlantic Ridge, while other hotspots that are farther from a ridge axis often appear to create a 'spike' in mid-ocean ridge chemistry of the section of the ridge that is closest to the hotspot (even in some cases where the hotspot is currently thousands of kilometers from the axis [e.g., Schilling et al., 1984]).

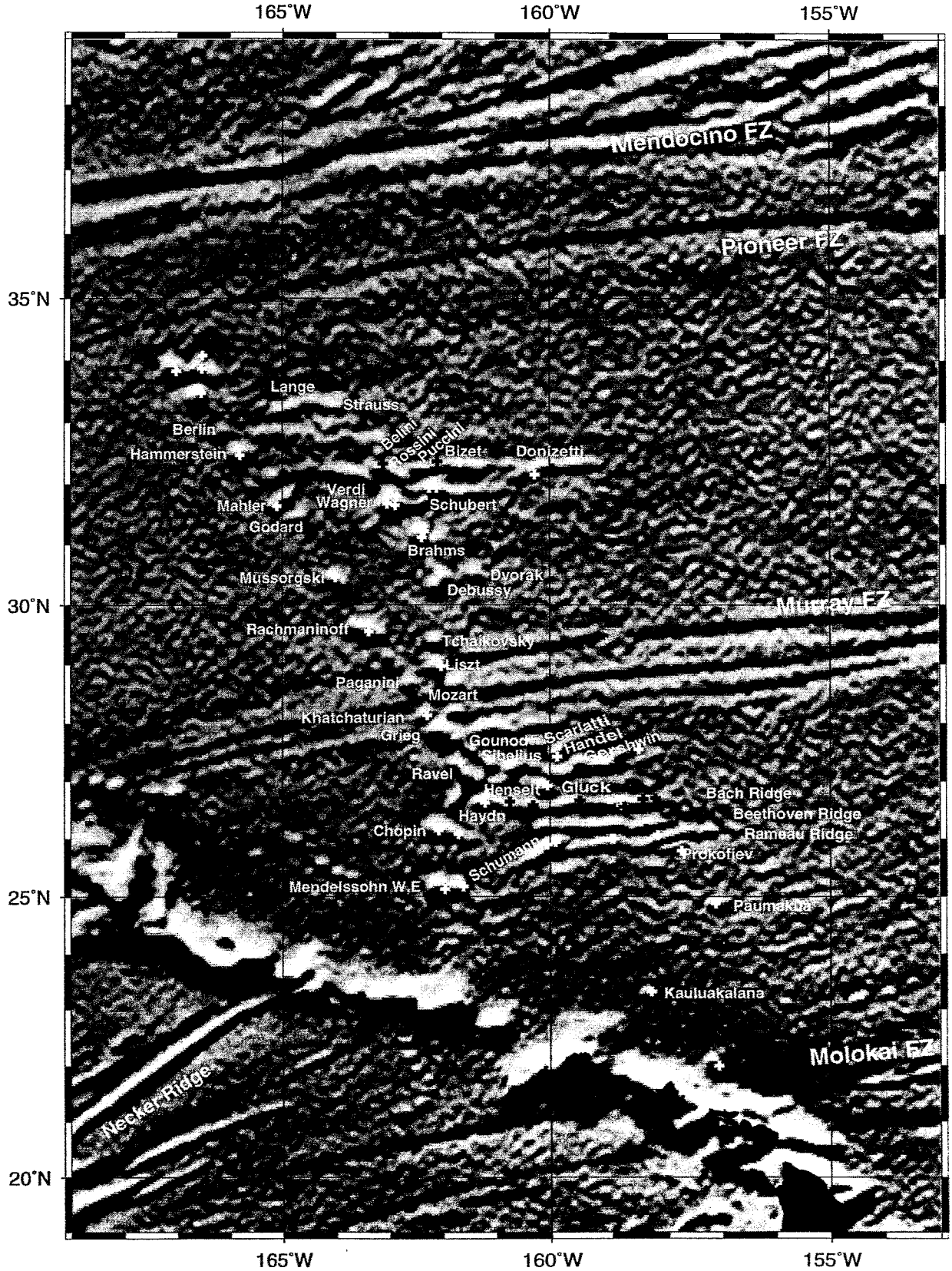

Figure 2.2.2.2.1: Previous + New Dredgesites in the Musicians Seamount Province.

In addition, at least two morphologic features are thought to be produced by the interaction between a plume/hotspot and a nearby mid-ocean ridge – oceanic plateaus and volcanic elongate ridges (cf. Fig. 2.3.1). Oceanic plateaus are known to form when a hotspot is near a slow or intermediate-spreading center. Two examples of this phenomena are the Iceland-Faeroes-Greenland Ridges associated with the Iceland hotspot and the Carnegie and Cocos Ridges associated with the Galapagos hotspot. Typically, plateaus form as conjugate pairs about the spreading center. The plateau on the hotspot-side of the ridge has both larger and more rugged relief, as it is produced both by enhanced ridge melting and by hotspot volcanism after the seafloor moves away from the spreading axis. The plateau on the opposite side of the ridge from the hotspot has much smoother and lower amplitude relief as it is created solely by the hotspot's influence to enhance crustal production at the spreading center. Because of the asymetric morphology of hotspot plateaus about the spreading center, this can often be used to decipher when the spreading center crossed over a mantle plume. Morgan (1978) proposed that the geometry of aseismic ridges and VERs will be related to the relative motion of the spreading center with respect to the hotspot and the absolute motion of the plate overlying the hotspot. This geometric construction is shown in Figure 2.3.2 (after Morgan, 1978).

Volcanic elongate ridges were first suggested by Morgan (1978) to be the products of hotspot-ridge interactions. These linear (often en-echelon) structures typically have ~2km of relief, are ~10-15km wide, and can stretch for up to ~700km (Figure 2.3.3). Besides the elongate volcanic ridges in the Musicians seamount province, many similar elongate volcanic(?) features appear to have been also created by other past and present ridge-hotspot interactions. For example, an even larger paleo example occurs at Necker Ridge which extends from the Mid-Pacific Mountains to the Hawaiian Island chain (Fig. 2.3.1). Other smaller paleo examples are evident on the eastern sides of the Line Islands, Manihiki Plateau, and Tuomatu Islands (see Figure 2.3.1). Even larger isolated ridges of this type may have been created by the interaction of the Kergulen and Reunion hotspots and their adjacent spreading centers as discussed by Morgan (his proposed "second type of hotspot island" [Morgan, 1978]). It seems likely that this type of hotspot-spreading center interaction is also presently producing oblique volcanic ridges along the Pacific-Antarctic spreading center (e.g. the oblique ridges within the Foundation chain [Maia et al., 1998] and the oblique Hollister Ridge south of the Eltanin transform system. The global significance of this overlooked class of volcanism only became obvious with satellite-altimetry-based gravity and 'predicted bathymetry' maps of the ocean basins. Figure 2.3.3 and Table 2.3.1 summarize the azimuths and lengths of VERs mapped using gravity maps such as Figure 2.1.1 based on global satellite altimetric data. Roughly half of these features are oblique to the local relative-plate motion, and thus clearly cannot be directly related to mechanisms of fracture zone formation. The musicians seamount province is unique in that long VERs formed while the hotspot was moving beneath the Pacific Plate in a direction that is strongly oblique to the direction of relative Pacific-Farallon plate motion. We hope in the current project to gain enough understanding about the surface and sub-surface structure of the Musician's VERs to be able to understand how, where, and why these enigmatic structures are sometimes produced when a hotspot is near an oceanic spreading center.

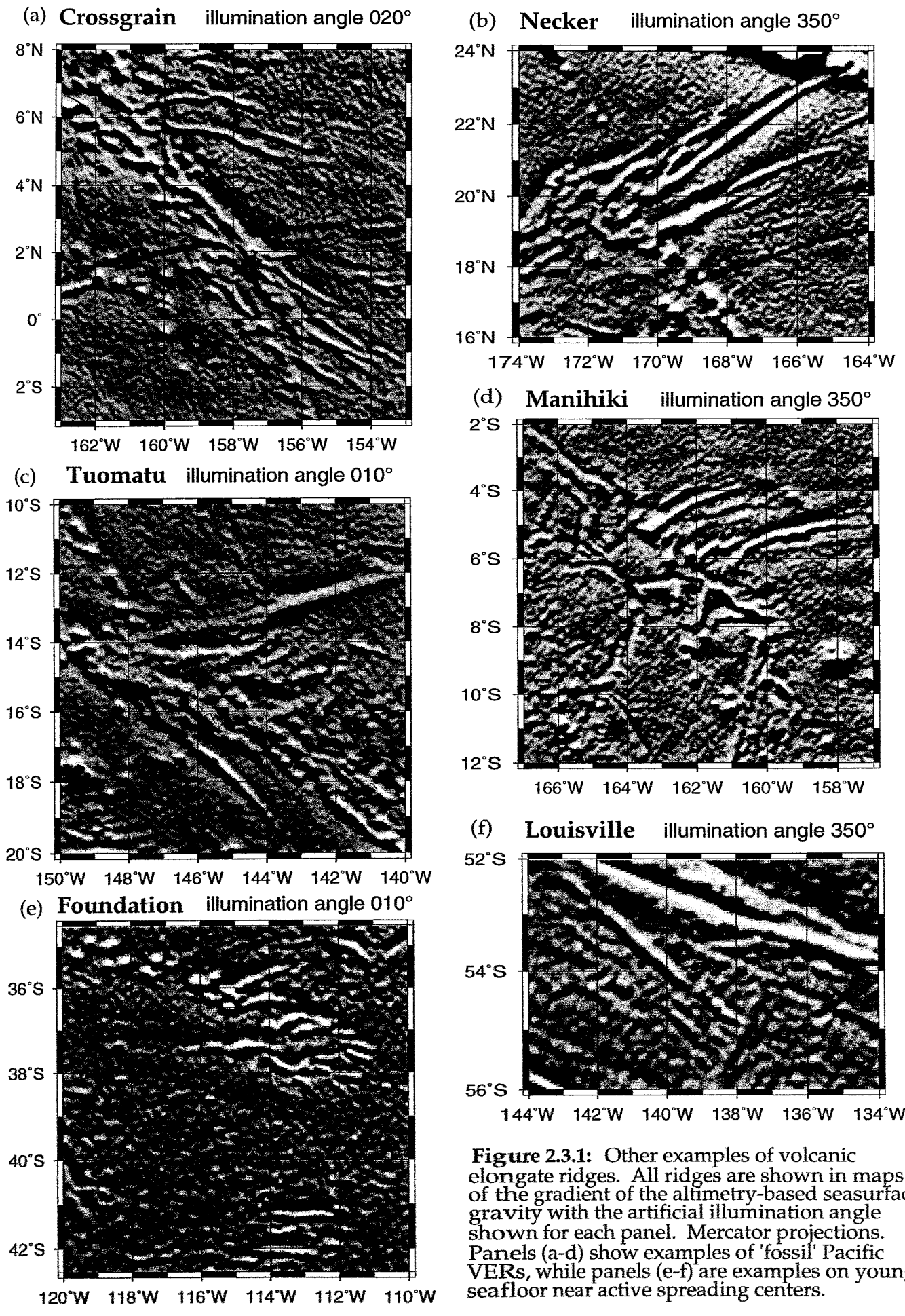

Figure 2.3.1: Other examples of volcanic elongate ridges. All ridges are shown in maps of the gradient of the altimetry-based seasurface gravity with the artificial illumination angle shown for each panel. Mercator projections. Panels (a-d) show examples of 'fossil' Pacific VERs, while panels (e-f) are examples on young seafloor near active spreading centers.

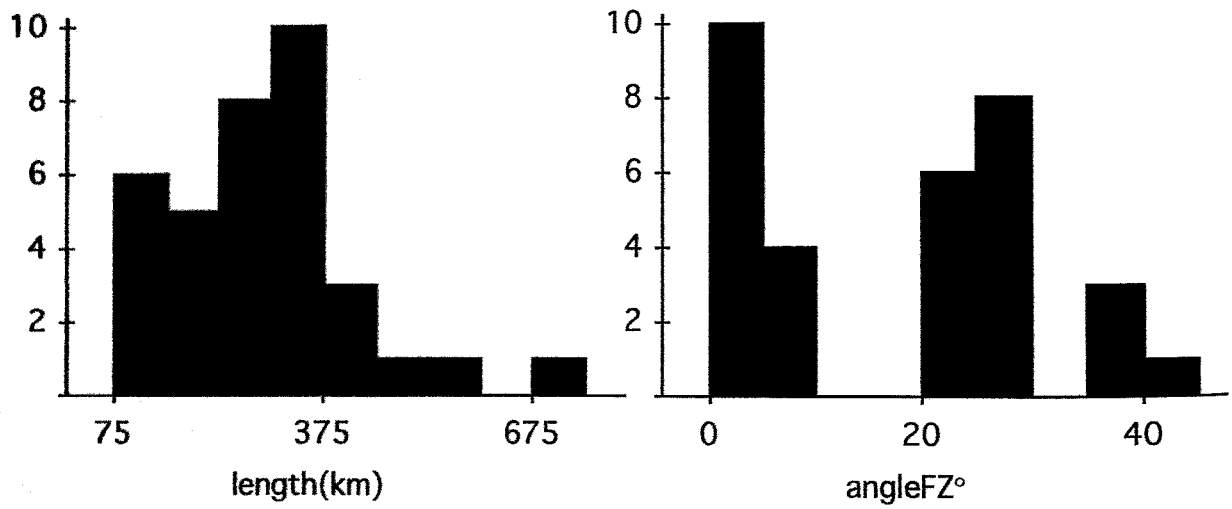

Figure 2.3.2: (Lhs) The lengths of Volcanic Elongate Ridges in the Pacific and Indian Ocean Basins measured from satellite-altimetry-derived maps of the seasurface gravity field. Lengths were measured from GMT-derived maps of the curvature of the gravity field. (rhs) Azimuths of VERs from the local direction of fracture zones (azimuth measured as the absolute value of the difference between a VER direction and the local FZ trend (if availible nearby).

Region	°from FZ	Length(km)
Del Cano	5	466
Kergulen1	27	444
Kergulen2	28	178
WolfDarwin	41	310
Louisville1	26	321
Louisville2	25	89
Louisville3	25	100
Louisville4	25	78
Austral1	22	111
Austral2	0	310
Austral3	0	244
Austral4	22	255
Austral5	22	244
Manihiki1		355
Manihiki2		111
Manihiki3		400
Necker1	21	688
Necker2	0	344
Necker3	9	277
Necker4	8	166
Crossgrain1	23	366
Crossgrain2	20	244
Crossgrain3	27	400
Crossgrain4	35	355
Crossgrain5	37	322
Crossgrain6	37	266
Crossgrain7	29	166
Musician1	0	133
Musician2	0	566
Musician3	0	222
Musician4	0	222
Musician5	0	288
Musician6	0	333
Musician7	0	244
Musician8	5	321

Table 2.3.1: Lengths and azimuths of Volcanic Elongate Ridges in the Pacific and Indian Ocean Basins measured from satellite-altimetry-derived maps of the seasurface gravity field. Lengths were measured from GMT-derived maps of the curvature of the gravity field. (rhs) Azimuths were measured from the local direction of fracture zones (azimuth measured as the absolute value of the difference between a VER direction and the local FZ trend. If no local FZ trend is availible, then the azimuthal trend was not measured.

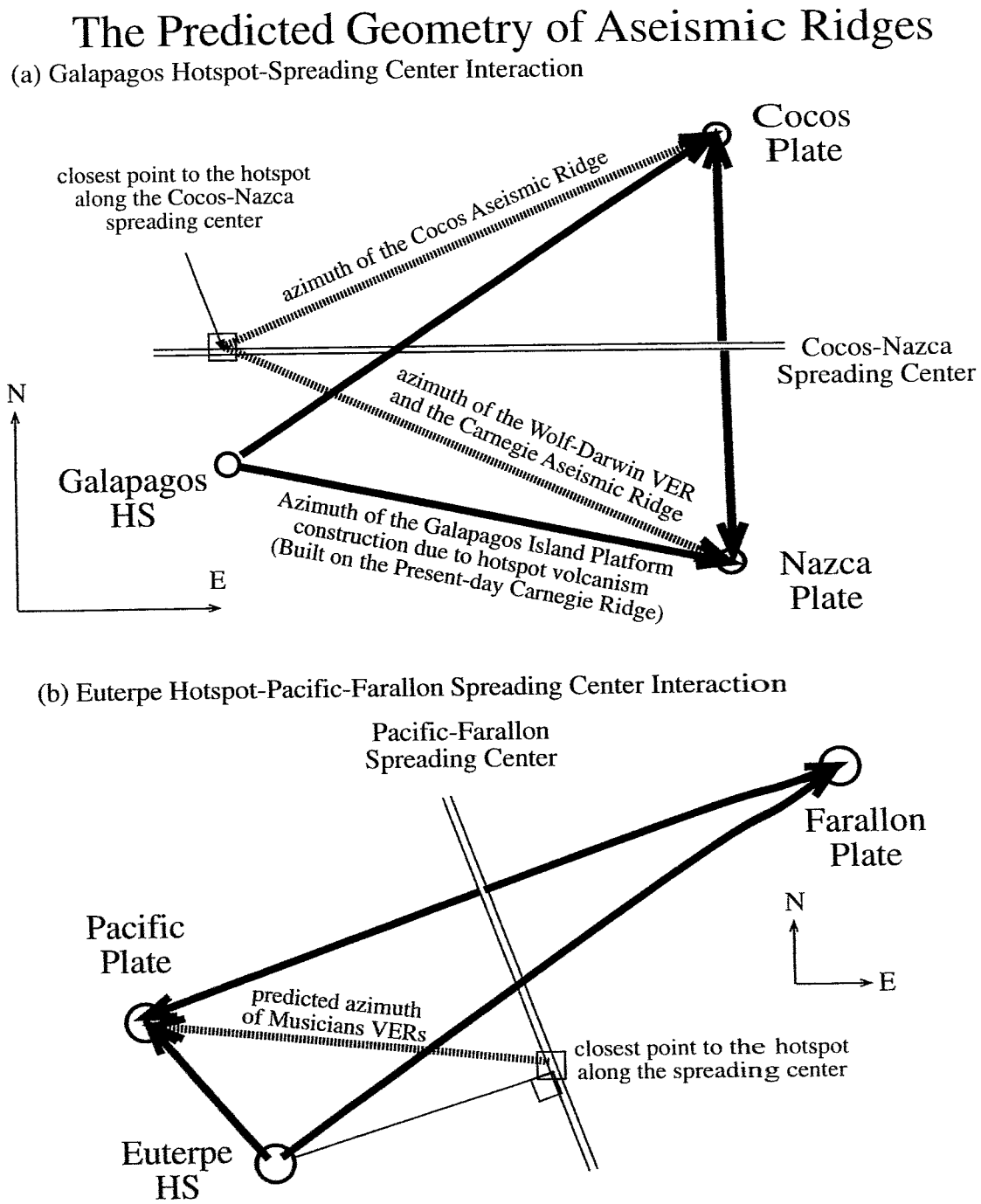

Figure 2.3.3: The geometric relations between a pair of aseismic ridges and the island platform. (a) The interaction of the Galapagos Hotspot and the Cocos-Nazca Ridge. (Redrawn after the construction in Morgan [1978].) The aseismic ridges are produced by anomalous volcanism at the neighboring mid-ocean spreading center and are created at an azimuth reflecting both the relative and absolute plate motions on both sides of the ridge. The island platform 'proper' is created (on the aseismic ridge) as the Nazca Plate passes over the Galapagos Hotspot and the rugged island relief reflects this direction of absolute motion. (b) The predicted geometric relations for the Musicians Seamount Province during the time interval between ~96-88 Ma, if these Volcanic Elongate Ridges (VERs) follow the trend predicted by Morgan (1978).

2.4. BIOLOGICAL OBJECTIVES

A number of recent biological cruises in the eastern North Atlantic (1986-1995) have included studies of the photobiology of the midwater fauna as a key objective. This research mainly comprises the linked elements of visual physiology and bioluminescence. It is important that the generalisations and hypotheses that have arisen from this work (for reviews see: Douglas et al., 1998a, Wagner et al., 1998) should be tested on a wider faunal and environmental range. The opportunity to extend these studies to the fauna of the Pacific is therefore a very timely one.

There are two basic aspects in the study of vision in deep sea animals. Firstly, since sunlight plays only a minor role between 500 and 1,000m of depth, and is no longer detectable below 1,000 m, bioluminescence is the major source of light; it is found in numerous species inhabiting this mesopolagic habitat (Herring, 1987, 1996). Observations in the "wild" from submersibles, and from specimens recovered alive from catches in the laboratory have shown a remarkable diversity of spatial and temporal patterns of bioluminescence. Unfortunately the biological significance of these often highly elaborate displays are largely a matter of speculation. The probable uses range from camouflage by counterillumination of the ventral surface (hatchetfish), disturbance of predators by release of luminous clouds; intraspecific signalling or identification of sexual mates; luminous lures (anglerfish); illumination of potential prey by "headlight photophores" (some lanternfishes). In general, the wavelengths emitted by the photophores match closely the colour of the downwelling sunlight at mesopelagic depths, i.e. the light produced is bluish-green (λ_{max} about 480nm). In very few cases (which are also of special interest during this cruise), however, dragonfish carry light organs emitting far red light under their eyes, in addition to the ordinary blue photophores elsewhere on their bodies. A better understanding of the biological significance of bioluminescence requires a detailed analysis of the temporal pattern and spectral composition of the light emitted by these animals.

Secondly, the receiver of this bioluminescence needs to be studied, including the special adaptations of the optical media (cornea, lens), and the visual pigments of the photoreceptors. A number of deep-sea fishes have conspicuously yellow lenses, or yellow pigments embedded in their retinae (e.g. some Scopelarchids). Douglas et al. (1998a) could show that this apparently counterproductive adaptation can be used to break the counterillumination camouflage of bioluminescent fishes such as hatchetfishes. Recent studies of the visual pigments in the outer segments of retinal photoreceptors have yielded a number of highly interesting observations. Bleaching of these visual pigments by photons triggers the stimulation cascade which ultimately leads to visual perception. Visual pigments contain a protein moiety, the amino acid composition of which ultimately determines their spectral sensitivity. In a broad comparative analysis of nearly 200 species of deep-sea fishes Douglas et al. (1995, 1998a) and Douglas & Partridge (1997) have shown that in these animals, the spectral sensitivity of the rhodopsins is so tuned as to make them maximally sensitive to both the residual sunlight and the bioluminescent emissions (λ_{max} 460-490nm).

Three genera of deep-sea dragon fish (*Malacosteus, Aristostomias* and *Pachystomias*), whose suborbital photophores have emission maxima beyond 700nm, have visual pigments very different to those of other deep-sea fish (see above). To enable them to see their own far-red bioluminescence, which will be invisible to all other animals in the deep-sea, these animals have been shown, using retinal extracts and microspectrophotometry, to posses two long-wave shifted visual pigments, giving them a private wave-band which they can use for covert illumination of prey or for intraspecific communication immune from detection by potential predators (Partridge & Douglas, 1995). These 2 pigments form a so called 'pigment pair'; in which both pigments

utilise the same opsin which in some photoreceptors is bound to the chromophore retinal (an aldehyde of vitamin A_1) forming a rhodopsin pigment, while in other receptors the same opsin is bound to the vitamin A_2-derived chromophore 3, 4 dehydroretinal, forming a porphyropsin pigment. Recently, using a retinal wholemount technique, we have demonstrated the existence of an additional longer-wave absorbing, pigment in the retinae of *Aristostomias tittmanni* (Partridge & Douglas, 1995) and *Pachystomias microdon* (Douglas et al., 1988a). This pigment is a rhodopsin, utilising retinal as its chromophore bound to a second, longer-wave absorbing, opsin. Perhaps surprisingly, we have been unable to find a similar third pigment in *Malacosteus niger*. This species instead employs a chlorophyll-derived photosensitizer to enhance its long-wave sensitivity (Douglas et al., 1998b). The demonstration of a chlorophyll-derived photosensitizer in *M. niger* is in many way astonishing. Firstly, it has never before been suggested that chlorophyll, which is central to plant photosynthesis, might have a role to play in animal vision. Secondly, photosensitizers were previously unknown in vertebrate eyes. We hope to collect additional specimens of dragon fishes in order to obtain new material which will enable us to continue these exciting investigations.

The morphological organisation of the retina in deep-sea fishes shows a number of striking adaptations which can be interpreted in terms of optimising the catch of the rare photons available in the mesopelagic habitat. Above all, deep-sea fish retinae, as a rule, contain only the more sensitive rods. In addition, the surface of the photoreceptive membrane, i.e. the number of discs in the rod outer segments has been greatly increased based on two alternative mechanisms: Either the rod outer segments are unusually long, far exceeding 100µm, or there are shorter rods, but arranged in multiple tiers, again adding up to a total length of up to 200µm or more. At the same time, the overall thickness of the neural retina and the density of retinal neurons is markedly decreased. Notably, however, every major transmitter system typically found in other vertebrate retinae is also present in the specialised retinae of deep-sea fishes (Wagner et al., 1988).

Interestingly, the adaptations especially of the photoreceptors and the retinal pigment epithelium bring about a number of problems for processes such as pigment regeneration and outer segment renewal which require a close spatial association and interaction of these cells. It is unclear how these processes are controlled in multibank rod retinae, and we want to collect living retinal tissue to address this question more closely.

A further specialisation of some deep-sea retinae is found in the ganglion cell layer (and sometimes also in the photoreceptor layer). It regards regions of particularly high cell densities (areae retinae) or even foveae (similar to primates) suggesting that some sectors of the visual fields are processed at high resolution. In these regions, the high convergence ratios from rods to ganglion cells, which usually are the hallmark of high sensitivity, are markedly reduced (Collin et al., 1997). We want to pursue these studies and refine them by using special labelling techniques which allow the unequivocal identification of retinal ganglion cells.

In addition to the study of the eye, material will also be collected that allows a more general assessment of the role vision plays among the other senses in the midwater fish fauna. This aspect is of particular interest because no observations are available to demonstrate to which extent and in what context these species make use of visually guided behaviour. Therefore, brains and cranial nerves are collected from a wide variety of species, and a quantitative analysis performed of the different afferent systems, with special emphasis on the olfactory and optic nerves

3. PARTICIPANTS

3.1. SCIENTISTS

Ernst R. Flüh, GEOMAR, chief scientist
Jason Phipps Morgan, GEOMAR, co-chief scientist
Benjamin Boormann, SOC
Hajnal Borús, GEOMAR
Ronald H. Douglas, CU
Ingo Grevemeyer, GEOMAR / GEOB
Ralf Hartz, AbisZ
Roger Hekinian, IFREMER
Peter J. Herring, SOC
Christian W. Kopp, GEOMAR
Camilla E. Larsen, UC
Heidrun Lelgemann, GEOMAR
Suzanne N. Lyons, SIO
W. Jason Morgan, PU
Carl-Urlich Nöske, AbisZ
John O'Connor, AWI / IFG
Yucheng Pan, HI
Klaus-Peter Steffen, KUM
Thimo Stender, IFG
Hans-Joachim Wagner, ANATÜ
R. Wilhelm Weinrebe, GEOMAR
Fritz Wolter, IFG

3.2. CREW

Hartmut Andresen	Master
Axel Bendin	Chief Officer
Lutz Mallon	1st Officer
Wolfgang Köthe	Radio Officer
Anke Walther	Surgeon
Uwe Thaysen	Chief Engineer
Helmut Grund	2nd Engineer
Peter Neumann	2nd Engineer
Rudolf Freitag	Electrician
Rainer Duthel	Chief Electronic Engineer
Heiko Buxel	Electronic Engineer
Kurt Stammer	System Operator
Jens Grigel	System Operator
Peter Schymatzek	Fitter
Frank Sebastian	Motorman
Helmut Meyer	Motorman
Manfred Siewert	Motorman
Udo Prinz	Motorman
Klaus Herrmann	Chief Cook
Adolf Cwienk	2nd Cook
Georg Horzella	Chief Steward
Justine Hasler	Stewardess
Peter Eller	2nd Steward
Winfried Jahns	Boatswain
Stefan Tamm	A. B.
Peter Schober	A. B.
Jürgen Vor	A. B.
Eugenius Dracopoulos	A. B.
Hermann Röpti	A. B.
Andreas Schrapel	A. B.

3.3. ADDRESSES OF PARTICIPATING INSTITUTIONS

AbisZ: Ing.-Dienstleistungen
Wischhofstraße 1-3
24148 Kiel
Germany
Tel. 0049 – 431 – 721 –115
Fax. 0049 – 431 –721 –256
e-mail: AbisZ@t-online.de

ANATÜ: Anatomisches Institut
Universität Tübingen
Österbergstr. 3
72074 Tübingen
Germany
Tel. 0049 - 7071 - 29 - 7301
Fax. 0049 - 7071 - 29 - 4014
e-mail: hjwagner@anatu.uni-tuebingen.de

AWI: Alfred - Wegener - Institut
für Polar- und Meeresforschung
Columbusstr. 10
27568 Bremerhaven
Germany
e-mail: joconnor@awi-bremerhaven.de

IFG: Christian Albrechts Universität zu Kiel
Institut für Geowissenschaften
Olshausenstr.40
24118 Kiel
Germany
Tel. 0049 – 431 – 880 – 2851
Fax. 0049 – 431 – 880 – 4376
e-mail: stu38261@mail.uni-kiel.de

IFREMER: Département Géosciences Marines
Ifremer Center de Brest
BP 70 – 29280 Plouzané
France
Tel. 0033 – 298 – 224 – 252
Fax. 0033 – 298 – 224 – 570
e-mail: hekinian@ifremer.fr

CU: Dept. of Optometry & Visual Science
City University
311-321 Goswell Rd
London EC1V 7DD
U.K.
Tel. 0044 – 171 – 477 – 8334
Fax. 0044 – 171 – 477 – 8355
e-mail: r.h.douglas@city.ac.uk

GEOB: Universität Bremen
FB Geowissenschaften
Postfach 330440
28334 Bremen
Germany
Tel. 0049 – 421 – 218 – 4911
Fax. 0049 – 421 – 218 – 7163
e-mail: ingo@geophysik.uni-bremen.de

GEOMAR: GEOMAR
Forschungszentrum für
marine Geowissenschaften der
Christian-Albrechts-Universität zu Kiel
Wischhofstraße 1-3
24148 Kiel
Germany
Tel. 0049 - 431 - 600 - 2972
Fax. 0049 - 431 - 600 - 2922
e-mail: nn@geomar.de

HI: Dept. Geology & Geophysics
University of Hawaii
1680 East-West Rd. POST 615C
Honolulu, HI96822
USA
Tel. 001 – 808 – 9569544
e-mail: ypan@soest.hawaii.edu

KUM: K.U.M.
Umwelt- und Meerestechnik Kiel Gmbh
Wischhofstr. 1-3, Geb. D5
24148 Kiel
Germany
Tel. 0049 – 431 – 7209 – 220
Fax. 0049 – 431 – 7209 – 244
e-mail: KUM.Umweltmeerestechnik@t-online.de

PU: Geosciences Dept.
Princeton University
Princeton, NJ 08544 – 1003
USA
Tel. 001 – 609 – 258 – 3596
Fax. 001 – 609 – 258 – 1274
e-mail: wjmorgan@geo.princeton.edu

SIO: Scripps Intitution of Oceanography
IGPP, MC 0225
La Jolla, CA 92093-0225
Tel. 001 – 619 – 534 – 6150
Fax. 001 – 619 – 534 – 5332
e-mail: slyons@ucsd.edu

SOC: Southampton Oceanography Centre
Empress Dock
Southampton So14 3ZH
U.K.
Tel. 0044 – (1) – 703 – 596 – 345
Fax. 0044 – (1) – 703 – 596 – 247
e-mail: p.j.herring(or: b.boormann)@soc.soton.ac.uk

UC: Geologisk Institut
Københavns Universitet
Øster Voldgade 10
1350 København K
Denmark
e-mail: lc030472@geo.geol.ku.dk

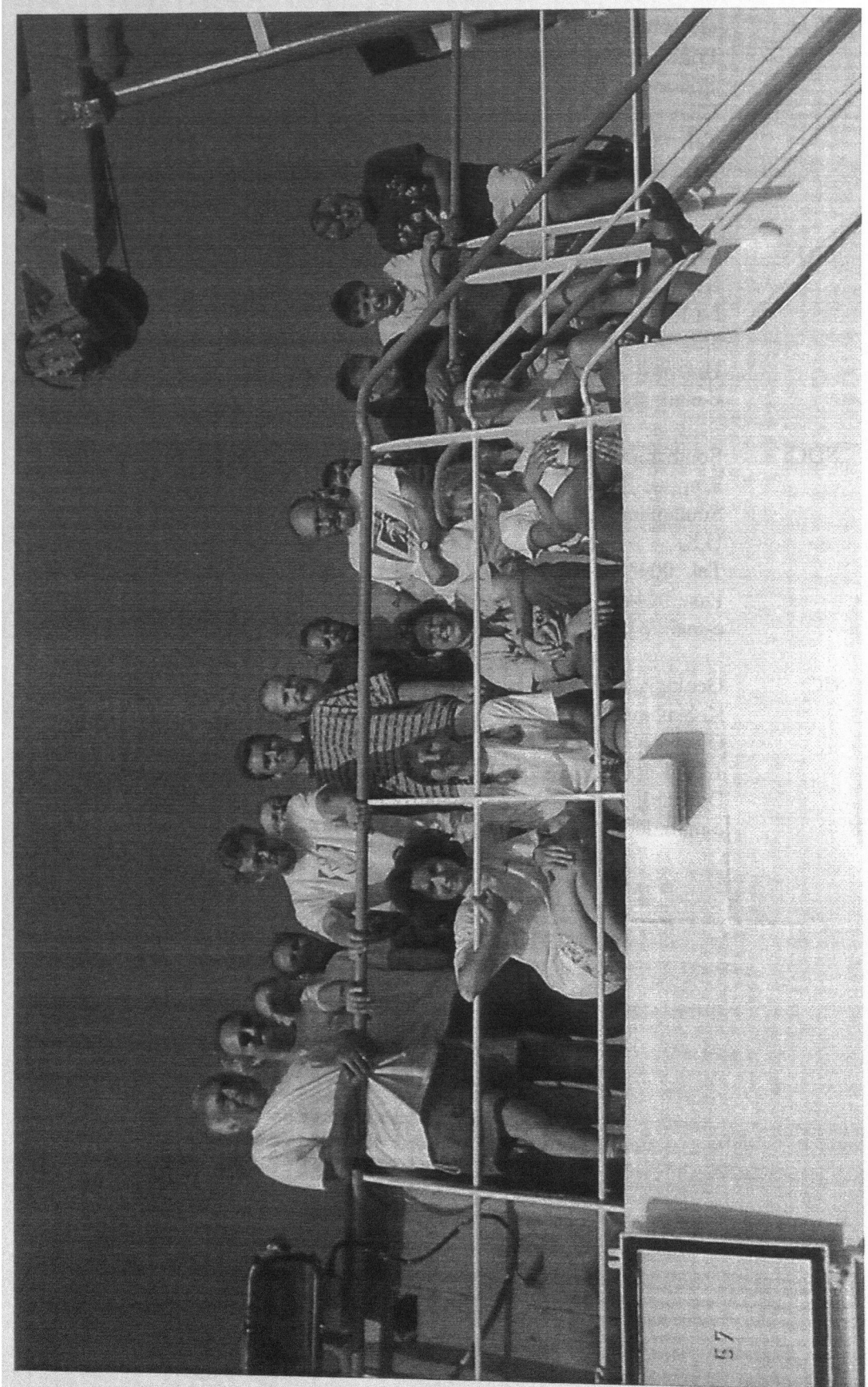

Figure 3.1: THE HULA SCIENTIFIC PARTY.

4. AGENDA OF SONNE CRUISE SO142

(E. Flueh)

SONNE cruise SO142 started on 30 May 1999 on Midway Island and ended 27 June 1999 in Honolulu. After the scientific equipment had been loaded and installed, SONNE left the pier on 30 May 1999 at 16:00 and headed in gale winds towards the Musician Seamounts. Continuous recording of hydroacoustics was performed throughout the cruise, with the exception of the approach to Honolulu. A complete track chart of cruise SO142 is shown in Figure 4.1.

Due to the short port time, most of the instrument preparation had to be performed at sea, despite adverse conditions during the first three days. Several tests of components of the Ocean Bottom Hydrophones (OBHs), especially the releasers and the pressure housings of the electronic recording packages were made using a W6 winch with up to 5600 m cable length. Unlike on previous cruises, both the ship mounted transducer and the inactive transducer failed to receive the acknowledgement commands of the releasers. Although the release commands were received and executed by the instruments, the acknowledgement and the range could only be read using the active transducer, which had to be put overboard and required the vessel to come to a complete stop.

During the transit, several trawls were performed with the Rectangular Midwater Trawl (RMT), each lasting 4 to 5 hours. The first trawl (F1) was made on 01 June from 10:00 to 14:00. During the cruise a total of 21 trawls was achieved, including shallow night trawls and deeper day trawls.

Before reaching the Musician Seamounts, a CTD was run to 5000 m depth in the evening of 02 June. For all subsequent hydracoustic profiles, the magnetometer was deployed, starting with Profile 101 at 23:00 on 02 June. The hydroacoustic survey of the northern Musician seamounts started at Mahler Seamount, where two complete swaths were run looking for the steepest walls, which are the most suitable for dredging. Profiling was interrupted for several trawls. The first dredge (G1) was made in the evening of 05 June.

A short seismic profile (SO142-01) using only one airgun and five instruments was made on 06 June; all instruments, including a test deployment, were recovered the same day. Two dredge hauls and two trawls were completed on 07 June. The magnetometer was then deployed and transit between stations was coordinated such that gaps in the swath bathymetry could be filled in. Another two trawls (F7 and F8), Dredge G4 and Profile 112 were all done in calm seas on 08 June; after completing profile 113, the first large seismic profile was started.

Between 05:50 and 10:20 on 09 June, 13 OBHs (OBH07 to OBH19) were deployed on a north-south striking line centered on the Italian Ridge. Instrument spacing was 3 nm with one additional instrument in the center. Sounding started about 35 nm to the south of the recording array and extended to 30 nm north of the array. While shooting, the line wind increased considerably to about 10 m/s, causing increased force on the two guns. Shooting was executed at a ship speed of about 3.7 kn with a shot interval of 60 s; this results in a shot spacing of about 115 m.

Shooting terminated at 18:00 on 10 June, about 30 nm north of the recording array. A profile parrallel to the line (115) was then run, extending to the start of the recording array (OBH19) in order to facilitate pickup of instruments against the wind. OBH19 was aboard at 01:15 on 11 June. Unfortunately, no release command was acknowledged, even when using the active transducer that was working well before. However, all instruments released upon the first command sent, as documented by the popup times. All OBHs were onboard at 13:30 on 11 June, when another trawl (F9) was started.

The magnetometer was deployed on the transit to the next dredge location (G5) at the eastern end of the Italian Ridge, and two trawls (F10 and F11) were made close to this position. An

additional hydroacoustic/magnetic profile completed the work in the northern working area and Sonne started its 350 nm transit to the Bach Ridge near midnight on 12 June.

The transit was interrupted at noon on 13 June when we crossed the Murray Fracture Zone and identified a promosing target for a dredge haul (G6). Two additional trawls (F12 and F13) were completed at this location before the transit to the south continued (profile 118) at 04:30 on 14 June. Bach Ridge was reached by 19:00. The magnetometer was deployed during transit, and three hydroacoustic profiles (119, 120, 121) were run on the western end of Bach Ridge before seismic profile S3 was started.

Deployment of 14 OBHs (OBH20 to OBH33) was accomplished along a north-south trending line from 05:00 to 10:00 on 15 June. Transit to the start of the shooting line about 40 nm to the north of OBH33 was made with the magnetometer deployed (profile 122) along a course-parallel line. Shooting started around 15:00 and terminated at 21:00 the following day. The starboard gun had to be repaired once in the middle of the profile when the airhose broke. Strong currents against the course slowed the ship down to less than 3.5 kn.

After the end of shooting, another night trawl was made (station F14), and the transit to OBH20 was run along another course-parallel track with the magnetometer deployed (profile 123). All OBHs were recovered between 05:00 and 14:00 on 17 June; all instruments recorded well. Among these recoveries was the 1000th successful recovery of a GEOMAR OBH. Again, no acknowledgement was received when release commands were sent, but apparently all release commands were executed immediately, even when sent from distances of 6 miles.

Before starting the next dredge haul on the western end of Bach Ridge, another RMT Trawl (F15) was made, this time to a depth of 2000 m. Transit to G7 was used for another magnetic profile (124). Dredge G7 was started at 20:30 on 17 June in a water depth of 4500 m. Following this dredge, several magnetic/hydroacoustic profiles were made along Bach Ridge in an attempt to achieve full bathymetric coverage. These profiles were occasionally interrupted by trawls and dredges. This was nearly completed on 21 June, when the fourth and final seismic profile began. Again, 14 OBHs were deployed (between 04:00 and 10:00) on a north-south oriented line, with a variable instrument spacing of two to four miles. Shooting started 40 nm north of the recording array at around 15:00 on 21 June and was completed without interruption at 20:00 on 22 June, despite ever increasing wind (force 5 to 6) and swell. Another trawl (F20) and magnetic profile parallel to the seismic line (129) were run before recovery of the OBHs began. Retrieval of OBH34 to 47 was achieved without any major delay between 04:00 and 16:00 23 June.

The last trawl (F21) of cruise SO142, which marked the end of the biological field program, was performed in the evening of 23 June; the remaining time was used for further dredges and magnetic profiles. Dredge haul G10, at the center of seismic profile SO142-04, was completed by 06:00 on 24 June, and was followed by G11, 15 miles immediately to the east.

A particularly strong bottom reflection was noted in wide areas around the Bach Ridge on the Parasound records, and therefore a GrabTelevision Video Bottom (GTVB) station was run for ground truthing. Unfortunately, the comminucation to the grab broke down shortly after bottom sight. After GTVB recovery and a magnetic transit line (profile 134), the last two dredges (G12 and G13) on Bach and Beethoven Ridges were completed in the evening of 25 June. Sonne then started its transit to Oahu. During the transit on 26 June, two more GTVB stations were run on the arch volcanic fields without producing any evidence for the existence of young volcanism. The scientific field program was terminated by 17:00 on 26 June, and Sonne headed south for its final destination.

The Honolulu pilot station was reached on 27 June at 11:00, and cruise SO142 HULA II ended with the docking of Sonne at pier 2 in Honolulu at 11:30 after 28 days at sea, cruising for more than 4400 miles.

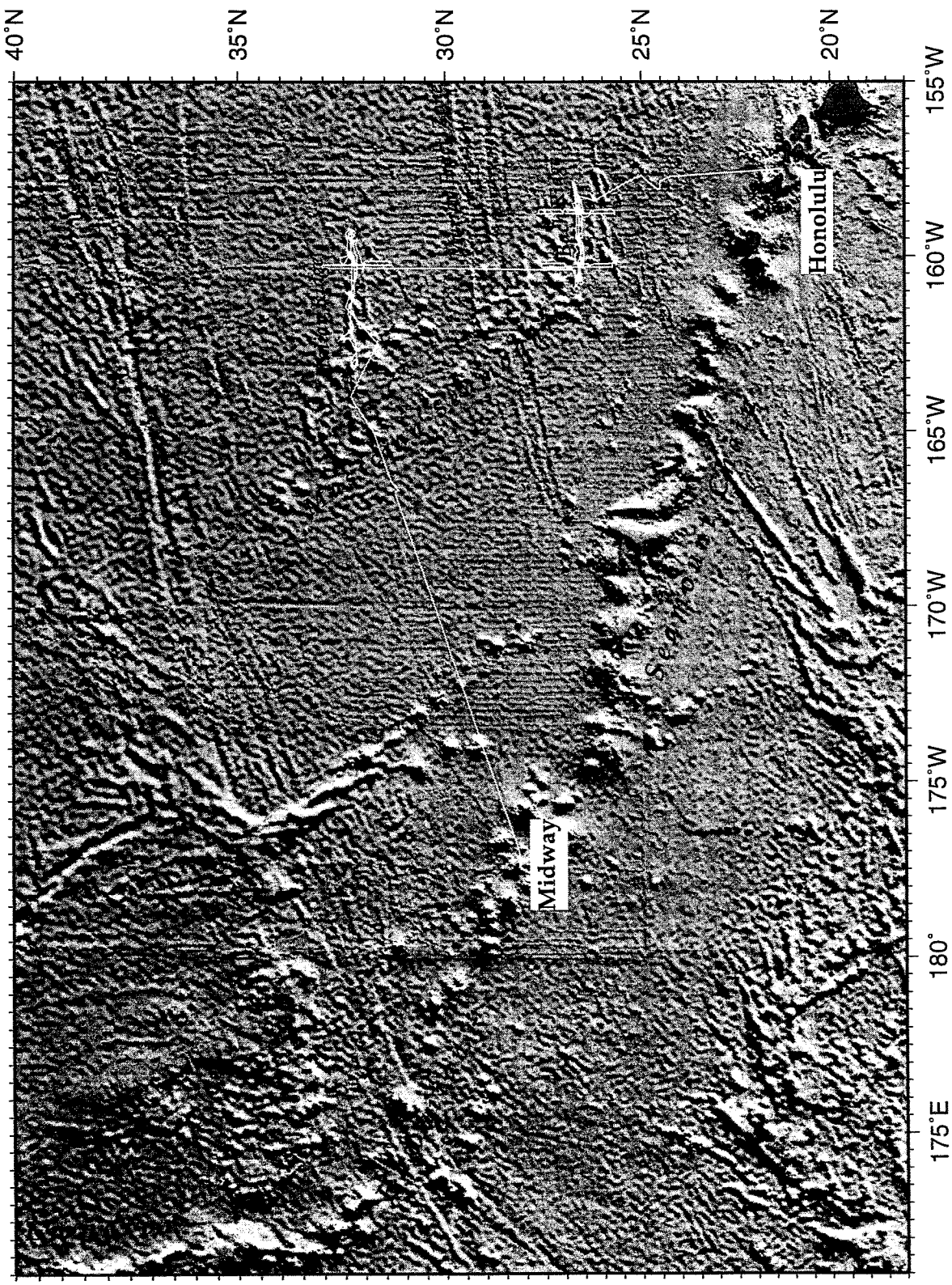

Figure 4.1: R/V SONNE cruise 142 total track.
Predicted bathymetry after Sandwell and Smith, (1996).

5. SCIENTIFIC EQUIPMENT

5.1 COMPUTER FACILITIES

(W. Weinrebe)

The experiments and investigations during SO142 required special computing facilities in addition to the existing shipboard systems. For processing of seismic data and analysis of HYDROSWEEP recordings, a workstation cluster was installed onboard comprising.

1	"neolithikum"	SUN Sparc 20	2 CPU, 256 MB memory	14 GB disks, DAT, Exabyte, CD	Sun Solaris 2.5
2	"devonia"	SUN Ultra 60	2 CPU 1 GB memory	112 GB disks, 2.3 GB MO, 2x DAT, 2x Exabyte	Sun Solaris 2.6
3	"avalonia"	SUN Sparc 5	1 CPU, 64 MB memory	13 GB disks, DAT, CD, Methusalem	Sun Solaris 2.5
4	"galicia"	SUN Sparc 10	1 CPU, 96 MB memory	12 GB disks, DAT, Methusalem	SunOS 4.1.4
5	"MBS"	Pentium II 350 MHz	1 CPU, 128 MB memory	9 GB disk, 3x PCMCIA	Windows95
6	"MBS"	Pentium II 350 MHz	1 CPU, 128 MB memory	9 GB disks, 3x PCMCIA	Windows95
7	"andean"	Pentium 133	1 CPU, 64 MB memory	5 GB disks, DAT, CD	Windows95

For seismic modelling four desktop Macintosh computers were installed:

1 PowerMacintosh G3/300 MHz

2 PowerMacintosh G3/233 MHz

3 PowerMacintosh 8200/120

4 PowerMacintosh 7100/66

In addition to these computers, two X-Windows-Terminals NCD-15r and several laptops/powerbooks were used.

For plotting and printing two HP Postscript Laserprinters (papersize A3 and A4), one OYO-11"-thermoplotter, as well as the shipboard color plotters were available.

The workstation cluster and the Macintosh desktops were placed in the magnetic/gravity lab and the Reinlabor.

The workstation cluster was set up according to a "client-server" model, with "neolithikum" being the server. All important file systems from the main server at GEOMAR were duplicated onto the "neolithikum"-disks. Using NFS-, NIS-, and automounter services the computing environment was identical to that at GEOMAR so every user found his/her familiar user interface.

The convenience of network mounted file systems has to be paid for with a heavy network load, particularly during playback of OBH-data from tape to disk (c.f. SO123 cruise report, Flueh et al., 1997). This required a high-performance network, which was accomplished by a switched twisted-pair ethernet. A 12-port ethernet switching-hub (3COM-SuperstackII 1000) with an uplink connection of 100 Mbps to the server "neolithikum" and dedicated 10 Mbps ports for the client workstations maintained the necessary network performance. In order to keep the shipboard network undisturbed by the workstation cluster, but to allow for communication between them, the server "neolithikum" was equipped with two network interfaces and served as a router. This provided the additional benefit of a simplified network configuration. Considerable setup work was dedicated to "neolithikum", while the other workstations used the same IP-addresses and network configuration as at GEOMAR.

This network setup showed a reliable and stable performance, and no breakdowns or bottlenecks were observed. The reconfigured shipboard network using twisted-pair technology and "star-"topology instead of BNC-cables along a linear "bus" with hubs in the main labs improved the flexibility to easily hook up systems to the network.

5.2 THE GEOMAR OCEAN BOTTOM HYDROPHONE (OBH)

(The Seismic Wide-Angle Group)

The Instrument

The first GEOMAR Ocean Bottom Hydrophone was built in 1991 and tested at sea in January 1992. A total of 14 OBH instruments were available for SO142. This type of instrument has proved to have a high reliability; in fact during, the cruise the1000th successful deployment was achived and celebrated. Altogether 47 sites were occupied during the HULA II cruise.

The principle design of the instrument is shown in Figure 5.2.1, and a photograph showing the instrument upon recovery can be seen in Figure 5.2.2. The design is described in detail by Flueh and Bialas (1996).

The system components are mounted on a steel pipe which holds the buoyancy body on its top. The buoyancy is made of syntactic foam and is rated, as are all other components of the system, for a water depth of 6000 m, except for the pressure cylinders holding the recording electronics. Here, various models for variable depths (2500 m, 3000 m, and 6000 m) are available. Attached to the buoyant body are a radio beacon, a flash light, a flag and a swimming line for retrieving from aboard the vessel. The hydrophone for the acoustic release is also mounted here. The release transponder is a model *RT661CE* made by *MORS Technology*. Communication with the instrument is possible through the ship's transducer system, and even at maximum speed and ranges of 4 to 5 miles release and range commands are successful. For anchors, we use pieces of railway tracks weighing about 40 kg each. The anchors are suspended 2 to 3 m below the instrument. The sensor is an *E-2PD* hydrophone from *OAS Inc.*, and the recording device is a *Methusalem* recorder of *DELTA t*, which is contained in its own pressure tube and mounted below the buoyant body opposite the release transponder (see Figures 5.2.1 and 5.2.2). Alternatively, the more advanced *MBS recorder of SEND GmbH* is used. The *Methusalem* consists of a preamplifier (26 dB), a highpass and antialias filter, a 13 bit A/D converter and a core memory of 0.768 MB. Signals are sampled at 800 Hz, and after FIR-decimation filtering, a resolution of 14 to 15 bits is achieved. Data are stored as 16 bit integers on a DAT cassette, which is run in audio-mode to save power consumption and which can store about 1.1 GB of data. The power supply is from alkaline batteries for long term deployments or from rechargeble lead batteries for short term deployments (up to 3.5 days). The instrument can be programmed before deployment through an RS232 interface. Up to 4 channels with different amplifications and sampling rates can be recorded. A DTCXO (0.05 ppm accuracy) is checked against GPS time before and after deployment. The DAT cassettes are read from a playback system, which simulates a SCSI interface, to a workstation for data reduction and analysis (see Chapter 6.3.2).

Marine Broadband Seismic Recorder (MBS)

Apart from the older DAT recording units a new generation of digital seismic recorders was used. The so-called *Marine Broadband Seismic recorder (MBS)*, manufactured by *SEND GmbH*, was developed based upon experience with the DAT based recording unit Methusalem (Flueh and Bialas, 1996) over the last years. This new recorder avoids mechanically driven recording media, and the PCMCIA technology enables static flash memory cards to be used as unpowered storage media. Read/write errors due to failure in tape handling operations should not occur any more. In addition, a data compression algorithm is implemented to increase the data capacity. Redesign of the electronic layout enables a decreased power consumption (1.5 W) of about 25% compared to the *Methusalem* system. Depending on the sampling rate data output could be in 16 to 18 bit signed data. Based on digital decimation filtering the system was developed to serve a variety of seismic recording requirements. Therefore, the bandwidth reaches from 0.1 Hz for seismological observations to the 50 Hz range for refraction seismic experiments and up to 10 kHz for high resolution seismic surveys. The basic system is adapted to the required frequency range by setting up the appropriate analog front module. Alternatively, 1, 2, 3 or 4 analogue input channels may be processed. Operational handling of the recording unit is similar to the

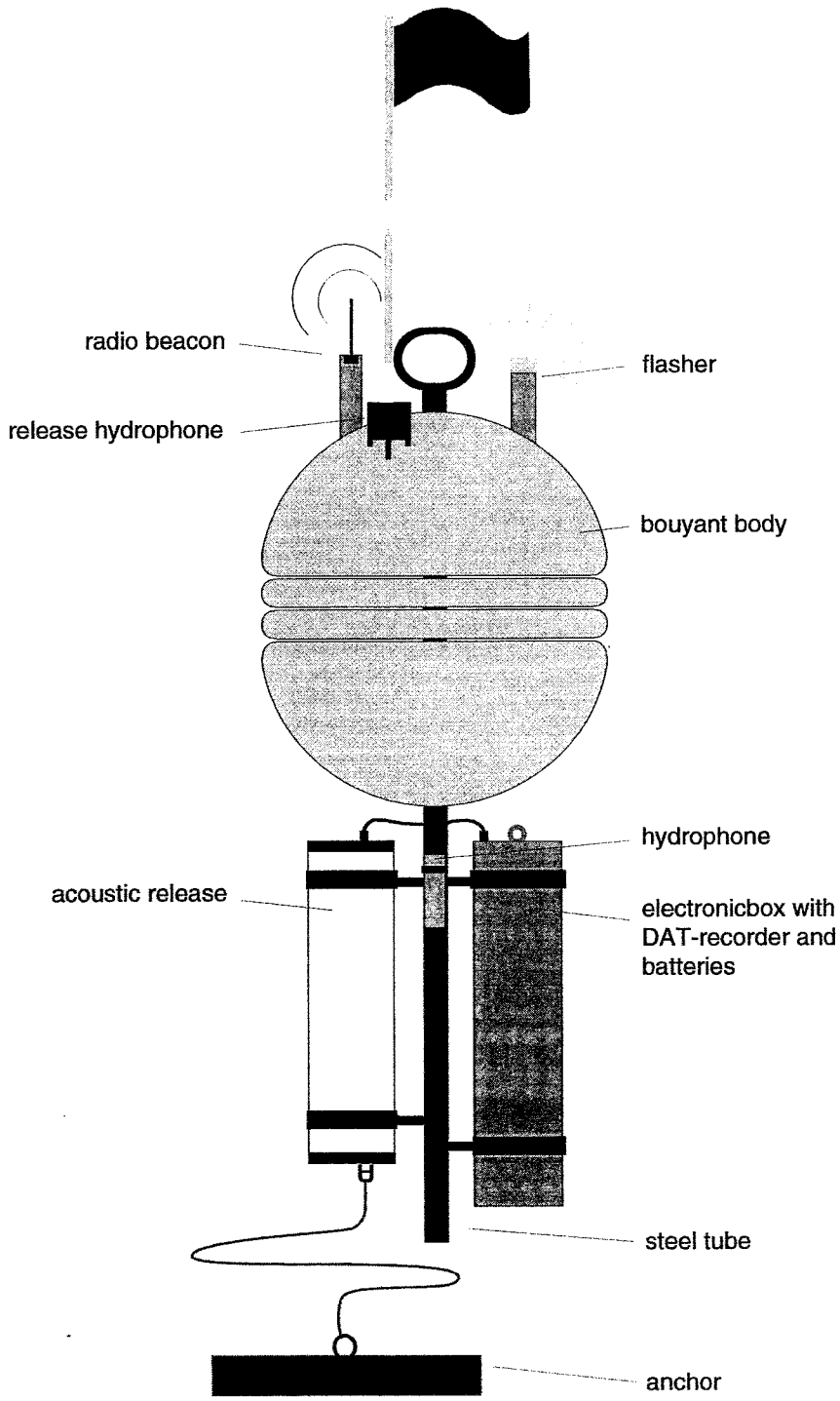

Figure 5.2.1: Principle design of the GEOMAR OBH

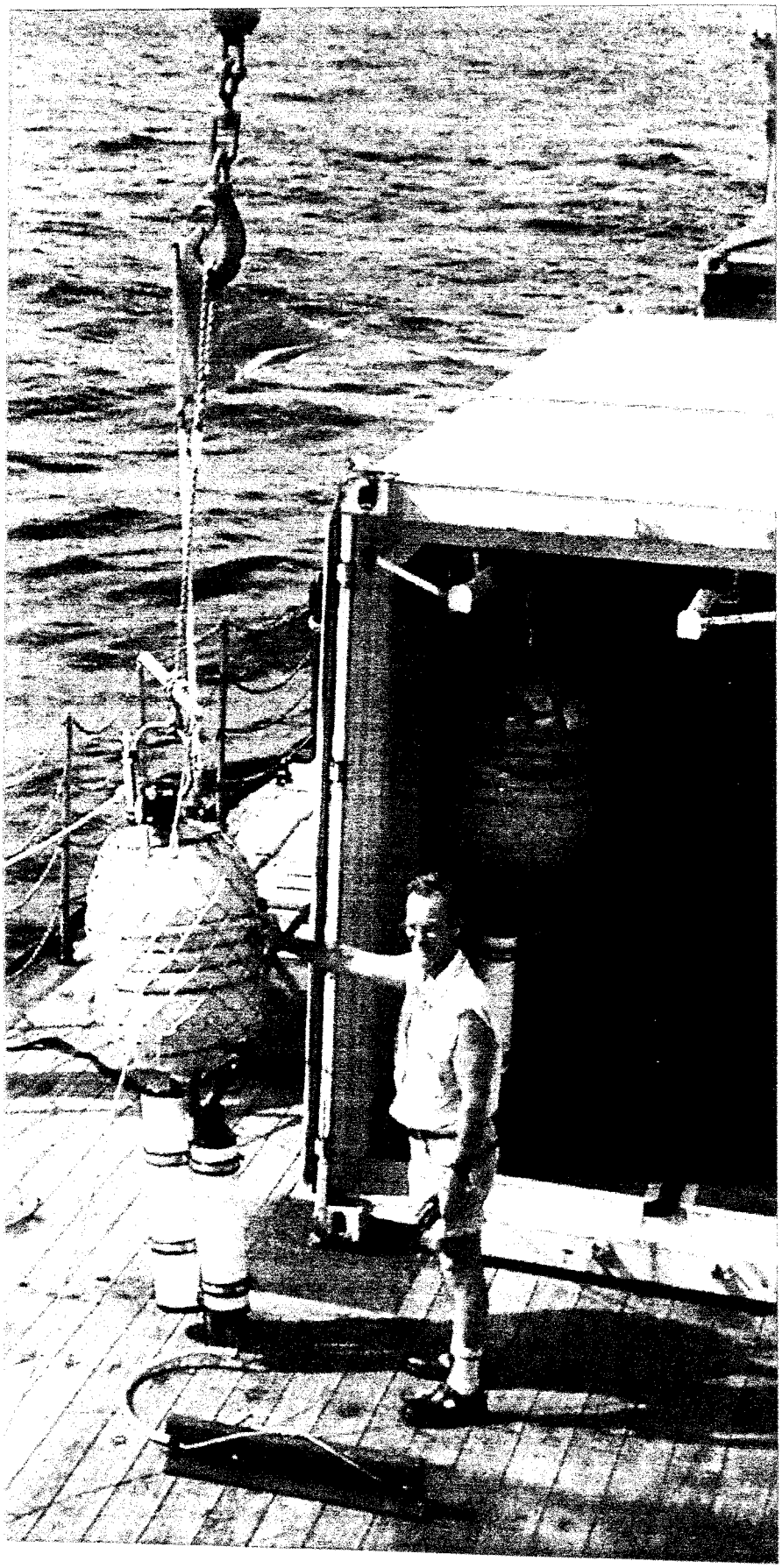

Figure 5.2.2: The GEOMAR OBH before deployment

Methusalem system or by loading a file via command or automatically after power-on. The time base is based on a DTCXO with a 0.05 ppm accuracy over temperature. Setting and synchronizing the time as well as monitoring the drift is carried out automatically by synchronization signals (DCF77 format) from a GPS-based coded time signal generator. Clock synchronization and drift are checked after recovery and compared with the original GPS units. After software preamplification the signals are low-pass filtered using a 5-pole Bessel filter with a -3 dB corner frequency of 10 kHz. Then each channel is digitised using a sigma-delta A/D converter at a resolution of 22 bits producing 32-bit signed digital data. After delta modulation and Huffman coding the samples are saved on PCMCIA storage cards together with timing information. Up to 4 storage cards may be used. Currently, up to 400 MB per card are available. Data compression allows more than 2 GB data capacity. After recording the flashcards need to be copied to a PC workstation. During this transcription the data are decompressed and data files from a maximum of four flash memory cards (up to 400 Mbyte each) are combined into one data set and formatted according to the PASSCAL data scheme used by the *Methusalem* system. This enables full compatibility with the established processing system. While the *Methusalem* system did provide 16 bit integer data, the 18 bit data resolution of the *MBS* can be fully utilized using a 32 bit data format.

Data Processing

The OBH data recorded on the *Methusalem* and the *MBS* have to be converted into standard SEG-Y format for further processing. The necessary program structure was mainly taken from the existing REFTEK routines and modified for the OBH requirements and GEOMAR´s hardware platforms. Because the GEOMAR OBH works in a continuous mode, most of the modifications on the existing program package had to be done in the program parts handling continuous data streams.

A flow chart shown in Figure 5.2.3 illustrates the processing scheme applied to the raw data. A detailed description of the main programs follows below:

- **mbs2pass**

For the PC-cards used with the MBS recorder data expansion and format conversion into PASSCAL data format is performed with DOS based PC. The program mbs2pass reads the data from the set of up to four flashcards used during recording. Decompressed data are written onto the PC´s hard disk using the PASSCAL data format, either 16 or 32 bit storage is available. This enables compatibility with the DAT recordings (s.b.). After ftp transmission to a sun workstation ref2segy and all other software can be used to handle and process the data files and store them as SEG-Y traces.

- **ref2segy**

Downloading the raw data from DAT tape on a hard disk of a SUN workstation is done by the program ref2segy. It will produce a pseudo SEG-Y trace consisting of one header and a continous data trace containing all samples. For each channel (different amplifications) one file will be created. The name of this file contains the start time, the serial number of the *Methusalem* and the channel number. In addition a log and an error file will track the download process. In a second mode PASSCAL disk files written by *mbs2pass* in either 16 or 32 bit format can be read in and included into the standard processing scheme. The file size of the data is directly related to the recording time. For example, a recording time of one hour sampled with 200 Hz will produce a file size of 1.44 MB per channel. A record with two channels and a recording time of two days will get a total data volume of 70 MB.

- **merge**

If a tape error has occurred during the download process, the ref2segy program has to be restarted. This will lead to several data files with different starting times. Merging these files into a single file is done by the merge program. The gap between the last sample and the first

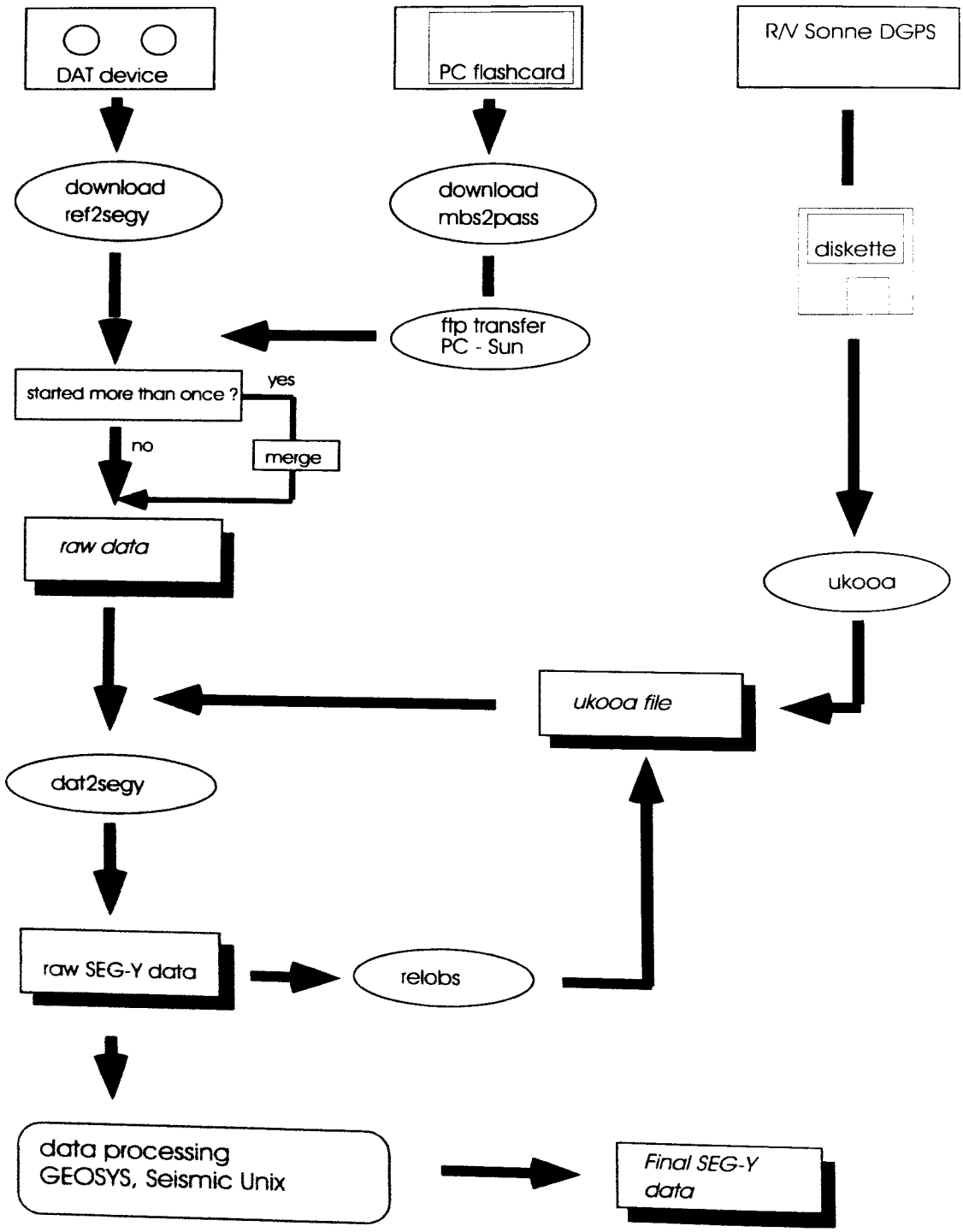

Figure 5.2.3: processing flow from raw data to SEG-Y records.

sample of the consecutive data trace will be filled up with zeros. Overlapping parts will be cut out.

• **segy2trig**

The trigger signal, which is provided by the airgun control system, is recorded simultaneously on an additional *Methusalem* during the shooting period. This tape is treated as a regular data tape and downloaded to the hard disk via the ref2segy program. The segy2trig program detects the shot times in the data stream. It determines the shot times by detecting the trigger signal through a given slope steepness, duration and threshold of the trigger pulse. The output is an ASCII table consisting of the shot number and the shot time. The accuracy of the shot time is one of the most crucial matters in seismic wide-angle work. It has to be reproduced with a precision of 5 ms. Due to this demand the shot times have to be corrected with the shift of the internal recorder clock. As additional information the trigger file contains the profile number and the start/end time of the profile and the trigger recording. The shot times are part of the UKOOA file which links the coordinates of the source and the hydrophones with the shot times.

• **ukooa**

The ukooa program is used to establish the geometric data base. It requires the trigger file containing the shot times, the ship's navigation and the position of each OBH for input. The ship's navigation is stored in a database about every two seconds (see Chapter 5.4.3). The program calculates the coordinates of each shot and creates a file in the UKOOA-P84/1 format as output. This file will be used when creating a SEG-Y section via the dat2segy program. During the cruise, the BGR system provided shot tables which already connected shot time, DGPS position and water depth. The ukooa program was therefore used to transform this table into UKOOA-P84/1 format.

• **dat2segy**

The dat2segy program produces standard SEG-Y records either in a 16 or 32 bit integer format by cutting the single SEG-Y trace (from the merged ref2segy file) into traces with a certain time length. It reads both the ukooa file with the geometry informations and the downloaded raw data as produced with the ref2segy program. In addition, the user can use several parameters for controlling the output. These parameters are information about the profile and the receiver station, number of shots to be used, trace length, time offset of the trace and reduction velocity (to determine the time of the first sample within a record (see Chapter 6.3.2)). Also the clock drift of the recorder is taken into account and corrected for. The final SEG-Y format consists of the file header followed by the traces. Each trace is built up by a trace header followed by the data samples. The output of the dat2segy program can be used as input for further processing with GEOSYS or Seismic Unix (SU).

Beside these main programs for the regular processing sometimes additional features are needed for special handling of the raw data:

• **divide**

The program divide cuts the raw data stream in traces with a given length without offset and time informations. The output is stored as SEG-Y format. The routine is useful for a quick scan at the raw data or if a timing error has occured.

• **segyhdr**

The routine segyhdr prints all the header values of the raw data on the screen.

• **segyshift**

The program segyshift modifies the time of the first sample, which means that the whole raw data trace can be shifted by a given value. This is very useful when shifting the time base from Middle European Time to Greenwich Mean Time or any local time. Because of recording problems, the data sometimes show a constant time shift, which can be corrected as well with segyshift.

- **castout**

The program castout allows you to cut out a specified time window from the raw data stream. When the shooting window is much smaller than the recording time, one can reduce the data volume by cutting out only the useful information. This will reduce the demand on diskspace.

- **relobs**

Due to a drift of the OBH during deployment and errors of the ship's GPS-navigation system the OBH positioning may have a mislocation of up to several 100 m. As this error leads to an asymmetry and wrong traveltime information in the record section it has to be corrected, which is done with the program relobs.

As input the assumed OBH location, shot locations and the picked traveltimes of the direct wave near to its apex are needed. By shifting the OBH position relobs minimizes the deviation between computed and real traveltimes using a least mean square fitting algorithm assuming a constant water velocity.

5.3 SEISMIC SOURCES

(K. P. Steffen, E. Flueh)

The seismic signals were generated by two Model CT800 *BOLT* airguns; a photo of one of the guns is shown in Figure 5.3.1. Each gun has a volume of 32 liters (2000 inch^3), and generates a signal with a main frequency centered around 6 to 8 Hz and including higher harmonics (see also 6.3.2). Both guns were towed attached to blocks on the outer side of the A-frame, with two pier winches controlling the towing. The trigger cable and airhose were deployed manually. Each gun was suspended on two floats with an additional float attached to the supply lines to prevent contact between the gun and the towing wire. A sketch of the towing configuration is shown in Figure 5.3.2. The guns were towed 50 to 70 m behind the vessel and operated at 133 bar in 7 to 8 m depth. For deployment and recovery of the airguns, an additional winch on the inside of the A-frame was used. The recent modifications on the deck (closing the slip) provided an easier launch and recovery operation compared to earlier cruises (e.g. SO103; Flueh, 1995). However, tight packing of additional instruments on both sides of the ship near the airgun array slips should be avoided in the future for easier launch and recovery of the airhoses and trigger lines.

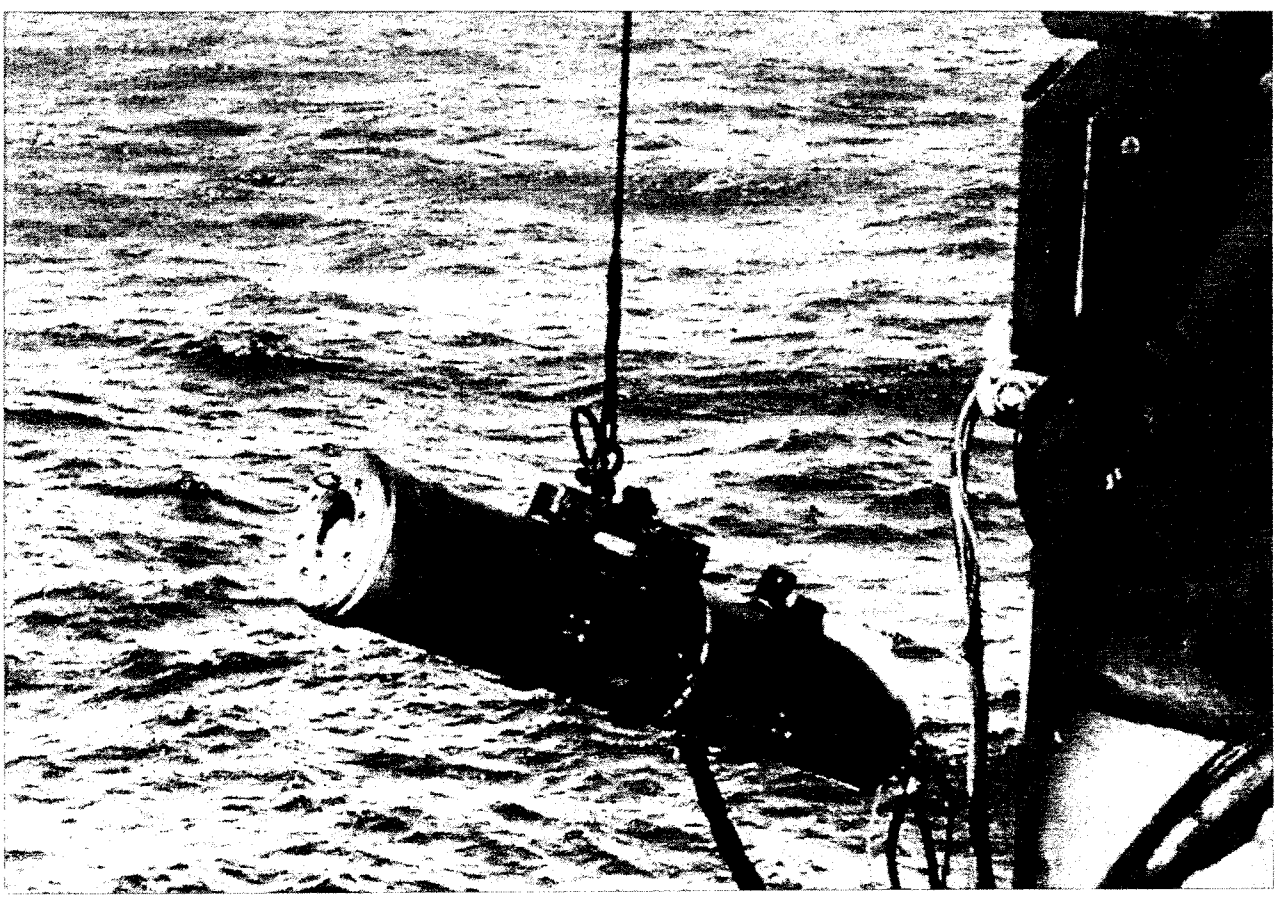

Figure 5.3.1: A CT800 BOLT airgun upon deployment.

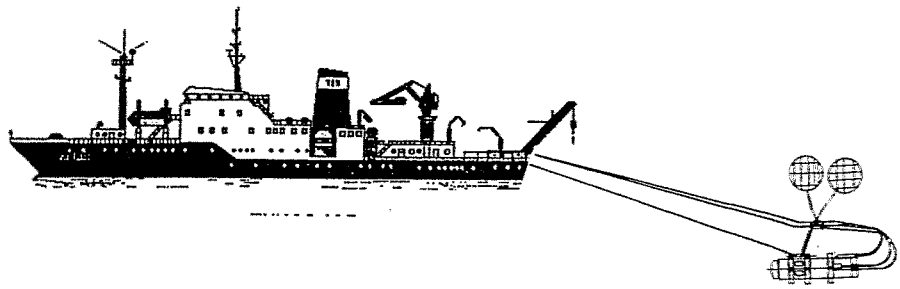

Figure 5.3.2: Sketch of the towing configuration of the CT800 *BOLT* airgun.

The trigger signal was supplied from the ships *Ashtech* GG24 GPS/Glonass receiver, and was available in the Geology Lab and the Seismic Lab. The receiver can provide a one millisecond long 5 V-TTL pulse at intervals between 0.2 and 999 s. The impulse should be stable to within the accuracy of the GPS Time, which is 70 nanoseconds. The impulse was delivered to the Par Airgun Firing Circuit FC300 of *BOLT*, which can handle up to three guns in parallel. The trigger signal as a 5 Volt TTl signal and was recorded on a MBS recorder to double check the shotbreaks, using the same time basis as for the OBH (see chapter 5.2).

During cruise SO142 HULA II, the guns were used along four seismic profiles, with the first profile utilizing only the starboard gun. The total operation time was close to 1000 hours, with about 5600 shots being fired, always at a 60 s shot interval. This was well within the capability of the ship's compressor system, which worked smoothly and caused no delays or interruptions. Despite rough weather conditions and considerable swell during some profiles, the airguns worked without any major problems. Only once did one of the guns need to be taken inside for repair of a broken airhose.

5.4 THE MAGNETOMETER

(C. Kopp)

During cruise SO142 we used a GeoMetrics G801/3 Marine Proton Magnetometer. This unit is comprised a gasoline-filled sensor with a 350 m marine cable and a control unit. Fig. 5.4.1 shows the magnetometer during deployment. On board RV SONNE , the winch was placed on the port-side back deck and the sensor was towed to the port side of the vessel. A boom leads the cable about 7 m to the side of the ship in order to prevent it from being tangled with the ship. The system worked well throughout the cruise, although the sensor was heavily attacked by fish (Fig. 5.4.2).

The measured values of the total intensity magnetic field were displayed on a console and written as digital output coded in BCD values. The system was set to deliver one data value every 3 seconds via a SCSI interface to a PC, where a special software was used to store the data together with UTC-time in ASCII tables.

After data backup the files were transfered to a SUN workstation. GPS-coordinates and time were taken from the ship's navigation system and assigned to each magnetic stamp on the basis of the recorded time. The magnetic and the navigation data were resampled to 10 s interval. After optional median filtering they were displayed using GMT plot routines (Wessel and Smith, 1995).

In total, 4100 km of magnetic data were recorded on SO142. Generally, the data quality on each of the 27 continuous lines was excellent with a noise level of about 5 nT, a higher noise level could only be observed on two profiles. Due to a significantly higher frequency content of the noise, it could be removed by amplitude clipping and filtering.

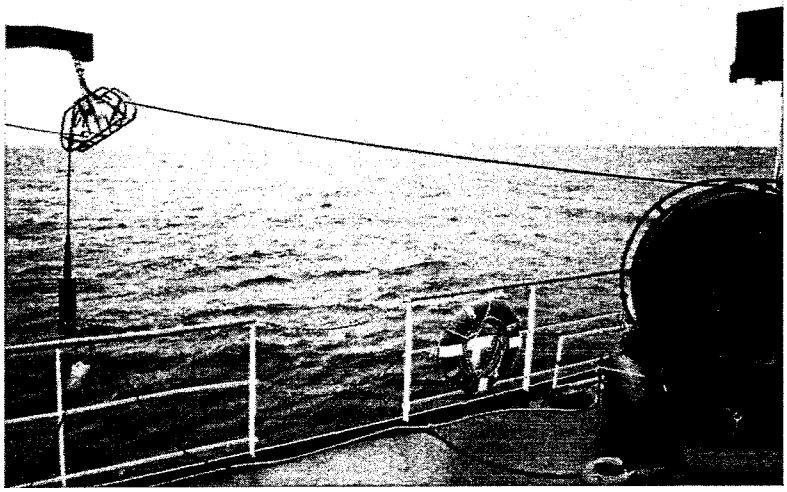

Figure 5.4.1: The GeoMetrics Proton Magnetometer onboard FS SONNE

Figure 5.4.2: The magnetic sensor after shark attack

5.5 DREDGES

(J. O'Connor)

The following selection of different chain bag and tube dredges were available for rock sampling during the SO 142 cruise.

Type	Name	Width (cm)	Length	Weight (kg)
Burkhardt	Oval	100	300	500
Hydrowerkstätten	Bella Maria	110	300	600
Preusag small	Tube	50	100	400
Preussag large	White Shark	135	390	900

The 'Oval' dredge (5.5.1) has very large 'teeth' attached to its outer rim. Due to the difficulty of dredging old MnOx encrusted seamounts/ridges, such as those encountered along the Musician Chain, it was used predominantly throughout the SO142 cruise. However, a new dredge 'Bella Maria', which does not have attached teeth, was used successfully to dredge the Murray Fracture Zone. The skill of the captain and crew of the F.S. SONNE contributed very significantly to the success of the SO142 dredge stations. This is clearly demonstrated by the fact that in addition to recovering rock sample at each station, no dredges were lost, nor was the safety cable attaching the dredge to the main winch broken on a single occasion.

During cruise SO142-HULA II a total of 13 successfull hauls were made at waterdepths between 6000 and 3000m, each one lasting between 6 to 10 hours.

5.6. THE SOC RMT 8+1 WITH CLOSING COD-END

(P.J. Herring)

The fishing gear developed and provided by Dr. Peter Herring and operated by Ben Boorman (SOC, Southampton) provide an optimal method for obtaining midwater animals in better physiological condition than can be achieved with standard trawls. For visual studies animals need to be maintained in dark conditions from the moment of capture, and for *any* physiological work the animals need to be retrieved as nearly undamaged as possible and protected from the thermal shock of transfer through the thermocline.

A thermally insulated closing cod-end on a midwater trawl of $8m^2$ mouth area achieves both these objectives. This sampling gear has been used at a variety of depths, as and when convenient within the broader programme of the cruise. Tows have been of between 3 and 5 h total duration, depending on the densities of animals encountered and the sampling depths required. The cod-end is fitted with a timing device which closes the cod-end at a pre-determined time (routinely: 3h), sealing the catch within a volume of water from the same depth. On recovery the samples are examined initially in a dark room under dim red light and particular specimens selected for further study.

Figure 5.6.1 shows the closing cod end during deployment, followed by the SOC RMT 8+1 (Fig. 5.6.2).

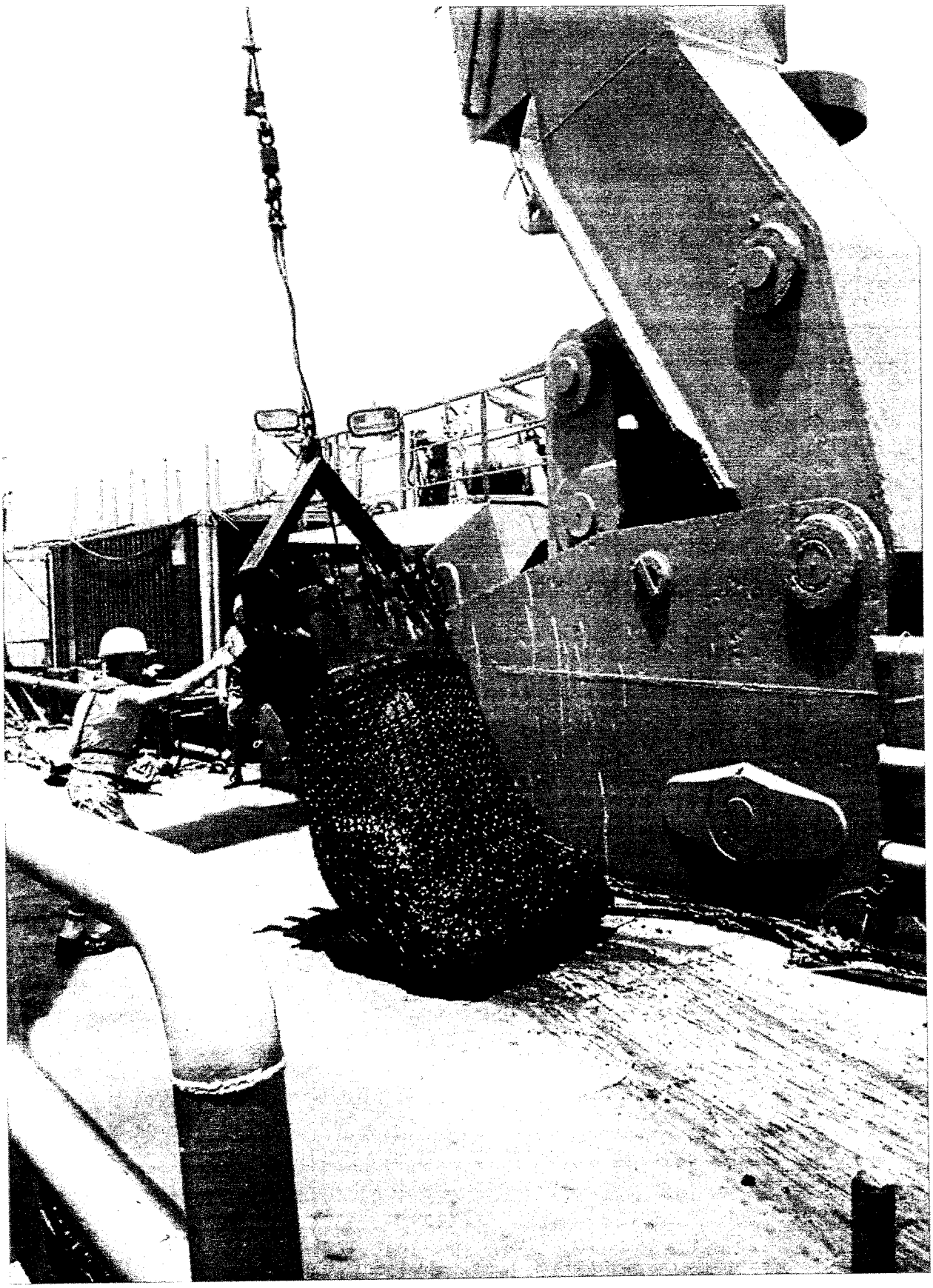

Figure 5.5.1: Oval dredge used during most SO142 dredge stations.

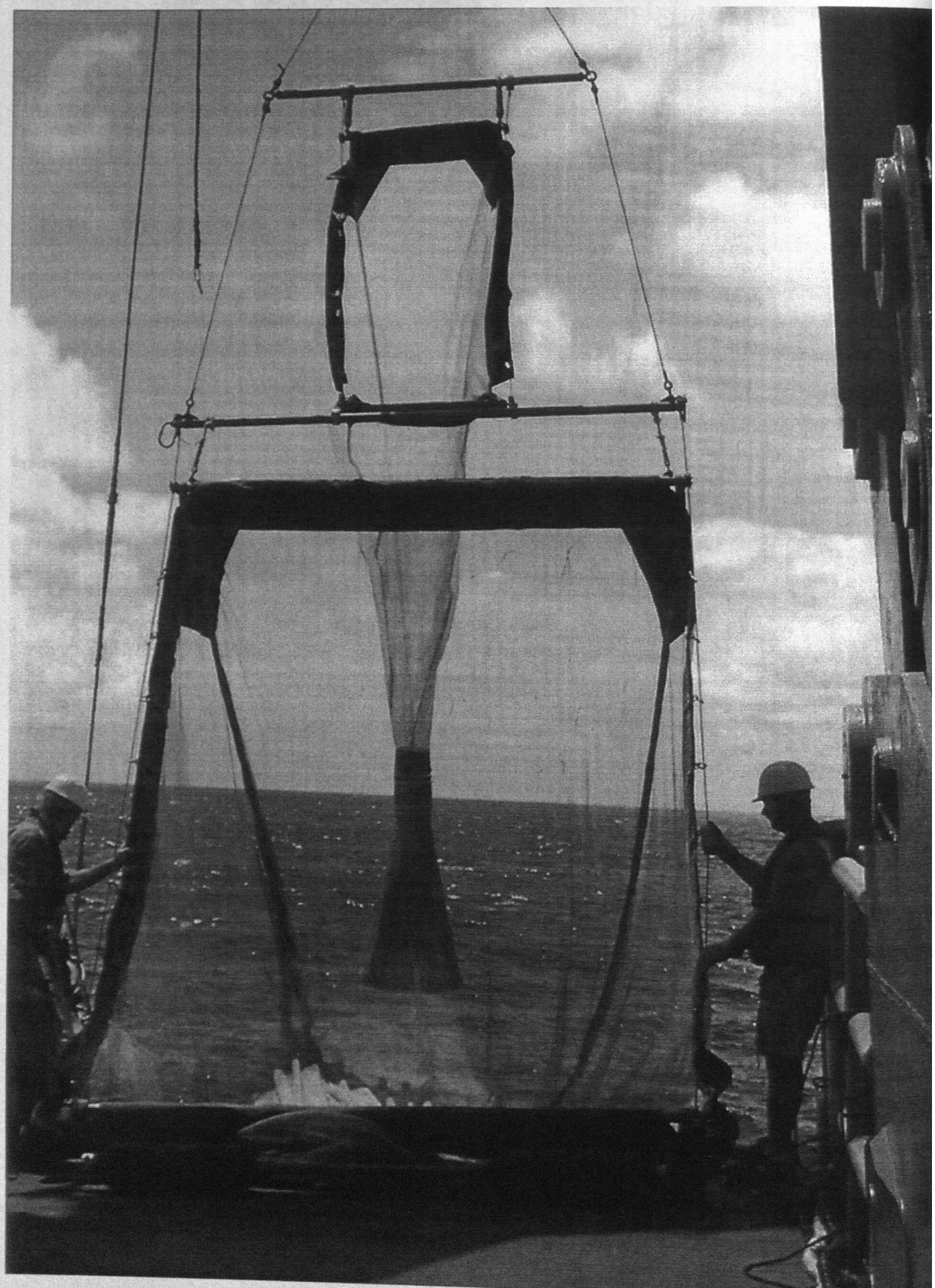

Figure 5.6.1: The Soc RMT2+1 upon deployment. The RMT1 (top) terminates into a conventional cod end. Its finer mesh is mostly designed to catch plankton. The weigt-bar of the RMT8 is still on deck and about to be lowered.

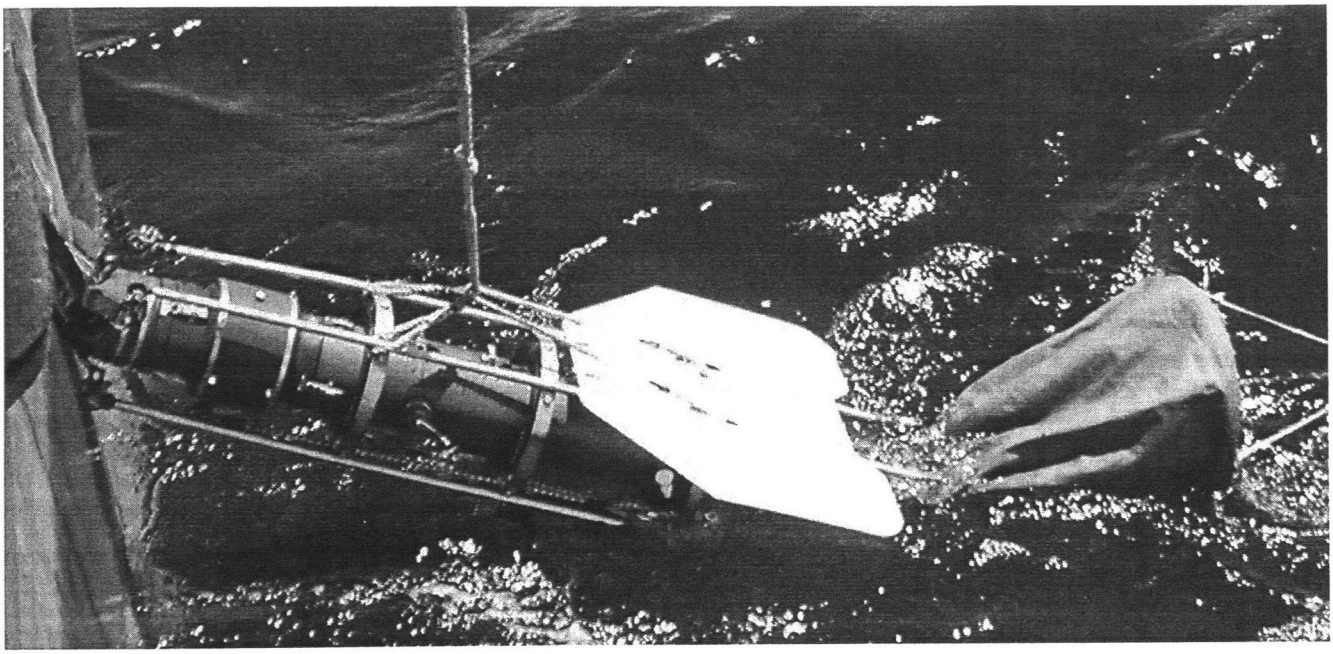

Figure 5.6.2: The closing cod - end recives the catch taken by the RMT8. It contains a thermally isolated container, the entance of which can be closed prior to heaving the net inorder to relieve the catch from the ensuing decrease in pressure. The closing cod-end is an essential prerequisite for preserving midwater fish in excellent conditions so that their visual physiology may be studied.

5.7. THE BIOLOGY LABS

(J. Wagner)

After the arrival of the catch, the material was transferred to the **Fotolabor (552)** which was used as a dark room. Under the light of red torches a first inspection of the specimens was carried out and those chosen for the analysis of visual pigments were removed. These particular specimens were stored in light tight containers and further analysed in the Fotolabor. The rest of the catch was then brought into the light and transferred to the **wet chemistry lab (560)** which was used as the main biology lab during cruise SO142. Two work places equipped with stereo microscopes and special lighting were set up for identification and dissection of the specimens. Labelling experiments with fluorescent dextranes, lipophilic DiI for the tracing of olfactory and optic neurons, as well as application of Lucifer Yellow for the visualisation of individual nerve cells and potentially newly formed outer segments were also performed here. Furthermore, a special aquarium was installed in the wet chemistry lab which allowed the photographic documentation of the specimens under optimal conditions. Furthermore, the on-board Zeiss Axioplan was set up in the **dry chemistry lab (562)** for the measurements of isolated rod outer segments.

In the **geology-lab (440)**, a deep-freeze chest (-80°C) was installed which was used for the storage of the preserved samples of visual pigments and fixed and labelled histological materials. We also used the ship's **cold room** to cool down large volumes of seawater into which the catch was transferred immediately after retrieval from the closing cod-end.

5.8 SHIPBOARD EQUIPMENT

5.8.1 HYDROSWEEP

(W. Weinrebe)

For continuous bathymetric profiling, the HYDROSWEEP multibeam system from STN ATLAS-ELEKTRONIK is available onboard RV SONNE. Using a frequency of 15.5 kHz and 59 beams in a swath of 90°, it can map the seafloor with a scanline width of up to twice the water depth. Range of the central beam is up to 10,000 m with an error of 1% and for the outer beams it is up to 7,000 m with a precision of about 1% if the roll is less than 10° and the pitch is less than 5°. Corrections for roll, pitch, and heave are automatically applied. Due to the fixed angle between beams, resolution is dependent upon the water depth and varies from about 170 m to 200 m in depths of 5,000 m to 6,000 m.

To calculate depths from echo time delays the velocity of sound in the different waterlayers is required. HYDROSWEEP uses a second set of transducers and a calibration scheme with soundings along track to determine an average water sound velocity profile (Schreiber und Schencke, 1990). However in certain areas this algorithm fails (c.f. Flueh and von Huene, 1994), so for better results, direct measurement of sound velocity at different depths using a CTD is required.

Postprocessing of HYDROSWEEP data is comprised of the merging of navigational data, the calculation of depth and positions of the footprints of the beams, removing artifacts and erroneous datapoints, and generation of a digital terrain model (DTM). The ATLAS HYDROMAP software, based on the CARIS software package, is available onboard for that purpose. However, for several reasons outlined in Flueh and von Huene (1994) and Weinrebe (1997), the academic software MB-System (Caress and Chayes, 1996) from Lamont-Doherty Earth Observatory is used for HYDROSWEEP data processing.

5.8.2 PARASOUND

(W. Weinrebe)

For the geological mapping of the uppermost sedimentary layer the parametric echosounder PARASOUND from ATLAS ELEKTRONIK is available onboard R/V SONNE. This system uses a parametric signal generated by the superposition of two slightly-offset, high frequencies to gain deeper penetration and higher resolution than that of ordinary echosounders. One signal is generated with a fixed frequency of 18 kHz, the other can be set to values between 20.5 kHz and 23.5 kHz (at 0.5 kHz increments), thus yielding a parametric signal of 2.5 kHz to 5.5 kHz with a (narrow) beam angle of about 4°. The footprint of a beam ensonifies an area of approximately 7% of the water depth. Due to the narrow beam, no echoes from the ocean floor or from sedimentary layers will reach the receiver if the seafloor is inclined more than 2°, thus restricting the application of PARASOUND to relatively flat areas.

5.8.3 NAVIGATION

(C. Kopp)

A crucial prerequisite for all kinds of marine surveys is the precise knowledge of position information (latitude, longitude, altitude above/below a reference level). Since 1993 the global positioning system (GPS) is commercially available and widely used for marine surveys. It operates 24 satellites in synchronous orbits, thus at least 3 satellites are visible anywhere at any moment (Seeber, 1996). The full precision of this originally military service yields positioning accuracies of a few meters, yet this is restricted to military forces and usually unaccesible to commercial users (Blondel and Murton, 1997). For civilian purposes the precision is in the order of 100 meters.

The resolution of GPS can be enhanced with the Differential GPS (D-GPS) scheme (Blondel and Murton, 1997, Knickmeyer, 1996). Using several reference stations the determination of the ship's position can be corrected in real time and enhanced to a 1 m to 5 m accuracy. Since the cruise SO-109 (1996) D-GPS service is available onboard R/V SONNE. The ships ASHTEC system provides a validated accuracy of approximately 5 m in the area of the HULA investigations.

5.8.4 The GTVG (Großer TV-Greifer; Large TV Grab)

(J. O'Connor)

The concept of the TV-Grab system (5.8.4.1) is based on the simultaneous transmission of video- and data signals in order to make possible visual observation of the seabottom and allow the operator to select suitable samples, e.g., *in situ* rock. The TV-Grab is equipped with a fibre-optic system that allows the use of up to four video-transmission lines. At this time, only one color and one black and white camera are used. Data transfer for controlling the grab and the tv-cameras is routed through two data transmission-channels leading to the subsurface unit and another two leading to the surface unit. All data channels work with a maximum speed of 200 kbit/s. The four video connections work with a bandwidth of 10 MHz, which makes very high quality transmisson possible. The surface unit allows monitoring and controlling of all neccesary functions of the subsurface unit. The size of the TV-Grab is 3m x 2.0m x 2.65m . The weight is appr. 3.2t. The TV-Grab is capable of holding 0.6m^3 , with a weight of up to 3.0 t. Power is provided by a 3 kW , 24 Volt DC-motor. The max. operational water depth is 6000m, with a maximum sediment penetration of 0.7m.

The TV grab was used three times during the cruise. On the first site the data channel collapsed imedeately before a grab attempt was planned. The second and third stations worked well.

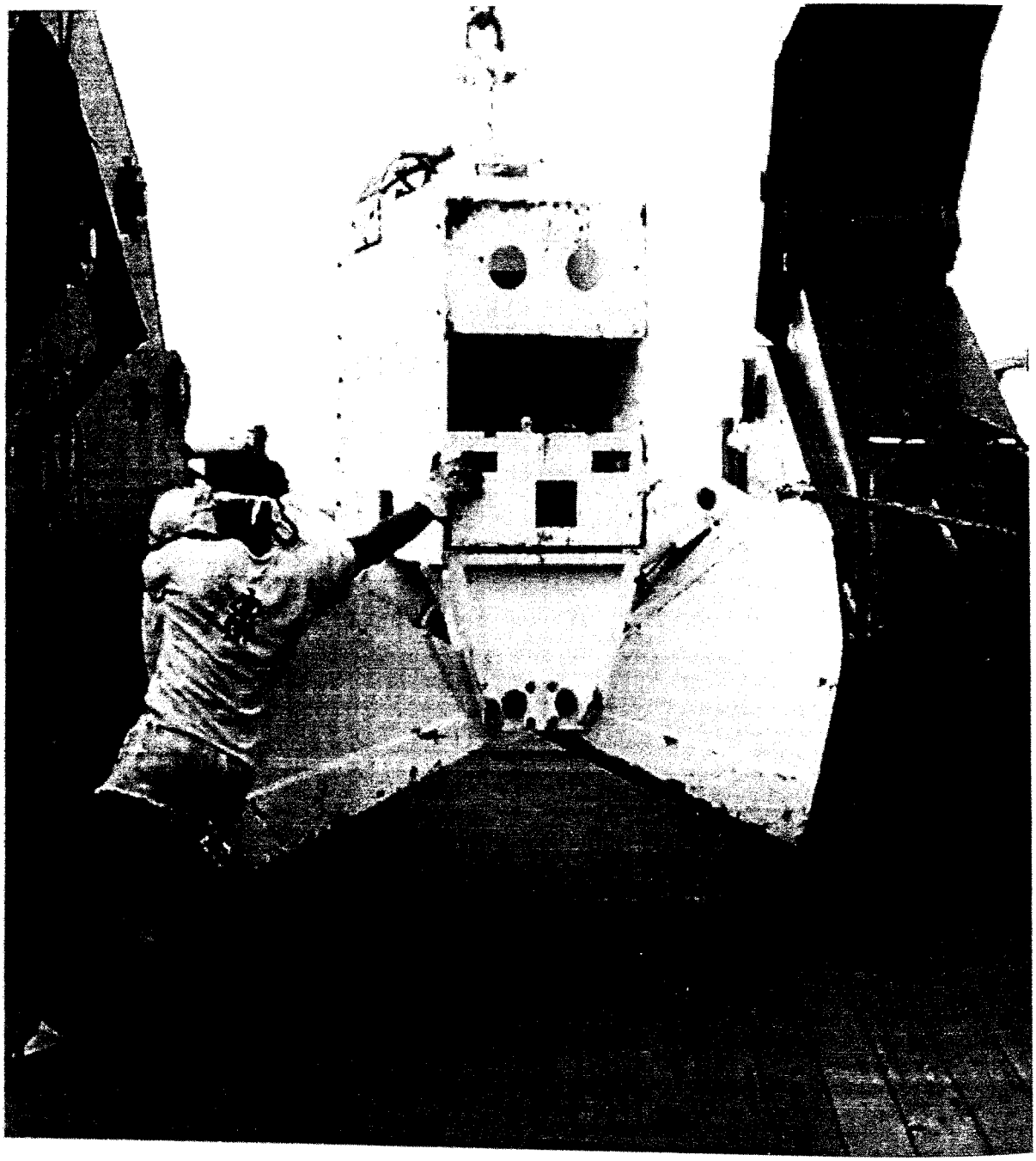

Figure 5.8.4.1: TV-Grab used to view and sample the young volcanic field near to the Hawaiian Islands.

6. WORK COMPLETED AND FIRST RESULTS

6.1 HYDROSWEEP

(W. Weinrebe, C. Larsen and watchstanders)

Data from the HYDROSWEEP system were continuously recorded during the cruise, beginning with Midway Atoll and ending in the Hawaiian waters. In total, for 570 hours, 96871 swaths (nearly 6 millions beams) were recorded. Due to stable weather conditions, data quality was usually good.

The HYDROSWEEP data were processed onboard using the MB-System software developed at Lamont-Doherty Earth Observatory (Caress and Chayes, 1996). Using a velocity function measured with a CTD, raw HYDROSWEEP echo-time data were converted to depth by complete ray tracing through the different water layers. Sweeps including all 59 beams were then displayed in profile on a screen and edited to eliminate erratic points. Edited sweeps were assembled, gridded, and contoured with the GMT software (Wessel and Smith, 1991). No filters were applied to smooth the edited data; thus, more small tectonic features, but also more noise, are visible in the maps. However, the viewer can usually distinguish between small tectonic features and map artifacts.

6.1.1 SOUND VELOCITY MEASUREMENT WITH A CTD

A water sound velocity profile was measured with a CTD "Seabird SBE9" on June 3, 1999, 04:30 UTC at 166°30.98' W, 31°14.35'N. Temperature, salinity, sound velocity, and oxygen content were continuously recorded during descent and ascent of the instrument; the recorded data is shown in Fig. 6.1.1.1. In general, results coincided with a CTD that was measured farther west during cruise SO141, so the CTD was not deployed to the full water depth of 5625 m, but to only 5000 m.

The water sound velocity profile, which is required for processing of the HYDROSWEEP data, shows high surface values of 1523 m/s, decreasing to a minimum value of 1480 m/s in 850 m to 900 m depth, and then continuously rising to 1540 m/s in 5000 m depth with a constant gradient below 3000 m. For processing of HYDROSWEEP data, the sound velocity profile in this area was extrapolated using this gradient down to the full ocean depth, reaching a velocity of 1554 m/s at 5700 m waterdepth.

6.1.2 NORTHERN MUSICIANS

The Musician Seamount province is comprised of a northwest-southeast trending chain of distinct seamounts, another generally north-south trending line of seamounts, and several east-west trending elongated ridges (Fig. 4.1). One of the elongated ridges in the northern part and one in the south were mapped in detail during cruise SO142. Fig. 6.1.2.1 gives an overview of the surveyed region in the north.

In the north, the "Italian Ridge" (so named because most of its single seamounts are already named after Italian composers) was mapped for over 400 km with dedicated profiles and additional HYDROSWEEP data recorded during seismic work and fish trawls. Table 9.3 in the appendix gives a summary of all dedicated HYDROSWEEP profiles. Nearly complete coverage of this ridge was achieved (Fig. 6.1.2.2). The general structure of the ridge is best seen in the contour map (Fig. 6.1.2.2) and in the perspective image (Fig. 6.1.2.3). The narrow (not more than 20 km wide) ridge rests on flat, approximately 5500 m to 5700 m deep ocean floor. The ridge is built of different en echelon segments, each around 100 km to 150 km in length, with

small lateral shifts or small changes in strike direction between them. A minimum depth of 2100 m was found in the ridge area, which means that the highest peaks are rising more than 3500 m above surrounding ocean floor. Numerous rounded, flat, pancake-like structures are found at the base and in the vicinity of the ridge. These features have a diameter of 5 km to 10 km and a height of 500 m to 1000 m. Several have a central crater. Figures 6.1.2.4 to 6.1.2.9 show different parts of the ridge in detail; refer to fig. 6.1.2.1 for the location of these maps. Though the general structure is quite uniform along the ridge and there is only 300 km between the eastern and western parts, morphological differences between the two sections are quite evident. In the west, in the Rossini (Fig. 6.1.2.4) and Bizet (Figs. 6.1.2.5 and 6.1.2.6) areas, the ridge is characterized by large cylindrical blocks with steep walls and flat tops, sometimes with very small secondary cones. The eastern part around Donizetti seamount (Figs. 6.1.2.7, 6.1.2.8, and 6.1.2.9) is dominated by generally steep and high cones. Though the dataset is very limited, a difference in age or origin between western and eastern parts is suggested by this morphological difference.

6.1.3 SOUTHERN MUSICIANS

A 300 km long segment of the Bach Ridge in the southern Musicians Seamount area was mapped with HYDROSWEEP (Fig. 6.1.3.1). To show more detail, the western and the eastern parts of the area are presented in different maps; refer to Fig. 6.1.3.1 for the locations. Although the gross structure of the Bach Ridge resembles that of the Italian Ridge, differences are evident. Minimum water depth in the southern Musicians area reaches 2000 m, whereas the surrounding ocean floor is around 5200 m to 5300 m deep, so the summits rise about 3300 m with respect to their surroundings. This is slightly less than in the northern Musicians.

The Bach Ridge does not show basic morphological differences between the western (Figs. 6.1.3.2 and 6.1.3.3) and the eastern (Figs. 6.1.3.4 and 6.1.3.5) parts. However, differences between "normal" ridge segments and parts with a dominating seamount are evident. Particularly in the perspective images (Figs. 6.1.3.3 and 6.1.3.5), the interruption of the uniform elongated structure by massive blocks with steep slopes is obvious. This is demonstrated with a sequence of depth profiles across the ridge (Fig. 6.1.3.6). Whereas the profiles 4, 5, 7, and 10 cross a "normal" ridge structure, the profiles 1, 2, 3, 6, 8, and 9 show depth sections across distinct seamounts or blocks on the ridge. The "normal" profiles have their summits below 3500 m depth, whereas the other sections rise to depths between 3500 m and 2600 m. The slopes of these sections are much steeper. Two of the larger cones (profiles 2, 6) are characterized by flat tops, while others have small craters on top (profiles 3, 8).

Pancake-like, rounded structures, which were also found in the northern Musicians, are abundant in the southern Musicians, particularly in the western part of Bach Ridge (Fig. 6.1.3.3). Most of them are found at the southern base of the ridge.

The preliminary results of the HYDROSWEEP survey during cruise SO142 show a morphology of the same type, yet of different style, for the two ridges: Italian Ridge in the north and Bach Ridge in the south.

SO142 CTD - 01

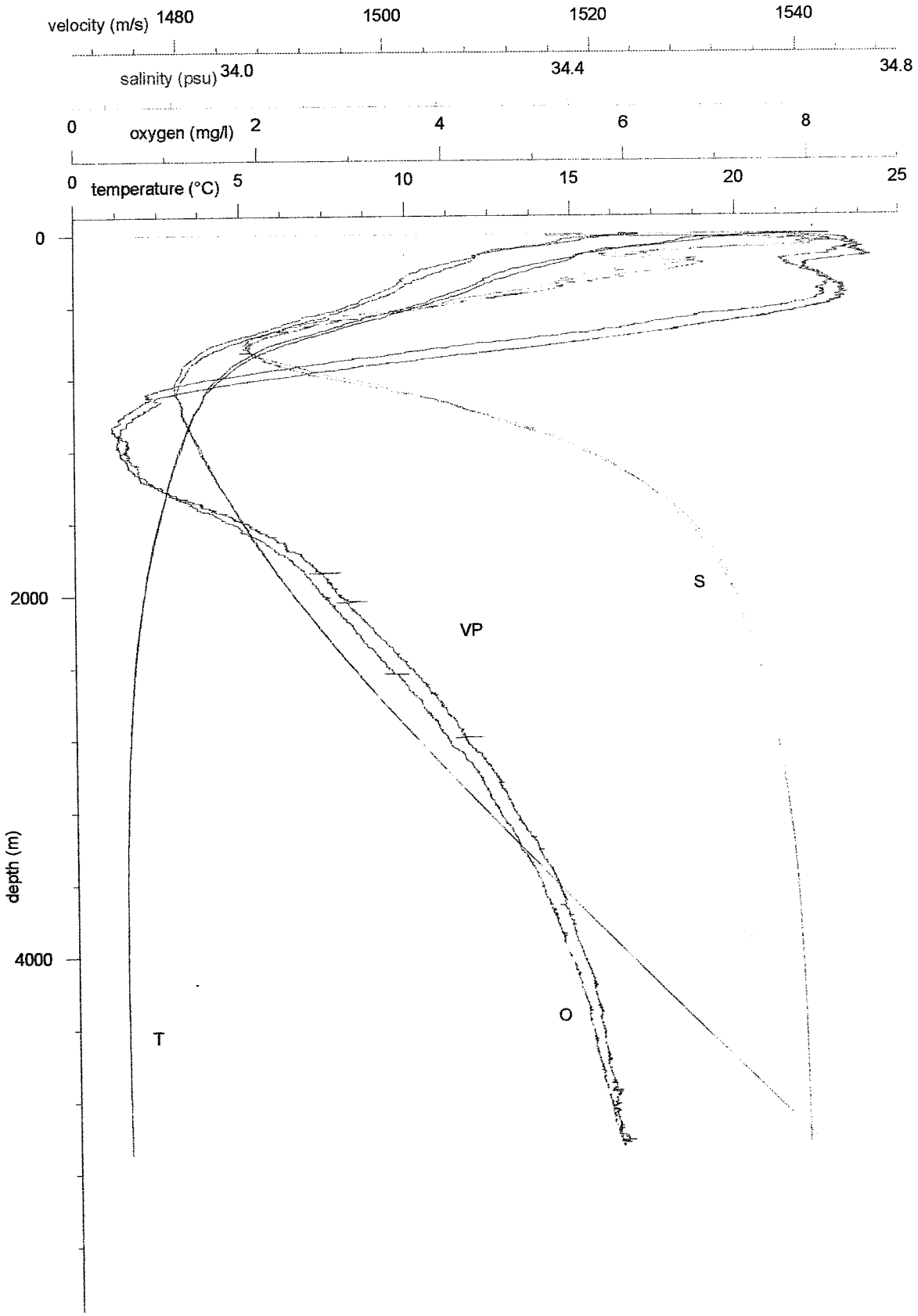

Figure 6.1.1.1: Data recorded from the CTD.
T: temperature, O: oxygen, VP: sound velocity, S: salinity.

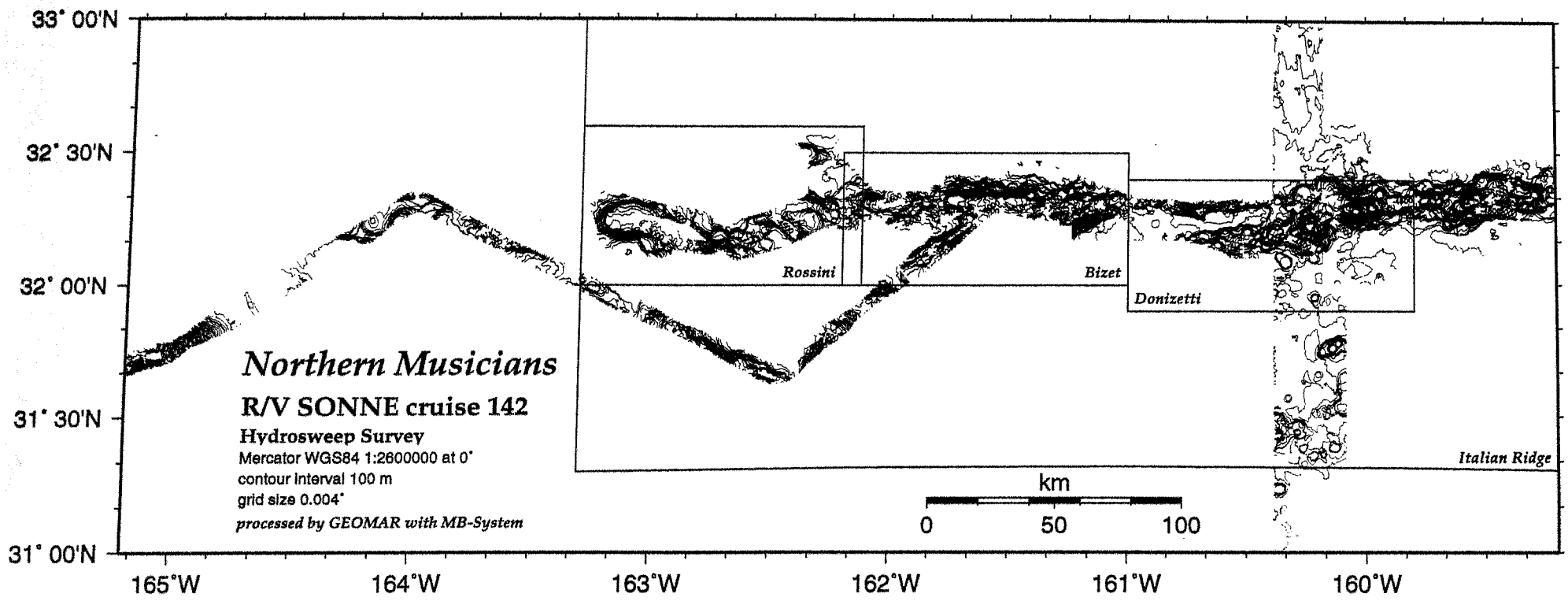

Figure 6.1.2.1: Areas mapped with HYDROSWEEP in the northern Musicians with locations and names of detailed maps.

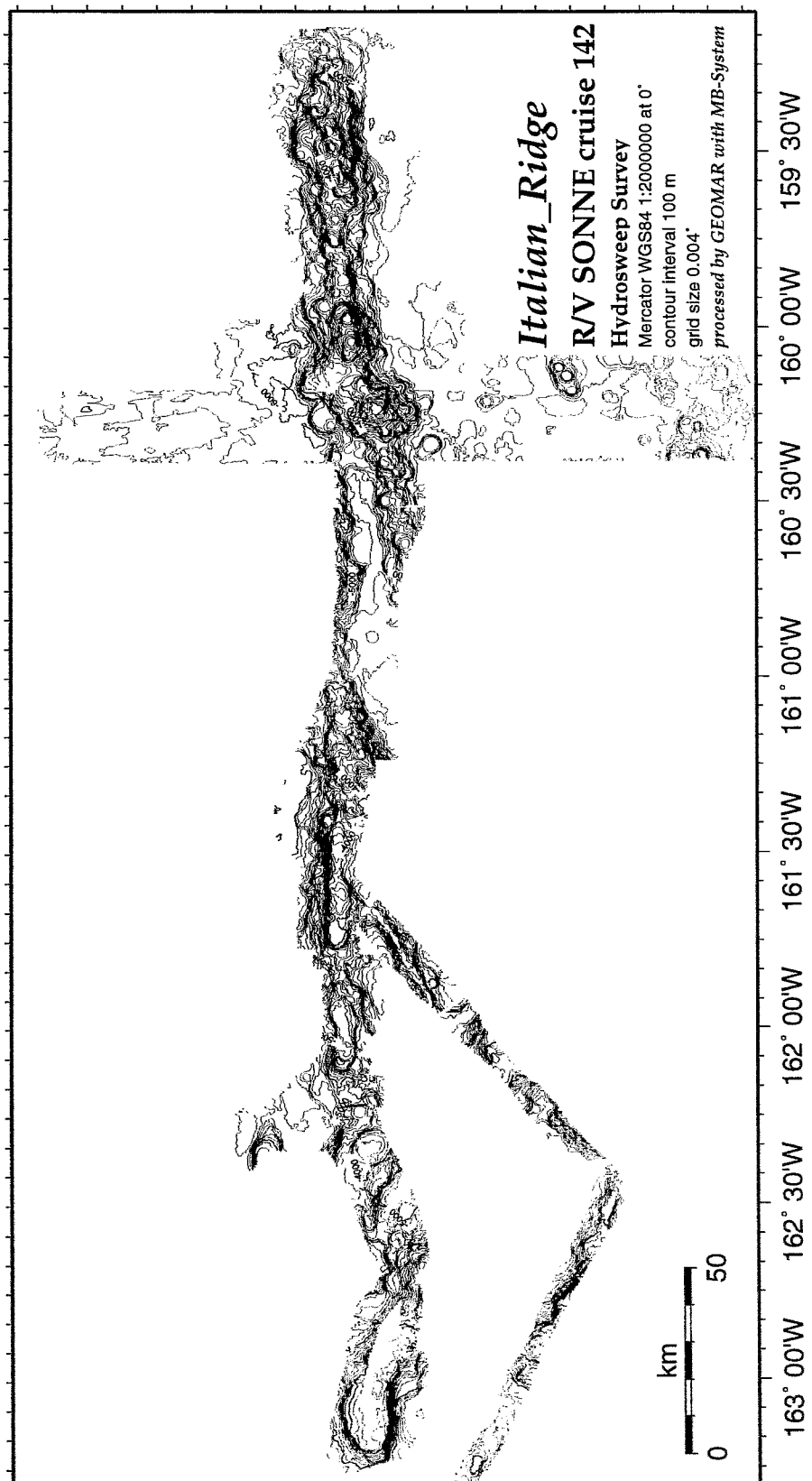

Figure 6.1.2.2: Bathymetric map of Italian_Ridge.

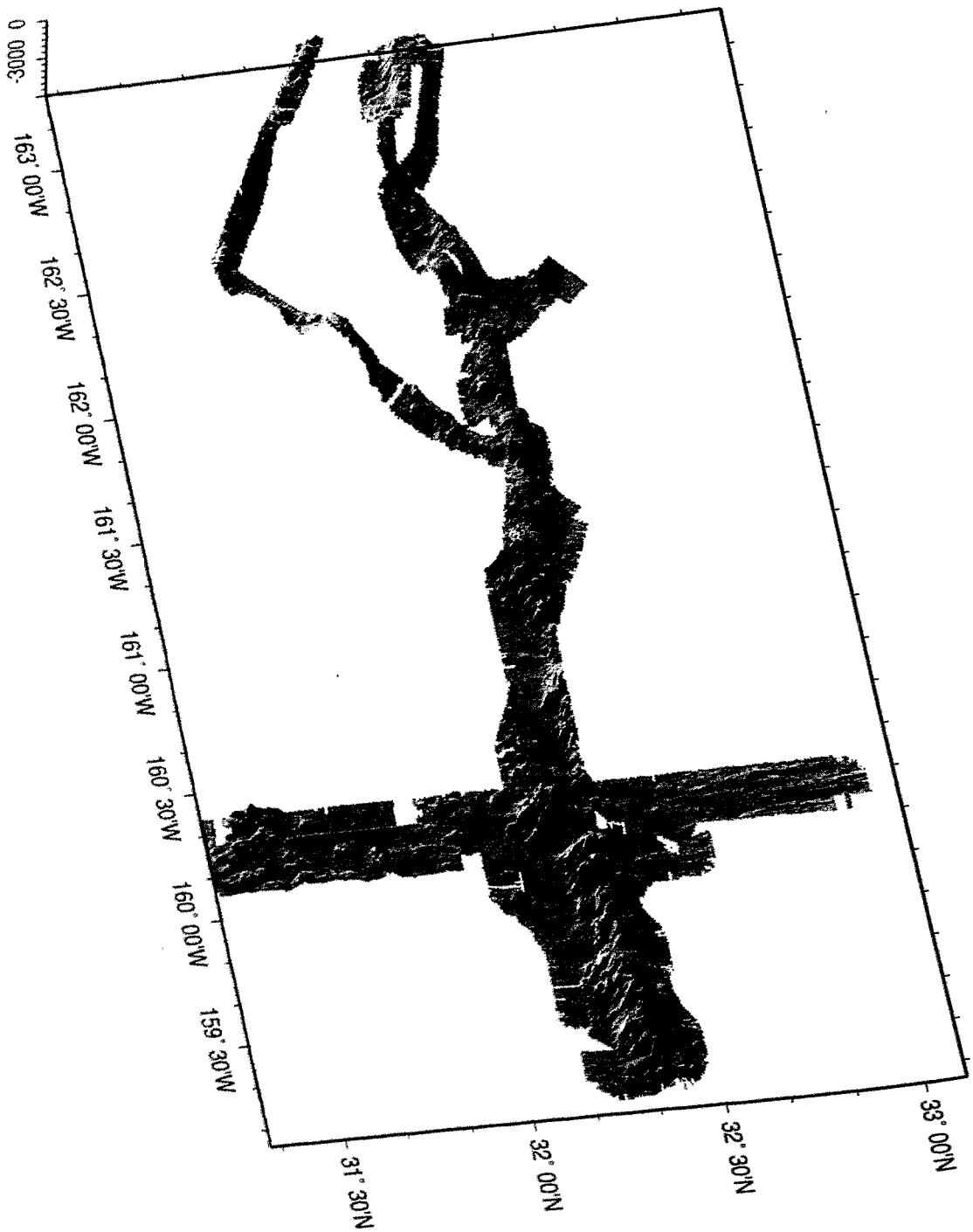

Figure 6.1.2.3: Perspective image of Italian_Ridge. View from east, illumination from we

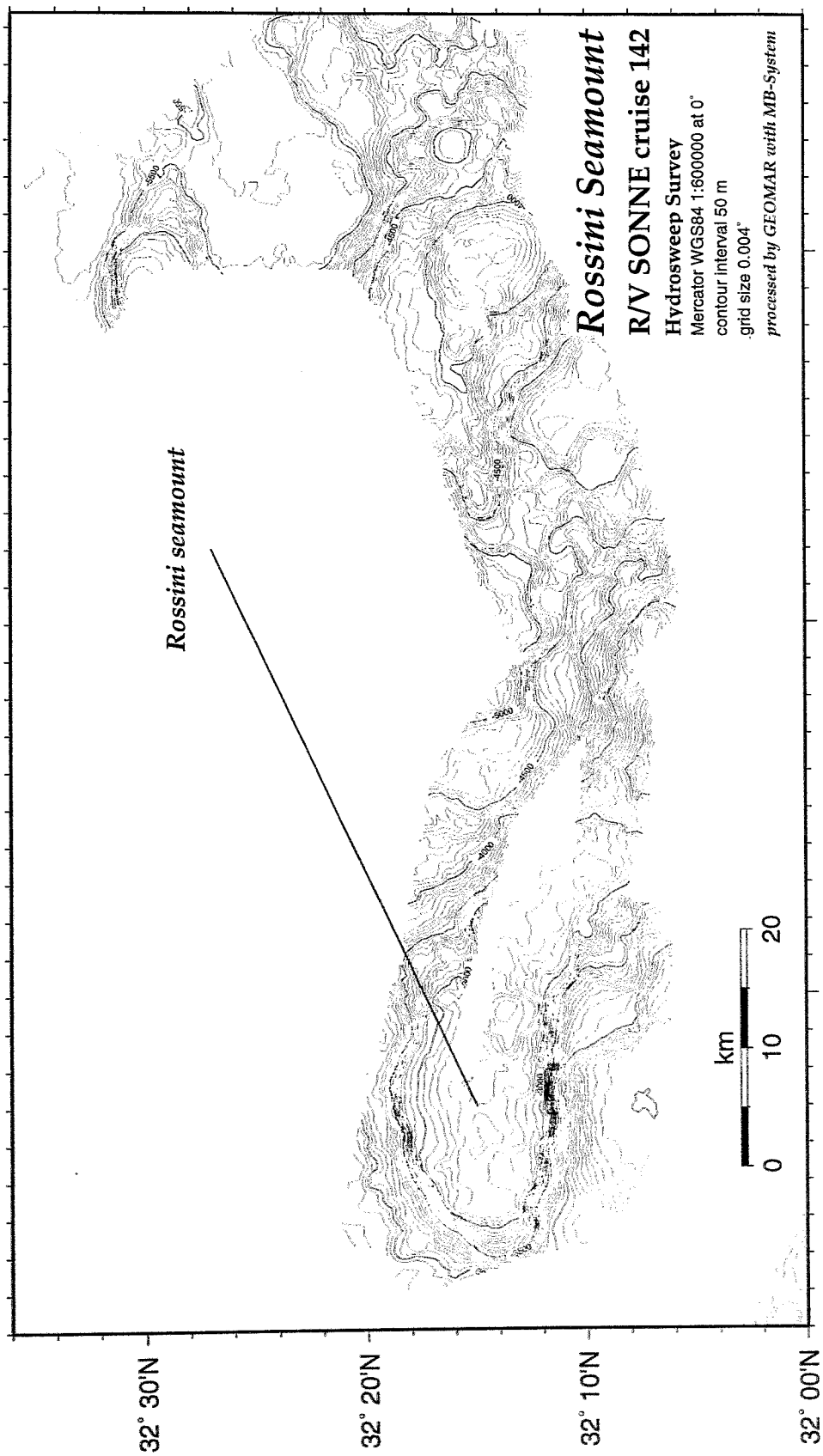

Figure 6.1.2.4: Bathymetric map of Rossini seamount.

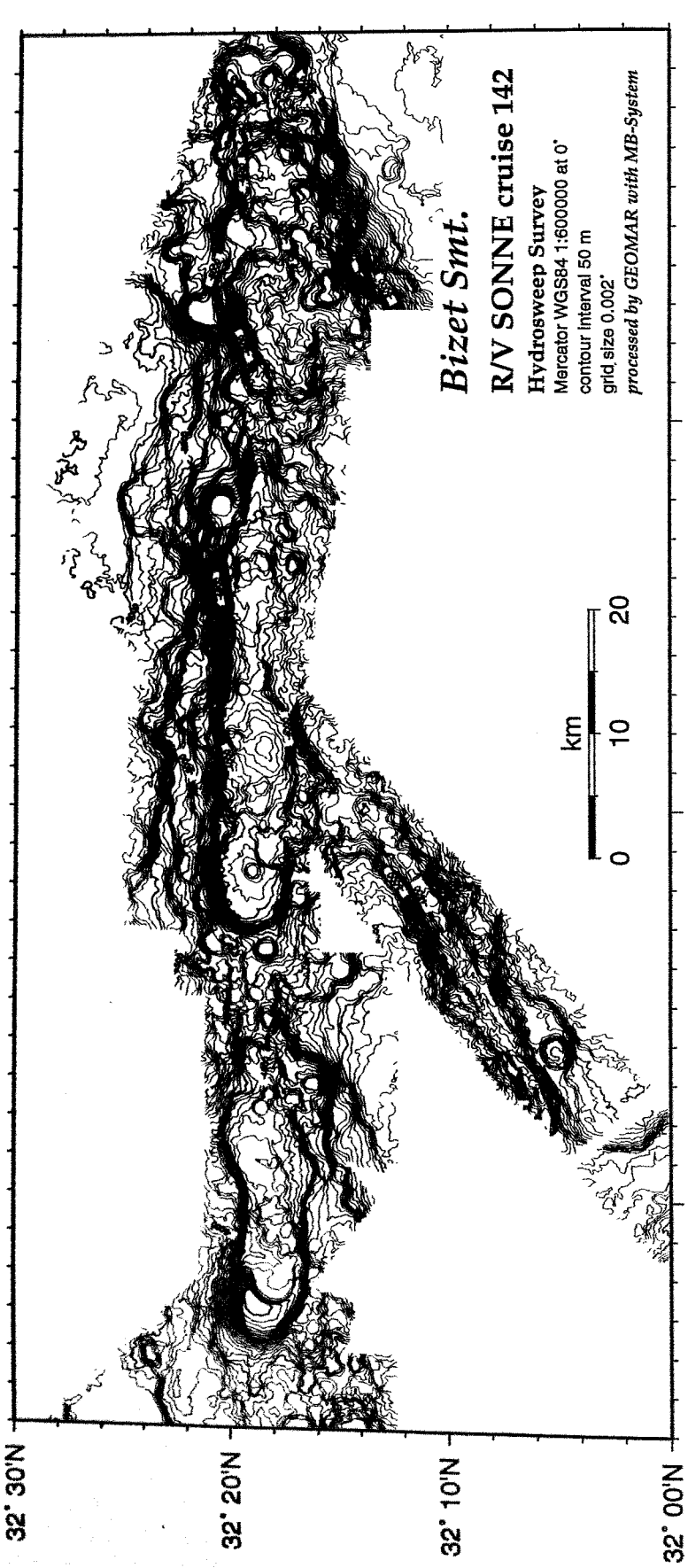

Figure 6.1.2.5: Bathymetric map of Bizet seamount.

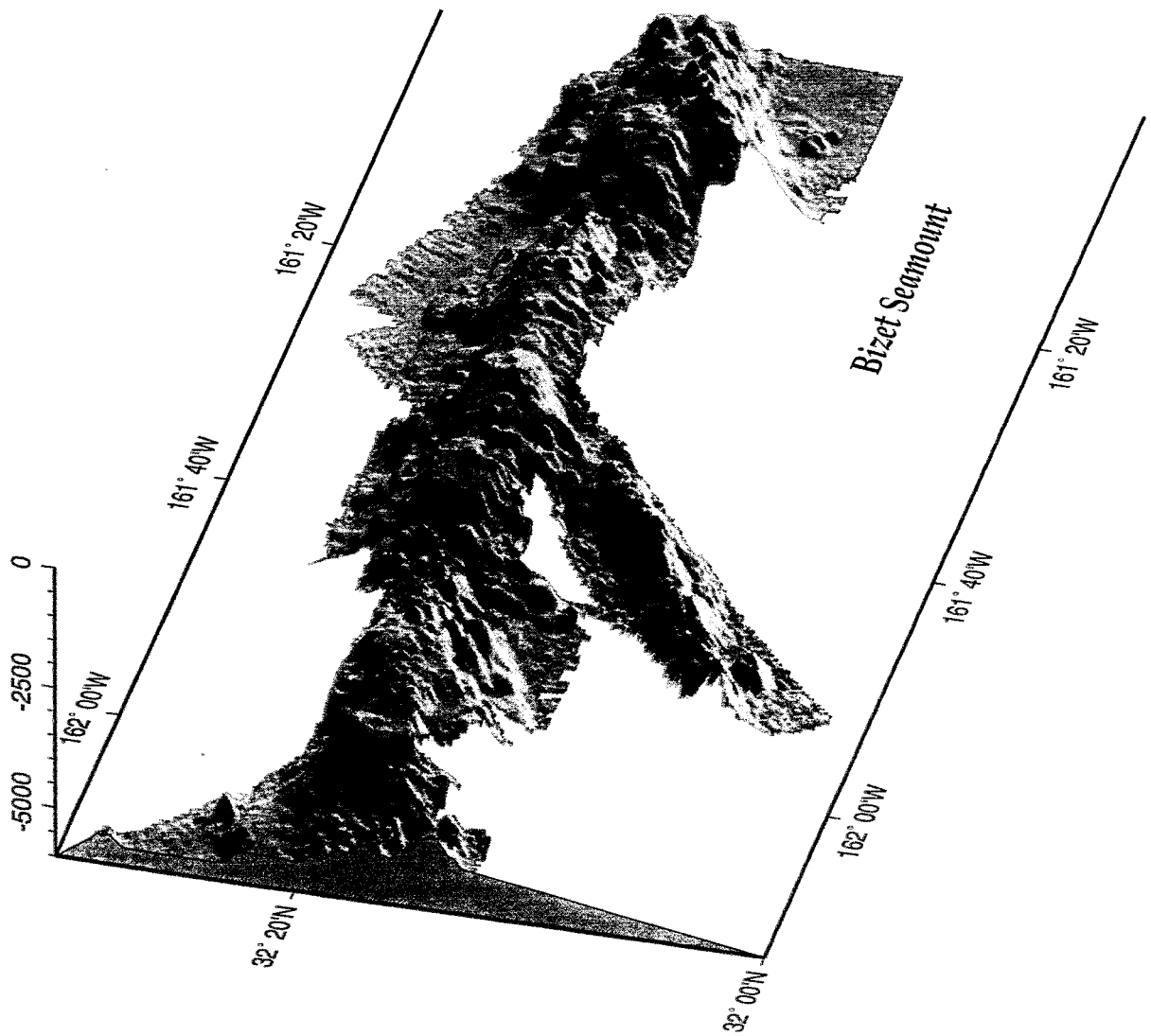

Figure 6.1.2.6: Perspective image of Bizet seamount. View from west, illumination from east.

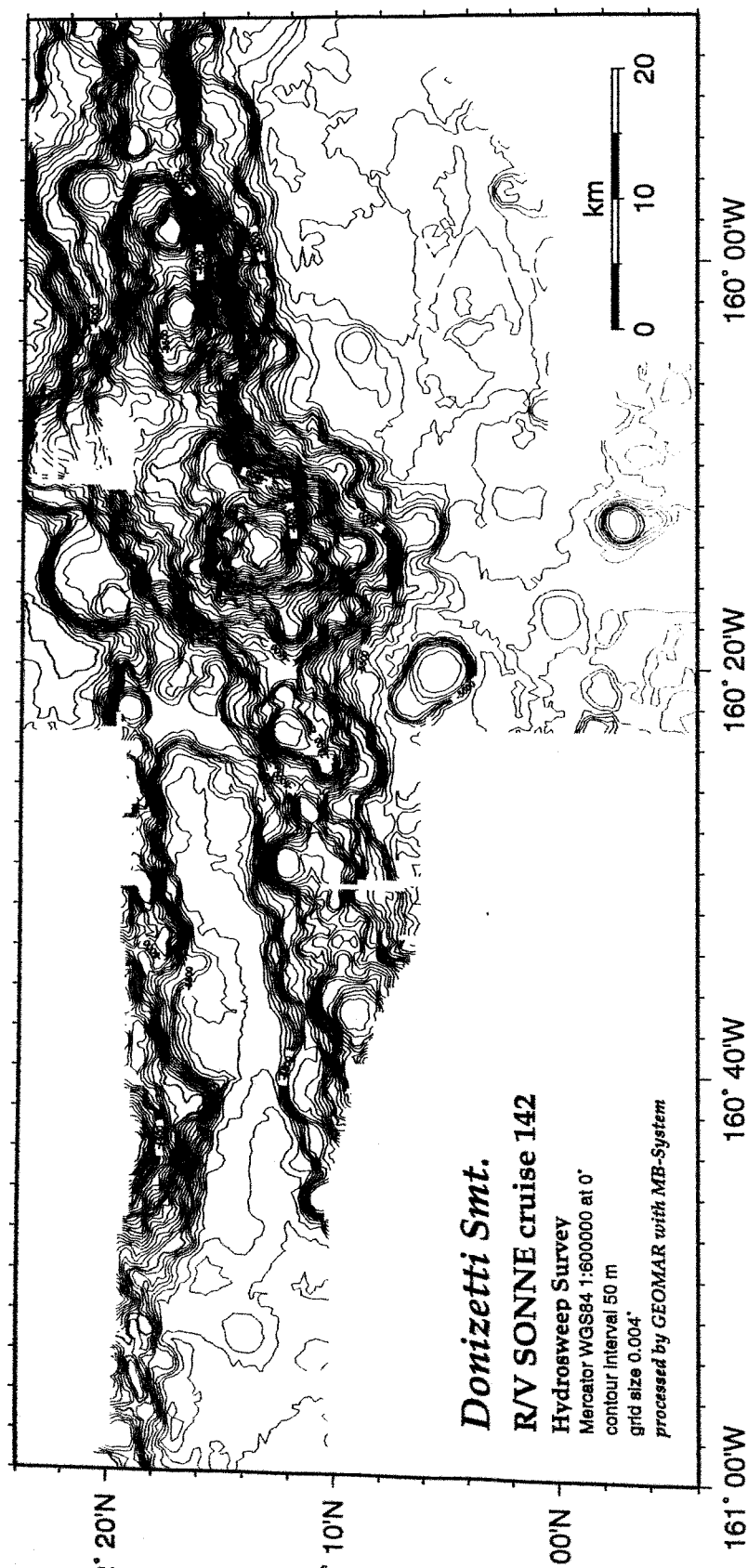

Figure 6.1.2.7: Bathymetric map of Donizetti seamount.

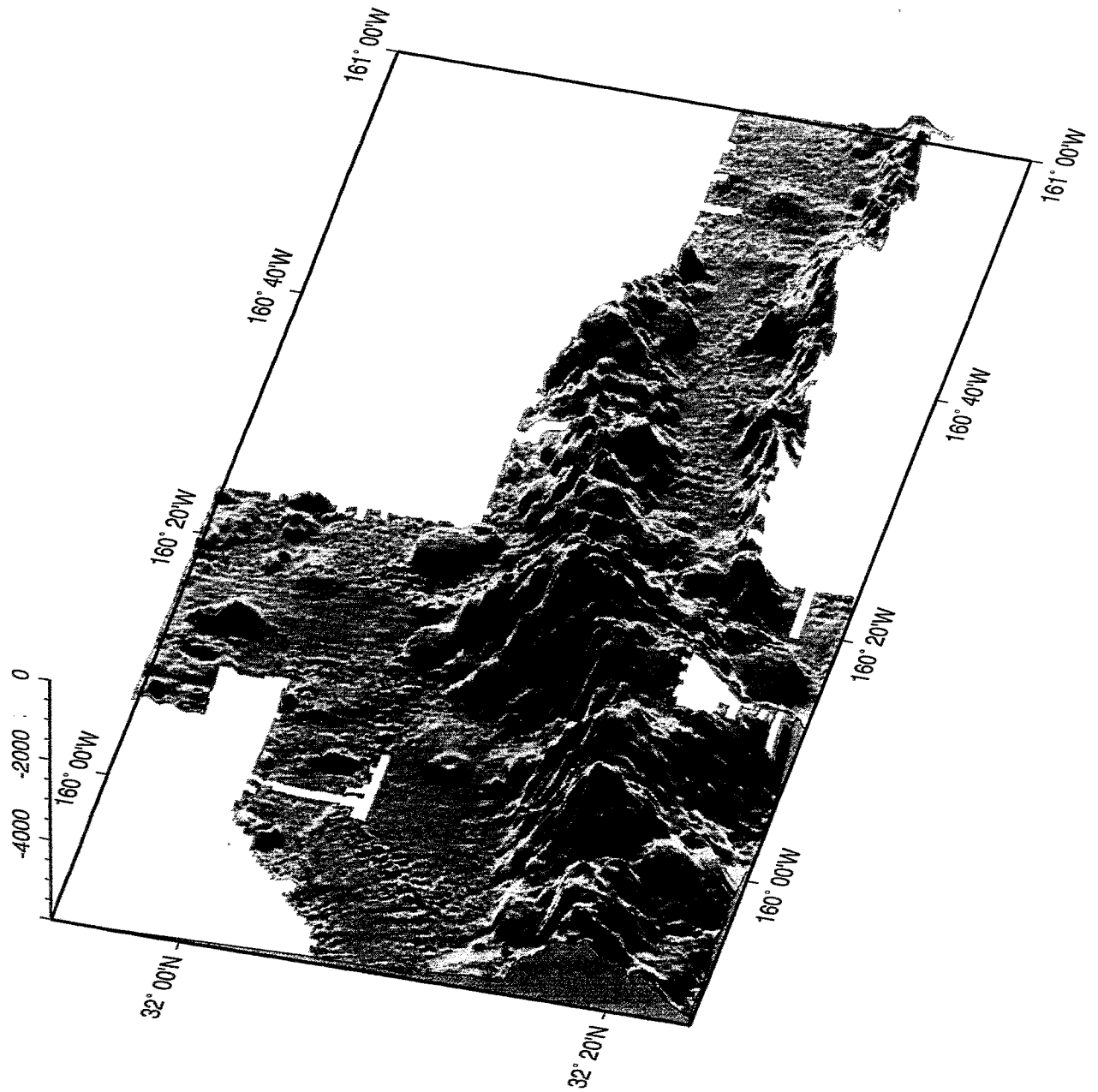

Figure 6.1.2.8: Perspective image of Donizetti seamount. View from east, illumination from west.

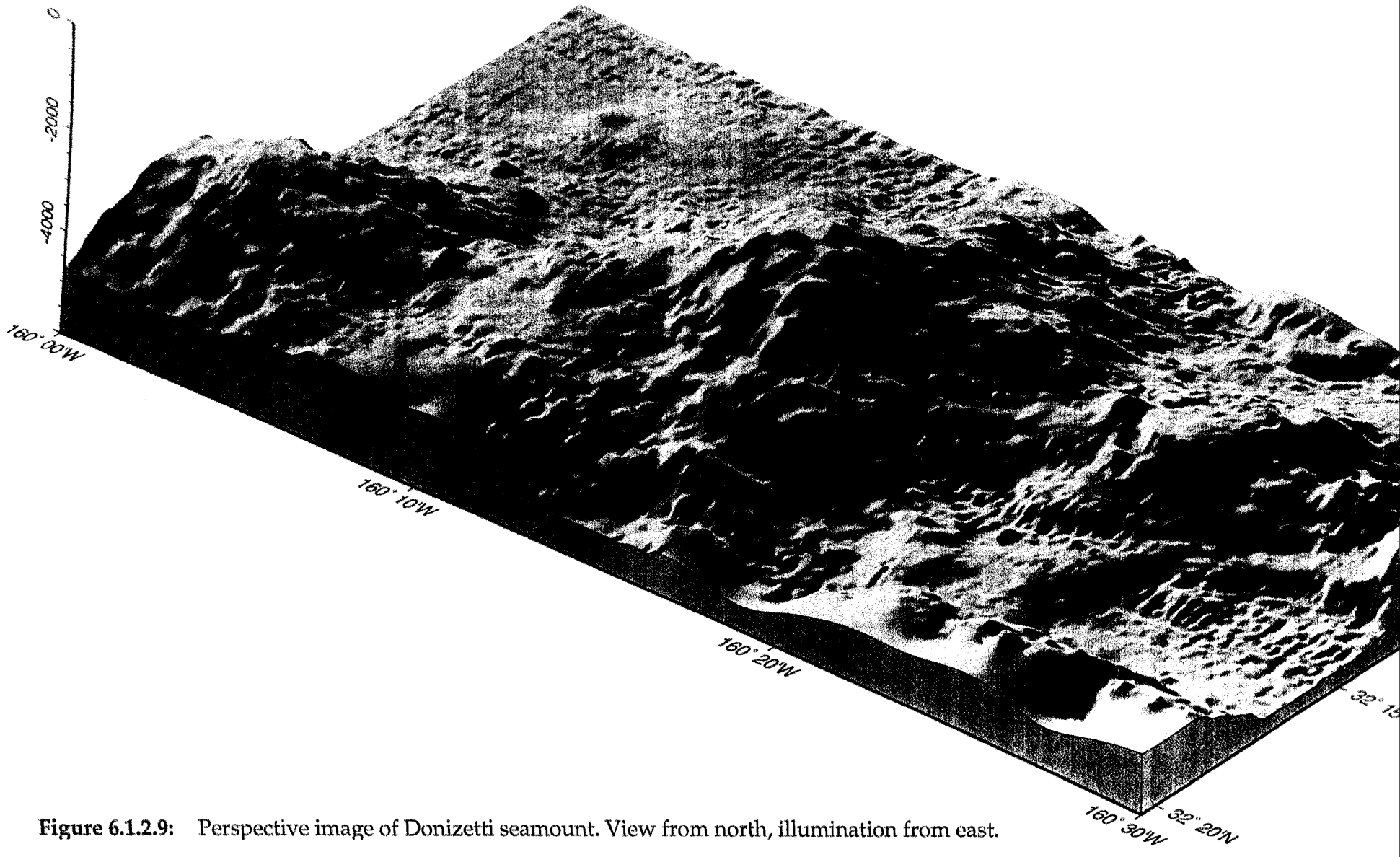

Figure 6.1.2.9: Perspective image of Donizetti seamount. View from north, illumination from east.

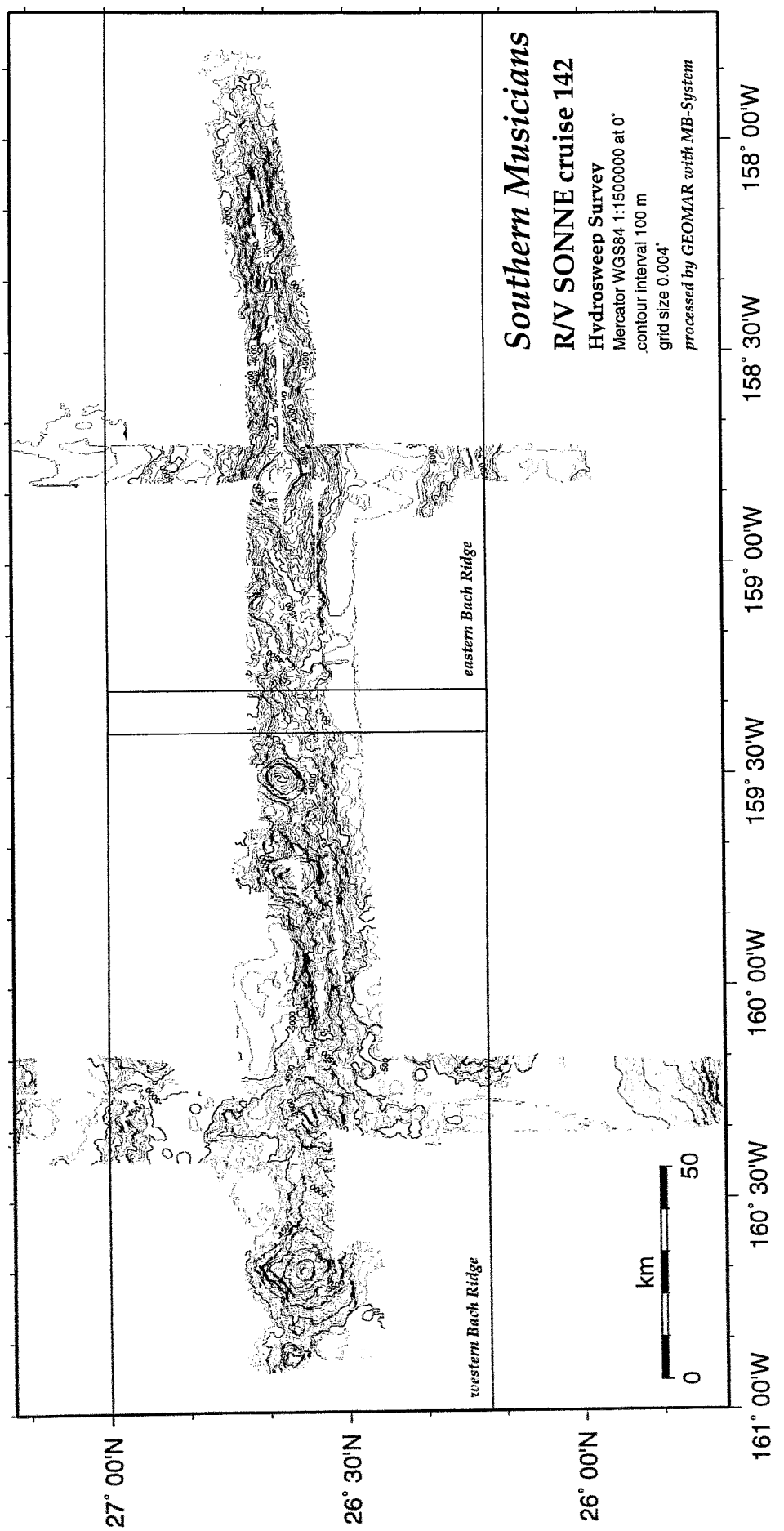

Figure 6.1.3.1: Areas mapped with HYDROSWEEP in the southern Musicians with locations and names of detailed maps.

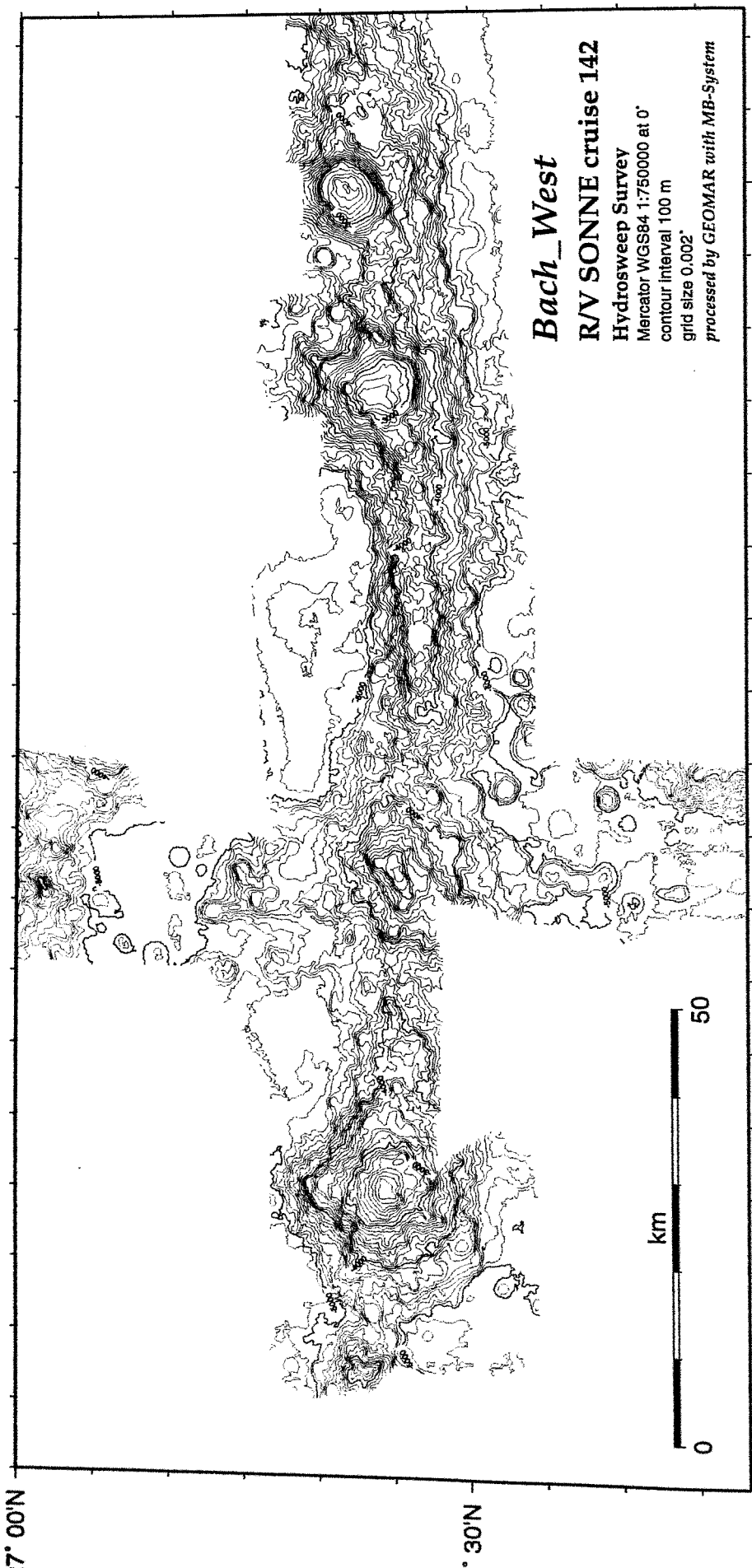

Figure 6.1.3.2: Bathymetric map of western part of Bach Ridge.

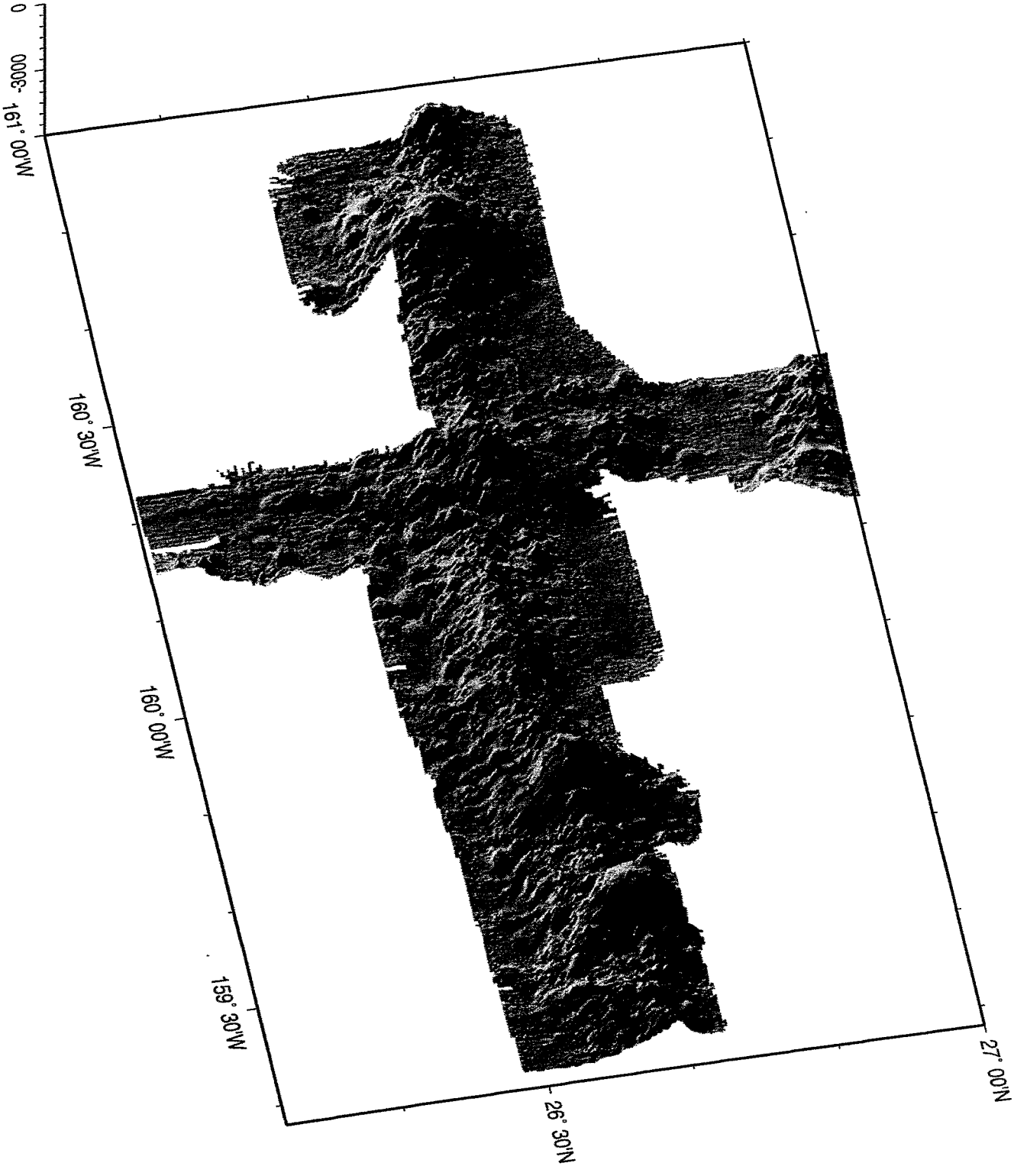

Figure 6.1.3.3: Perspective image of western Bach Ridge. View from east, illumination from west.

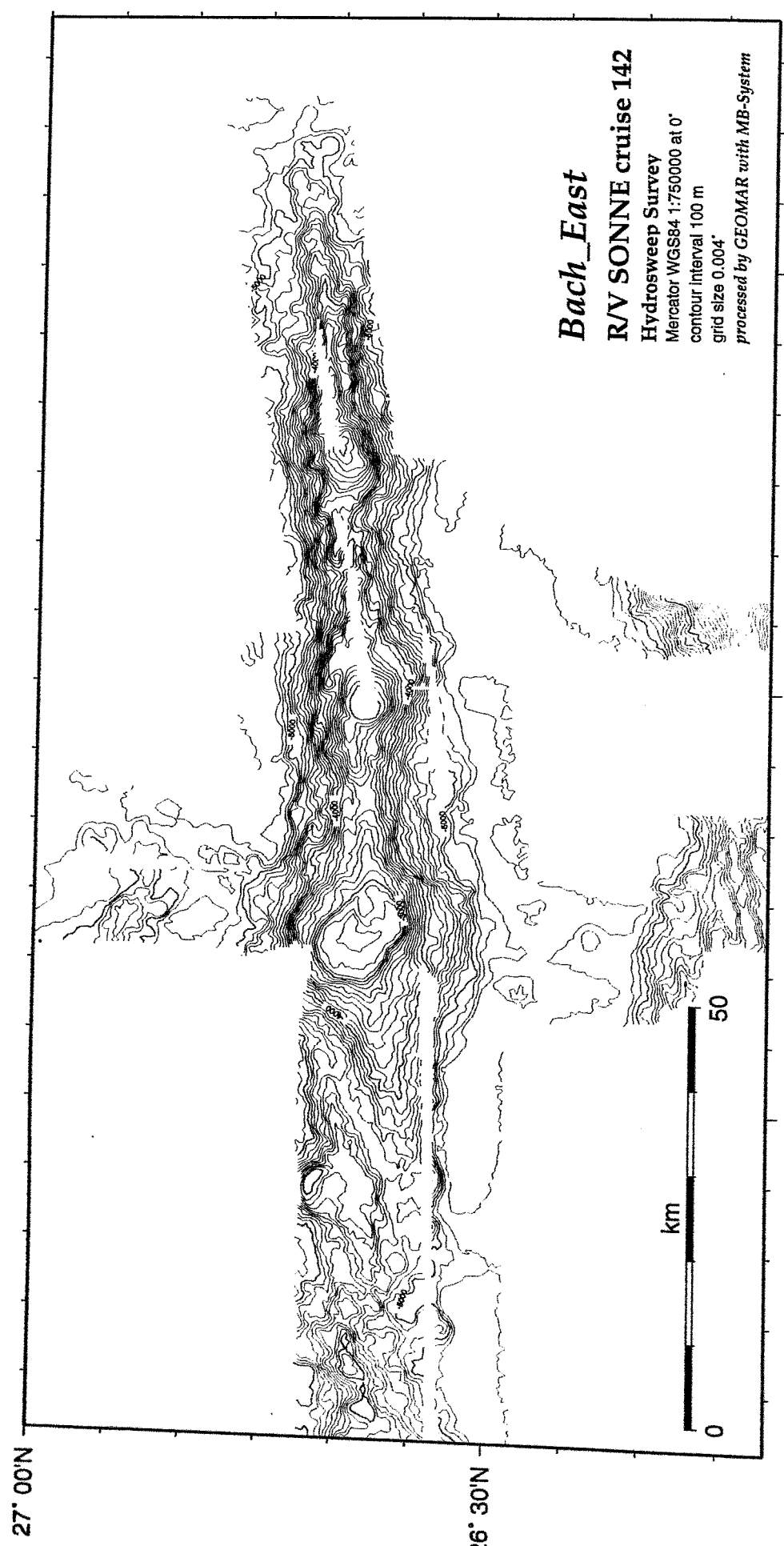

Figure 6.1.3.4: Bathymetric map of eastern Bach Ridge.

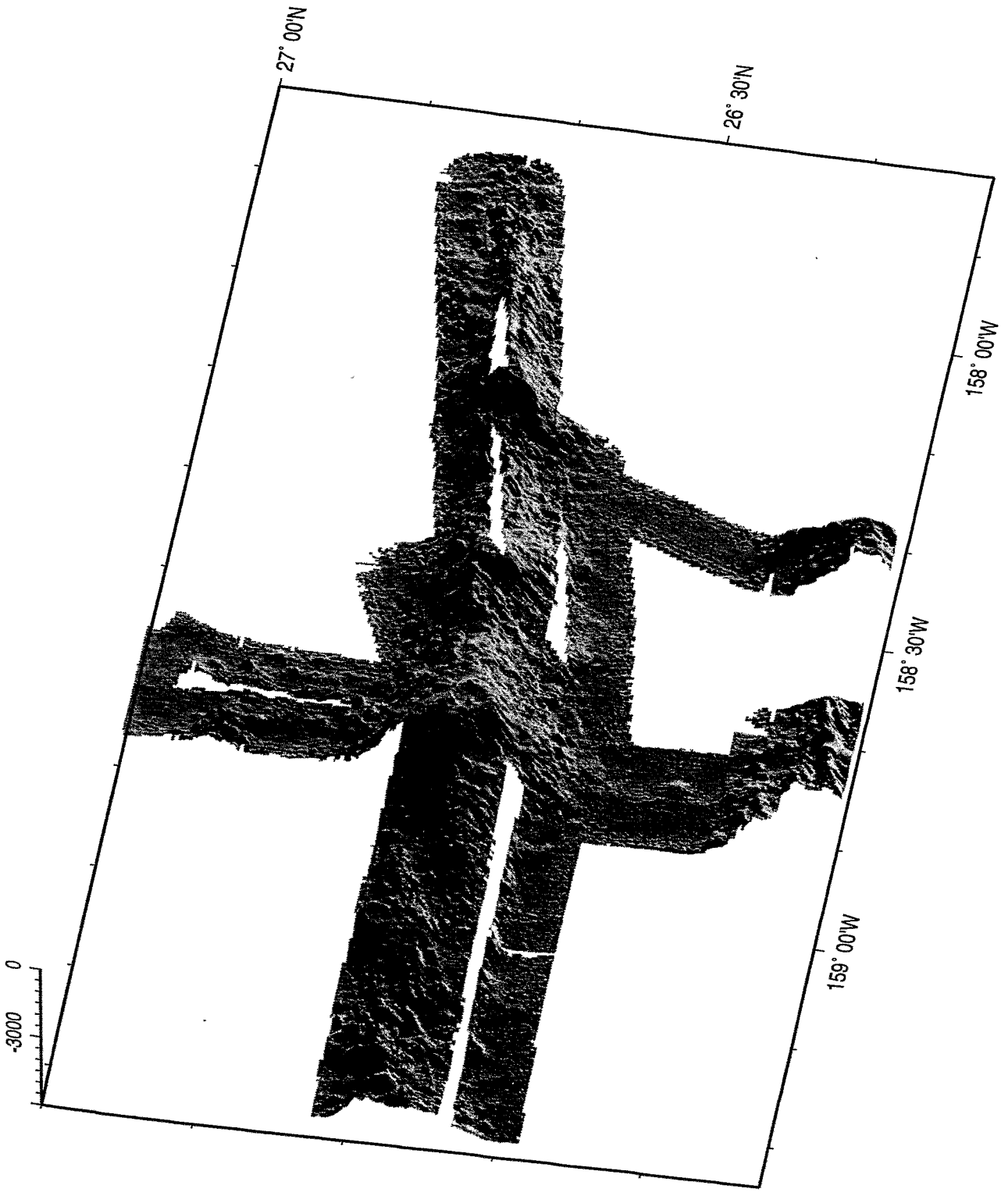

Figure 6.1.3.5: Perspective image of eastern Bach Ridge. View from west, illumination from east.

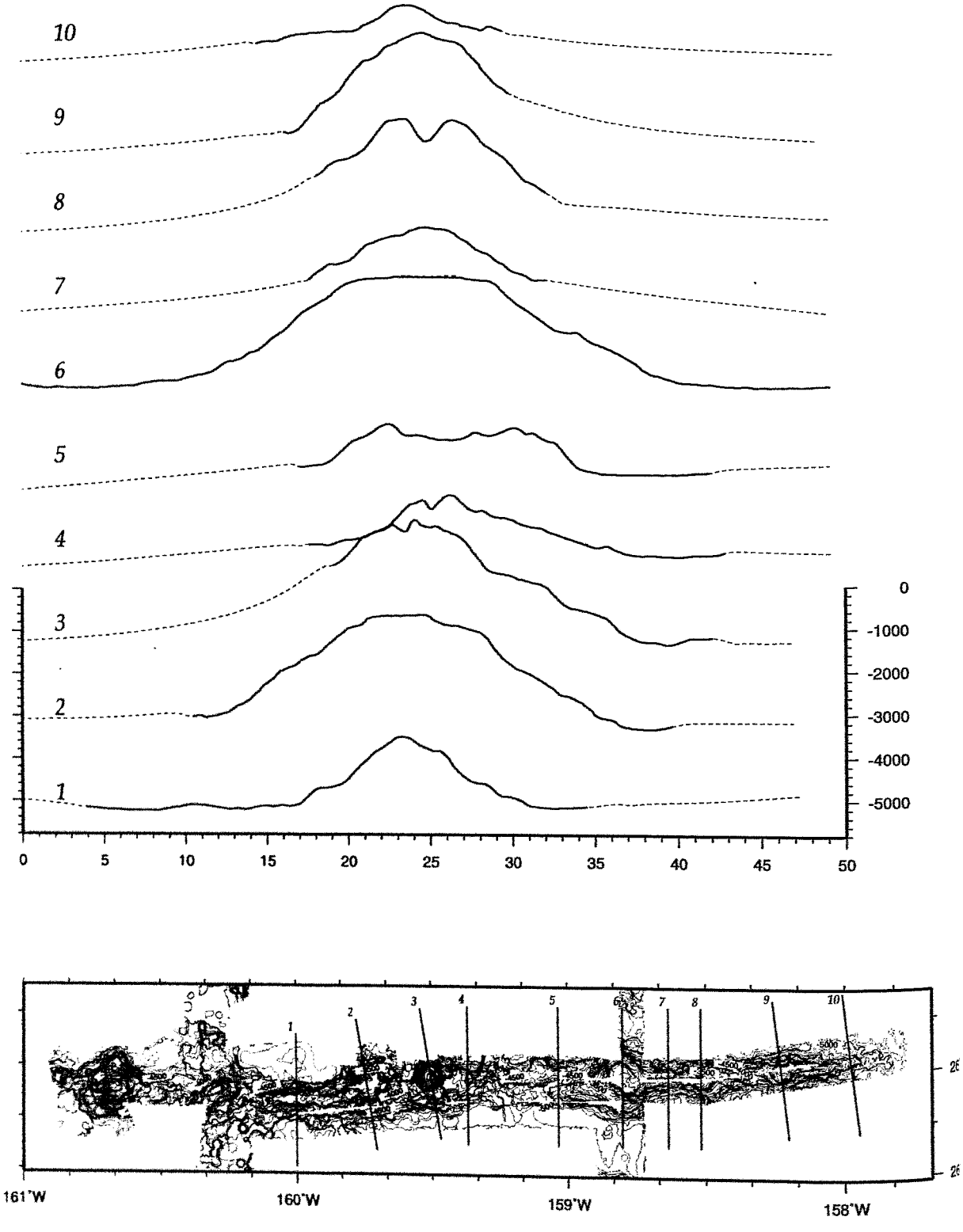

Figure 6.1.3.6: Depth profiles across Bach Ridge (top), from west (bottom) to east (top), each shifted vertically. Horizontal scale in km, vertikal scale in m, vertical exaggeration 2.5. North on the left, south on the right. Position of depth profiles across Bach Ridge (below).

6.2 PARASOUND

(S. Lyons, C. Larsen and watchstanders)

Parasound data were collected during the hydrosweep and magnetic surveys and along all seismic lines. Data were recorded continuously on both a color plotter and a black and white plotter. Due to the narrow beam width of the parasound, data will not be reflected back from surfaces with more than ~2° slope, so the parasound system is only effective in generally flat or gently-sloping regions. For areas in which the bathymetry was sufficiently shallow, the data quality was good throughout the cruise at the ship's speed of 4-12 knots. In mildly sloping regions, including the crests of some of the ridges, penetration of the parasound beams reached 50-65 m; in flat areas, imaging of up to 100 m into the uppermost sedimentary layers was achieved.

Ridge systems and sediment ponds

Good Parasound images were obtained from the relatively flat ocean floor in the eastern regions of the Musician Seamounts between the elongate volcanic ridges, as well as along the seismic profile lines. Sediments in the flat areas between ridges show little deformation and deposition layers of sediments are clearly parallel to the seafloor (Figure 6.2.1). Penetration depth is about 70 m in this figure, which is located at 26° 19'N, 160° 18'W, between the western segments of Bach and Beethoven ridges. The reflectance in these regions is quite good and the gentle slope of the deeper sediments under the flat layers is easily identifiable. In other shallow, flat areas, there are regions in which the sediment is highly reflective and massive, with indistinguishable layers. Penetration depth is of similar magnitude as the layered regions. Finally, there are areas of rolling seafloor which yield a parasound image with both characteristics. Figure 6.2.2 shows a section of the northern Musicians, south of the Donizetti Ridge, (31° 31'N, 160° 14'W) in which reflectance is good, penetration depth is about 50 m, and some layering is apparent. These regions show depositional arcs of sediment, indicating some compression within the region.

Northern Musicians

In the northern region of the Musicians, there is evidence of normal faulting near the elongate ridges, as seen in Figure 6.2.3, between Rossini Ridge and Puccini Seamount (32° 32'N, 162° 21'W). The signature of the hanging walls and footwalls is evident and indicates extension within this area. The image has a maximum penetration depth of about 80 m, with average quality reflectance. In the semi-flat regions to the southeast of the ridges, sediment layering is mostly parallel to the ocean floor, indicating little deformation. In some of these images, as in Figure 6.2.2, there are signs of mild compression.

Murray Fracture Zone

While the parasound system could not produce well-defined images of the Murray Fracture Zone due to its steep slopes, there is evidence of deformation north of the fracture zone. Faulting similar to that in Figure 6.2.3 is apparent, as well as regions of folded terrain, such as seen in Figure 6.2.4, northwest of the fracture zone (29° 45'N, 160° 20'W). These indicate both compressional and extensional strain within the region surrounding the fracture zone. The average penetration depth in these images is 70 m, with good reflectivity.

Southern Musicians

In the southern region of the Musican seamount province, there is evidence of compression between the elongate ridges. This is apparent in the folded layers of sediment in Figure 6.2.5, near the northern end of the Schumann Ridge, south of the Beethoven Ridge (25° 56'N, 160° 13'W). The maximum penetration depth in this area is about 60 m with high reflectivity of the layers. To the west of the Beethoven and Bach ridges, north of the area in Figure 6.2.5, we can see a zone with little deformation (Figure 6.2.1). The top sediment layers in this region lay parallel to the ocean floor, with arched layers further below. This could indicate past compression, but it is apparent that no recent tectonism has occurred in this area.

West of the Rameau Ridge (25° 48'N, 158° 46'W), parallel sediment layers were highly defined in the parasound images to a depth of about 50 m (Figure 6.2.6a). This is in sharp contrast to the images obtained just south of the central portion of the Bach Ridge (Figure 6.2.6b, 26° 28'N, 158° 46'W). In this region, where the first TV grab of the cruise was performed, the seafloor appeared enormously reflective, with the deeper layers showing up much more sparsely in comparison. The reflectance level of the seafloor in this area was on the order of 2-4V, compared with a normal seafloor reflectance of 100-200mV. This high value is typical of very shallow continental shelves, not deep oceanic sediments. The cause of this is unknown, but it is believed to be a real signal, due to its consistency, rather than just an artifact in the data.

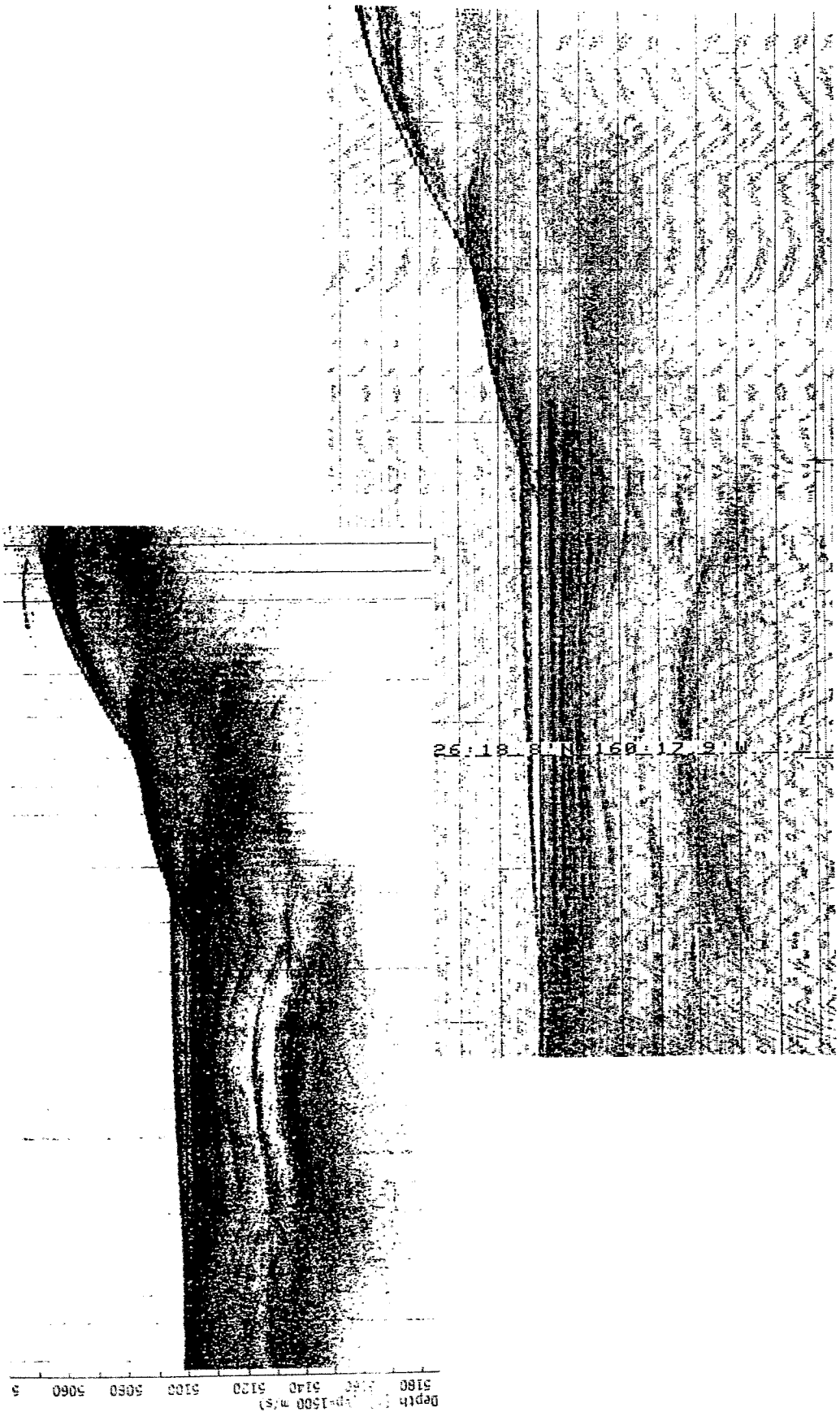

Figure 6.2.1. Parasound images of sedimentation between the western segments of the Bach and Beethoven ridges, in the southern Musician province (26° 19'N, 160° 18'W). The upper sediment layers are parallel to the ocean floor and show little or no deformation, while the arched lower layers could be indicative of either compressional or erosional processes. Penetration depth is about 70 m.

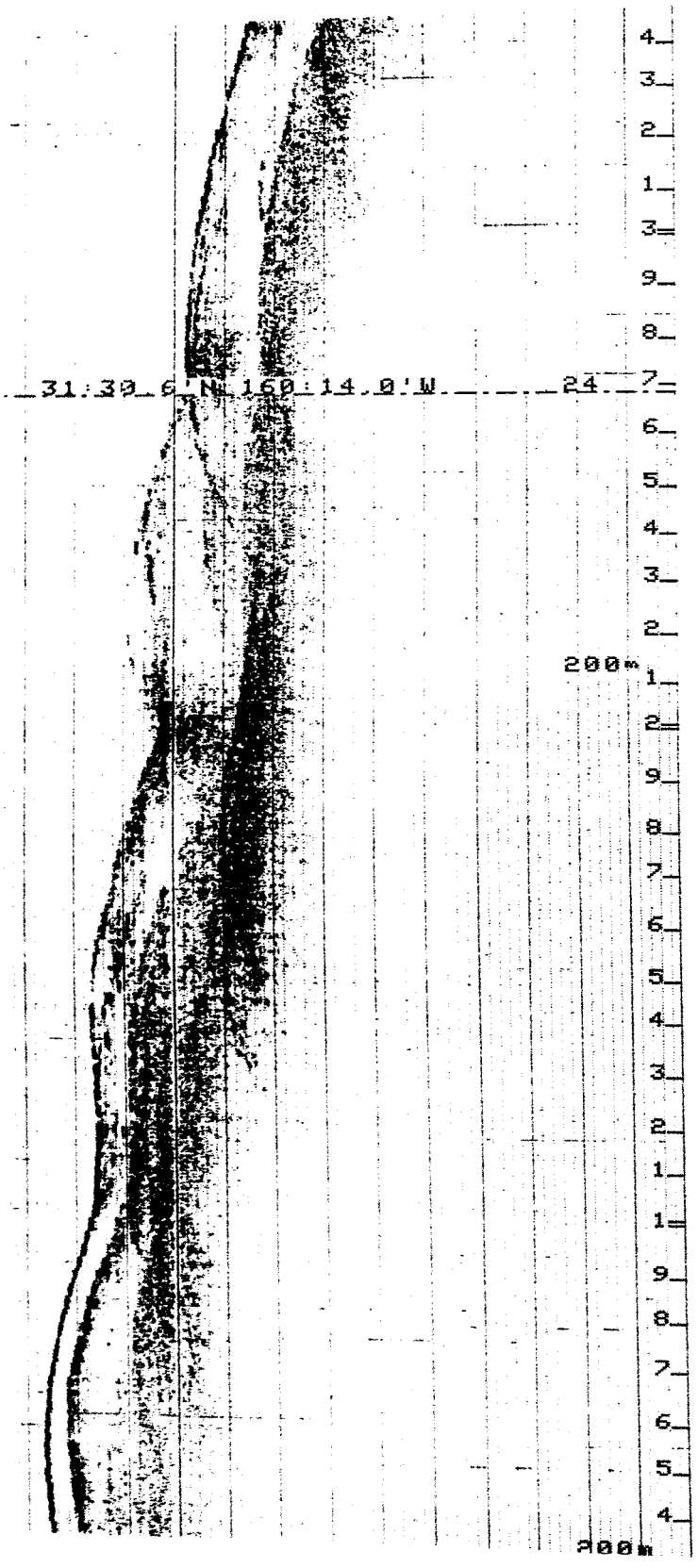

Figure 6.2.2. Parasound image south of the Donizetti Ridge in the northern Musicians (31° 31'N, 160° 18'W). Minor compression has occurred in this region, as seen by the depositional arcs in the sediment. Penetration depth is 50 m.

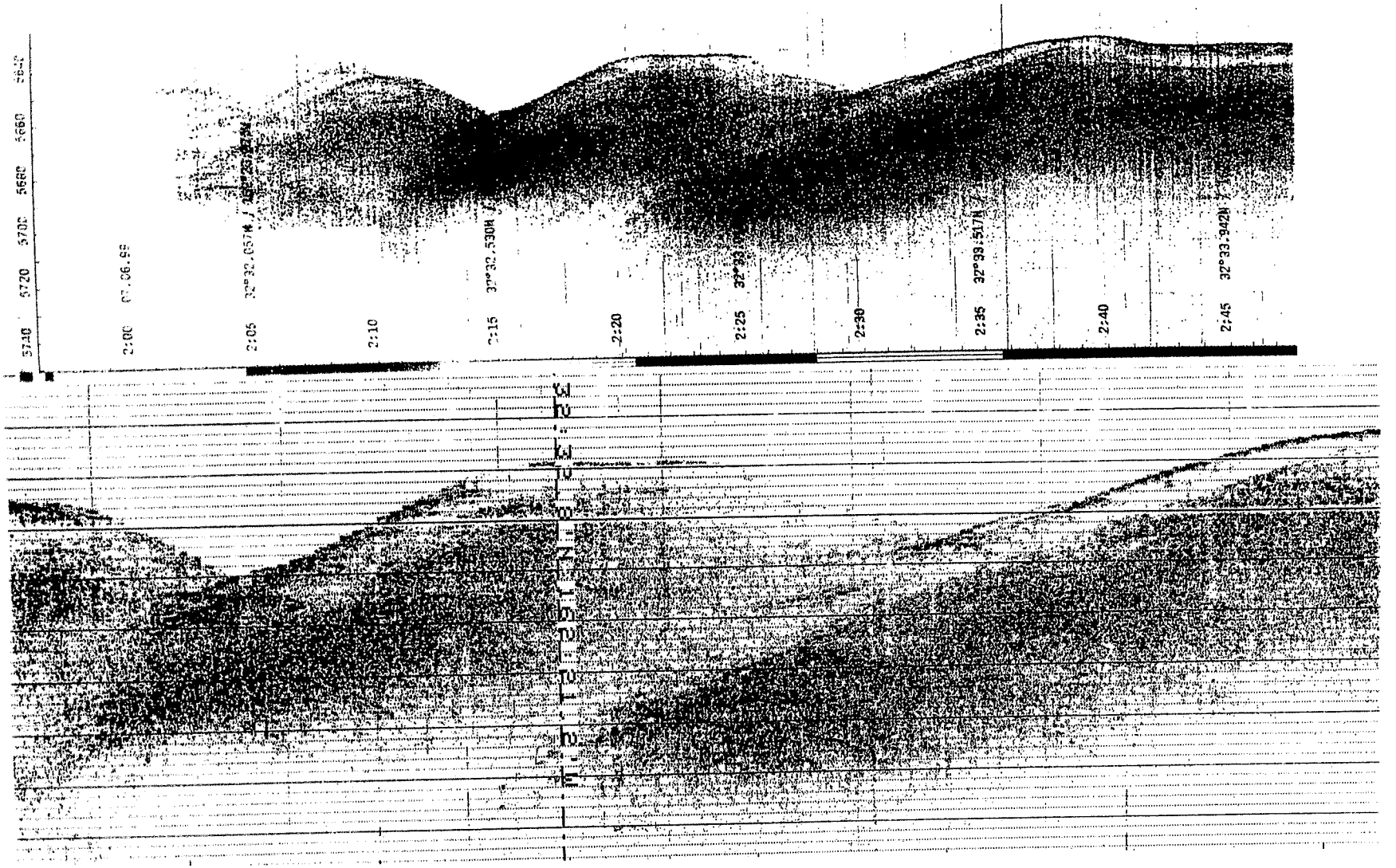

Figure 6.2.3. Image indicating faulting between the Rossini Ridge and the Puccini Seamount in the northern Musicians (32° 32'N, 162° 21'W). Penetration depth is about 80 m.

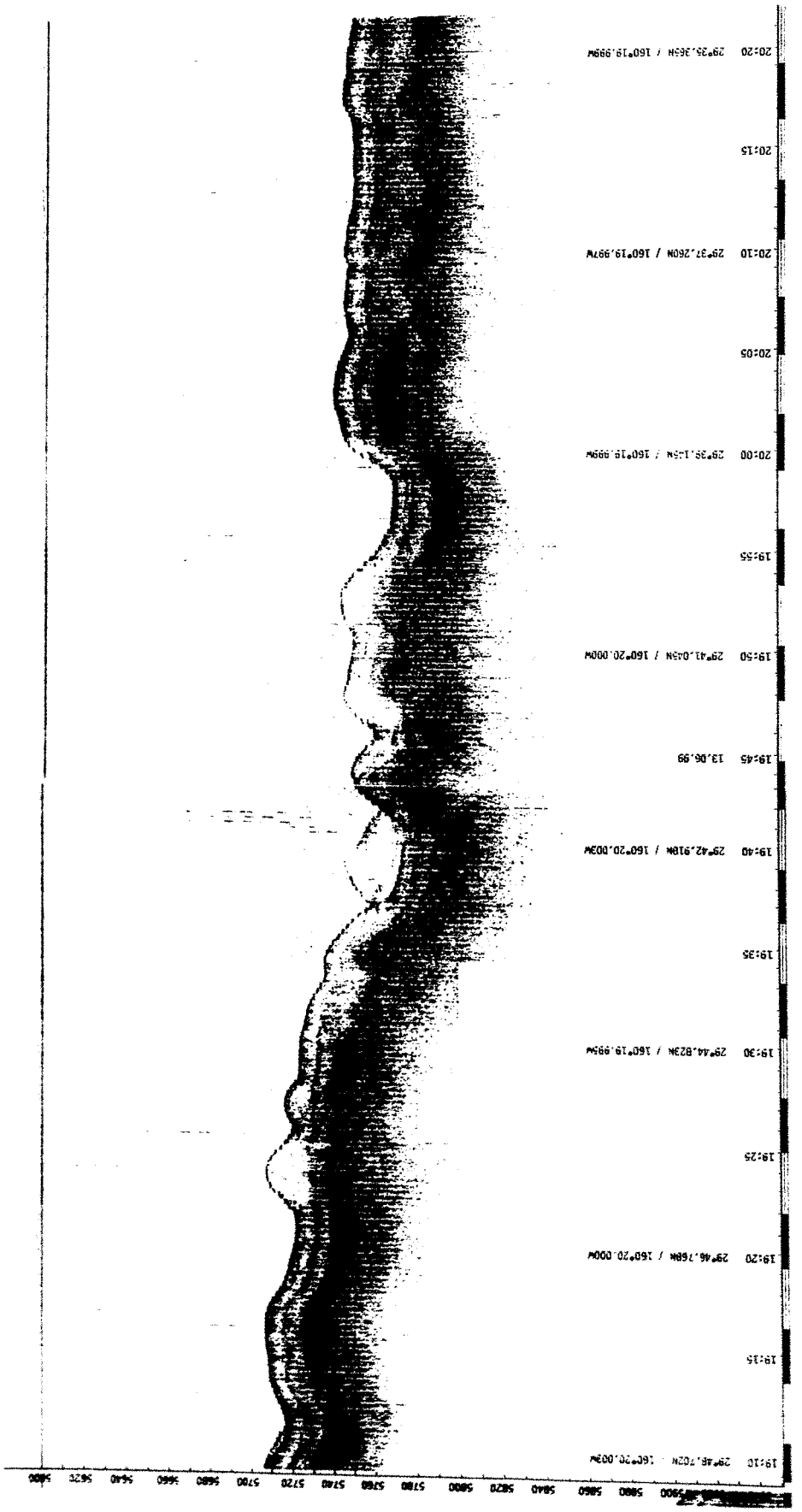

Figure 6.2.4. Parasound image north of the Murray Fracture Zone (29° 45'N, 160° 20'W). The folded terrain indicates compression within this region, which has a penetration depth of about 70 m.

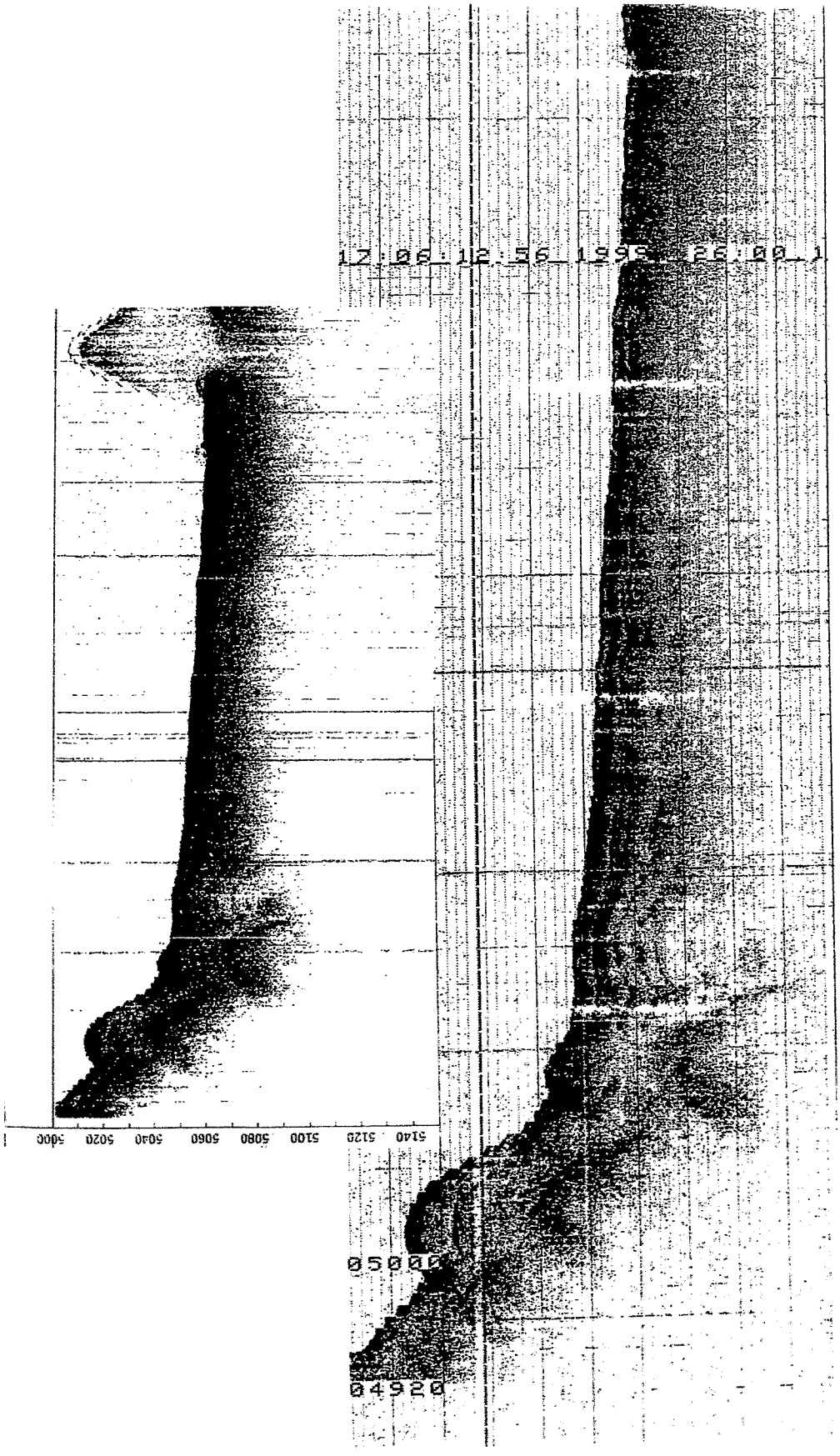

Figure 6.2.5. Deformation signature north of the Schumann Ridge, south of the Beethoven Ridge in the southern Musicians (25° 56'N 160° 13'W). Compression is evident from the folded layers in the image. The large anomaly on the far right of the image is of unkown origin, but is probably an error in the parasound system due to temporary poor reflectance. Maximum penetration depth is about 60 m.

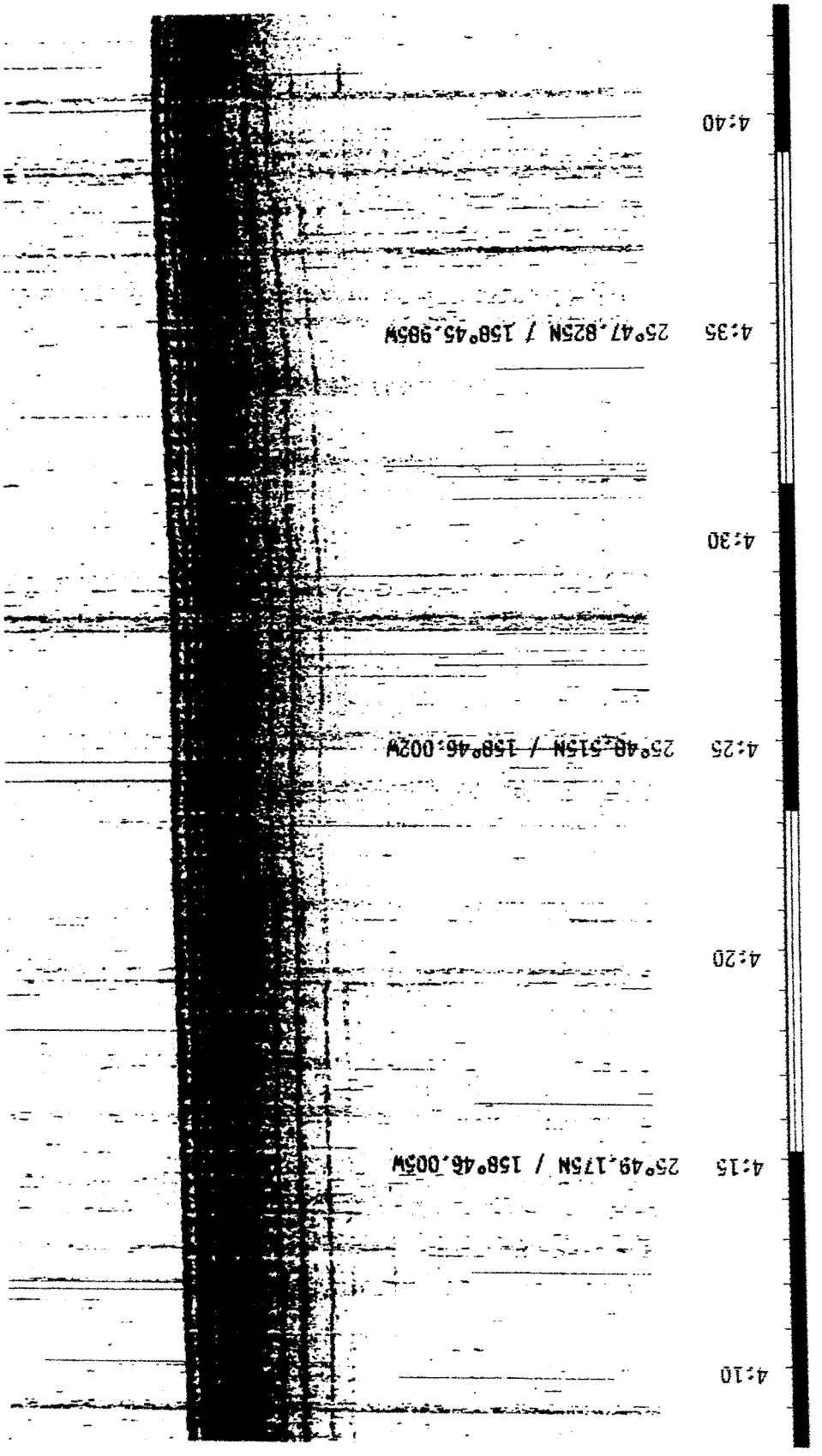

Figure 6.2.6a. Sedimentation west of the Rameau Ridge in the southern Musicians (25° 48'N, 158° 46'W). Penetration depth is about 50 m and the individual sediment layers are well-defined throughout the image.

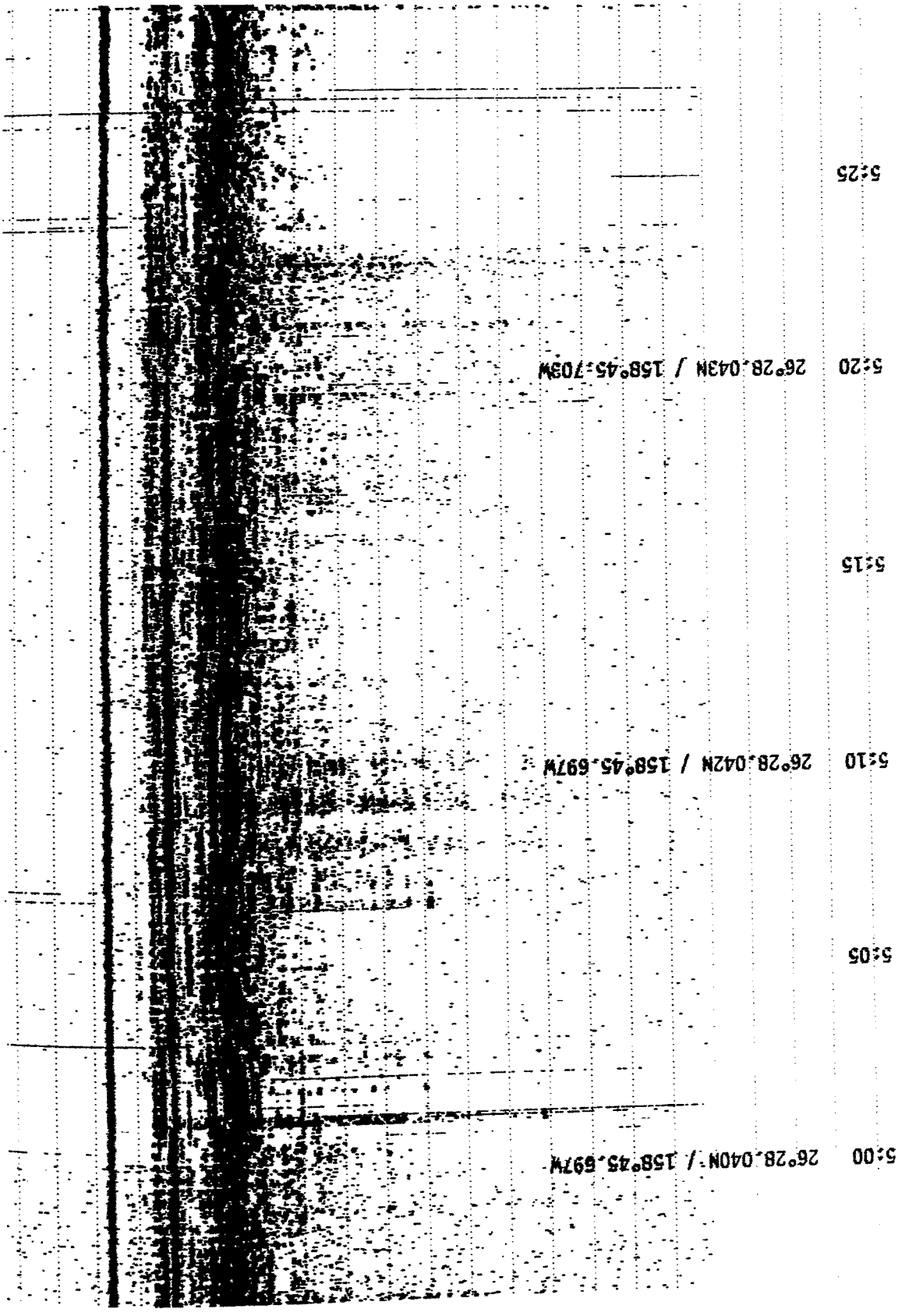

Figure 6.2.6b. Parasound image south of the central Bach Ridge (26° 28'N, 158° 46'W). The seafloor in this region has an extremely large reflectance value, causing the other layers to be poorly defined. The cause of this anomalously high reflectivity is unknown, but the value is typical of very shallow continental shelves rather than deep oceanic sediments.

6.3 SEISMIC WIDE-ANGLE WORK

6.3.1 INTRODUCTION

(E. Flueh, I. Grevemeyer, C. Kopp, H. Lelgemann, H. Borús, C. Larsen and watchkeepers)

An important component of the work during cruise SO142-HULA II was the collection of seismic wide-angle data. A total of 47 OBHs were deployed along 4 lines, with one of the lines (SO142-01) as a short test line for new instrumentation. Up to 14 instruments were available for use along each line. All instruments were safely recovered. A summary of all deployment sites and profiles is shown in Figure 6.3.1; technical details are summarized in Appendices 9.1. The data quality is generally very good, and on a number of sections it isof superb quality, with clear arrivals at distances of 150 km (the maximum observation distance).

Problems with recording errors, especially a strong dc-shift, became apparent during the past cruise (Flueh et al., 1999c), and extensive tests were made to understand this phenomenon. Although the problem is not fully understood, it appears that a switch that regulates a resistor on the preamplifier was not grounded well. After isolating the switch from the housing, the dc-shift was only noticed on two instruments, however, this still requires further investigation to avoid future deterioation of the recordings.

Shooting was performed using the two large *Bolt* airguns, which provided a total volume of 64 liters (4000 inch^3). For nearly 100 hours the guns worked without any problems or delays, despite a moderate swell; only one repair had to be made on one of the supply hoses. In total nearly 5600 shots were fired along the profiles with a total length of about 600 km. Details are given in Appendix 9.1.5. Although the signal is far from being well-tuned, it could be compressed through processing techniques to an acceptable waveform which allowed good resolution. In generel energy transmission was surprisingly good, with strong arrivals seen at maximum recording offsets of 150 km in places.

Although originally intended, we did not deploy a short streamer, since the guns were often too close together to risk a safe operation of the streamer. However, with the rather low main frequency of the gun signature, the absence of noticeable sediment cover, and only occasional near-vertical reflections seen on the OBH record sections at near-offset, we feel that this is not a major loss. Also, the magnetometer was not deployed during shooting of the seismic profiles, for safety reasons.

All seismic data collected were initially processed. Unfortunately, both of the playback devices for the DAT recorders failed and therefore these records (4 instruments out of 14) could not be displayed onboard. The remaining data were copied, processed, and plotted during the cruise. They are archived in standard SEG-Y format. The excellent cooperation between the scientific parties onboard and the ship's crew enabled a very smooth operation. Due to the presence of other working groups onboard and the small number of instruments used during the cruise, the workload was moderate for both people and computer facilities. No shortcomings were noticed. Preliminary interpretations were made for some of the profiles, especially for those collected early during the cruise. In the following chapters the applied processing (chapter 6.3.2) and modelling techniques (chapter 6.3.3) are described. This is followed by a description of each profile, which includes the chronology of the experiment (all times given correspond to local times:GMT minus 11 for Profiles SO142-01 and 02; GMT-10 for SO142-03 and 04), the most important data; and some initial results. Naturally, these first results should be read with caution. Incorporation of the remaining data and more detailed analyses of the recorded wavefields will lead to a much more detailed image of the crustal structure and its variation across the Italian and the Bach Ridges. The data needed to achieve the aims of the project were acquired during the cruise and provide asolid foundation for the interpretation to be done in the forthcoming months.

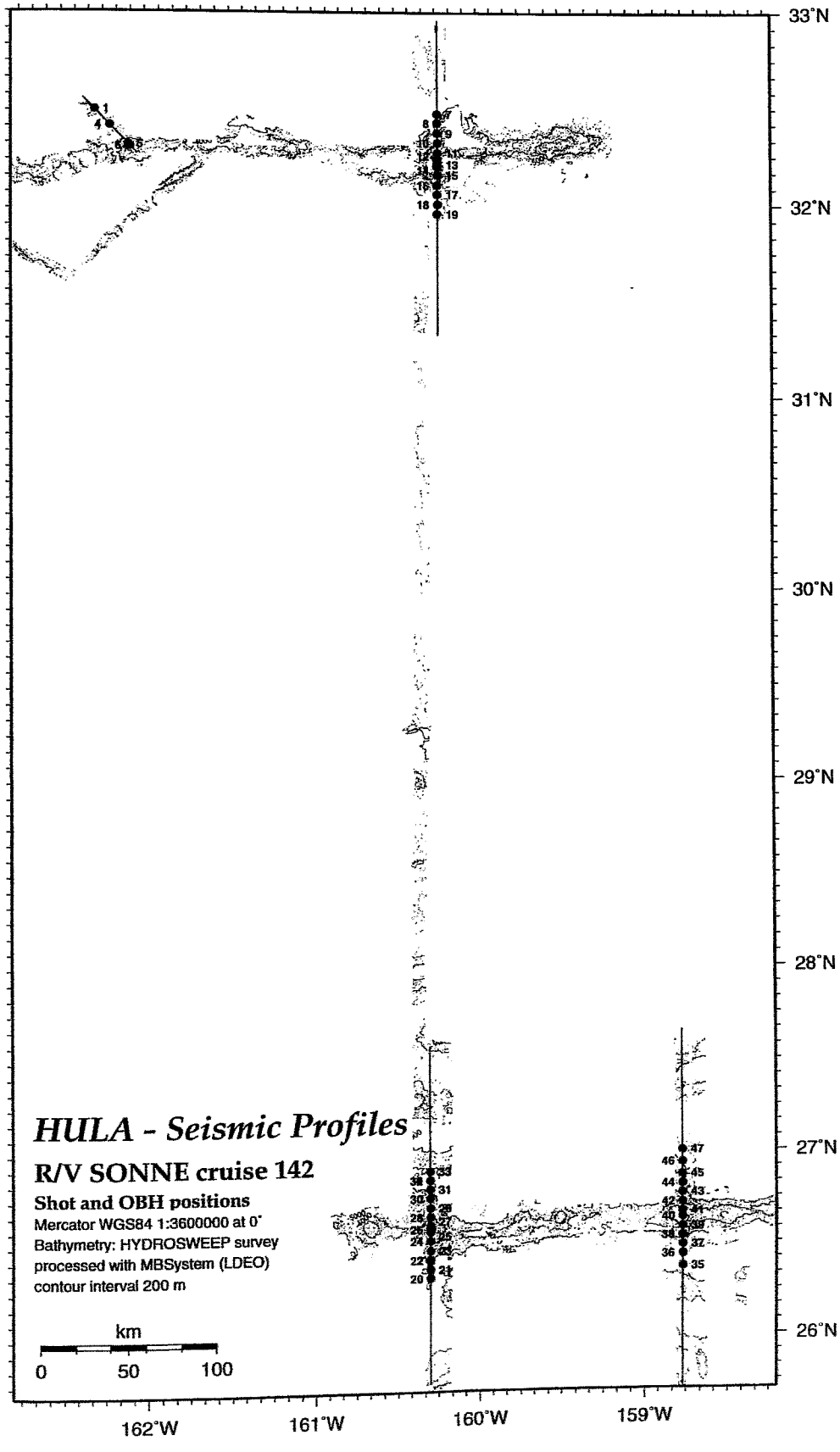

Figure 6.3.1.1: Shot and OBH positions during cruise SO142 HULA.

6.3.2 SEISMIC PROCESSING AND DATA ARCHIVING

Raw seismic field data are usually heavily contaminated by noise from different sources. Even though there is no good way to supress real random noise, e.g. noise with a white frequency spectrum, there are several processes to supress spectral non-white components. The preprocessing steps applied to the wide-angle data were designed mainly to contract the original airgun signal with a strong bubble to a shorter wavelet, to supress the high-amplitude, low-frequency noise occuring on many receivers, and to exclude frequencies without useful information content.

Figures 6.3.2.1 and 6.3.2.2 display spectral analyses of seismic recordings at offsets between 5 km and 8 km. Figure 6.3.2.1 shows the signal on profile SO142-01, where only one airgun was used. Several peak frequencies at 6 Hz, 12 Hz, 18 Hz, 24 Hz and 30 Hz can be identified clearly, with the highest energy at 12 Hz. Amplitudes below 5 Hz seem rather uncorrelated and are presumably due to noise. Figure 6.3.2.2 analyzes profile SO142-02 with two airguns in operation. The spectrums in these figures look very similar: peak frequencies are the same and the largest amplitudes occur at 12 Hz. The main difference when operating two airguns, is that energy above 12 Hz is more damped due to inteference of the two guns.

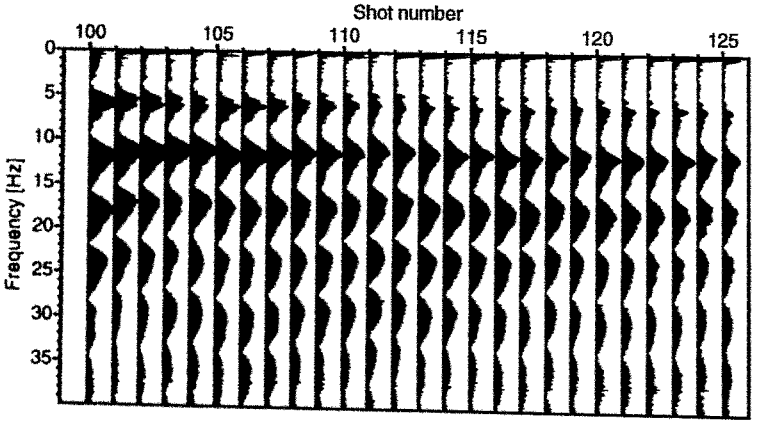

Figure 6.3.2.1: Frequency analysis OBH 05, offset 5-8 km, only one airgun used.

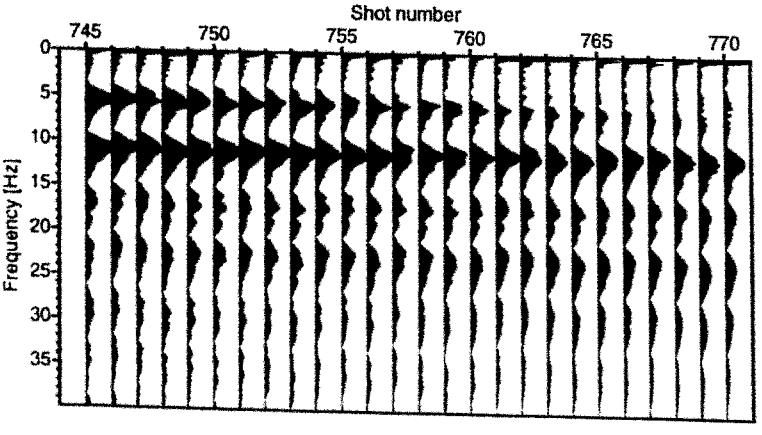

Figure 6.3.2.2: Frequency analysis OBH 17, offset 5-8 km, two airguns used.

The following section describes all preprocessing steps; processing parameters were determined in offset ranges of 2-8 km (OBH06) and 30-36 km (OBH05).

Deconvolution test:

To improve the temporal resolution of the seismic data, a deconvolution is applied to compress the basic seismic wavelet. As the amplitude spectra of seismic wide-angle data vary with time and offset, the deconvolution must be able to follow these time- and offset-variations. Each trace is therefore divided into 2 s data gates with 1 s overlap, in which time-invariant deconvolution operators are computed from the autocorrelation function of the data segment and subsequently applied to the data. The deconvolved trace results from a weighted merging of the independently deconvolved gates.

The deconvolution test panels are shown in Figures 6.3.2.3 and 6.3.2.4 for two different offset ranges. Above the data, an autorrelation function (AKF) is attached. Input for the deconvolution process is raw data, 5 Hz lowcut filtered with 48 db slope. The input data (panel labeled 'no deconvolution' in Fig. 6.3.2.3) shows strong low-frequency noise (trace 350-380) and 6 Hz / 12 Hz reverberations following the direct wave (trace 380-400). In the AKF, this noise appears clearly in the repeating phases up to the end of the AKF window. For the deconvolution tests, a constant operator length of 480 ms was chosen and the predictive length was modified from 0 ms (spike) to 320 ms as displayed in the different panels in Fig. 6.3.2.3. With decreasing predictive lengths, the monofrequent noise level reduces and the wavelet compresses, indicated by a shorter AKF. The best resolution is obtained for a predictive length of 0 ms but with a reduction of signal-to-noise ratio. For this dataset, a predictive length of 80 ms was chosen, which is a compromise between temporal resolution and signal-to-noise-ratio. For display purposes of the deconvolution test, the far offset panels in Fig. 6.3.2.4 are filtered with a 3-25 Hz Ormsby filter after deconvolution.

Frequency filter test:

After deconvolution an offset- and time-variant Ormsby filter was applied. As the seafloor depth changes rapidly along the seismic lines, each trace was statically corrected to a fixed seafloor travel time of 6 s based on the water depth. This information is available in the trace headers. The time- and offset-variant filter depends on the reduction velocity. After this filter was applied, the data were shifted back to their original travel times.

Filter panels for offset ranges of 2-8 km and 30-36 km, respectively, are shown in Figs. 6.3.2.5 - 6.3.2.8. The autorrelation function is shown above the data. The amplitude spectra of the Ormsby frequency filter operators are characterised by linear slopes. The filter is described by four corner frequencies: Lower stop / pass band boundary and upper pass / stop band boundary. The frequency labels on the filter panels are mean values between pass and stop frequencies of the filter slopes.

To determine the corner frequencies of the seismic signals at each offset, only one filter slope was varied at a time. The result of the filter tests is given in the table below as a compromise between passing the best part of the signal and cutting the worst part of the noise at each offset range.

Final processing sequence:

- Input: SEGY-data, 5 ms (DAT recorder) or 4 ms (MBS recorder) sampling rate with complete geometry information. Trace length: 20 s, reduction velocity profile 1: 6 km/s, else: 8 km/s.
- Low cut frequency filter 5Hz with 48 db slope.
- Gated Wiener deconvolution: gate length 2 s, overlap 1 s, operator length 480 ms, prediction interval 80 ms.

- Static correction to a fixed seafloor travel time of 6 s
- Time and offset-dependent Ormsby frequency filter.
  On time-shifted traces with a reduced time scale of 6 km/s:

offset (km)	100%-time (s)	lower stop/pass	upper pass/stop (Hz)
0	5	5/9	20/30
	13	3/5	16/26
	20	3/5	12/22
20	1	5/9	20/30
	5	3/5	16/26
	13	3/5	12/22
40 - max	0	5/9	20/30
	0	3/5	16/26
	5	3/5	12/22

On time shifted traces with a reduced time scale of 8 km/s:

offset (km)	100%-time (s)	lower stop/pass	upper pass/stop (Hz)
0	5	5/9	20/30
	13	3/5	16/26
	20	3/5	12/22
20	1	5/9	20/30
	5.75	3/5	16/26
	13	3/5	12/22
40 - max	0	5/9	20/30
	0	3/5	16/26
	6.5	3/5	12/22

Data archiving

Unfortunately During the cruise it was impossible to process the recordings made by OBHs equipped with a Methusalem DAT recorder. Both playback units failed and could not be repaired with shipboard equipment. Therefore, the original tapes had to be stored for later playback and processing. However, a quality check was performed using the recorder interfaced to the PC, where the data could be displayed in real time through the RS232 interface. This was routinely applied to all recordings.

Data recorded with the MBS recorder on flash discs were transferred via a PC to a Sun workstation. On the workstation they were transformed into a so-called PSEUDO-SEGY format. Both the raw data from the flash discs and the PSEUDO-SEGY data were archived on DAT or Exabyte tapes. Generally, we were able to store the data from 5-6 MBS instruments on a single tape. After navigation data had been merged and SEGY formatted traces of 20 sec length with the appropriate header words had been created, the data were also archived. Finally, a third set was stored and archived after the shipboard processing, as described above, had been applied. All final processed SEGY data were archived on a single tape. For safty reasons, we did every backup twice. Thus, in total, 14 DAT tapes were used for archiving all seismic data.

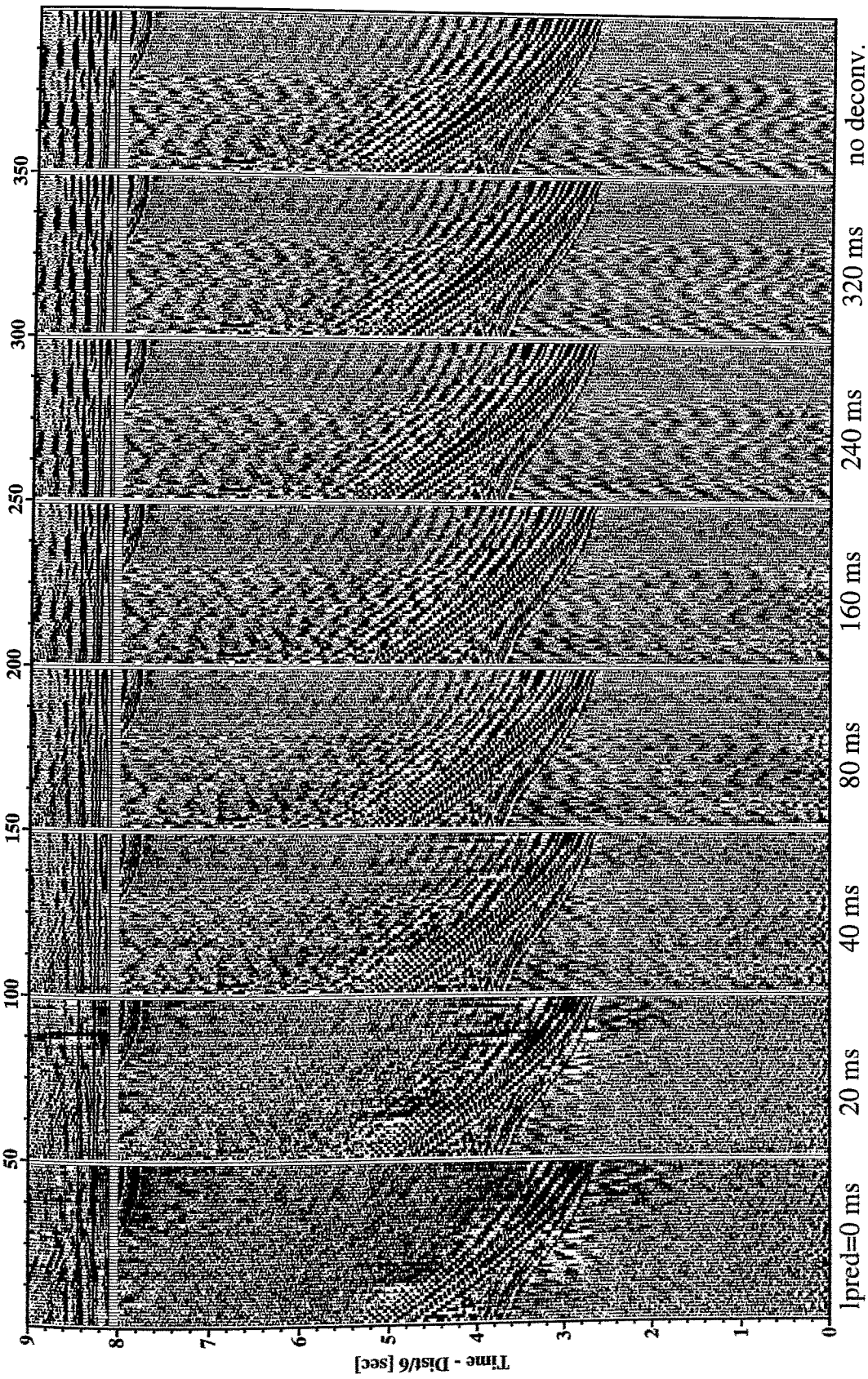

Figure 6.3.2.3: Deconvolution test obh06, offset range 2-8 km, gated with 2 s window, operator length 480 ms, different predictive lengths. Autocorrelation is given between 6 and 7 s.

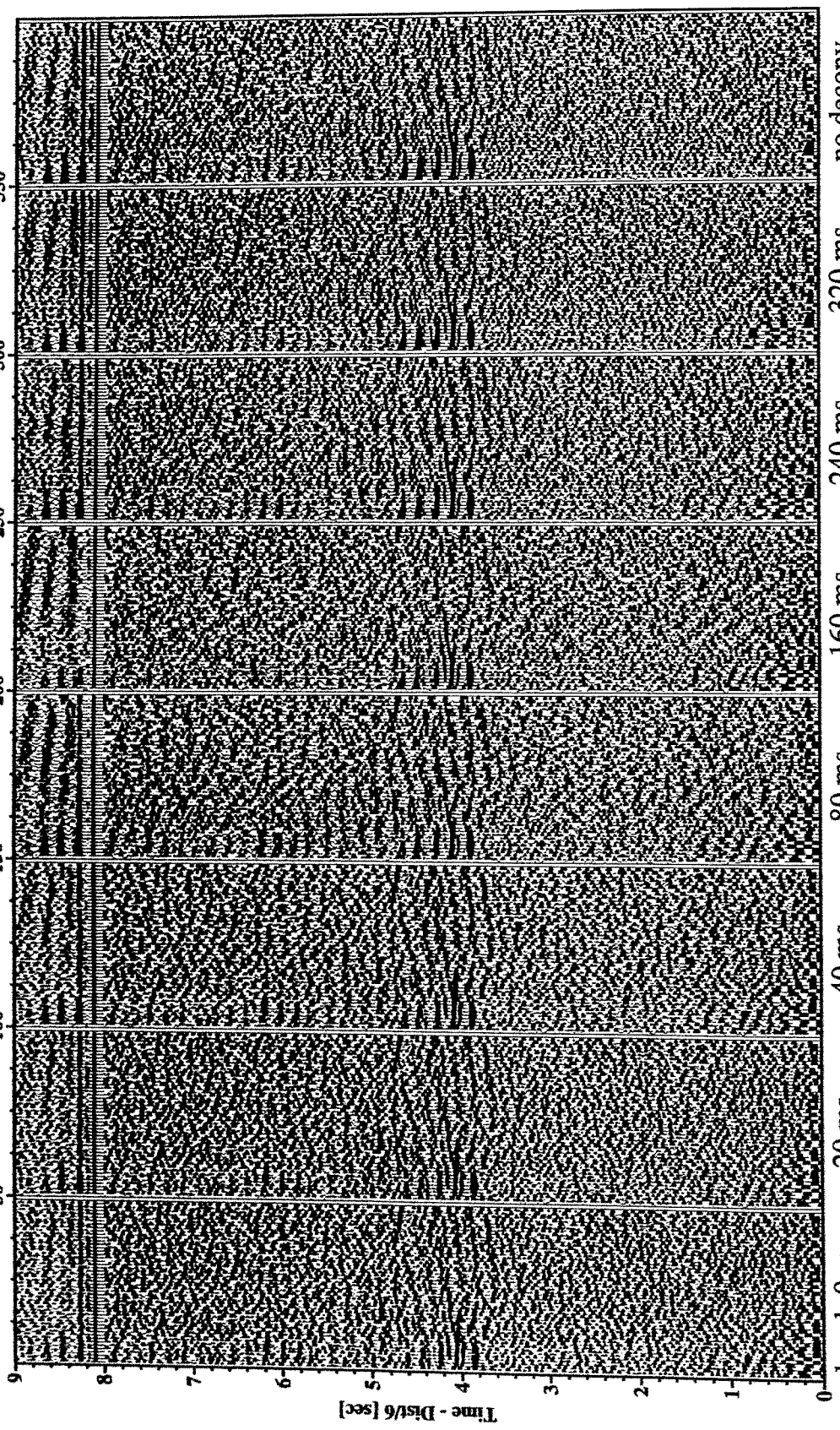

Figure 6.3.2.4: Deconvolution test obh05, offset range 30-36 km, gated with 2 s window, operator length 480 ms, different predictive lengths. Autocorrelation is given between 6 and 7 s.

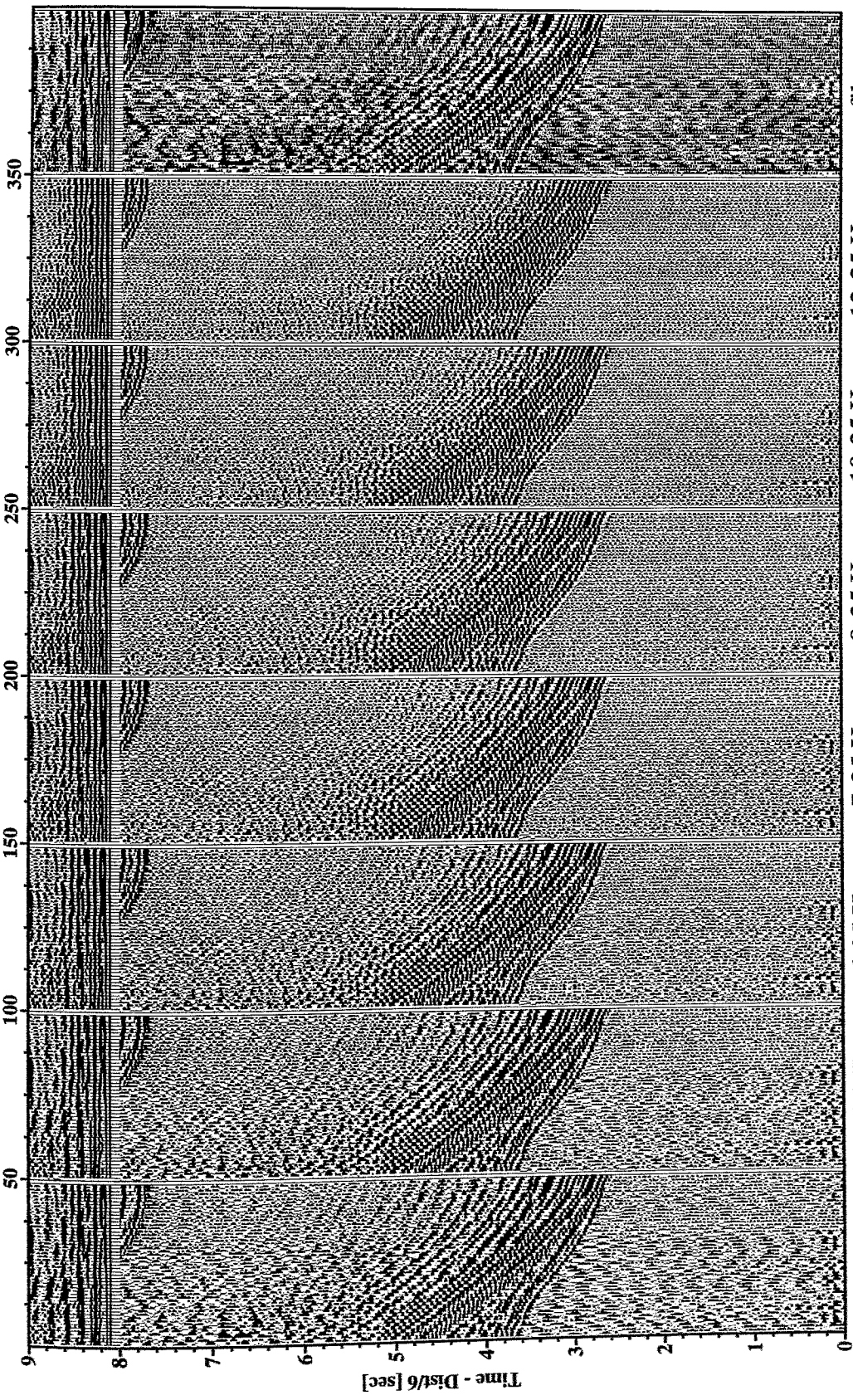

Figure 6.3.2.5: Filtertest obh06, offset range 2-8 km, different bandpass filters. Autocorrelation is given between 8 and 9 s.

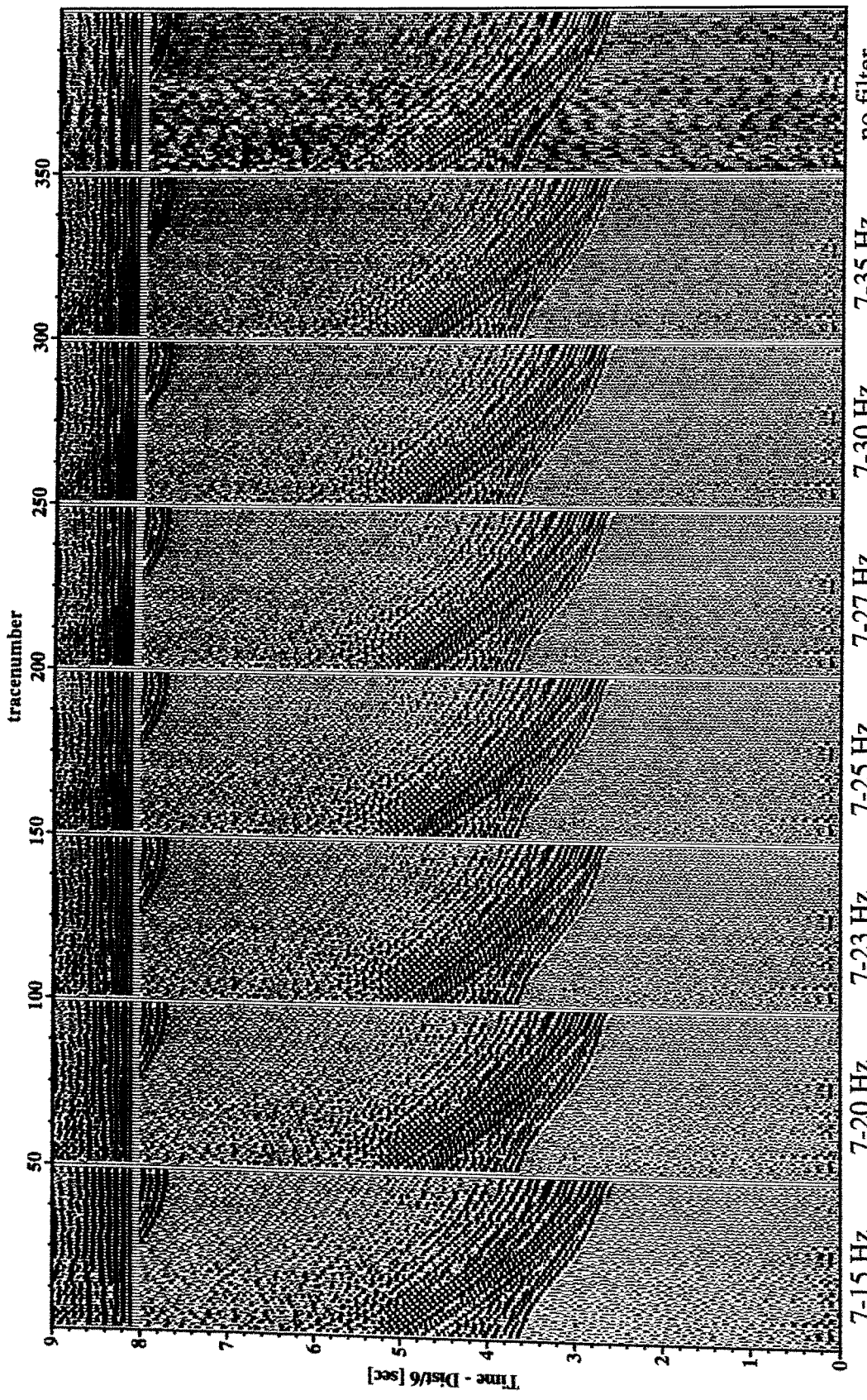

Figure 6.3.2.6: Filtertest obh06, offset range 2-8 km, different bandpass filters. Autocorrelation is given between 8 and 9 s.

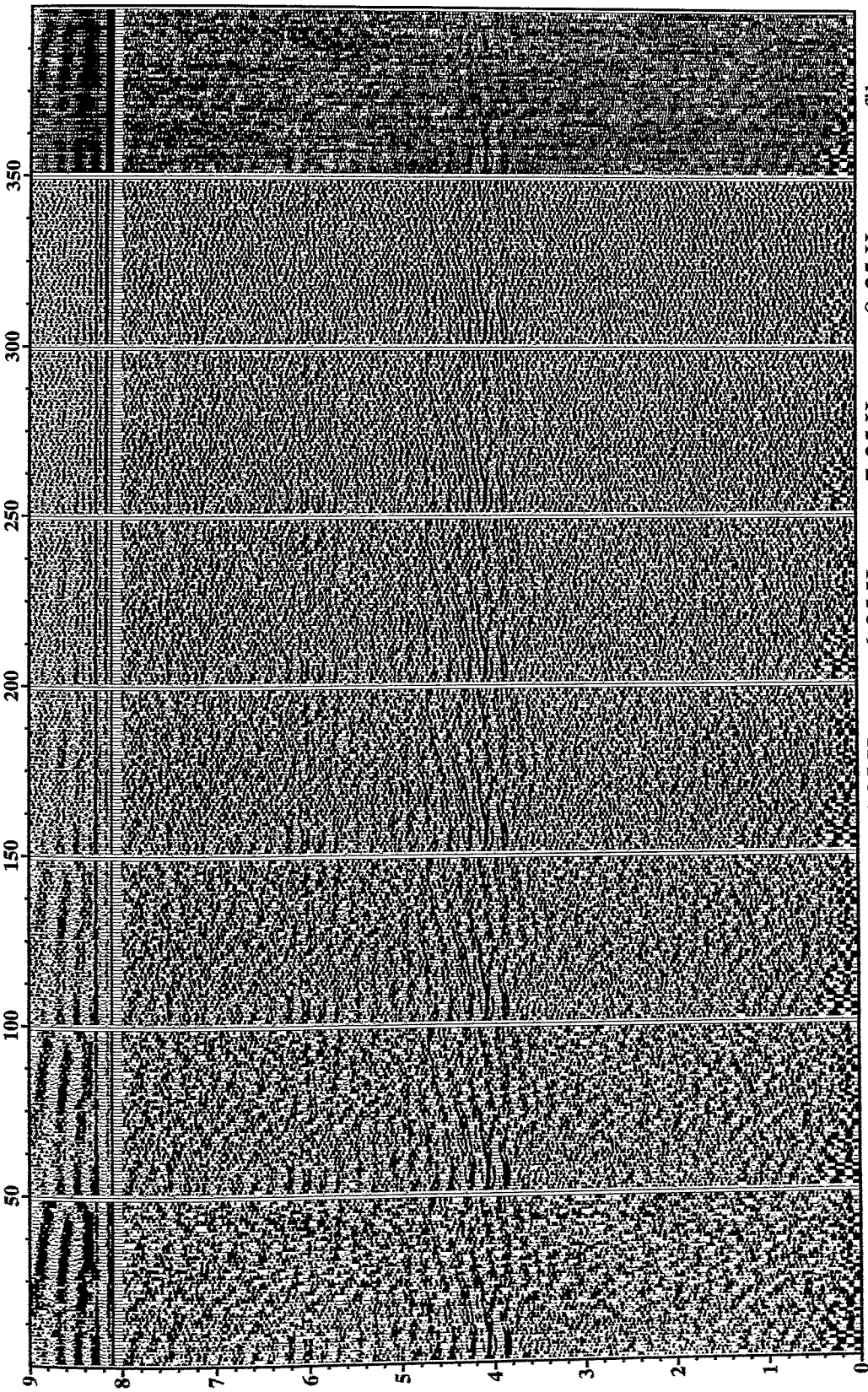

Figure 6.3.2.7: Filtertest obh05, offset range 30-36 km, different bandpass filters. Autocorrelation is given between 8 and 9 s.

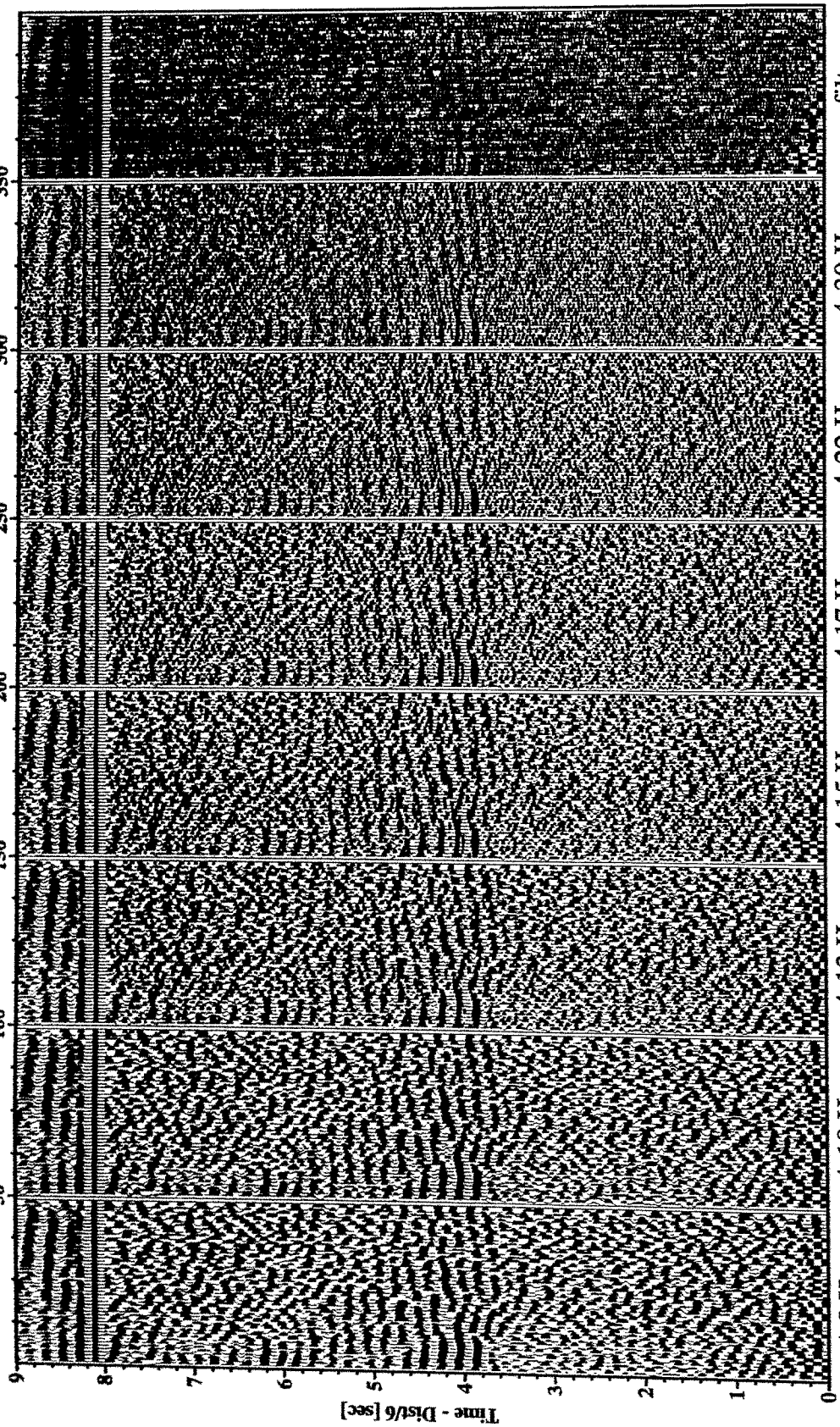

Figure 6.3.2.8: Filtertest obh05, offset range 30-36 km, different bandpass filters. Autocorrelation is given between 8 and 9 s.

6.3.3 WIDE-ANGLE DATA MODELLING

The ocean-bottom hydrophon data were analyzed for crustal and upper mantle velocity structure. The modelling sequence of the wide-angle data involves different steps:

Picking of seismic phases

The travel times of the observed phases are interactively picked using the ZPLOT-program written by Colin Zelt of Rice University, Texas. Generally, we observed two crustal refraction branches sampling the lava pile forming the upper crust and lower crustal grabbros. In addition, the record sections indicate strong PmP-Phases (wide-angle reflections from the crust/mantle boundary) and clear Pn-Phases of energy turning within the uppermost mantle. The PARASOUND-echosounder supports only insignificantly sedimented volcanic bedrock; thus the sediment blanket is too thin to provide any refaction branch. The picked arrivals are archived as ASCII tables containing source/receiver distance, travel time and phase identification. These informations are used later for modeling and inversion.

Modeling and Inversion

First, 1-dimensional velocity-depth modeling was performed on some of the record sections. This first approach was choosen to estimate the velocity structure along the different lines and allows an assessment of preliminary velocity-depth models, which are used as starting point for 2-dimensional ray tracing. The software used for this purpose is an interactive program "MacR1D" (Luetgert, 1992) for calculating travel times from 1-dimensional velocity-depth functions. It allows a quick manipulation of velocity-depth functions and the resulting travel times can be seen immediately. Thus, "MacR1D" gives useful insights into the effects of changing gradients, low-velocity zones, etc.

Two-dimensional models have been created for all profiles. The water depth is taken from the UKOOA-files. The models are capable of predicting the correct offset/time of as many of the observed phases as possible. During the cruise, we used the program "MacRay" (Luetgert, 1992), an interactive application for calculating travel-time curves from 2-dimensional velocity models. It is based upon the RAY84 and RAY86 seismic raytracing programs written for the DEC VAX/VMS environment and adapted to the Apple Macintosh graphical interface for display and manipulation of the velocity models. A second code available is the 2-dimensional forward modeling and inversion packaged "RAYINVR" described by Zelt & Smith (1992). This program runs on the Sun-Workstations and allows the rapid calculation of travel times through laterally heterogeneous structures.

For both codes the velocity models are defined by two or more interfaces extending across the model. Any pair of successive interfaces describes a layer, within which the velocity may be defined in terms of the velocity at the top and bottom of the layer. Within any layer the velocity may be inhomogeneous but continuous. First or second order discontinuities in velocity may occur at the interfaces. A ray tracing algorithm calculates the propagation of rays within a layer by the stepwise integration of a system of first order differential equations, i.e. using asymtotic ray theory (Cerveny et al., 1977). Lithologic interfaces are represented in the models as first or second order velocity discontinuities. When an interface is encountered in the calculation of a ray, Snell's law is applied and the calculation is continued. "MacRay" is very useful for quick

manipulation of velocity models while the "RAYINVR"-code is useful for modeling profiles with densly spaced OBHs.

In addition, we applied a 2-dimensional tomographic inversion to yield a crustal structure model from first arrivals. The tomographic method of RAYTOMORF relies on travel time computation of first arrivals using a finite difference (FD) algorithm and on a nonlinear inversion of arrival times for subsurface slowness (Parson et al., 1996). The FD algorithm is based on equations developed by Vidale (1988) and modified by Ammon and Vidale (1993) to handle media with stong velocity variations. After determination of the travel time field rays are traced through it and ray length segments are computed for each cell. Then the ray length matrix is inverted for a set of slowness correction values. The inversion of the slowness correction vector is performed using conjugate gradients (LSQR). The code enables to vary the weigthing factor for the minimazation of the Laplacian smoothness of the slowness correction vector as well as the number of iterations in the LSQR matrix inversion. Model calculations were done within a recursive loop using the last inverted model as the input for the next inversion.

6.3.4 SEISMIC PROFILES
6.3.4.1 PROFILE SO142-01

Profile SO141-01 was a test line to study energy propagation and gather some first information on crustal velocities for optimization of later deployments. It was also a practice run for the deployment / retrieval of the airguns, had never been made after the recent refitting of the ship. Five OBHs (OBH1, OBH03-to OBH06) were deployed between 05:15 and 07:30 on 06.06. The instruments were all placed in groups of two in order to allow a simultaneous release of two instruments instantaneously, thereby reducing recovery time. In addition, OBH02 was deployed without a recorder for test purposes only. Deployment of the one airgun lasted a little more than 30 minutes, and shooting was done from 08:40 to 16:00 along a 25 nm profile, with a shot rate of 60 s. Details on shooting and instrumentation can be found in Appendices 9.1.1 and 9.1.5., and the location of the profile and the instruments is shown in Figure 6.3.4.1.1. All instruments were recovered between 16:00 and 22:30. During each recovery two neighboring stations were released using the hull-mounted transducer of the vessel from a distance of 3.5 to 4 nm during transit. The rising of the instruments was then monitored using the active transducer on the W6 winch, once the ship had come to a complete stop.

Four of the five instruments recorded well, the data were processed as described in chapter 6.3.2 and the record sections for the data are shown in Figures 6.3.4.1.2 to 6.3.4.1.5. OBH03 showed only clipped signals, a discussion of this malfunctioning is given in 5.2. OBH01 was unfortunately placed close to an unknown seamount (see Figure 6.3.4.1.1), and diffracted water waves from this seamount caused the first arrivals near the instrument to be masked.

Modeling results and interpretation

P-wave first arrivals and major wide angle reflections were picked from the seismic sections. Based on the traveltime data of these 4 OBHs, a ray tracing forward modelling was performed using the interactive *MacRay* program (Luetgert, 1992). Subsequently a velocity model of profile SO142-01 was achieved, which is shown in Figure 6.3.4.1.6. On most record sections there is no evidence for any noticeble sediment on the oceanic crust. Clear PmP arrivals are seen starting around 20 km distance and also clear S-waves can be recognized, especially on OBH01, 04, and 05. However, no Pn-arrival is evident and all sections are too short to fully describe the subsurface structure. OBH06 has the poorest signal-to-noise ratio, and since it is go close to OBH05, it was not taken into account during modelling. First arrivals from the oceanic crust are generally strongly disturbed by the seafloor topography, but nevertheless can be followed throughout the sections. The northwestern end of the profile passes close to a ridge and seamount (see Figure 6.3.4.1), and diffractions from this seamount mask the first arrivals from the oceanic crust in the record section from OBH01 (Figure 6.3.4.2), and out of plane arrivals are also evident on OBH04 to the NW. A simple model with a two layer oceanic crust without any velocity discontinuity satisfies all first arrivals. The upper crust is about 2 km thick and characterized by a high velocity gradient (5.0 to 6.0 km/s), in the 4 km thick lower crust the velocity increase to about 7.2 km/s. Assuming a velocity contrast from 7.2 to 8.0 km/s, the critical distance for the PMP arrival is closely matched. OBH05 is located on Donizetti seamount, and first arrivals are somewhat reduced. Here a layer with velocities increasing from 4.0 to 4.5 km/s was introduced. This indicates that the seamount seems to be resting on the normal oceanic crust. It should be mentioned however, that there is no PmP coverage below the seamount, and that the lower crustal velocities and possible changes along the line are not constrained by the data. Around OBH04 in the deepest part of the basin a 200 m thick layer with an average velocity of 2.0 km/s was introduced to match a slight delay of all arrivals in this part of the model. A more detailed study of the seamounts and volcanic ridges was achieved on the other three profiles. In comparison to those profiles, the model obtained for profile SO142-01 fits into the general picture and results.

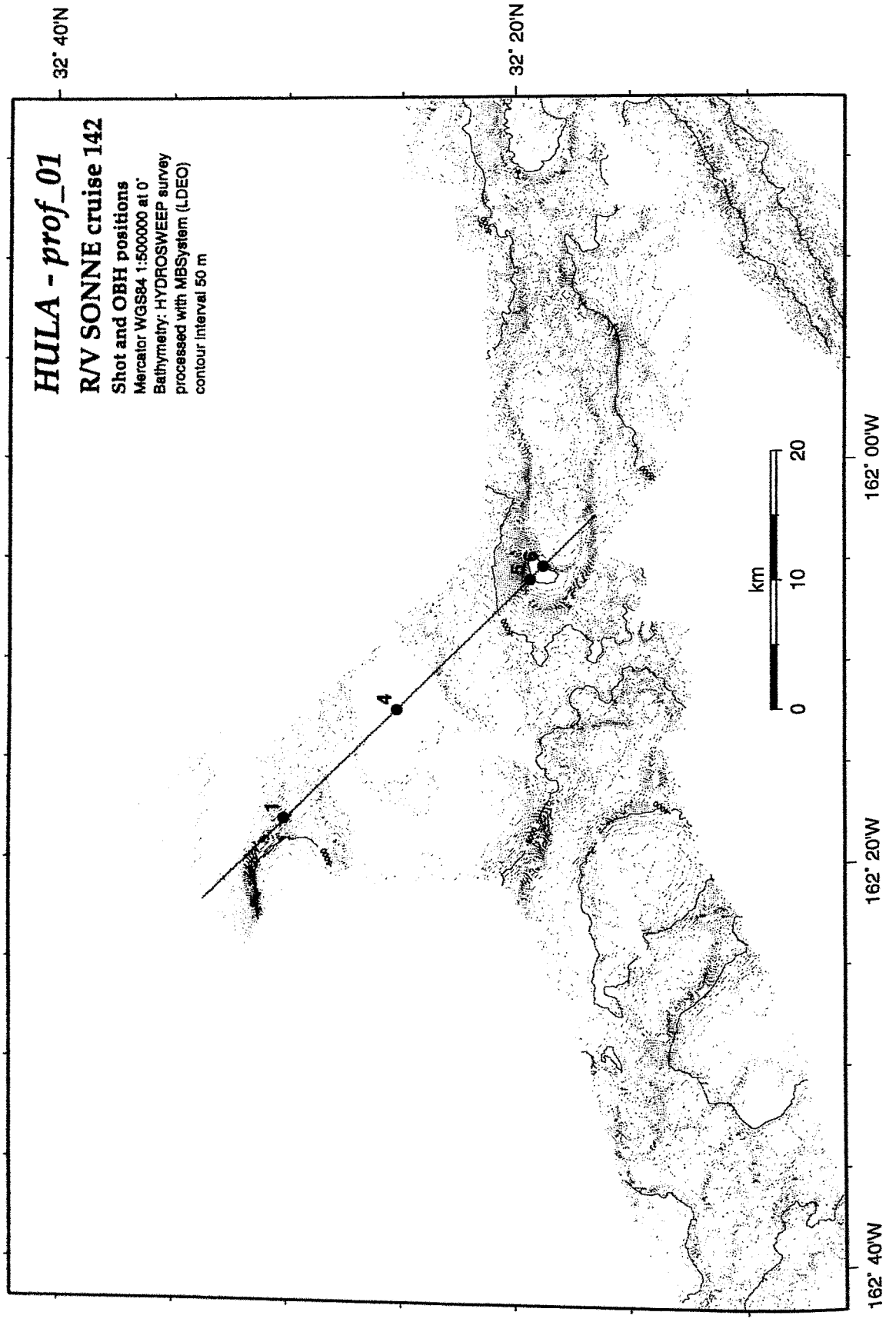

Figure 6.3.4.1.1: Profile 01 - Shot and OBH positions.

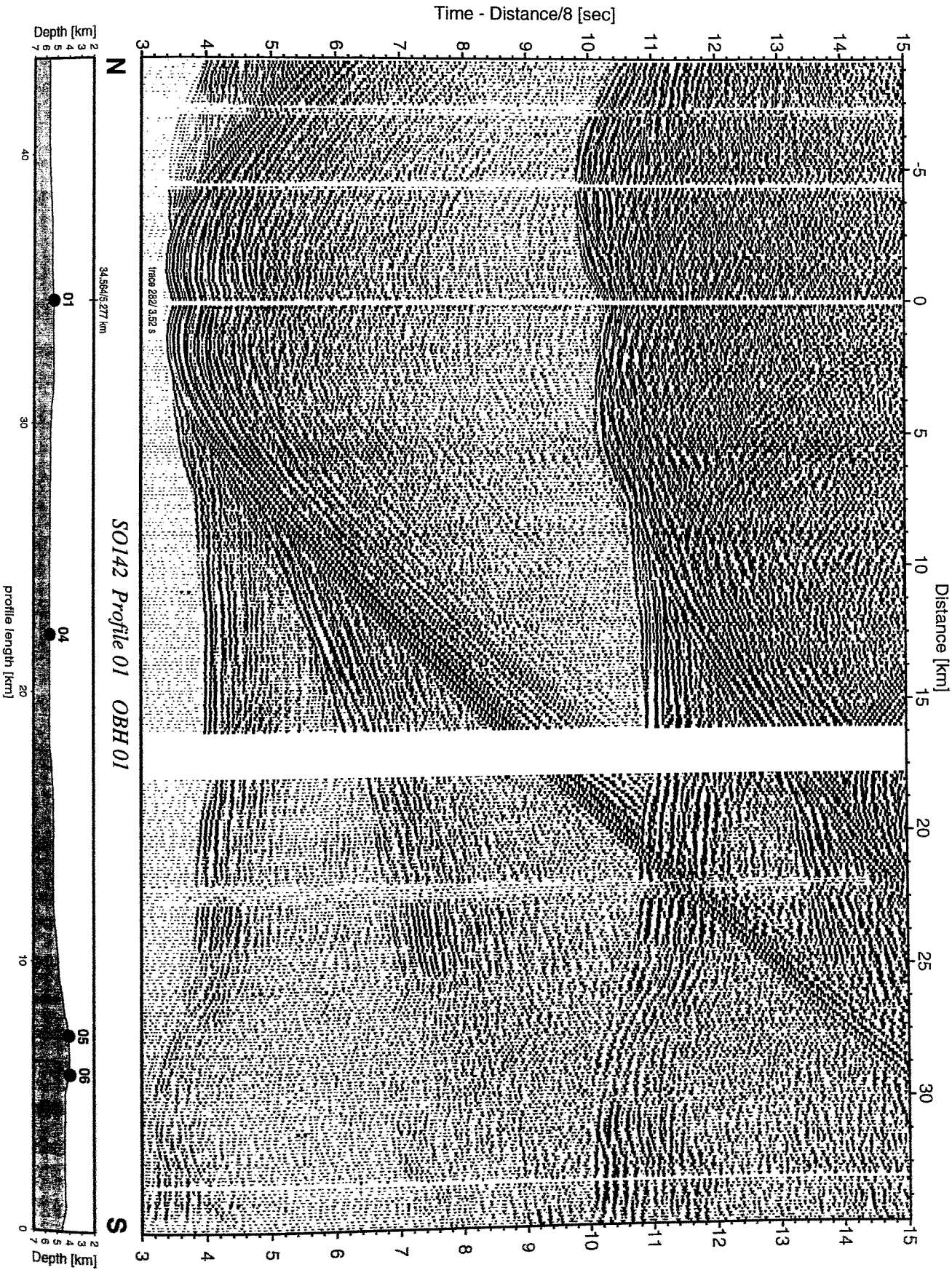

Figure 6.3.4.1.2: Record section from OBH 01 , Profile 01.

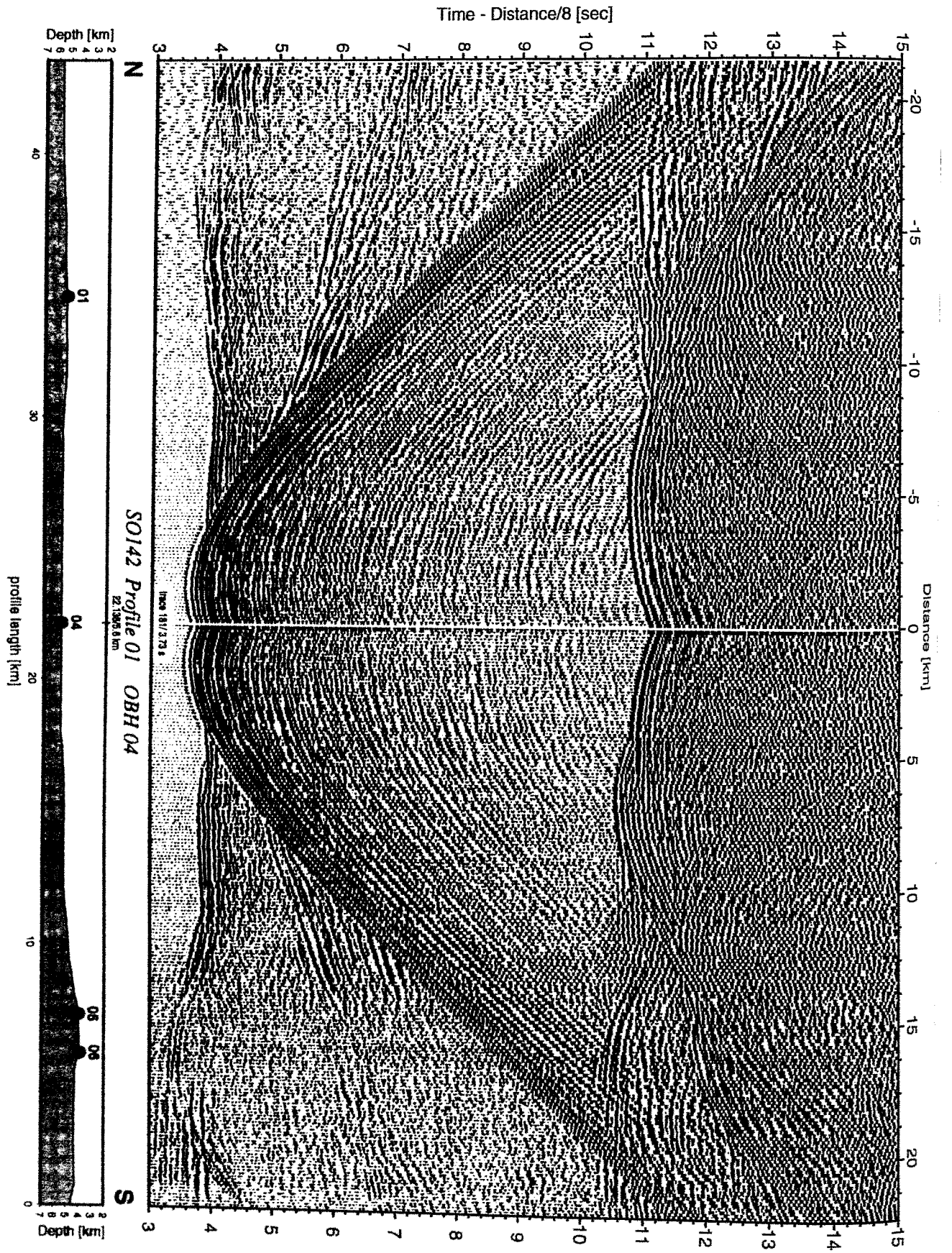

Figure 6.3.4.1.3: Record section from OBH 04 , Profile 01.

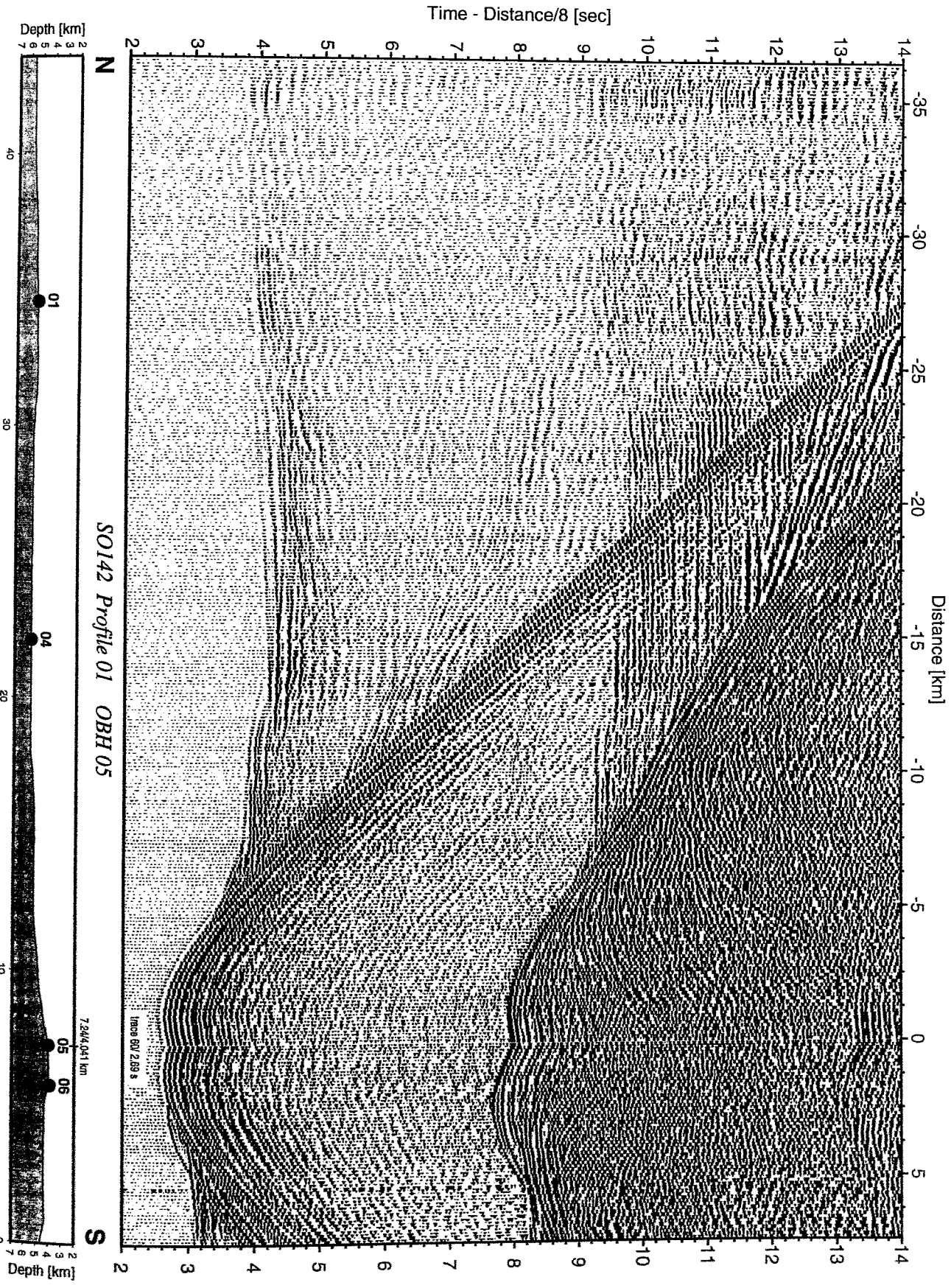

Figure 6.3.4.1.4: Record section from OBH 05 , Profile 01.

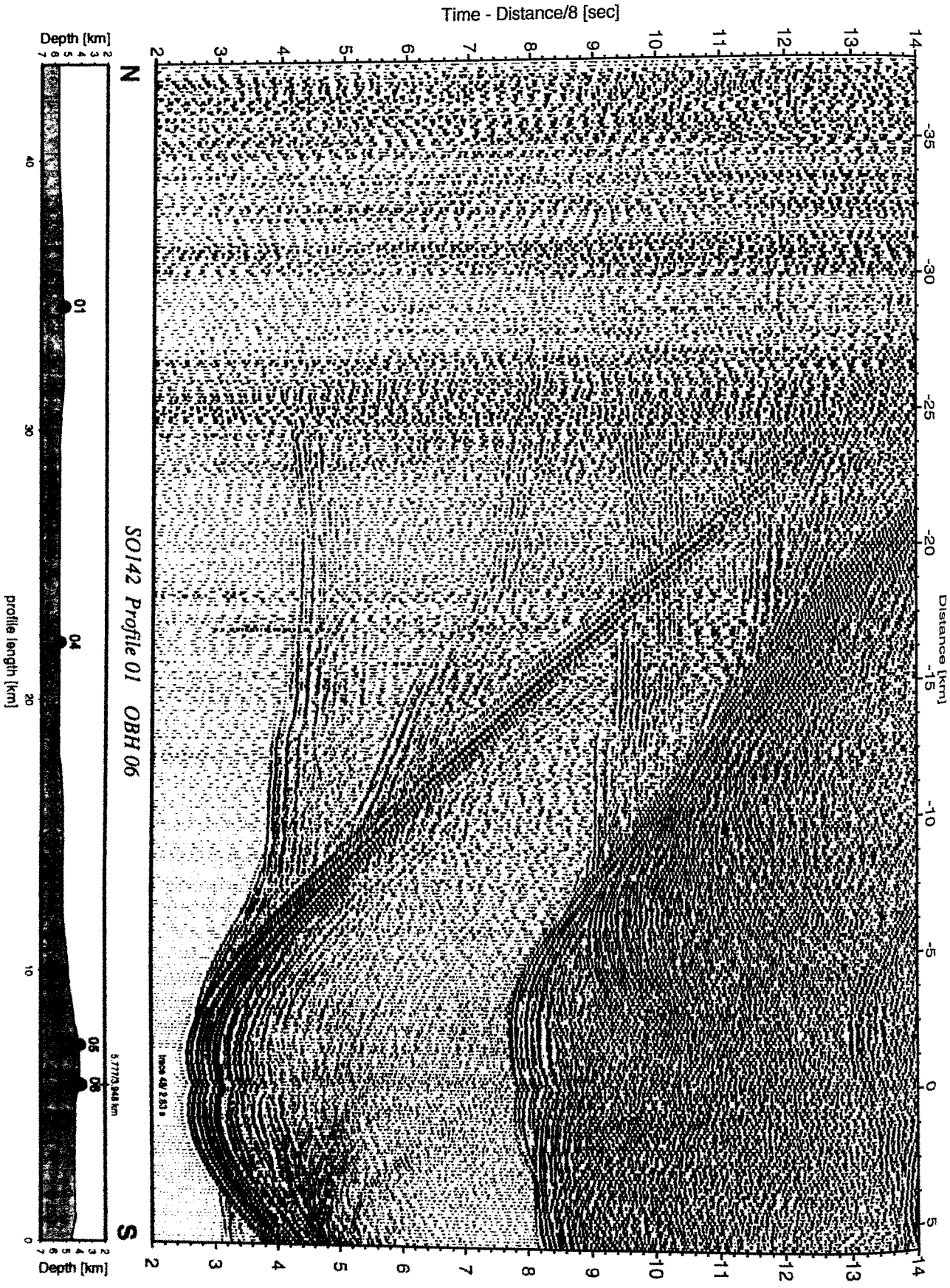

Figure 6.3.4.1.5: Record section from OBH 06 , Profile 01.

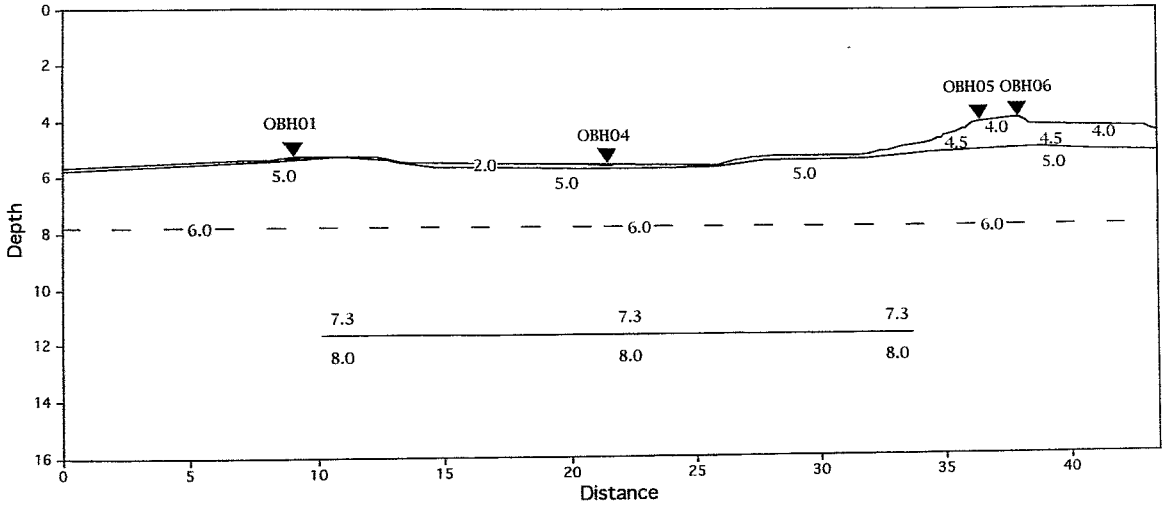

Figure 6.3.4.1.6: 2D-velocity model for profile SO142-01gained from ray tracing forward modelling. No significant sediment layer is found on the oceanic crust. A two layer oceanic crust model consisting of a 2 km thick upper crust and a 4 km thick lower crust fits all first arrivals.

6.3.4.2 PROFILE SO142-02

Profile SO142-02 is a dip profile across the Italian Ridge in the northern Musican Seamount survey area at about 32°15'N and crossed the ridge near its eastern end. Many seamounts along this ridge are named according to famous italian componists; we therefore called the ridge the Italian Ridge. The profile was choosen after swathmapping the ridge and crosses it at the location of one of the major seamounts, reaching to depth of less than 3000 m. The profile strikes N-S and therefore is located along an isochron regarding the age of the oceanic crust. Based on preliminary inspection of the data from profile SO142-01, an instrument spacing of 3 nm was choosen, and shooting was extended by 30 nm on both ends, thus assuring a good PmP and Pn coverage.

Along the profile 13 instruments (OBH07 to OBH19) were deployed between 06:00 and 11:00 on 09. June. Details on instrumentation can be found in Appendix 9.1.2, the location of the instruments and the extension of the shooting lines is given in Figure 6.3.4.2.1. Deployment of the two airguns started 40 nm ahead of the first instrument on 09.06.1999 at 15:00 and both guns were operational at 16:00, after some initial trigger problems were solved. The shot intervals was set to 60s, and the average speed was 3.7 kn, resulting in a shot spacing of about 115 m along profile SO142-02. It was terminated on 10.06.1999 at 18:00 about 30 miles north of the recording array. No malfunctioning of the guns was encountered, despite increasing winds during shooting, reaching force 6, and a course against the wind. At a few places the supply cable showed signs of high mechanical forces, these were reinforced before the next deployment. After a transit line parallel to the shooting line the instruments were all recovered between 01:00 and 13:30 the next day. Since also the active transducer failed, no release command was acknowledged from any instrument, but judging from the pop-up time all instruments were released upon the first command send, usually from a position about 3.5 to 4.0 nm away of the instrument. These early release commands reduced the waiting time for rising instruments considerably.

Apparently all instruments recorded all shots rather well, but the record sections from the instruments equipped with DAT recorders could not be produced onboard, but could be checked for functionality. The remaining record sections are all of superb quality, they are shown in Figures 6.3.4.2.2 to 6.3.4.2.8. A preliminary interpretation was attempted and is described below.

Modeling and interpretation of profile SO142-02

For modeling and interpretation of profile SO142-02, the record sections of OBH 07, 09, 10, 11 and 16-18 were used, which show arrivals of up to 100 km offset. The main phases to be identified on all record sections are the water-wave, two crustal refraction branches from upper and lower crustal rocks and PmP and Pn arrivals from the crust/mantle boundary and the uppermost mantle. As described in chapter 6.3.3. these arrivals were picked interactively. A low ambient noise level and the good quality of waveforms made picking of the first breaks relatively straightforward. However, rays turning within the ridge and those transiting it are often plagued with diffractions, multipathing events and out-of-plane scattering from a rough seafloor. Thus for these arrivals and for larger shot/receiver distances the signal-to-noise ratio decreases. The largest uncertainties of about 100 ms have been assigned to some Pn arrivals.

To derive structural models of crust we used two different approaches: i) forward modeling all travel time data using the 2-dimensional ray tracing algorithm of Zelt and Smith (1992) and ii) applying a non-linear tomographic inversion of first arrivals (Parson et al., 1996). Examples of the ray tracing calculations and the final velocity-depth model are shown in figure 6.3.4.9 and 6.3.4.10, respectively. Figures 6.3.4.11 and 6.3.4.12 are presenting some results from the tomographic inversion. The resulting models, however, are basically the same and a number of conclusions can be reached:

Velocities at the top of the cretaceous crust adjacent to the elongated ridge are about 4.4 km/s and are therefore in excellent agreement with upper crustal velocity versus age trends derived by recent studies (Grevemeyer and Weigel, 1996; Carlson, 1998; Grevemeyer et al., 1999). The basaltic upper crust or layer 2 is 1.8 to 2 km thick and therefore as well typically oceanic. Other large size seamounts, like the Marquesas (Wolfe et al., 1994), the Hawaiian Islands (Rees et al., 1993) or the Great Meteor Seamount (Weigel and Grevemeyer, 1999) very often provided thick

sequences of volcaniclastic material that cover the adjacent oceanic crust. These deposits form while a seamount reach a shallow water to submarine environment. Velocities of such deposits are 3-4 km/s (Rees et al., 1993; Wolfe et al., 1994). Because these values are quite similar to velocities of basement rocks seismic refraction studies may not reveal the boundary between igneous basement and volcaniclastic fill in sediments. Consequently, the resultant seismic model may provide a reasonably thick layer-2-type sequence at the top of oceanic crust adjacent to a seamount (Weigel and Grevemeyer, 1999). However, the typical layer 2 properties indicate that mass wasting processes have not been improtant during the creation of the Italian Ridge. The crust has a thickness of about 7 km, which is as well clearly oceanic (White et al., 1992). We therefore conclude that the preexisting crust can be classified as typical matured oceanic crust.

For the edifice of the elongated ridge, the data analysis yielded reasonably low velocities (3.6-4.0 km/s) at the top and values of less than 6.5 km/s are abundant within the feature. Typical velocities of gabbroic rocks (> 6.5 km/s) are encountered at 3-4 km beneath the edifice and the transition from crustal to upper mantle velocities occurs at 15-16 km below sea level, which indicates a Moho depression of about 2-3 km. To made a structural comparision of the ridge and the adjacent crust, we used the correlation between P-velocity as a function of sub-basement depth (see figure 6.3.4.2.12). Most profoundly, the gabbroic section with velocity of more than 6.5 km/s is more or less constant along the profile, indicating that the Italian Ridge is mainly built up of basaltic rocks. In terms of its structure the ridge is similar to off-axis seamounts frequently found along fast spreading ridges (Grevemeyer et al., 1998).

A comaprision between the Italian Ridge and other large size intraplate volcanoes or aseismic ridges (Klein, 1978; Hammer et al, 1994; Weigel and Grevemeyer, 1999; Flueh et al., 1999a) reveals at upper and mid crustal levels striking similarities (figure 6.3.4.2.12), suggesting that the transition from extrusive to intrusive rocks occurs at a similar depth interval. Nevertheless, at lower crustal level and within the uppermost mantle stong differences are evident, such as a thickening of both upper and lower crust at major hotspot islands. Another common feature of hotspot islands are high lower crustal velocities (7.4-7.8 km/s) which are interpreted in terms of intrusions at the base of crust (ten Brink and Brocher, 1987; Caress et al., 1995; Flueh et al., 1999b). The Italian Ridge, however, does not indicate any evidence for thickening of the lower crust or high velocity material added at Moho level. Consequently, the processes acting on typical hotspot islands or seamounts may be quite different than those forming the elongated ridges.

To place additional constraints on the structure of the ridge we calculated a simple gravity model. Using the Fourier method of Parker (1972) we compute the expected gravity anomaly from the observed seafloor topography (which is due to the insignificant sediment blanket coincident with the volcanic basement) and an admittance model and we compare this anomaly with the observed one. Details on the admittance technique are given elsewhere (e.g., McKenzie and Bown, 1976; Watts, 1978). The code used in this study was provided by Helene Herbert from the University of Paris and is describe by Diament and Goslin (1986). The free air anomaly results from the emplacement of a load which deflects the lithospheric plate. The parameter which controls the bending of the plate is the elastic plate thickness (Te). The gravity anomaly depends on the geometry of the main density interfaces, i.e. seafloor and Moho topography, the later being controlled by Te. Classical Airy-type compensation would correspond to a zero rigidity plate (i.e., Te=0). In our model we used a crustal thickness of 7 km, given by the seismic study. Densities for the upper and lower crust and the upper mantle are 2600 kg/m^3, 2850 kg/m^3 and 3300 kg/m^3, respectively. Figure 6.3.4.2.13 shows the best fitting model calculated using a value for Te of 5 km. The excellent fit of the seismically detected Moho boundary with the flexural Moho boundary clearly supports the idea that the ridge was formed primarily by extrusive volcanism which has loaded preexisting oceanic crust.

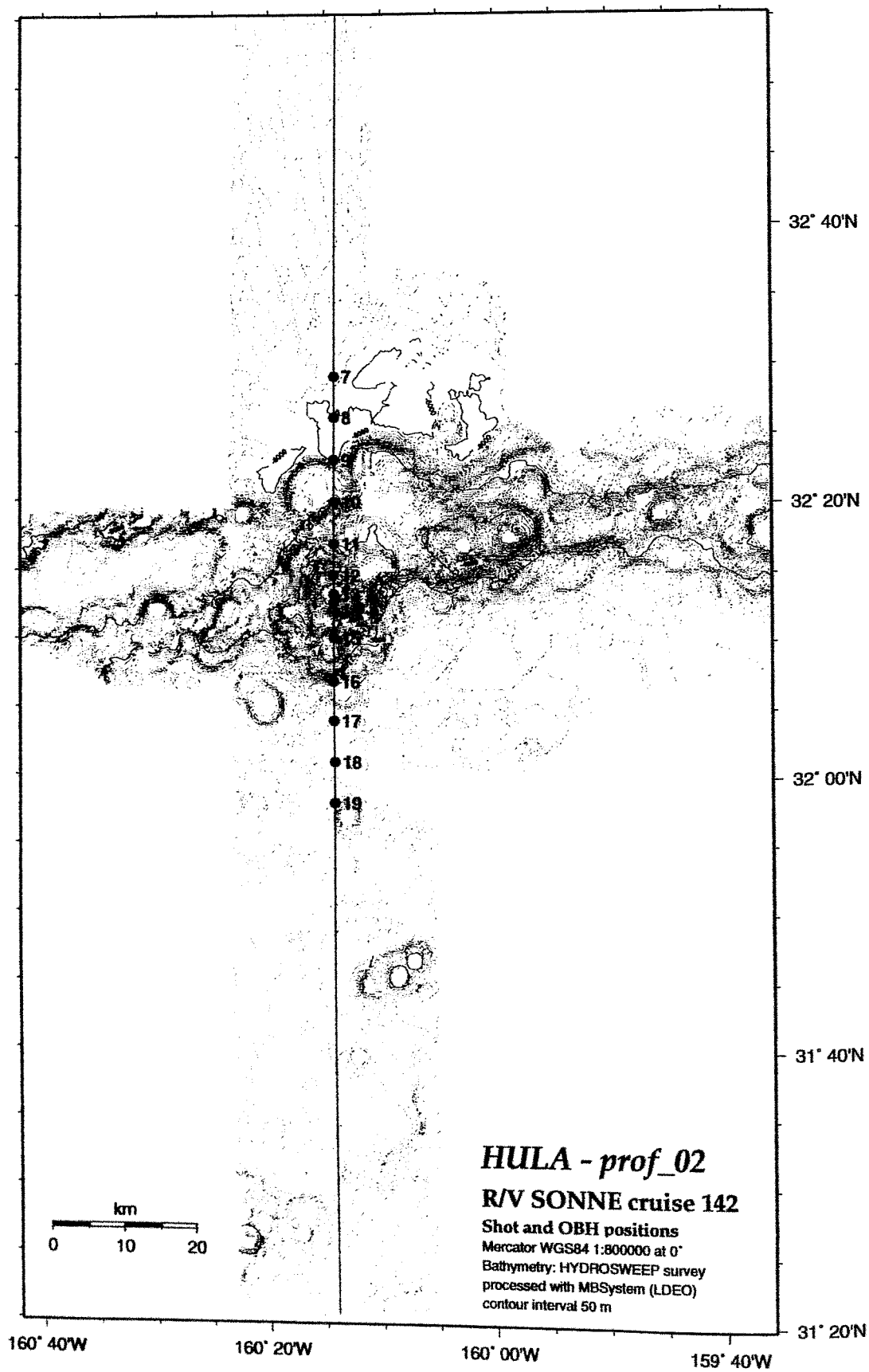

Figure 6.3.4.2.1: Profile 02 - Shot and OBH positions.

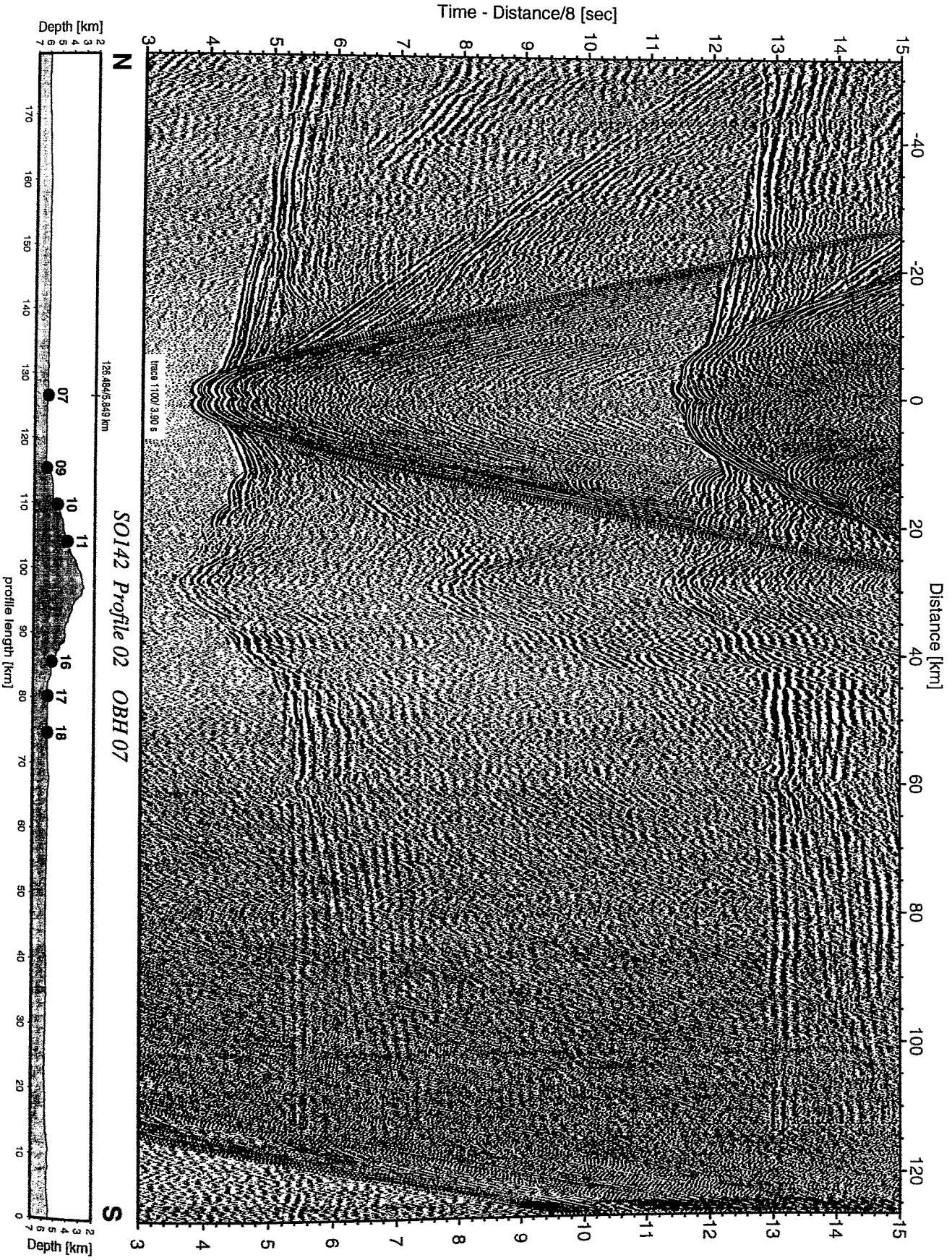

Figure 6.3.4.2.2: Record section from OBH 07 , Profile 02.

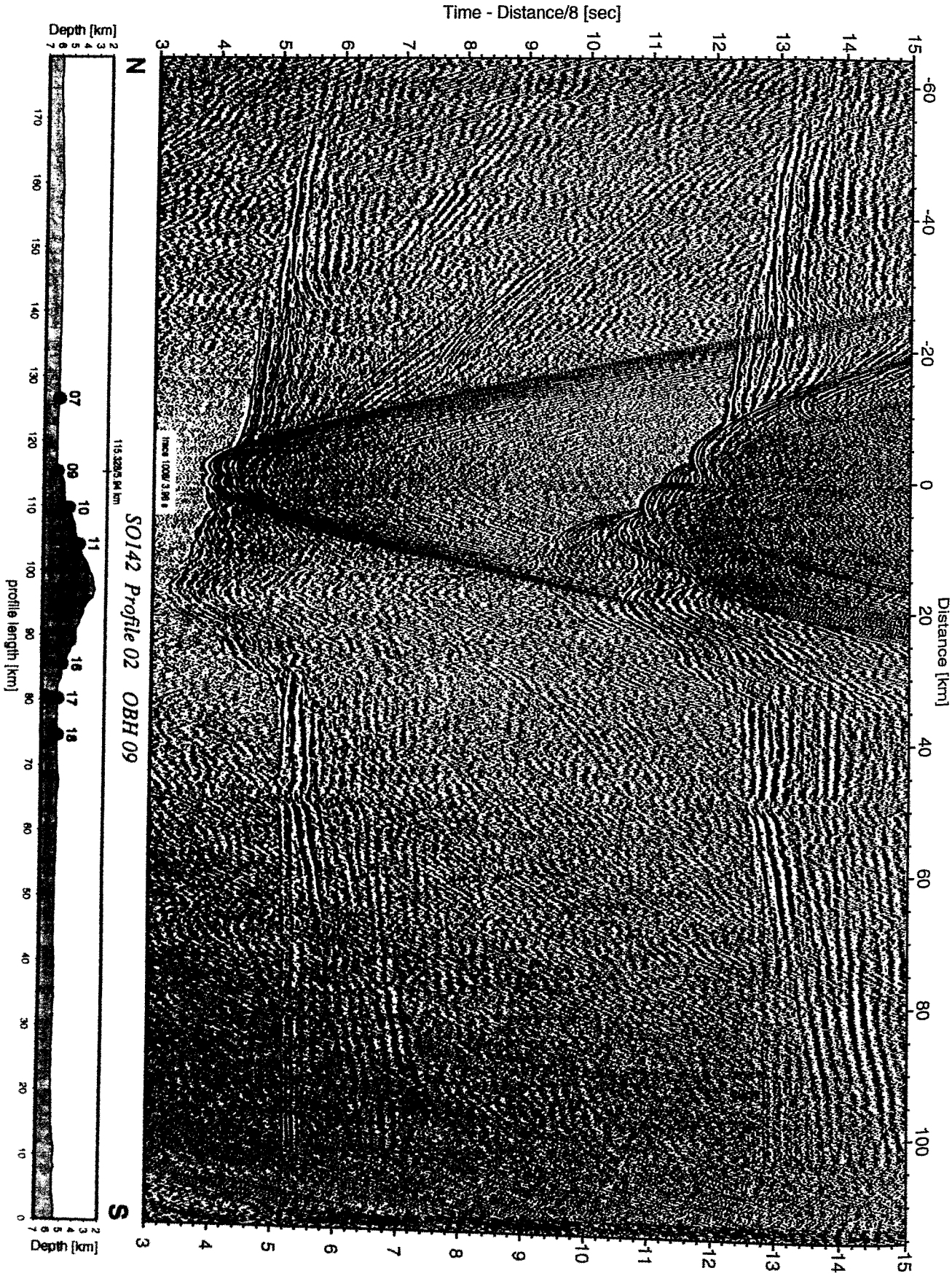

Figure 6.3.4.2.3: Record section from OBH 09 , Profile 02.

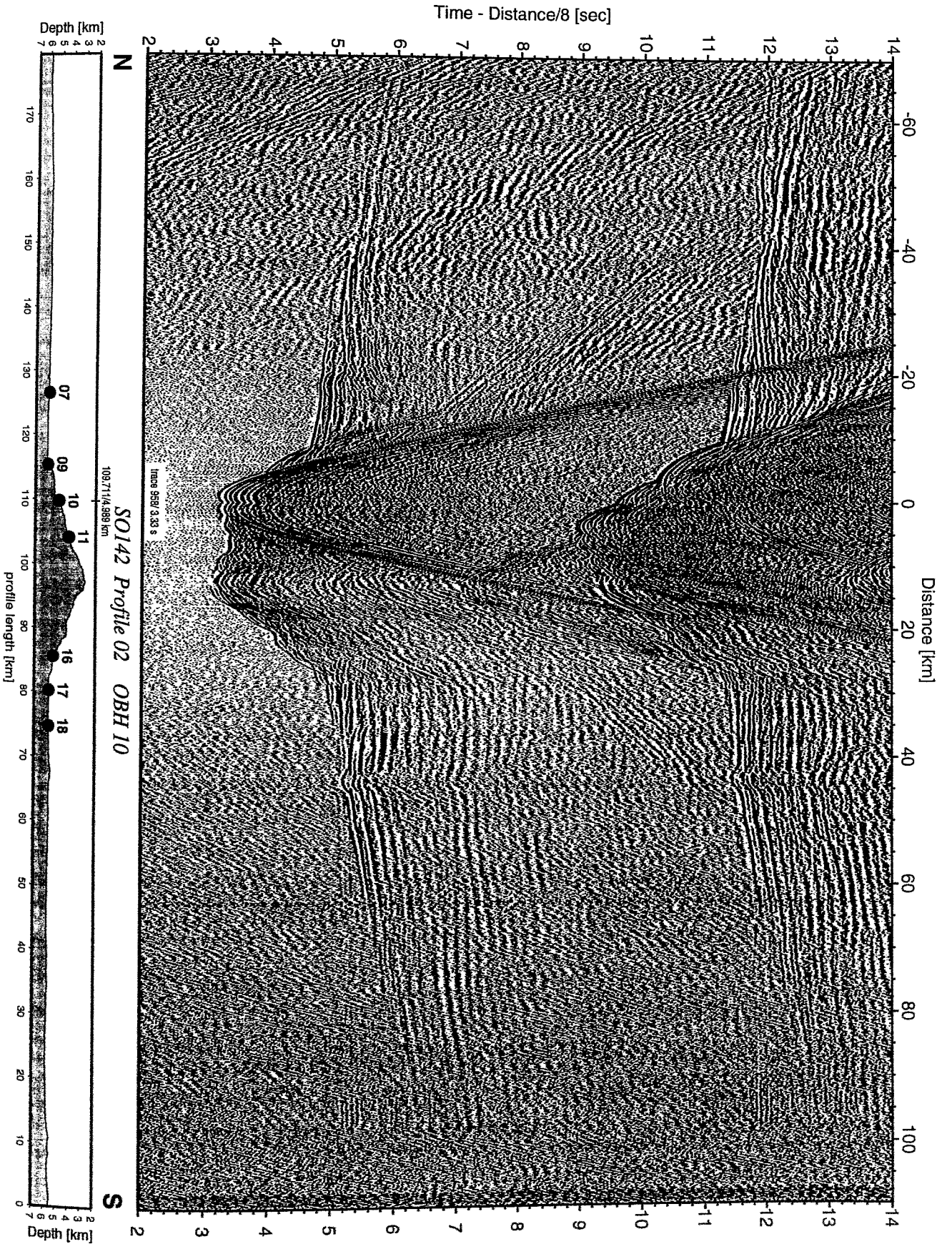

Figure 6.3.4.2.4: Record section from OBH 10 , Profile 02.

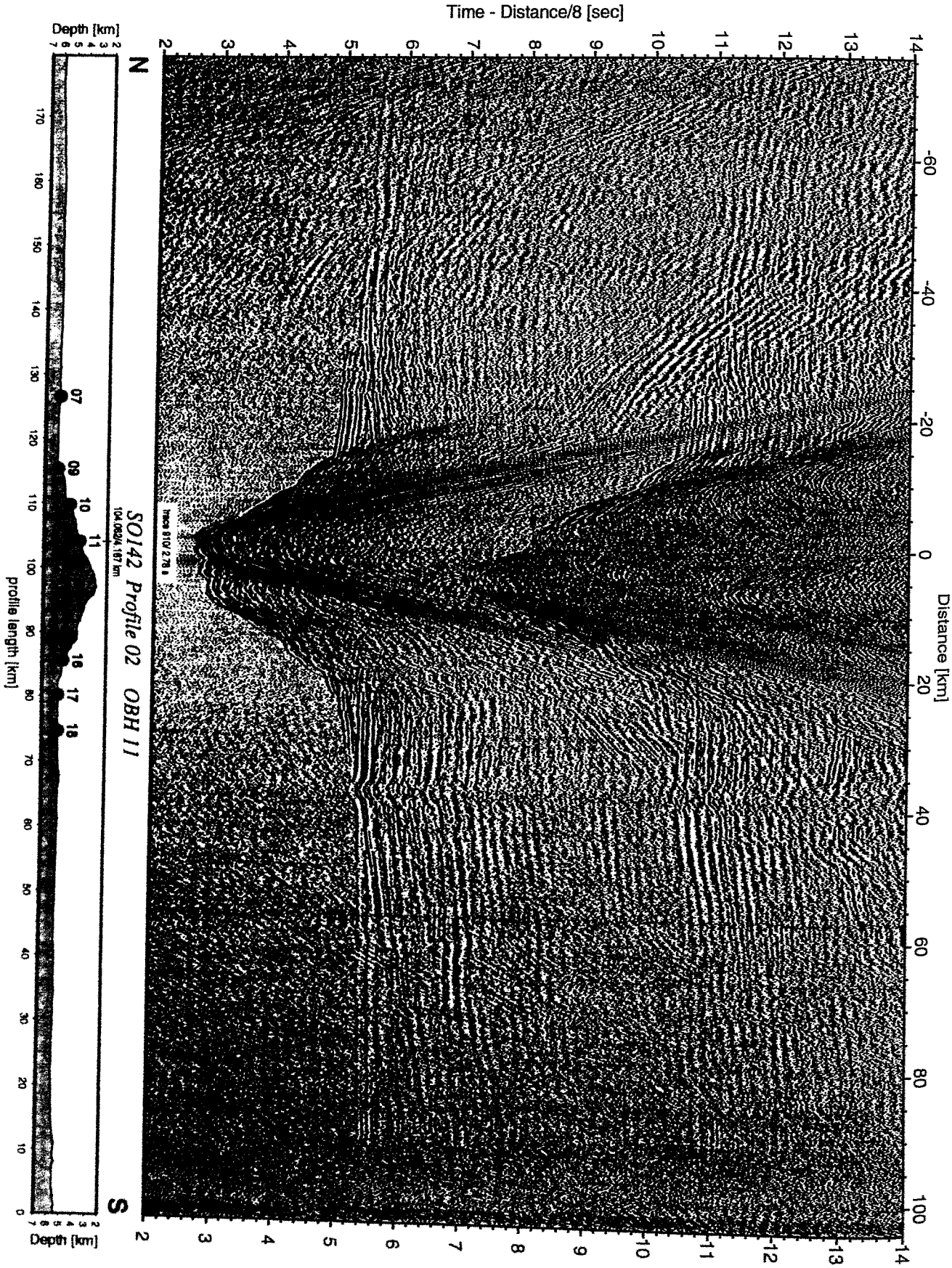

Figure 6.3.4.2.5: Record section from OBH 11 , Profile 02.

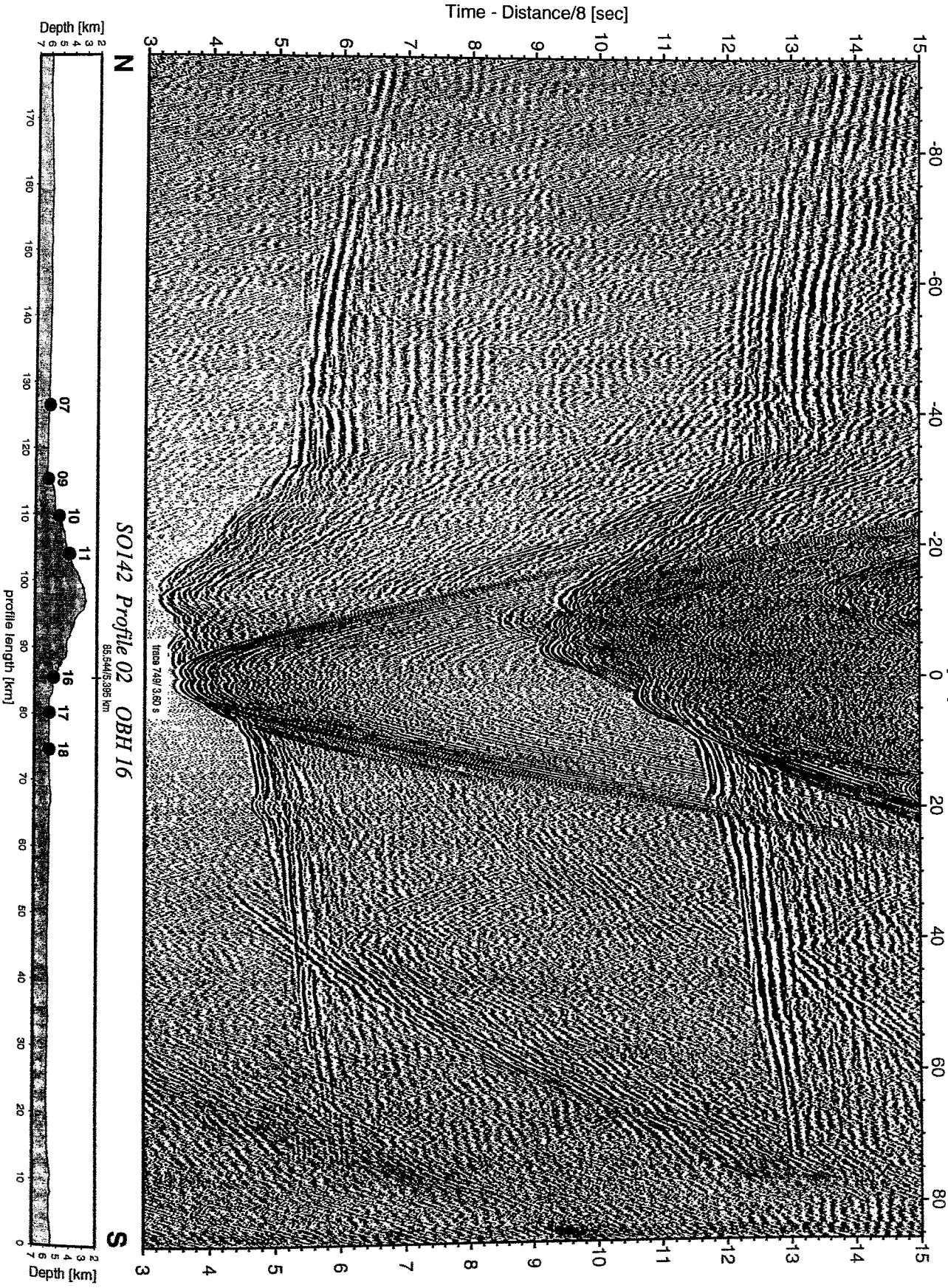

Figure 6.3.4.2.6: Record section from OBH 16 , Profile 02.

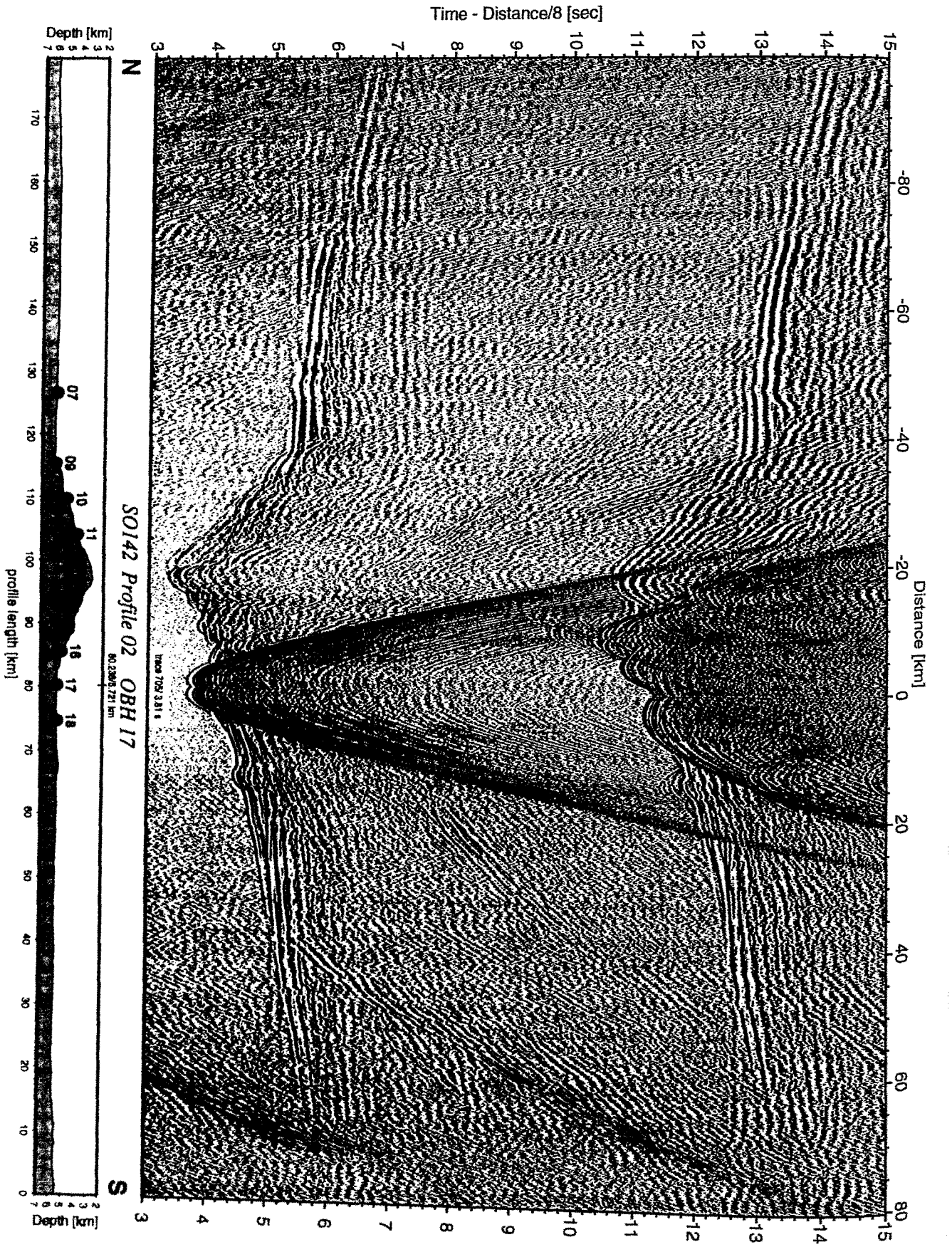

Figure 6.3.4.2.7: Record section from OBH 17 , Profile 02.

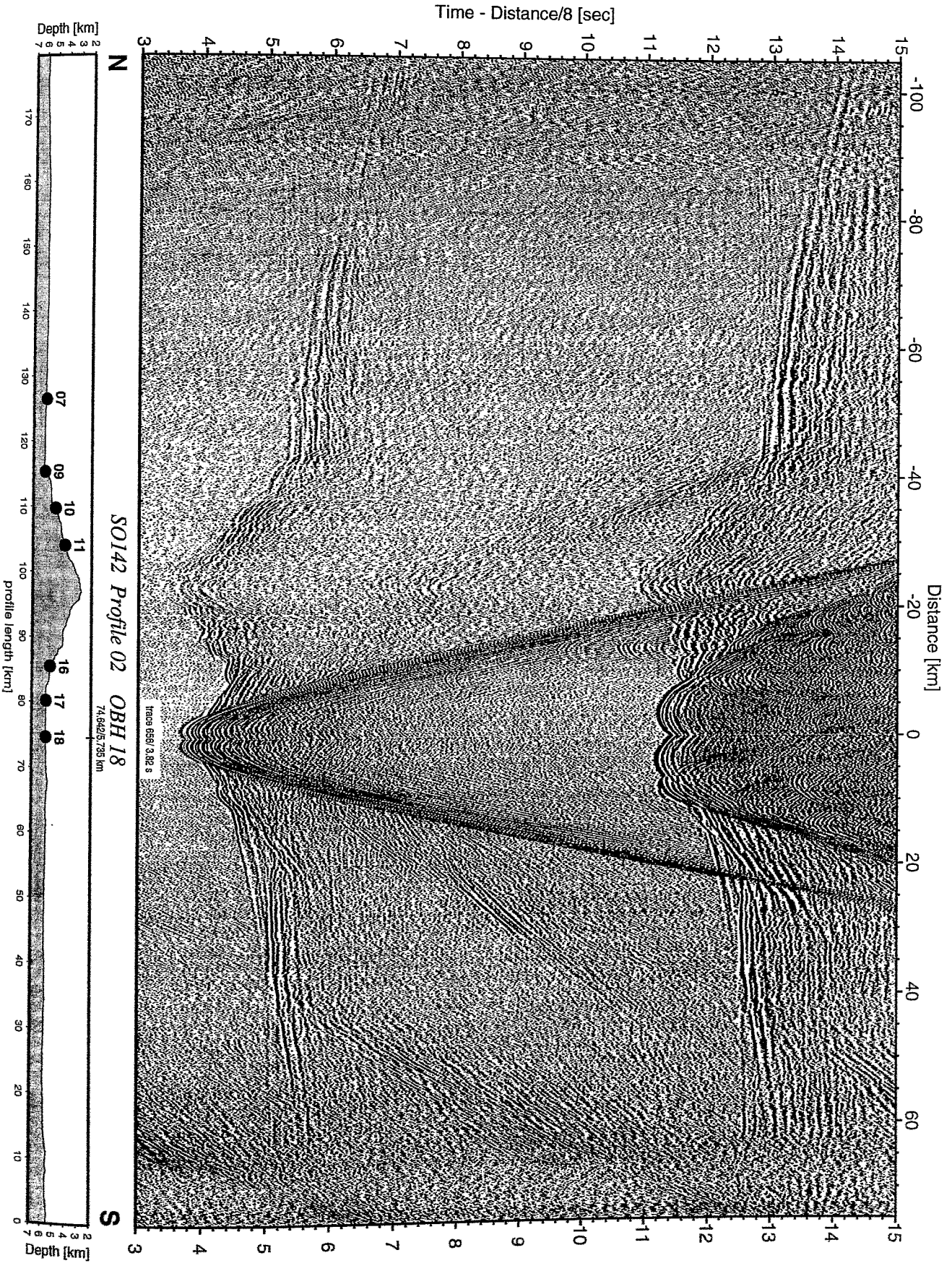

Figure 6.3.4.2.8: Record section from OBH 18 , Profile 02.

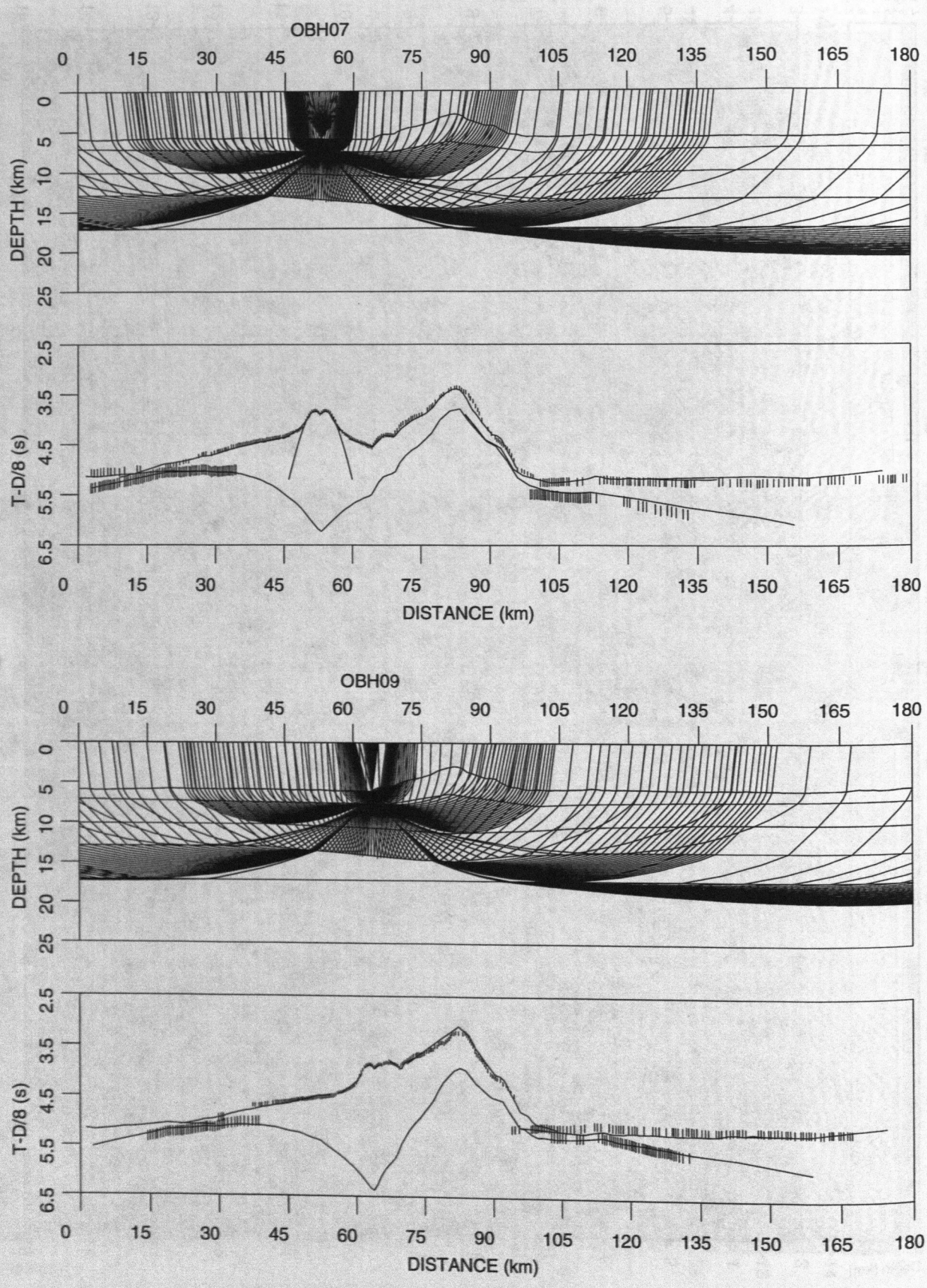

Figure 6.3.4.2.9a: Calculated (-) and observed (|) travel times and ray paths from OBH07 and 09.

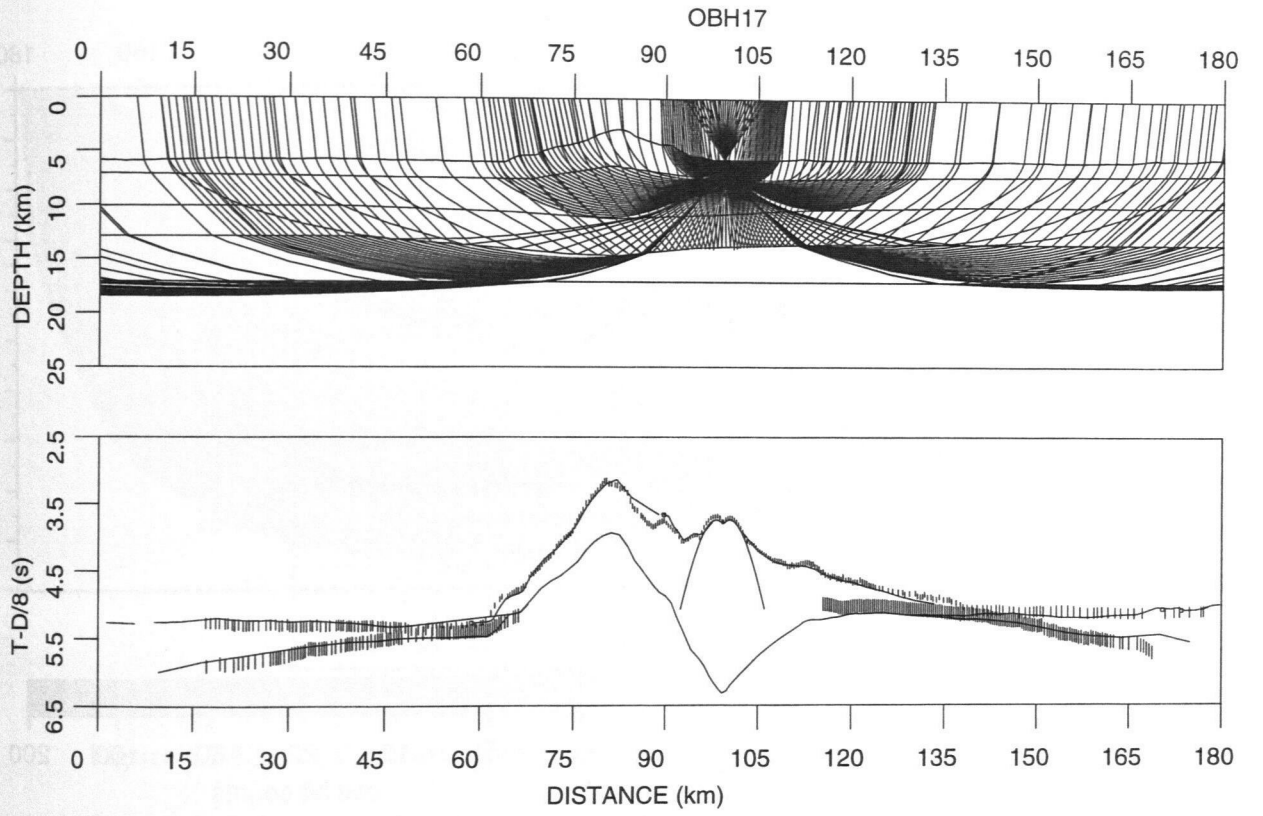

Figure 6.3.4.2.9b: Calculated (-) and observed (|) travel times and ray paths from OBH17.

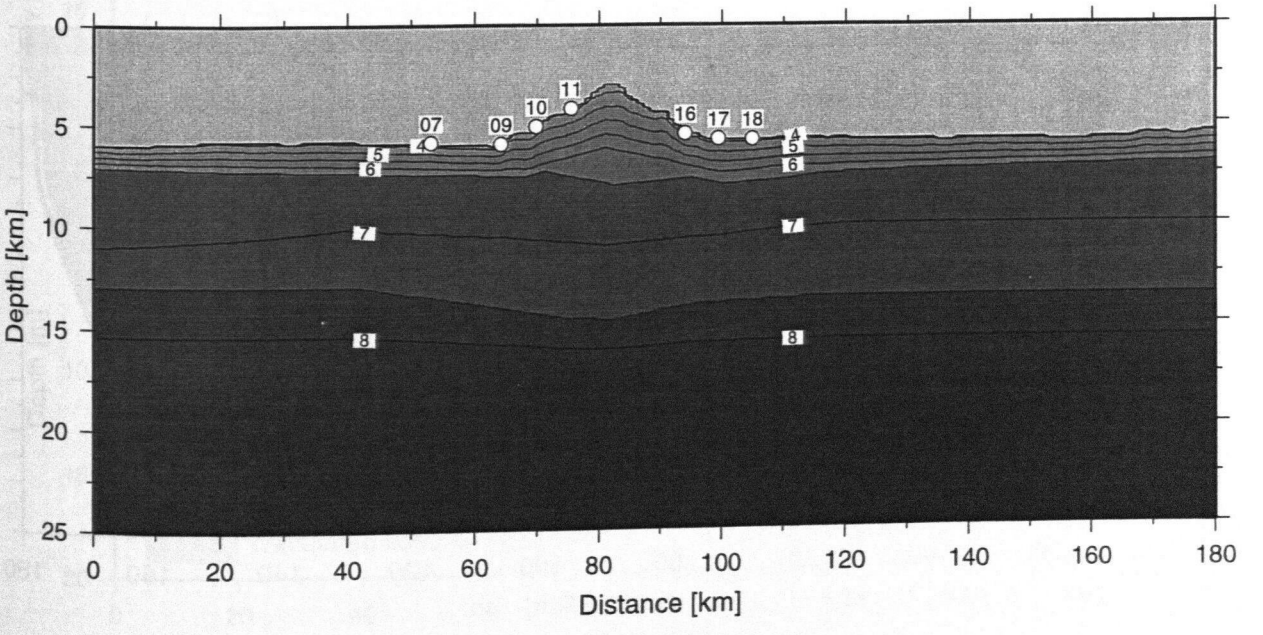

Figure 6.3.4.2.10: Velocity model derived from 2-dimensional forward modeling of profile 2.

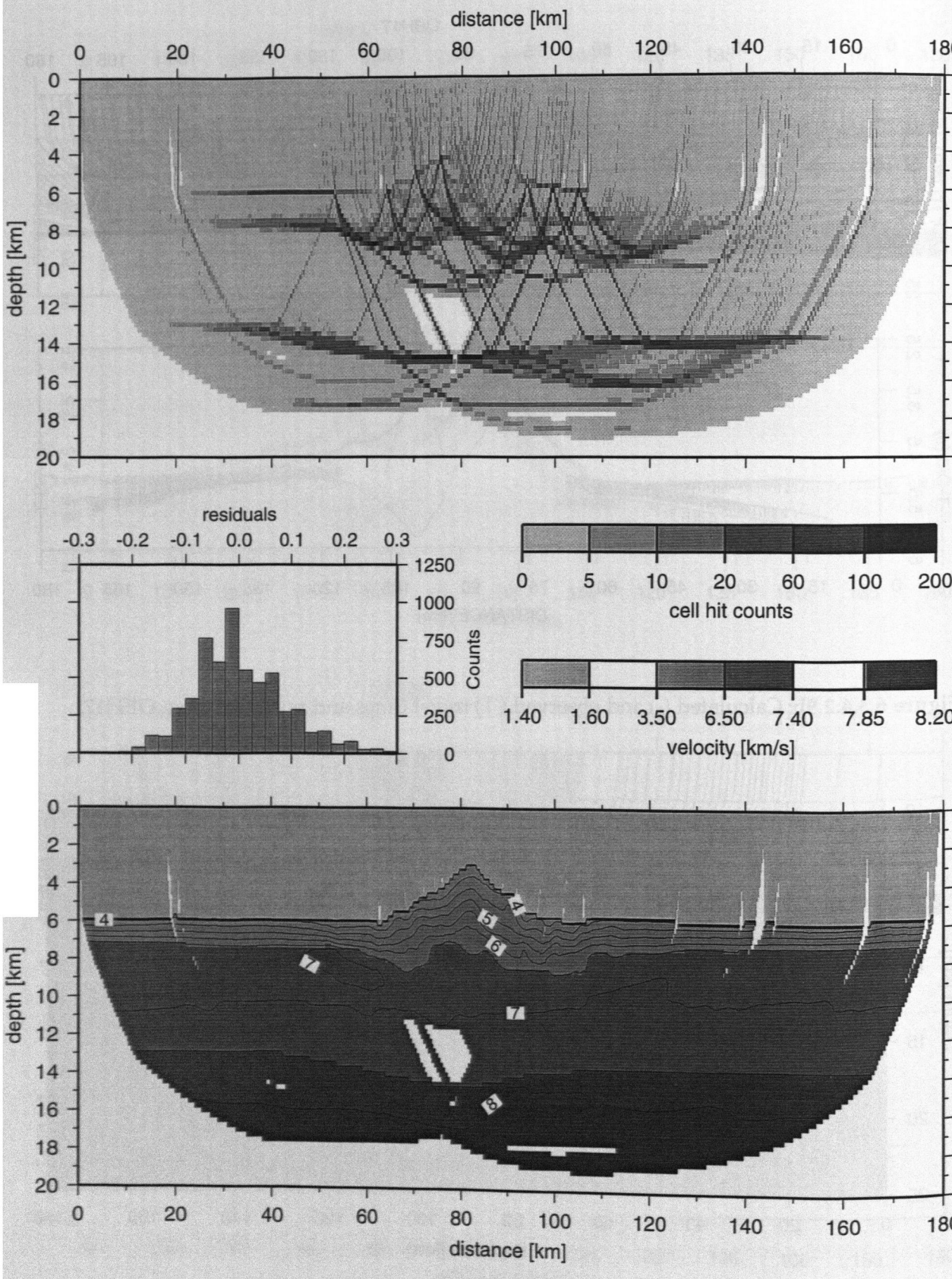

Figure 6.3.4.2.11: Results from the tomographic inversion of first arrivals recorded along profile 2.

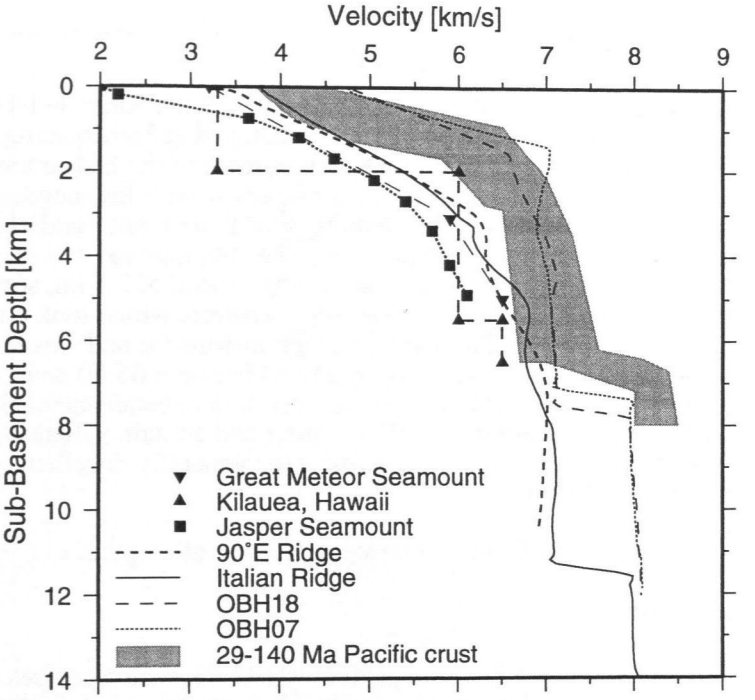

Figure 6.3.4.2.12: P-velocity from profile 2 as a function of sub-basement depth.

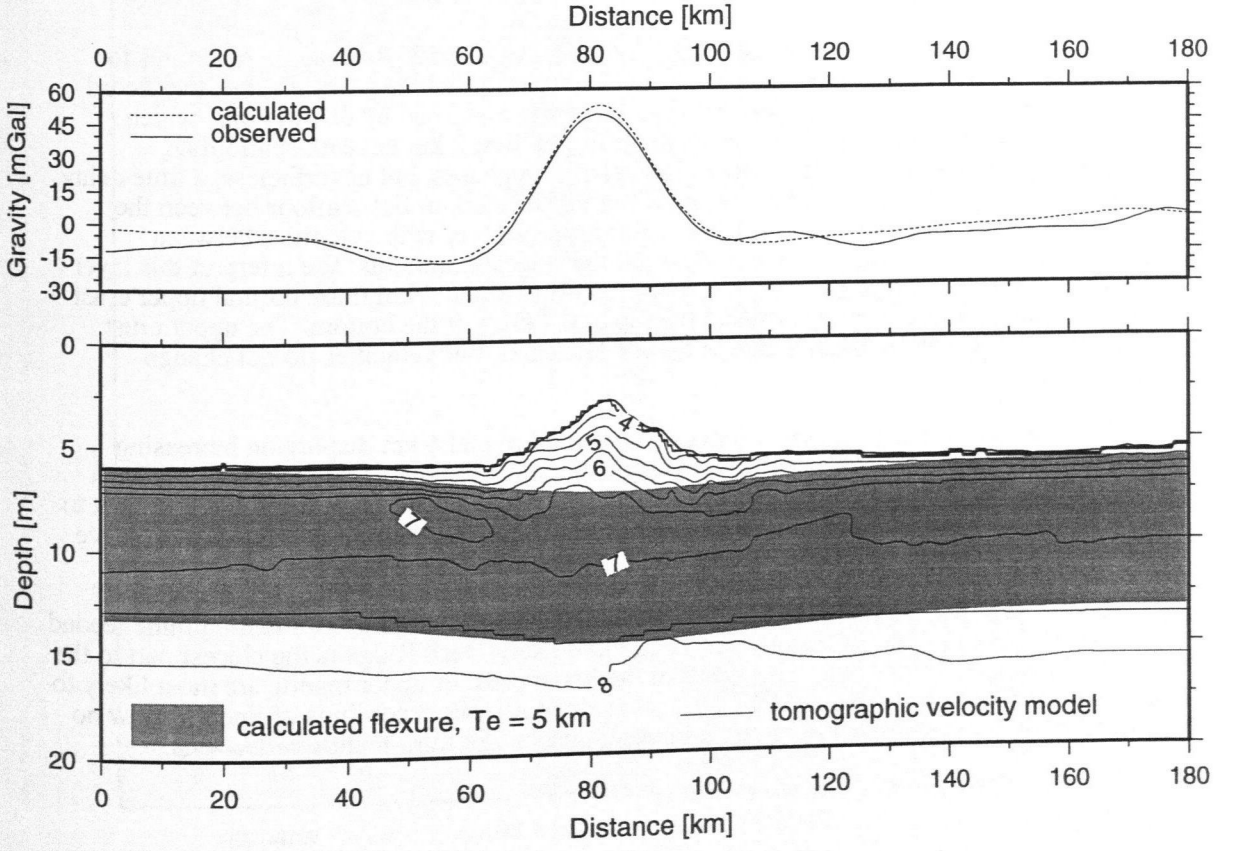

Figure 6.3.4.2.13: Gravity/flexural study along profile 2 using admittance technique.

6.3.4.3 PROFILE SO142-03

Profile SO142-03 is a north-south oriented dip line across the Bach Ridge at ist western termination.. Fourteen instruments (OBH20 to 33) were deployed at 3nm spacing with one additional instrument in the center (Figure 6.3.4.3.1). Deployment of the instruments started on 15 June 1999 at 05:00, and was finished at 10:00. A transit profile with the magnetometer deployed (profile 122) was run to the start of the shooting line about 6 nm parallel to the shooting line. Shooting started on 15 June 1999 at 15:00. The shot interval was 60 s, and the strong current against the course slowed the ship to an average speed of 3.5 kn, sometimes less. At midnight, one gun showed an air leakage, and had to be repaired, which took about two hours.. Shooting extended for about 35 miles across the first instrument and was terminated on 16 June 1999 at 21:00. All instruments were safely recovered between 05:00 and 14:00 on 17 June. Further details on instrumentation and shooting are given in appendices 9.1.3 and 9.2. The record sections of the OBH that were using an MBS recorder and contain valuable data are shown in Figures 6.3.4.3.2 to 6.3.4.3.11. The data quality was generally excellent, with clear signals at distances well above 100 km.

Despite limited time onboard, a preliminary interpretation was attempted.

Modelling and Discussion

9 OBH record sections along the 215 km long profile SO142-03, which crosses the Bach Ridge on its western tip, were analysed for a 2D velocity depth model. All data along the profile are of high quality, showing clear wide angle Pn and Pmp phases on most sections (Figs. 6.3.4.3.2 to 6.3.4.3.11) Modelling was attempted using the interactive *MacRay* (Luetgert, 1992) program to modify and alter the velocity-depth model. The program *RayInvr* (Zelt, 1992) was subsequently used for raytracing. Traveltimes were calculated using a 'top-down' approach, modelling velocity and depth for each layer before moving to the next.

Fig. 6.3.4.3.12 shows a preliminary velocity model of line S3. Raytracing examples for OBH30 and OBH23 are displayed in Figs. 6.3.4.3.13 and 6.3.4.3.14. On most of the record sections, the first phases of the upper layers are heavily disturbed by diffractions, which makes the velocity determination very difficult for the first 2 km beneath seafloor. A sedimentary cover could not be observed by refraction phases, but nevertheless, a time delay of the first refraction phases occurs on some stations located on flat seafloor between the volcanic highs. To account for this delay, a 500 m thick layer with velocities between 3.0 km/s and 3.5 km/s was introduced between the ridges/seamounts. We interpret this layer as volcanic debris. Crustal phases were modelled by an about 2 km thick normal upper crust with velocites ranging from 4.5 km/s at the top to 6.4 km/s at the bottom. The upper crust thickens to 4.5 km at the Bach Ridge in the model center, but velocities do not change significantly.

The thickness of the lower crust ranges between 4 km and 6 km displaying increasing velocities from 6.9 km/s to 7.2 km/s. As expected, the lower crust is thickest beneath Bach Ridge with a root-like geometry, but the crustal thickening seems asymmetric with respect to the ridge. Further modelling with more receivers will probably help to constrain or disprove this structure of the lower crust.

According to the idea that Bach Ridge was created when 75 Ma ago a mantle plume feeded the near mid ocean ridge in eastern direction, the western Bach Ridge is the closest part to the assumed Hotspot. Hence, heterogeneities of the lower crust or upper mantle are most likely to occur on this line. Nevertheless, the so far interpreted seismic recordings of line S3 show no distinct hints for unnormal velocities or unusual phases like intra-mantle reflections.

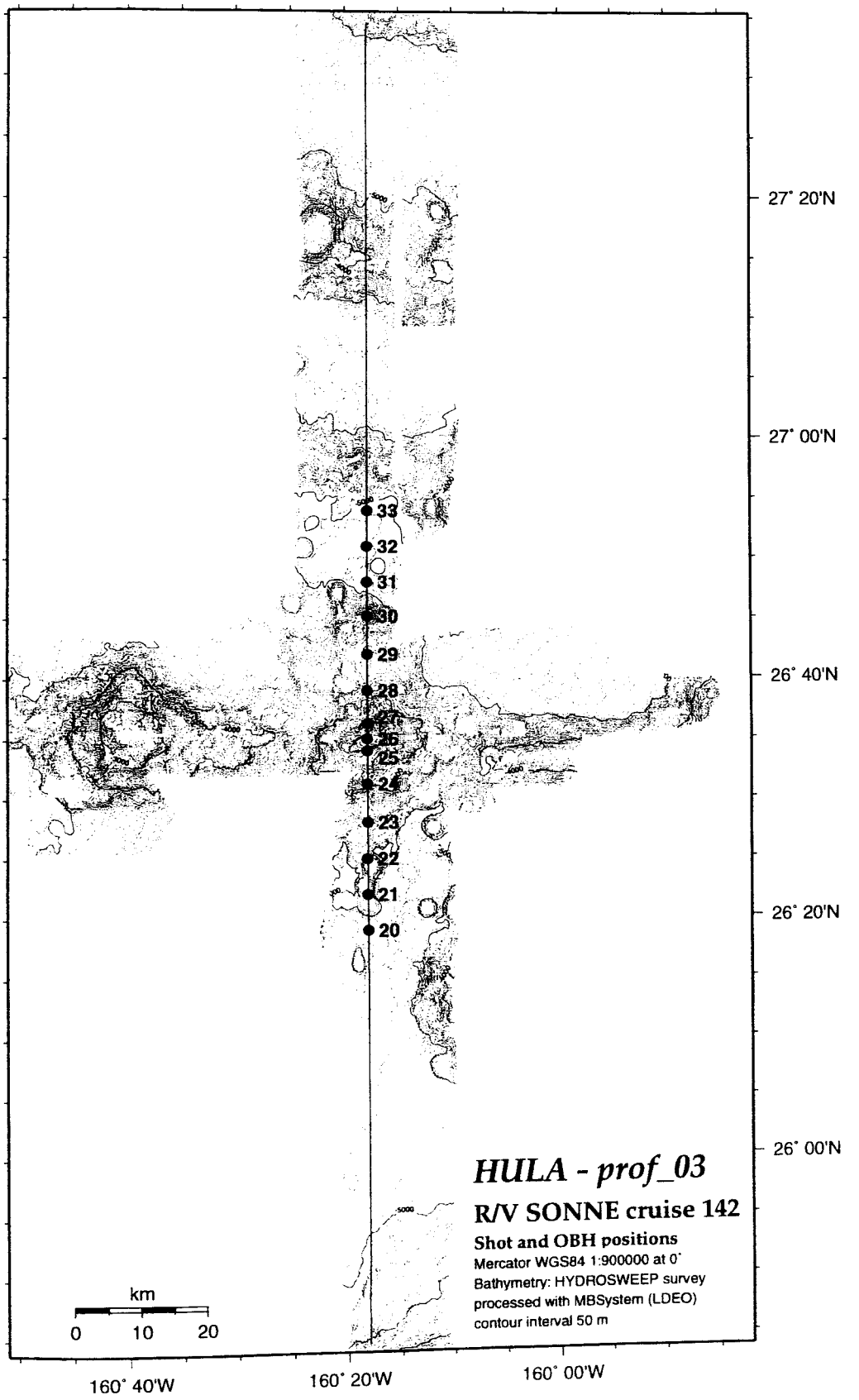

Figure 6.3.4.3.1: Profile 03 - Shot and OBH positions.

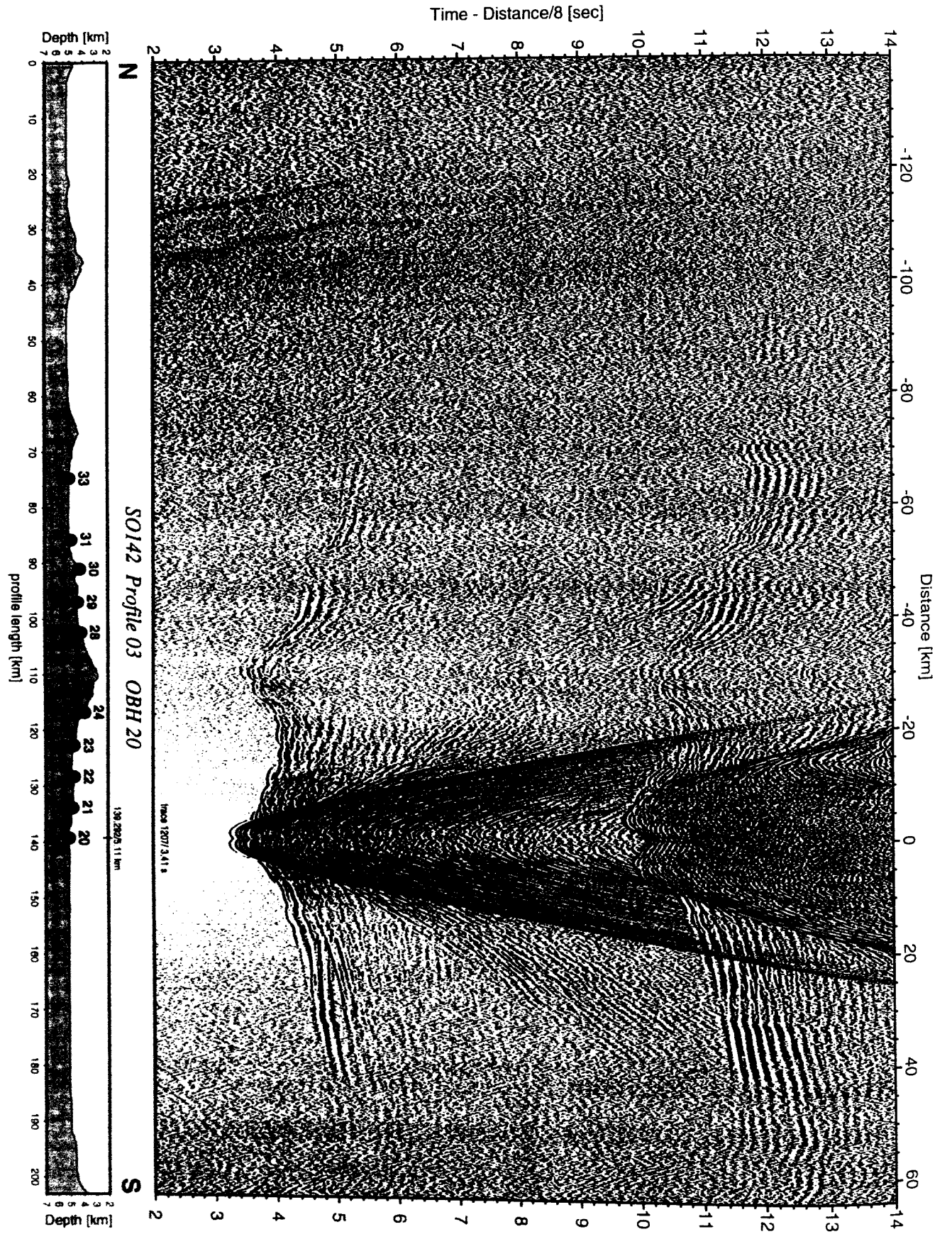

Figure 6.3.4.3.2: Record section from OBH 20 , Profile 03.

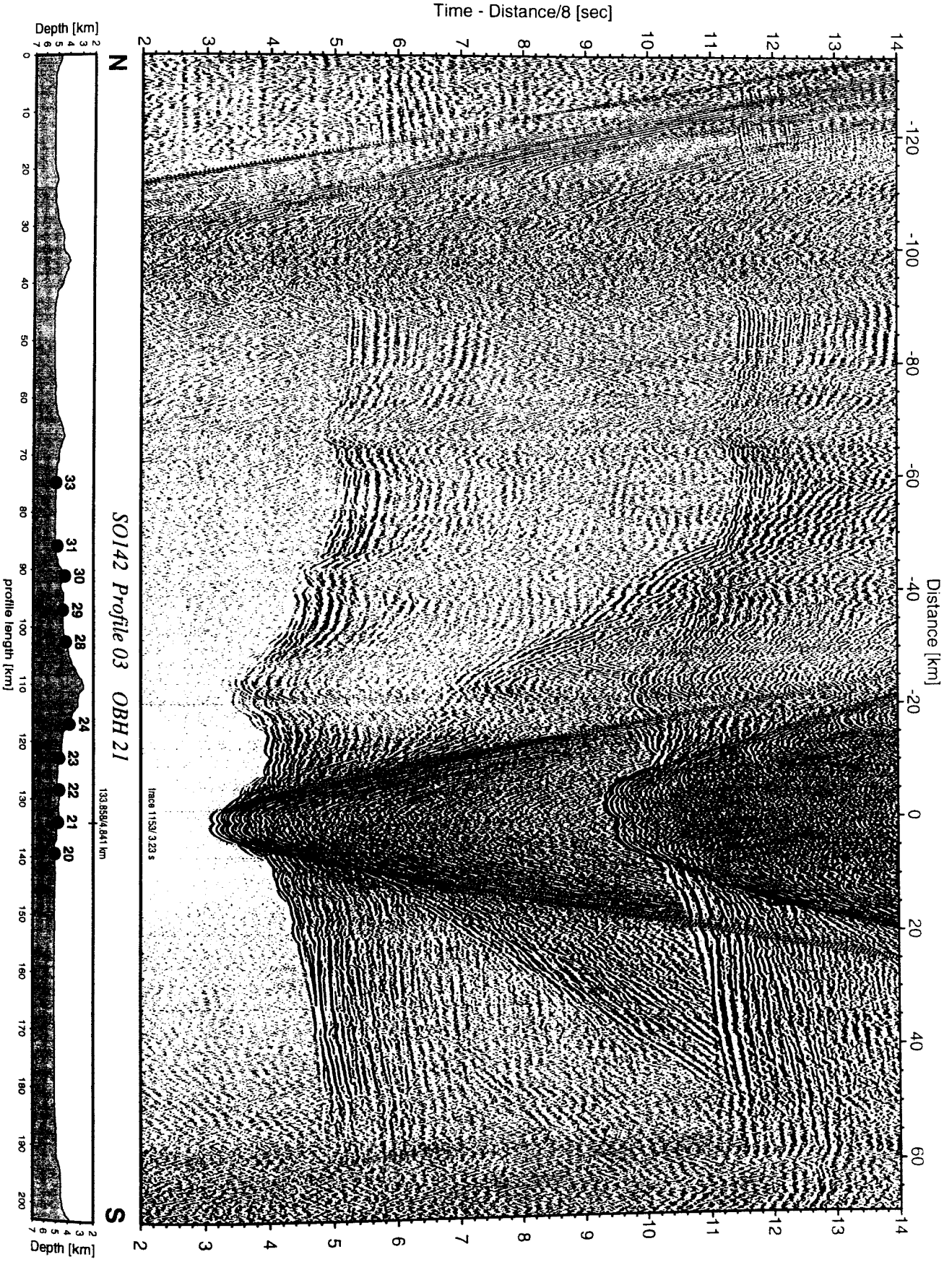

Figure 6.3.4.3.3: Record section from OBH 21 , Profile 03.

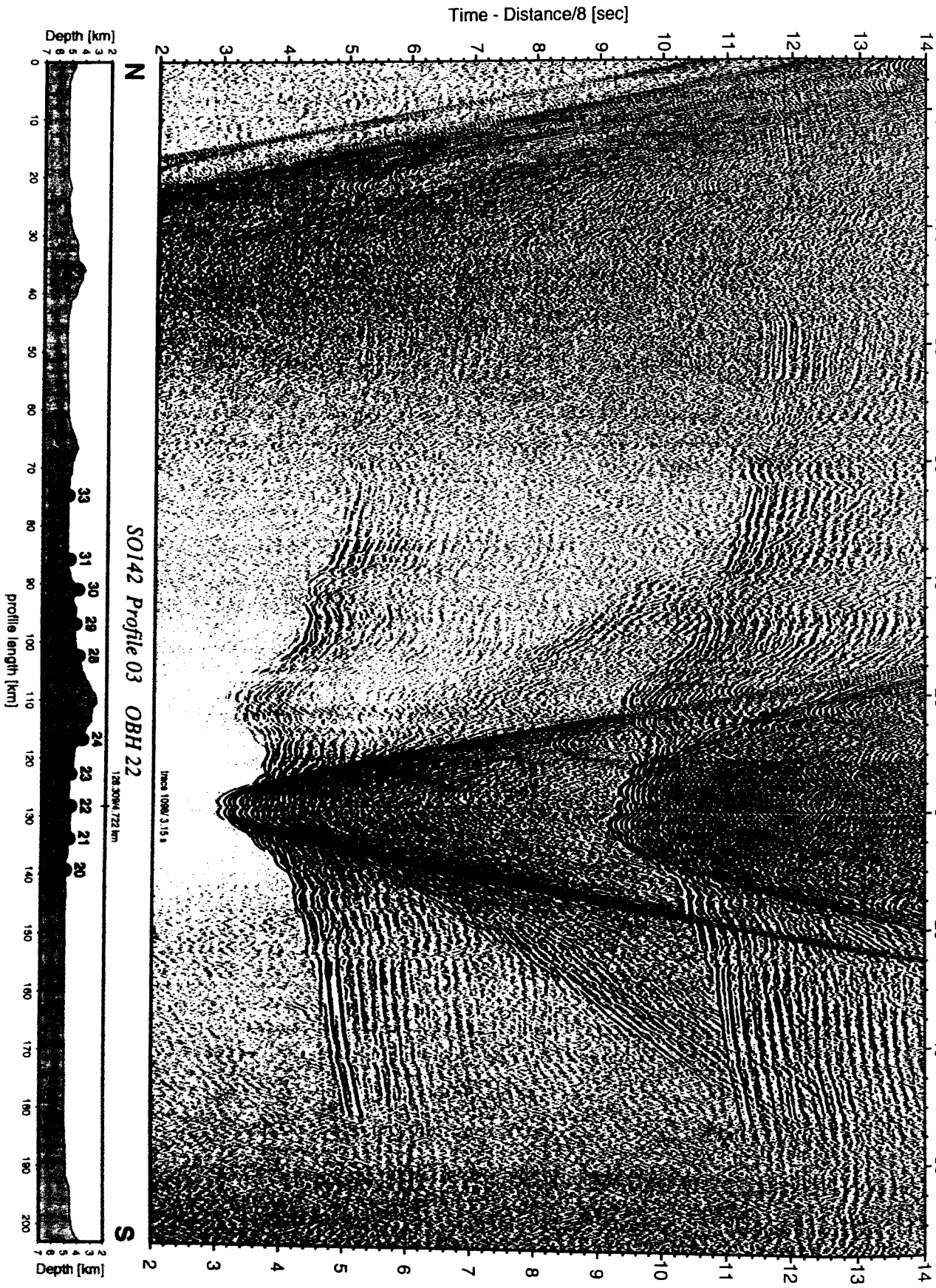

Figure 6.3.4.3.4: Record section from OBH 22 , Profile 03.

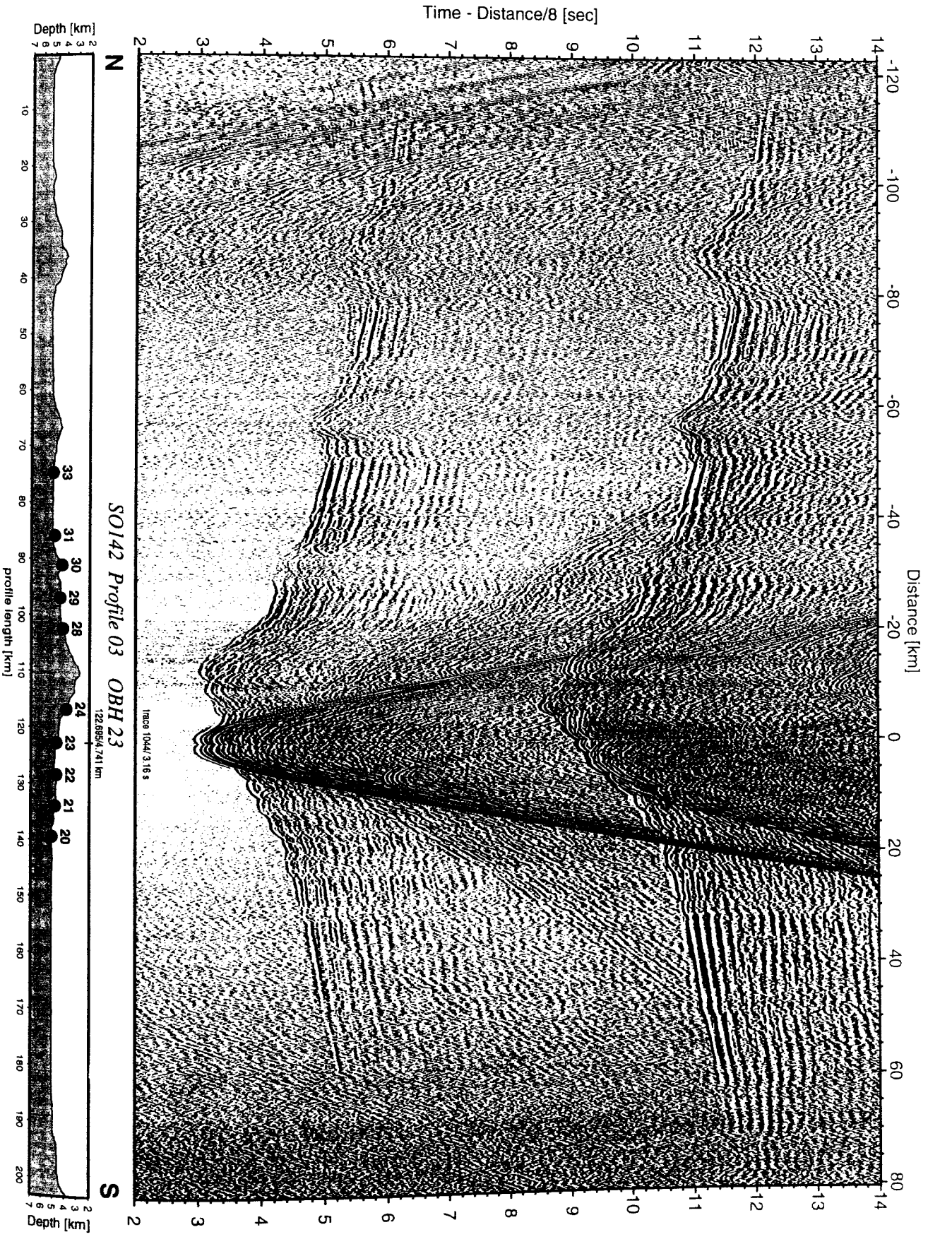

Figure 6.3.4.3.5: Record section from OBH 23 , Profile 03.

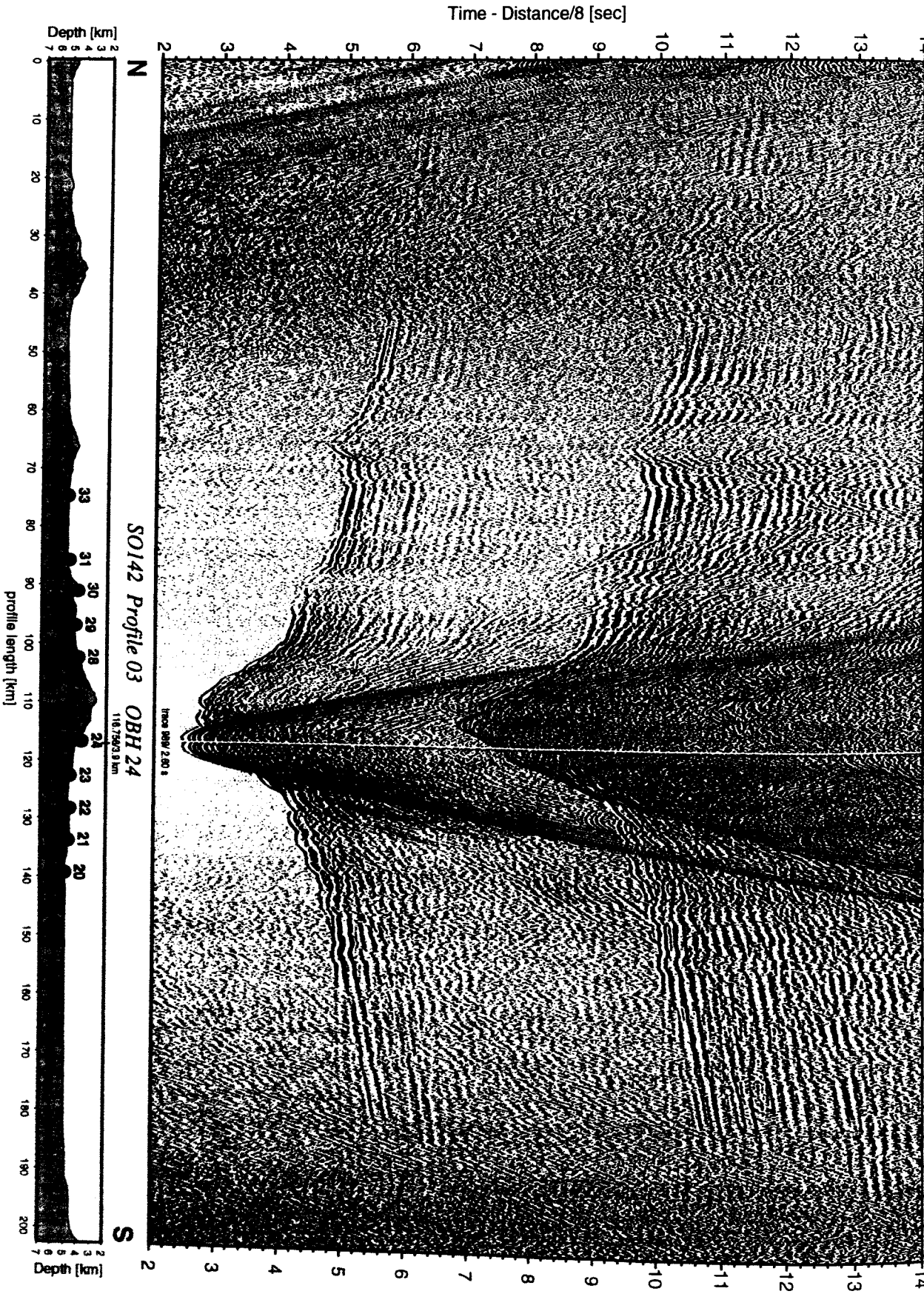

Figure 6.3.4.3.6: Record section from OBH 24 , Profile 03.

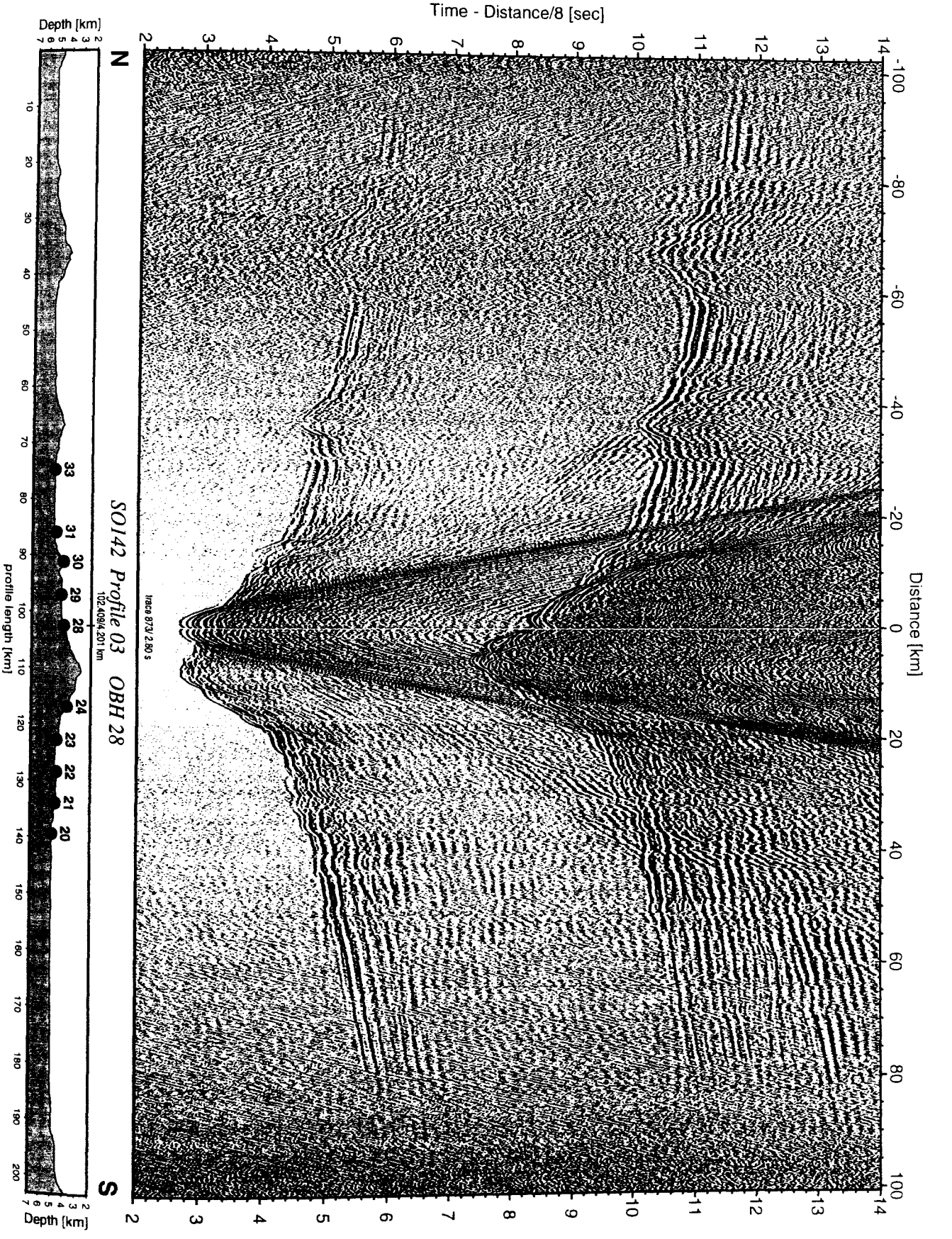

Figure 6.3.4.3.7: Record section from OBH 28 , Profile 03.

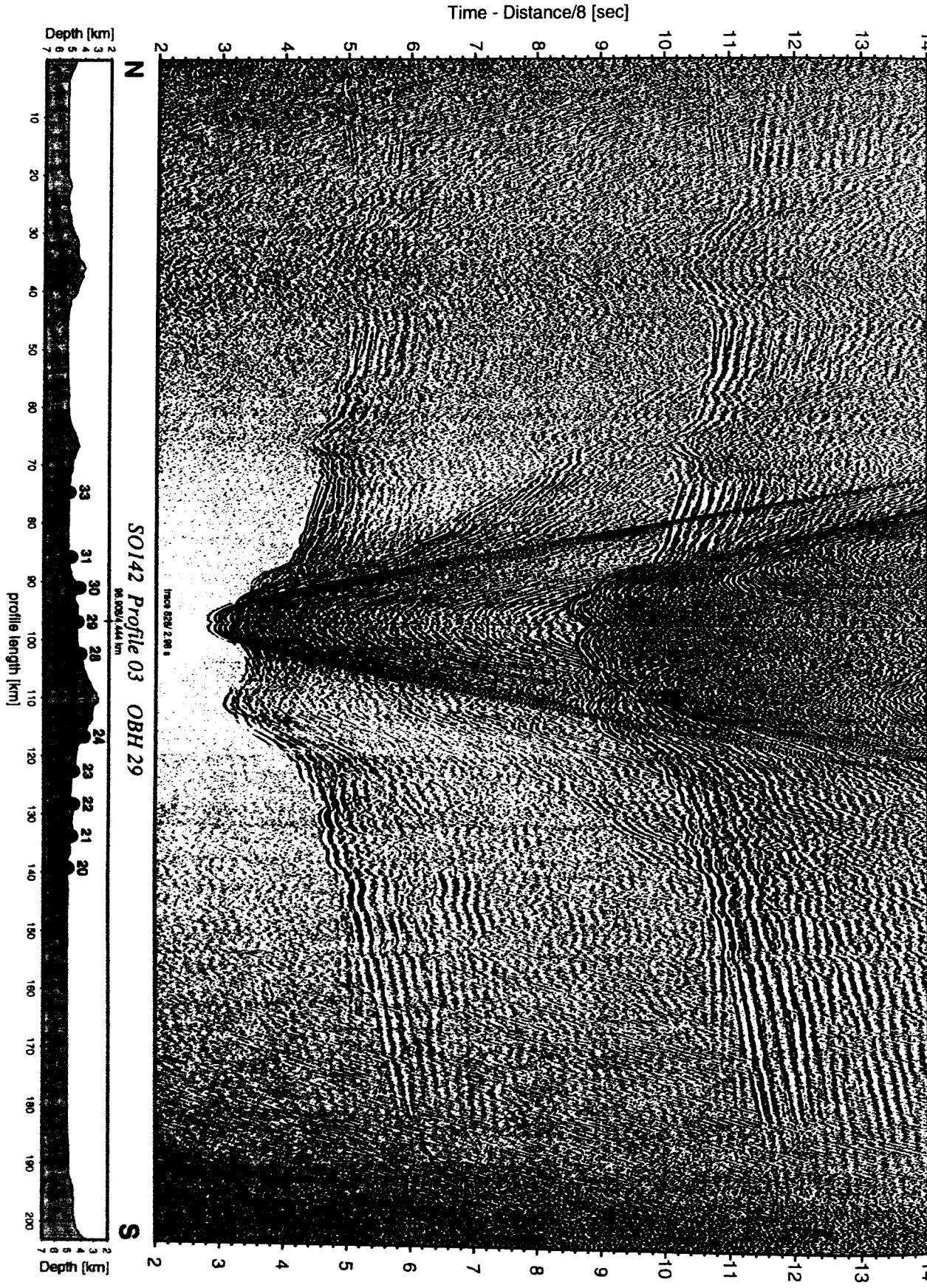

Figure 6.3.4.3.8: Record section from OBH 29 , Profile 03.

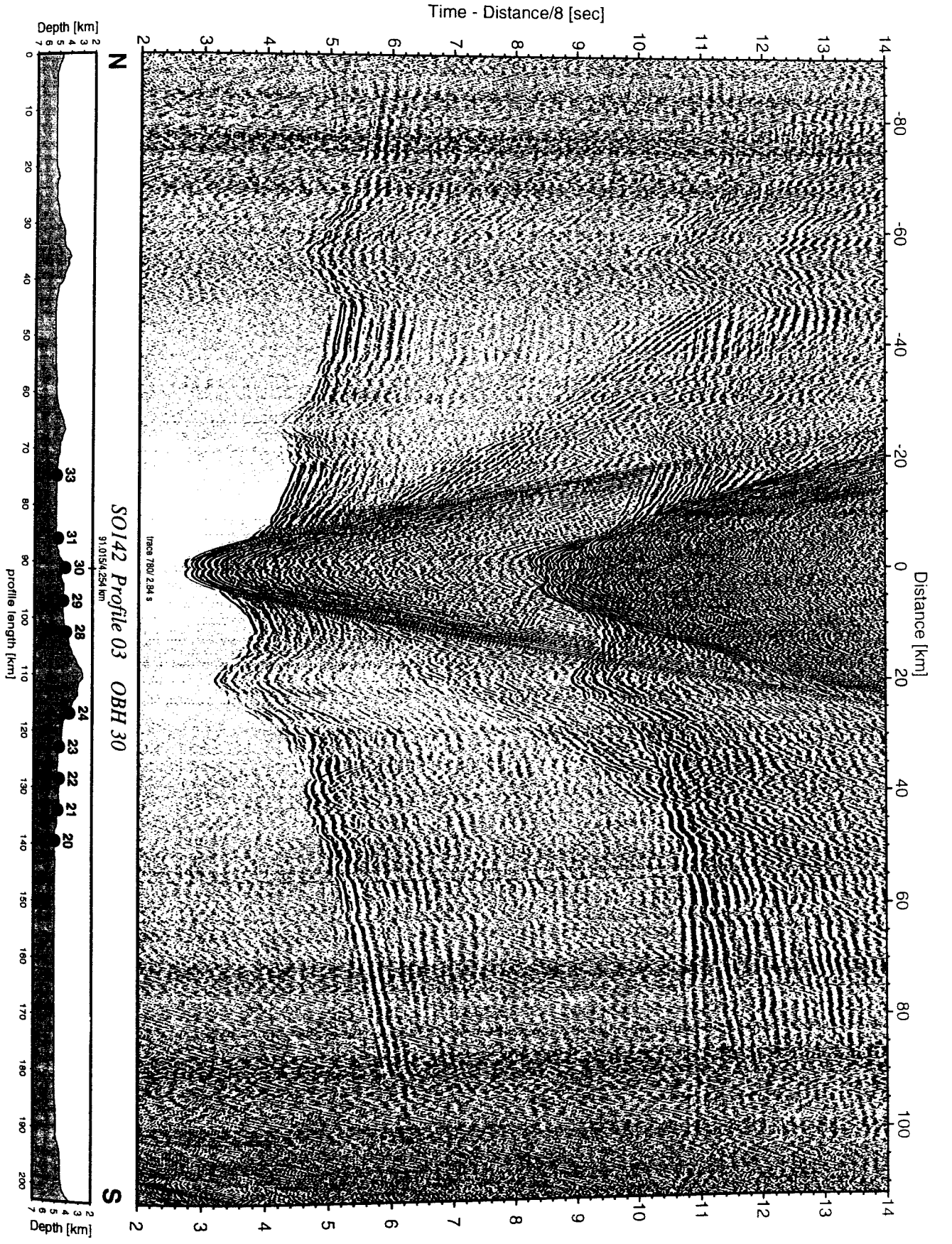

Figure 6.3.4.3.9: Record section from OBH 30 , Profile 03.

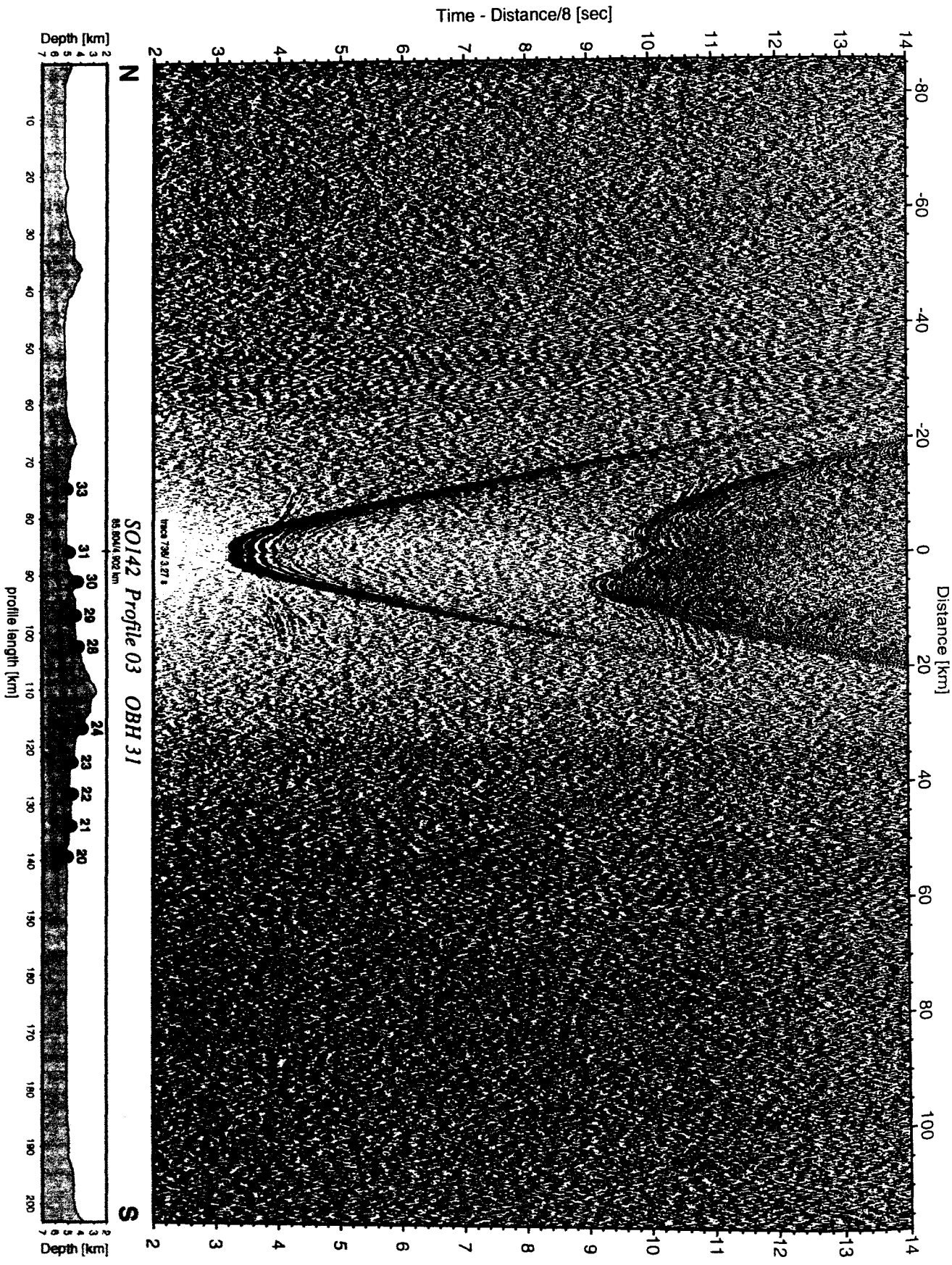

Figure 6.3.4.3.10: Record section from OBH 31 , Profile 03.

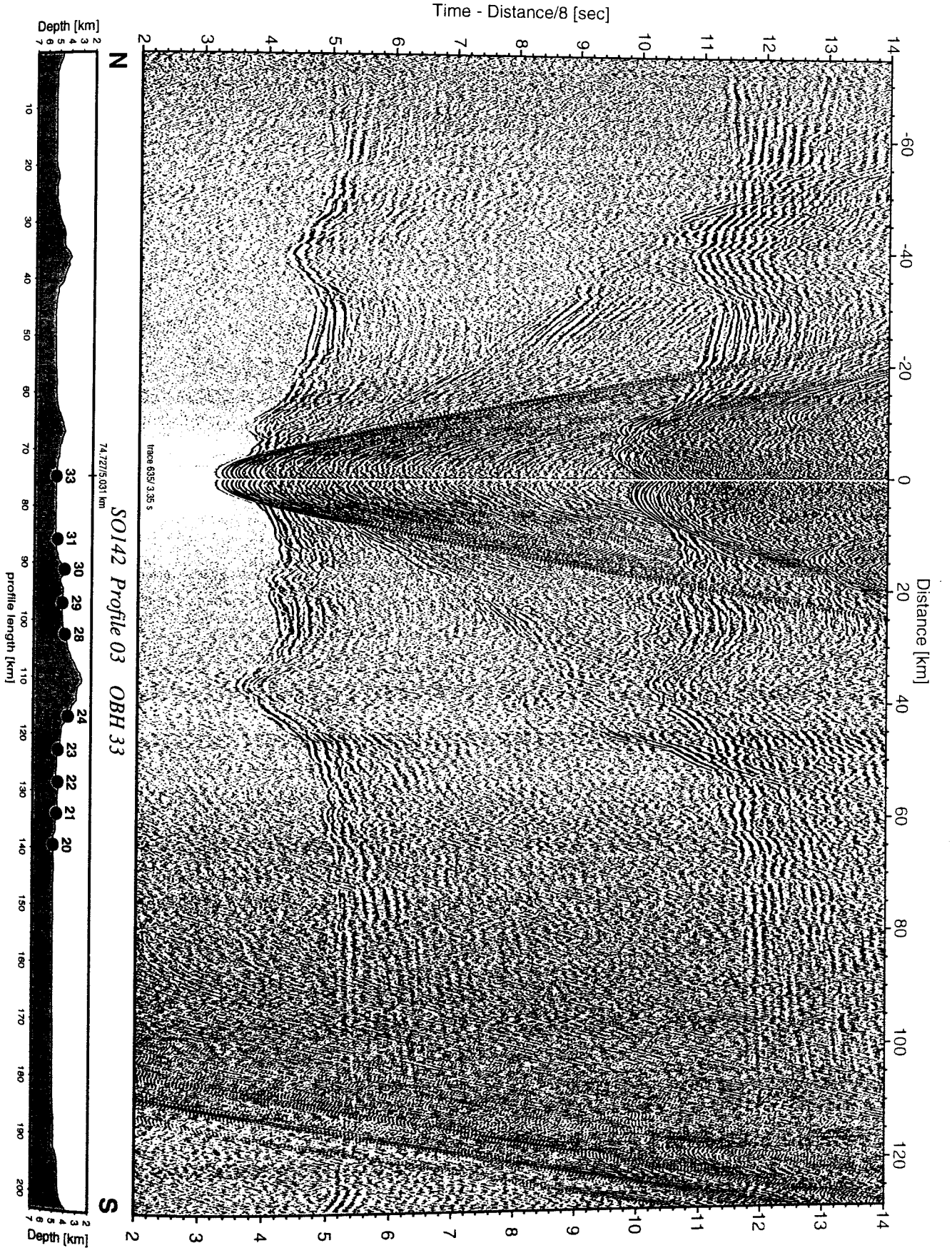

Figure 6.3.4.3.11: Record section from OBH 33 , Profile 03.

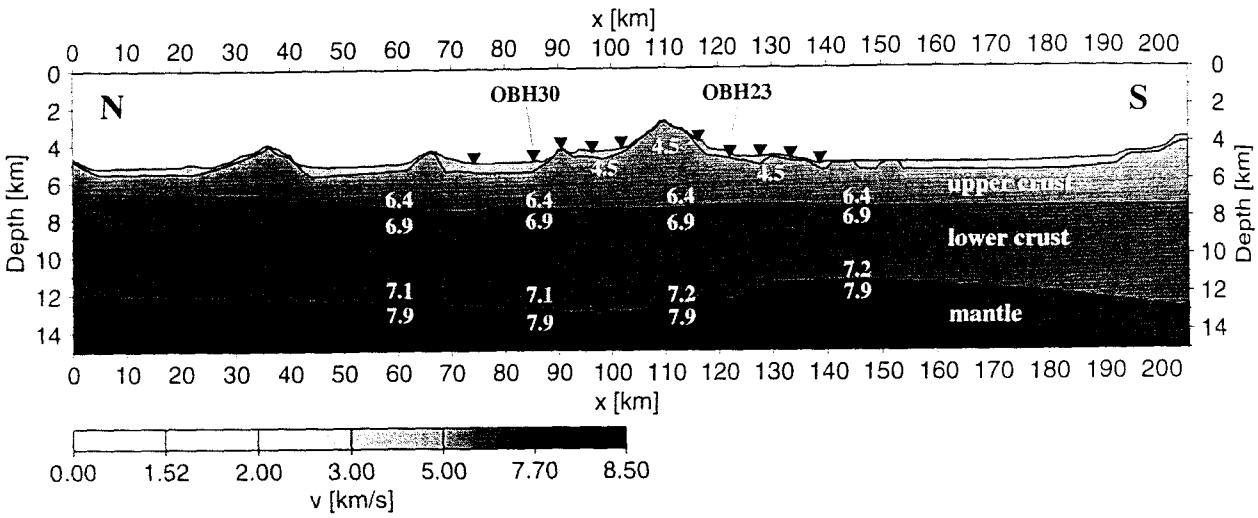

Figure 6.3.4.3.12: Velocity model of profile S3, labels in km/s. For the two marked OBH raytracing examples are shown in the following two figures.

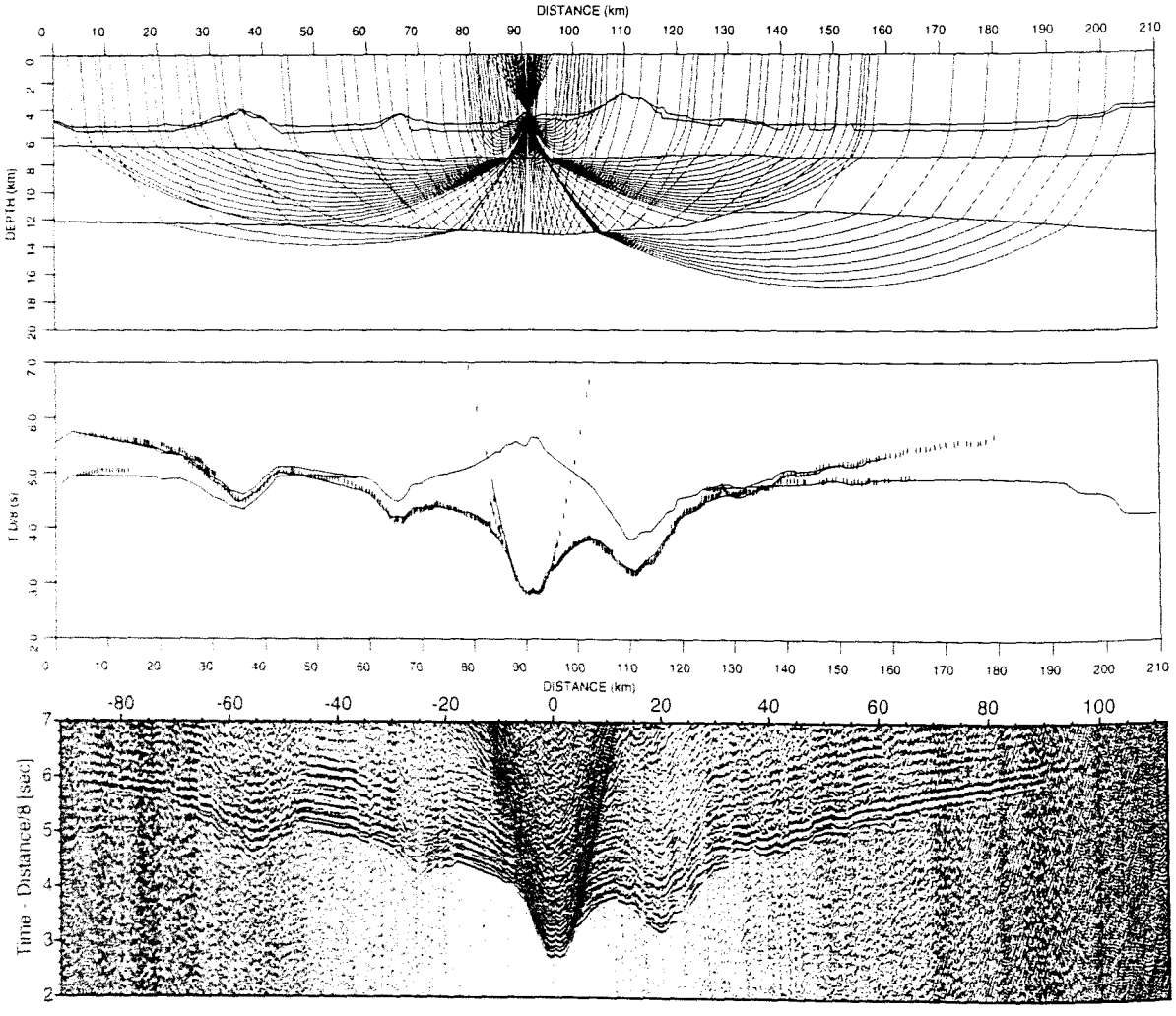

Figure 6.3.4.3.13: Seismic velocity modelling of profile S3, OBH30. Upper: raypaths through structural model; Middle: observed traveltimes (vertical bars) and calculated traveltimes (lines); Bottom: seismic section of OBH23.

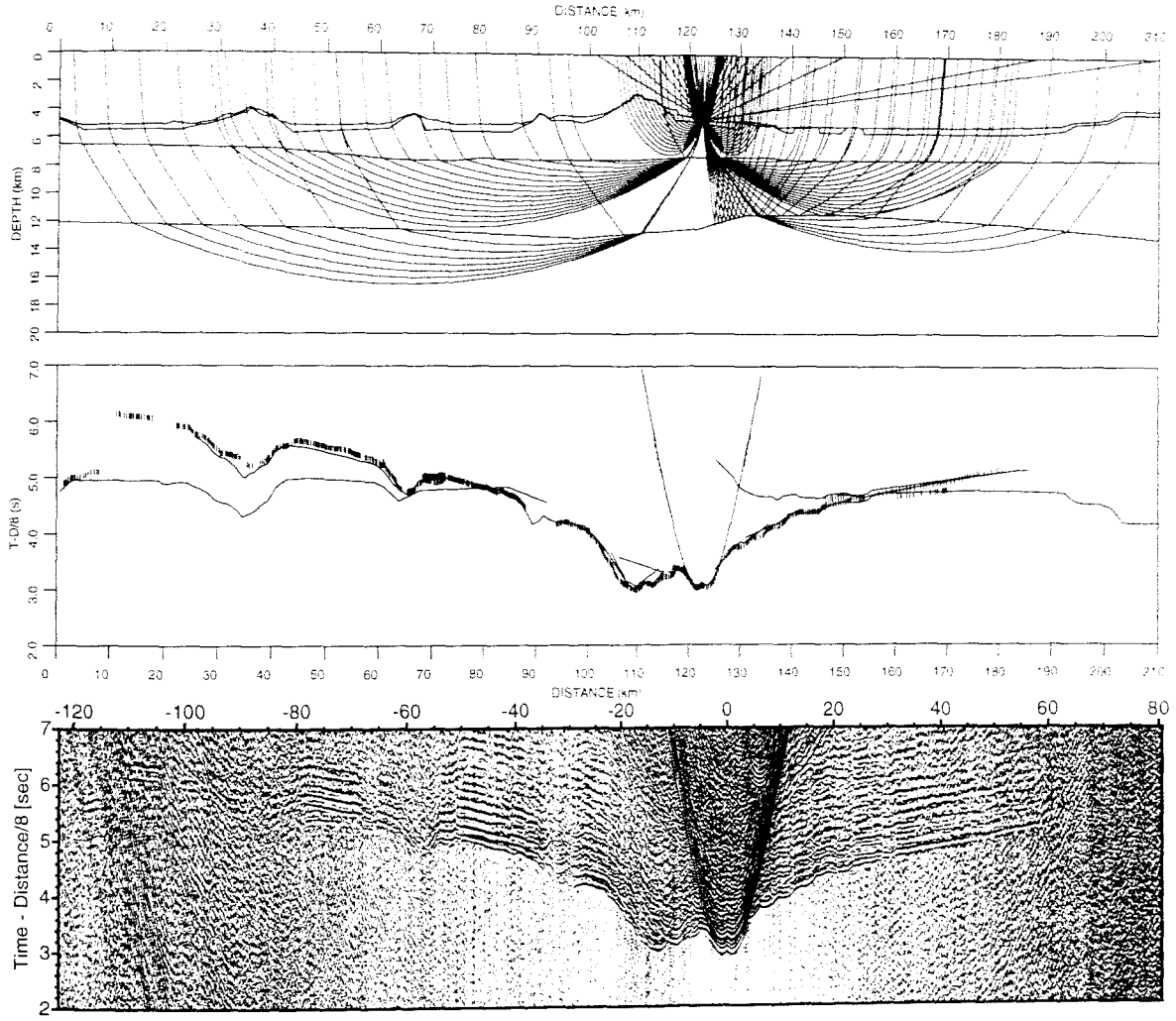

Figure 6.3.4.3.14: Seismic velocity modelling of profile S3, OBH23. Upper: raypaths through structural model; Middle: observed traveltimes (vertical bars) and calculated traveltimes (lines); Bottom: seismic section of OBH23.

6.3.4.4 PROFILE SO142-04

Profile SO142-04 is another north-south oriented dip line across the Bach Ridge, located at its eastern termination close to the assumed ridge axis of its formation. Fourteen instruments (OBH34 to 47) were deployed at 2 to 4 nm spacing, with the wider spacing at the ends (Figure 6.3.4.4.1). The profile also covered parts of the Beethoven Ridge. Deployment of the instruments started on 21 June 1999 at 04:00 and was finished at 10:00. A transit profile with the magnetometer deployed (profile 128) was run to the start of the shooting line in the north about 6 nm parallel to the shooting line. Shooting started on 21 June 1999 at 15:00. The shot interval was 60 s, and the average ship speed was just below 4 kn, but changing currents and strong winds made it somewhat variable. Shooting extended for about 35 miles from the first instrument and was terminated on 22 June 1999 at 20:00. There were no gun failures, despite strong winds (force 5 to 6) and moderate swells and currents. All instruments were safely recovered between 04:00 and 16:00 on 23 June. Further details on instrumentation and shooting are given in appendices 9.1.4 and 9.2. The record sections of the OBHs that were using an MBS recorder and which contain valuable data are shown in Figures 6.3.4.4.2 to 6.3.4.4.10. All of the signals recorded on OBH34 show a complete dc-shift and are thus not possible to read. Otherwise, the data quality was excellent, with clear signals at distances well above 140 km on some stations.

Despite limited time onboard, a preliminary interpretation was attempted.

Modelling and Discussion

The north-south running profile runs across strike of the east-west trending Bach Ridge. An age of 75 Ma is estimated for this ridge.

All data acquired along this 215 km profile are of high quality, displaying low ambient noise and a high quality waveform, which made the picking of arrivals by eye relatively straightforward. Water depth for the model was taken from the navigation data. P-wave first arrivals were picked from the seismic sections, which contain no significant wide-angle reflections or near-vertical reflections. Based on the traveltime data of all 9 OBHs, which could be played back onboard SONNE, a ray tracing forward modelling was performed using the interactive *MacRay* program (Luetgert, 1992). Subsequently, a velocity depth model of profile SO142-04 was achieved, which is displayed in Figure 6.3.4.4.11. It consists of three layers with different gradients and a Moho depth of approximately 12 km.

As several seamounts as well as the Bach Ridge are located along the profile, crustal refraction arrivals are dominated by the seafloor topography. Since virtually no sedimentary cover could be identified in the sections, a sedimentary layer was not introduced in the model.

In the preliminary model, two layers were used to trace the upper crustal phases. The first layer is a high-gradient layer with velocities ranging from 4.0 km/s at the top to 5.0 km/s at the bottom. The transition to the next layer is characterized by a strong velocity discontinuity with velocities raised to 6.0 km/s. This strong increase in velocites could best fit the refraction data (eg. Figure 6.3.4.4.12), however it must be mentioned that no corresponding reflection branches can be identified in the data and, thus, the dynamics of the wavefield may not be reproduced by the somewhat simplified model.

The lower crust is modelled using a low-gradient layer with velocites varying from 6.8 km/s at the top to 7.2 km/s at the bottom. This low-gradient layer is needed to model lower crustral phases, which arrive at later traveltimes than refractions from the underlying upper mantle (e.g. Pn) (Figure 6.3.4.4.12).

In addition to the crustal refraction branches, a very strong wide-angle Pn which penetrates the upper mantle is observed on several stations (eg. Figure 6.3.4.4.12). The crust-mantle boundary is modelled at a depth of 11-12 km, displaying a normal velocity discontinuity from 7.2 km/s to 8.0 km/s. A small root was introduced under the Bach Ridge to trace upper mantle arrivals from instruments on both sides of the ridge. Modelling of the remaining 4 OBHs which could not be played back onboard will further constrain the geometry of the root and the crustal thickening underneath Bach Ridge. The root suggests an isostatic compensation of the structure.

Overall, a very smooth velocity field with little lateral velocity variations is proposed as a preliminary model. To conclude, the structure obtained from preliminary seismic data analysis is in reasonably good agreement with other structures deduced from geophysical data that are believed to be of the same origin. A post-cruise data analysis considering all the data acquired in the Musician Seamounts region will help to constrain and improve these preliminary results.

Also evident are clear S-wave arrivals on some record sections (eg. OBH 35, 38, 39, 42, 44, 46, 47), which should later enable us to determine Poisson's ratio. Additionally, some records (eg. OBH 35, 36, 46, 47) show prominent wide-angle reflections from the upper mantle, with critical distances of about 90 km. These have not been analysed on board, but a simple estimate places this discontinuity at a depth of about 22-25 km.

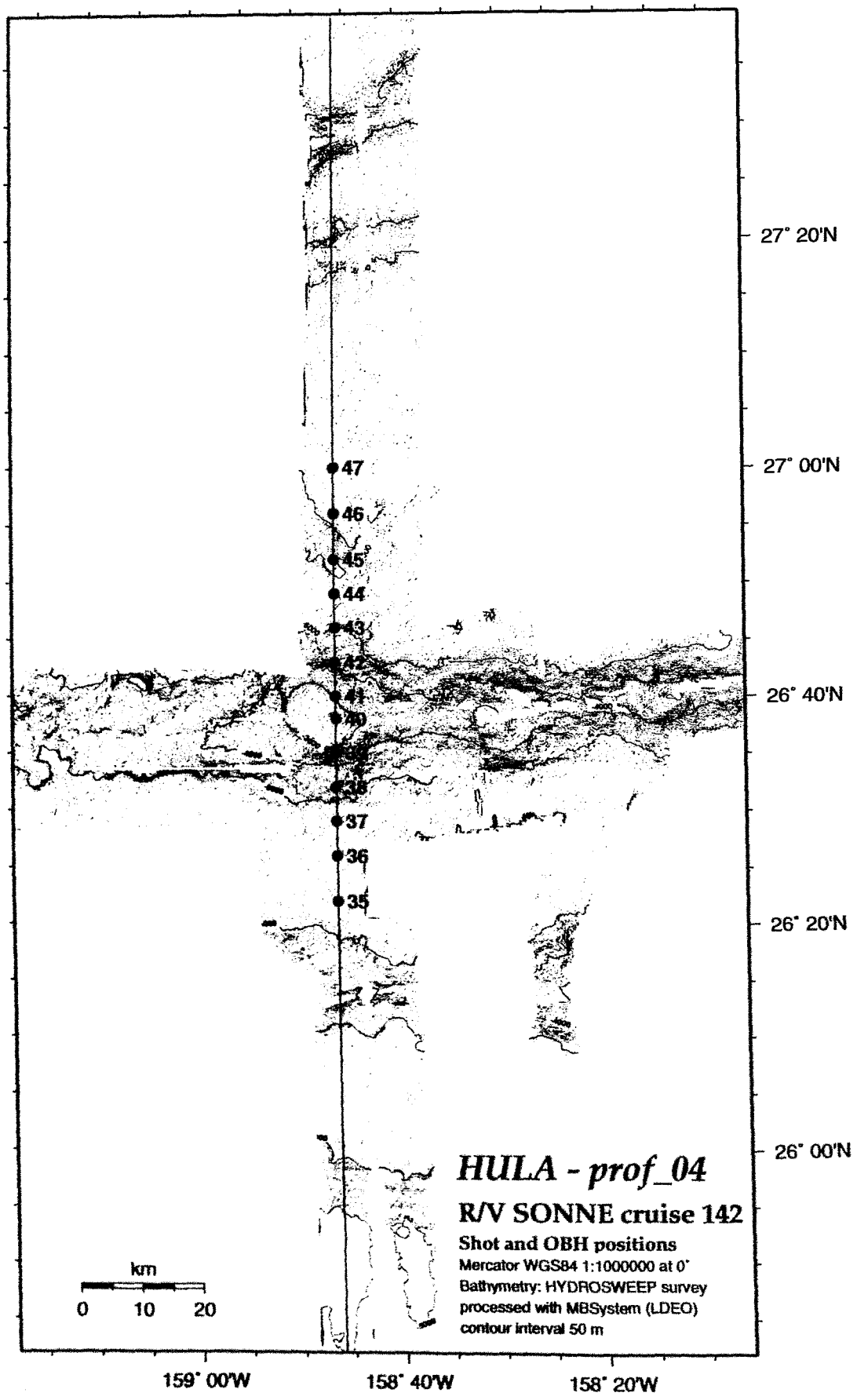

Figure 6.3.4.4.1: Profile 04 - Shot and OBH positions.

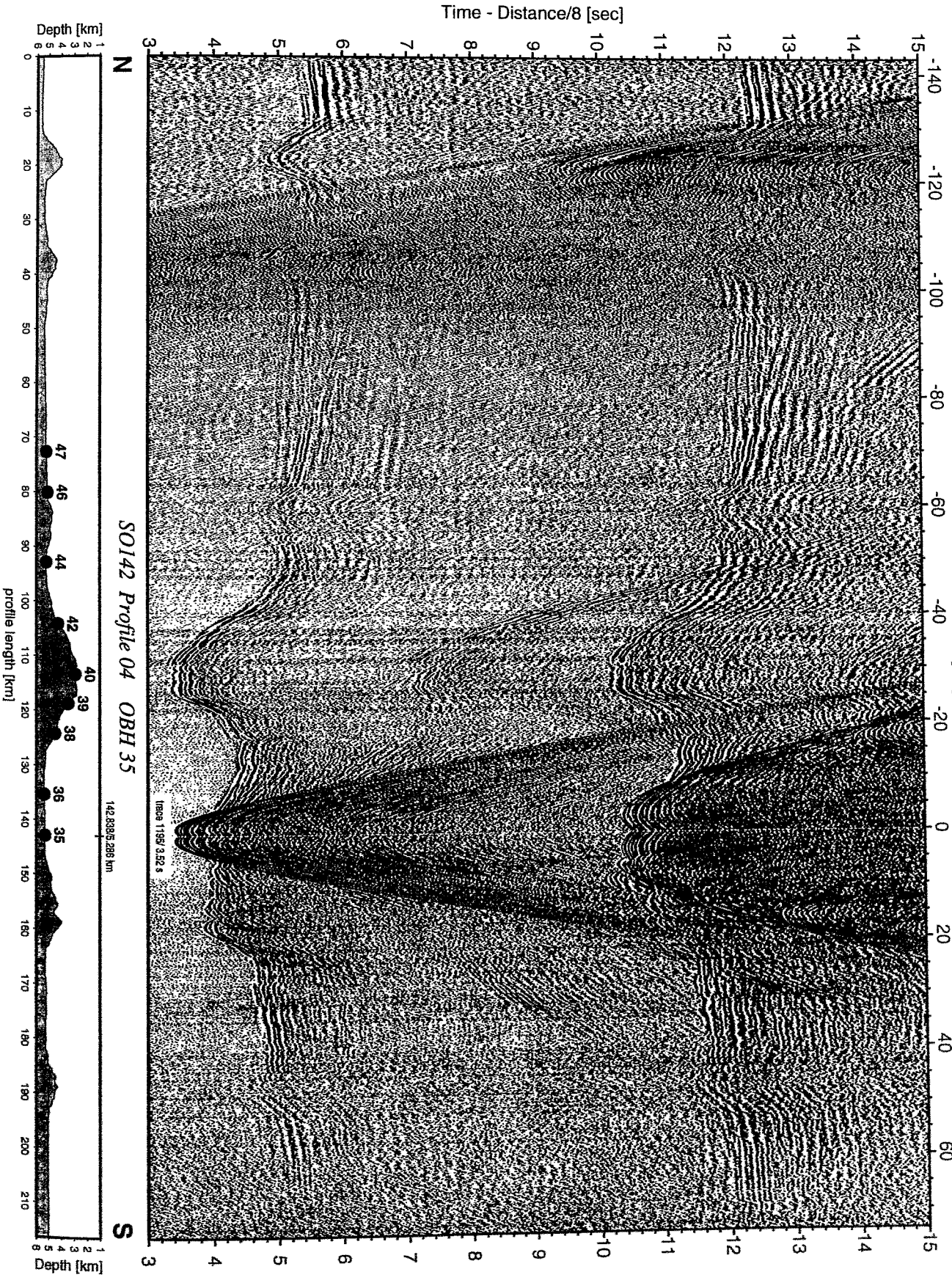

Figure 6.3.4.4.2: Record section from OBH 35 , Profile 04.

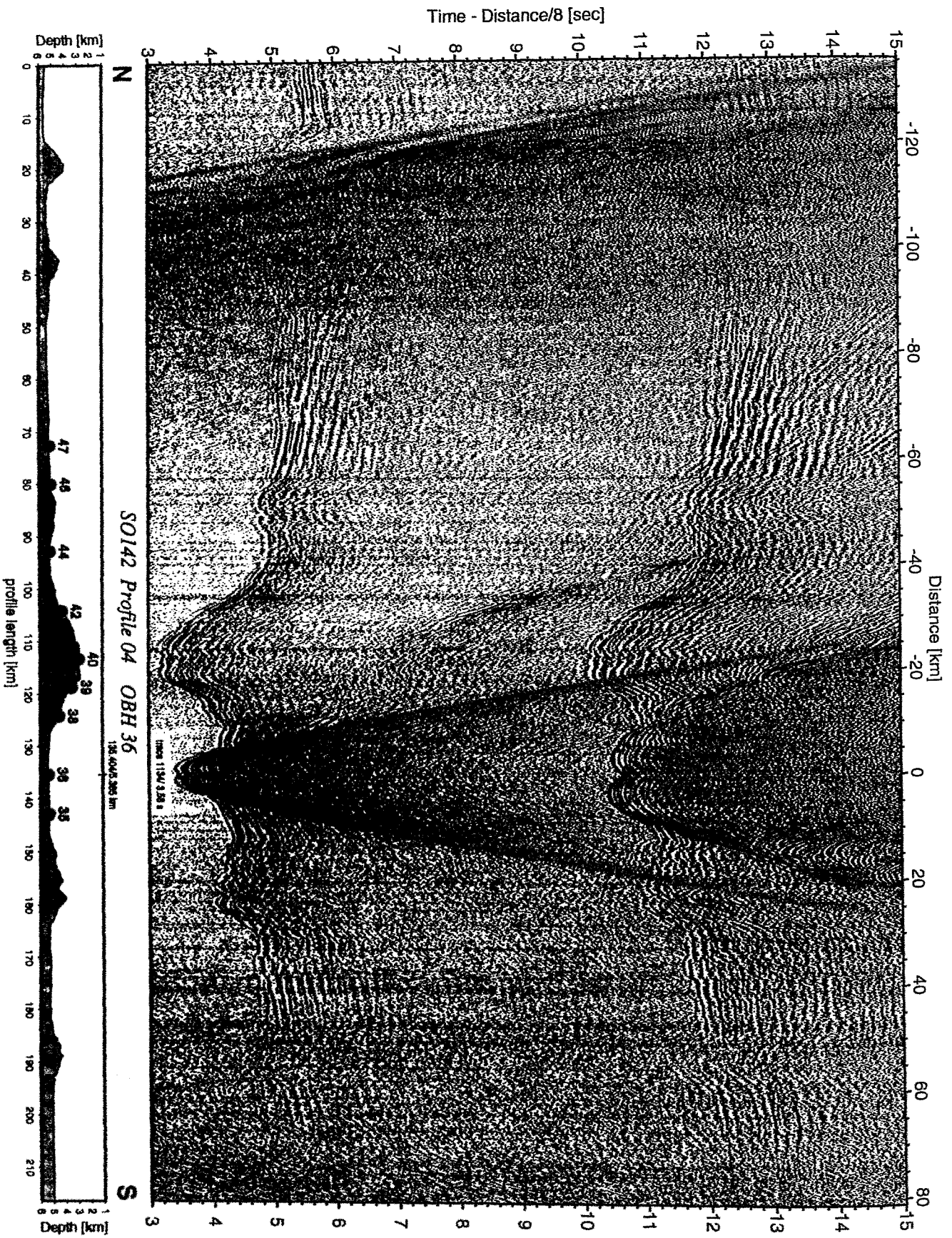

Figure 6.3.4.4.3: Record section from OBH 36 , Profile 04.

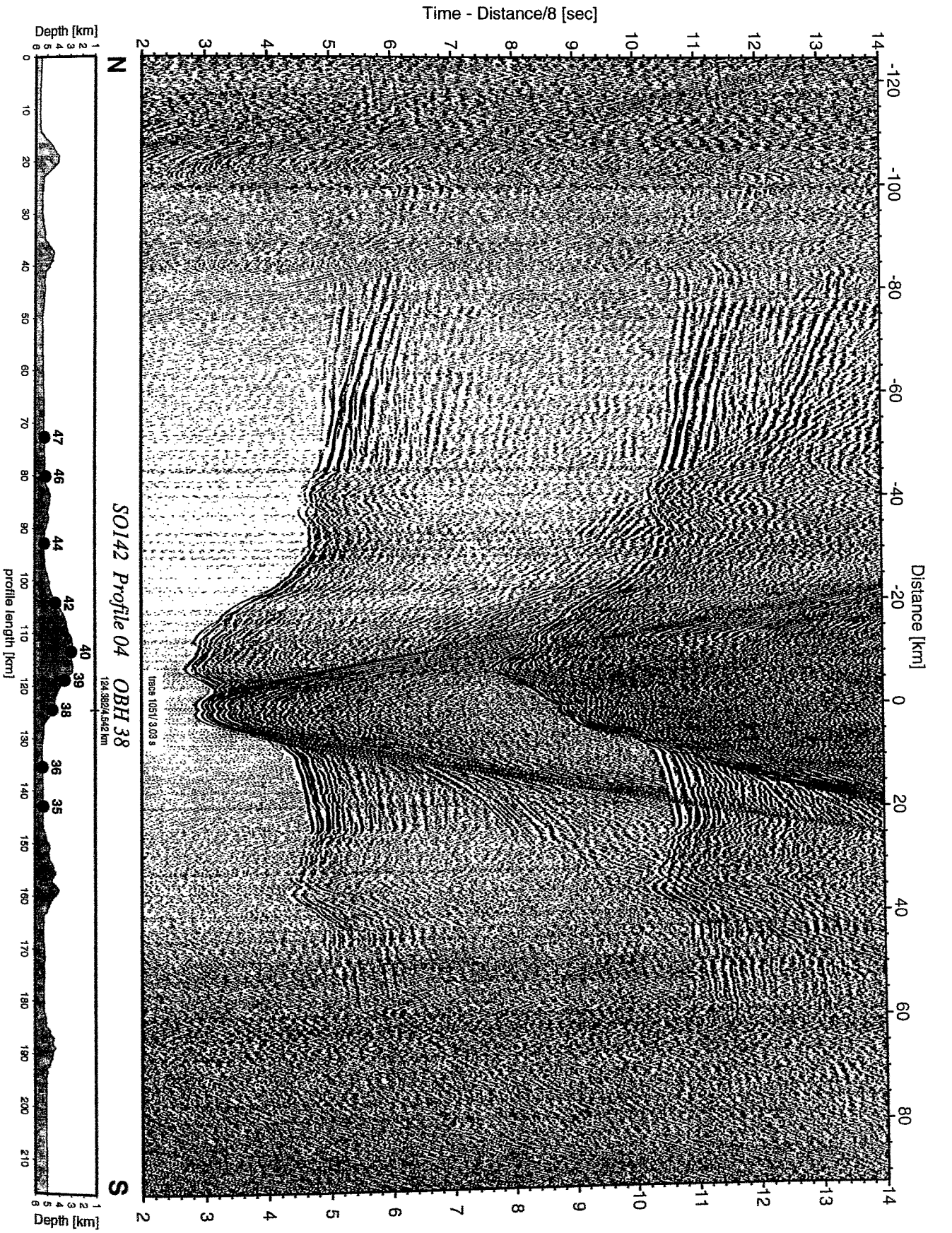

Figure 6.3.4.4.4: Record section from OBH 38 , Profile 04.

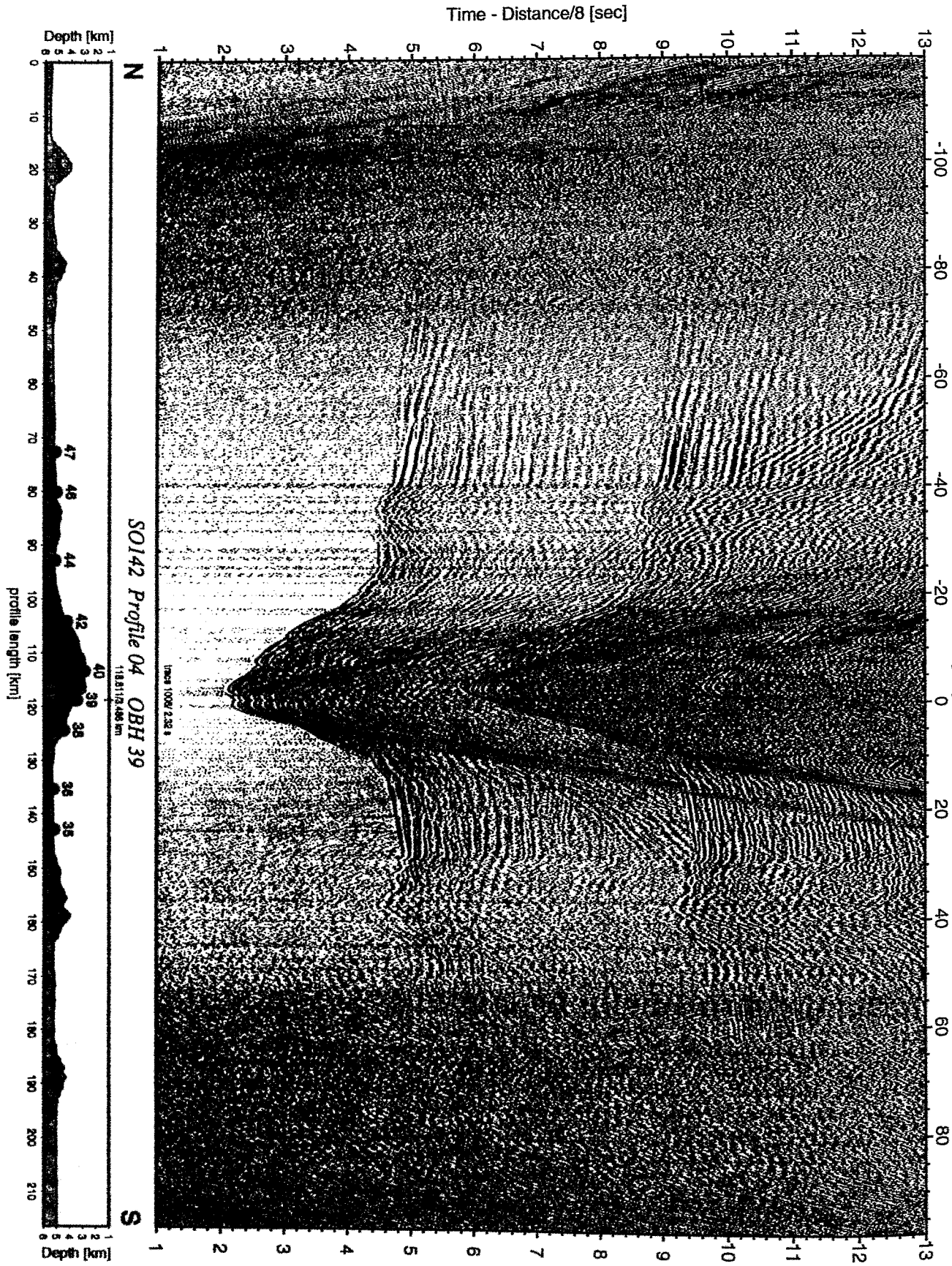

Figure 6.3.4.4.5: Record section from OBH 39 , Profile 04.

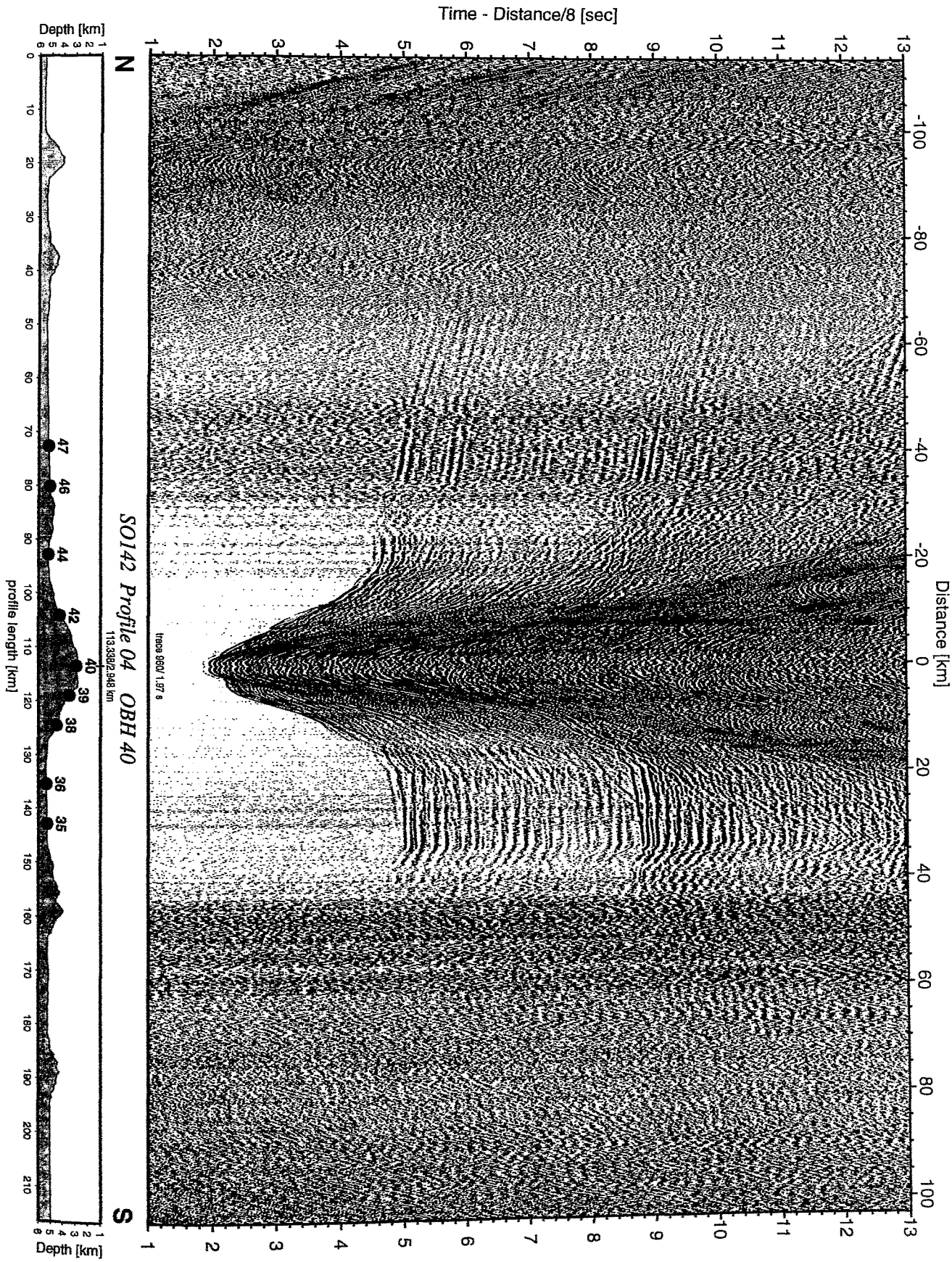

Figure 6.3.4.4.6: Record section from OBH 40 , Profile 04.

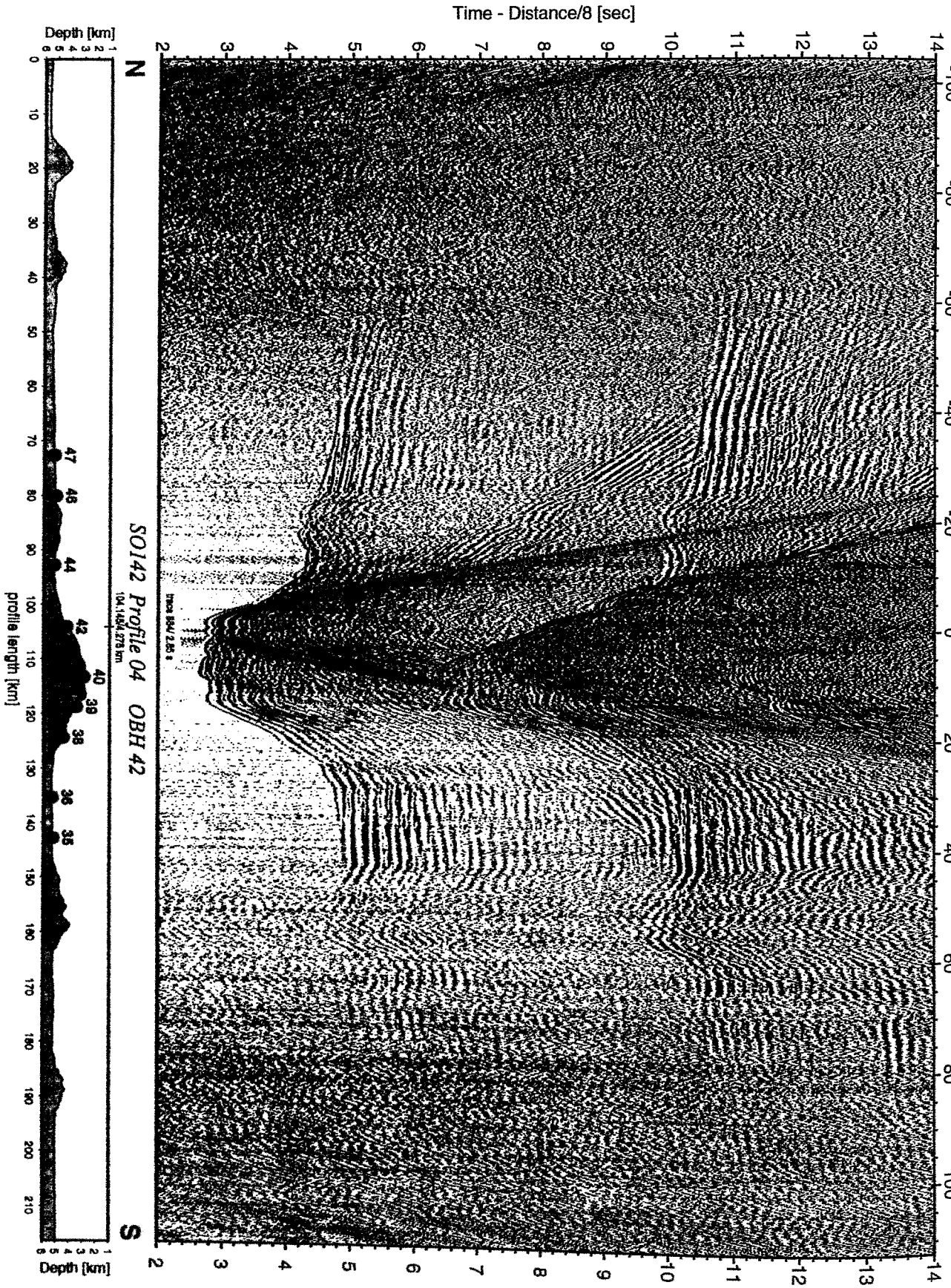

Figure 6.3.4.4.7: Record section from OBH 42 , Profile 04.

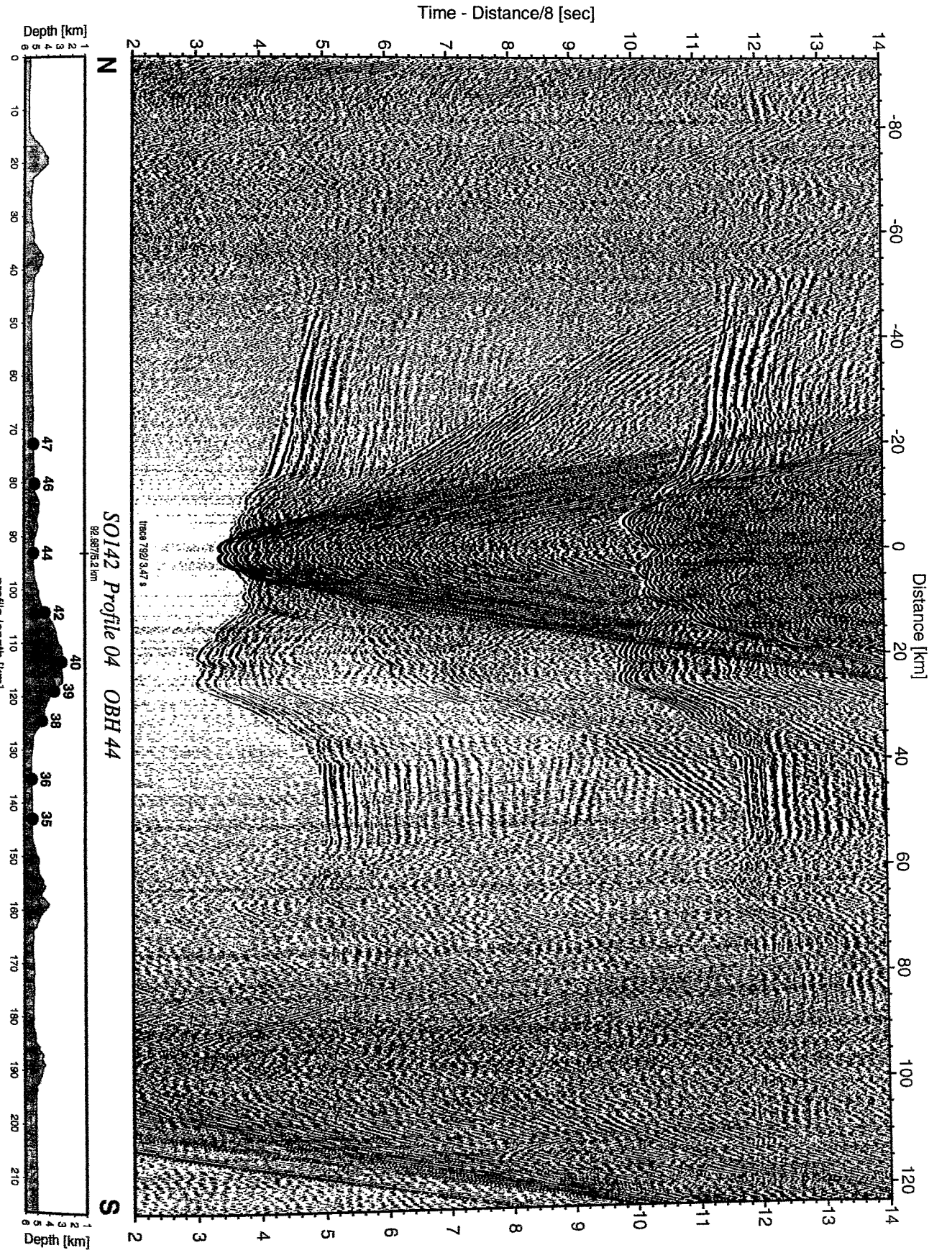

Figure 6.3.4.4.8: Record section from OBH 44 , Profile 04.

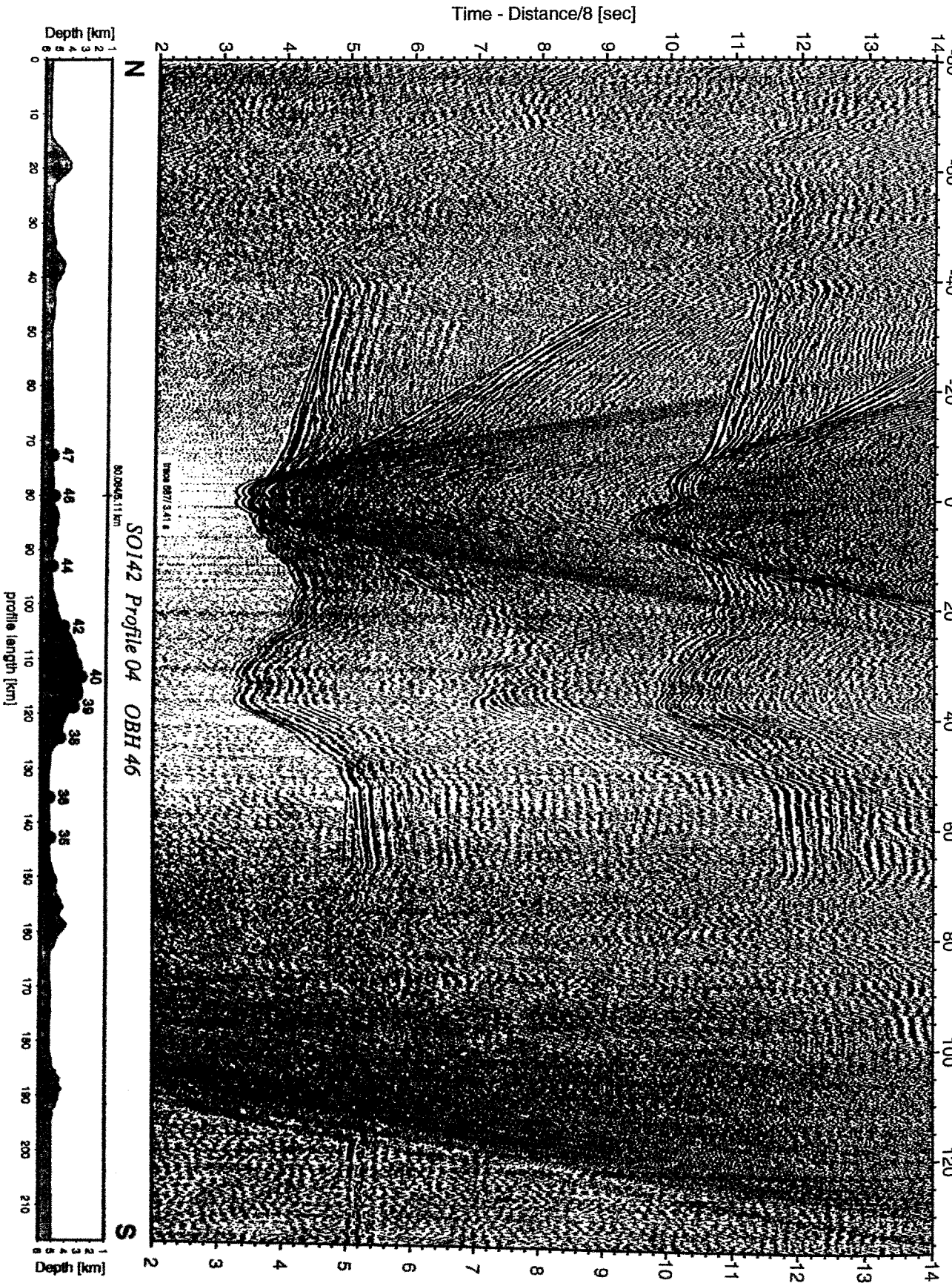

Figure 6.3.4.4.9: Record section from OBH 46 , Profile 04.

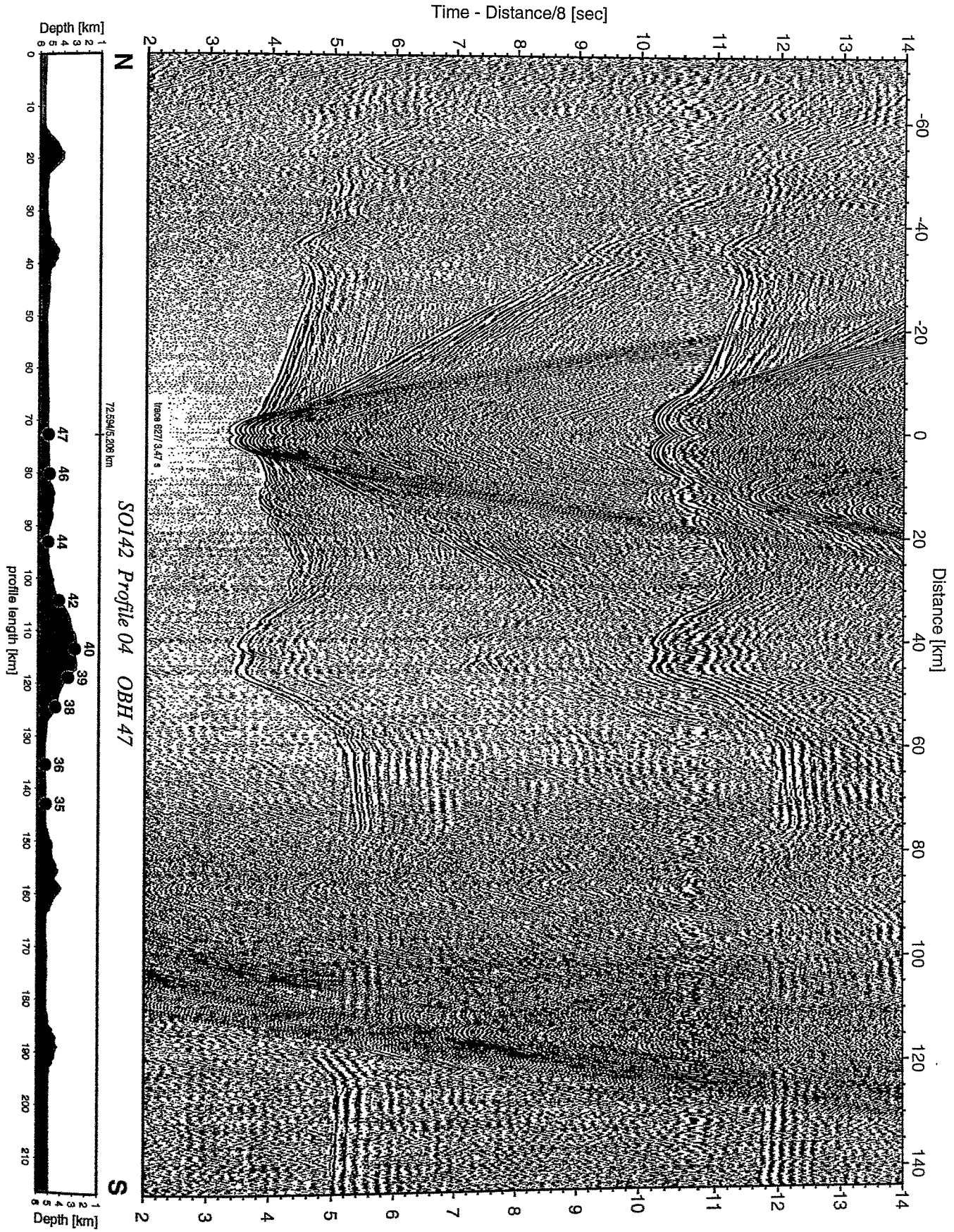

Figure 6.3.4.4.10: Record section from OBH 47 , Profile 04.

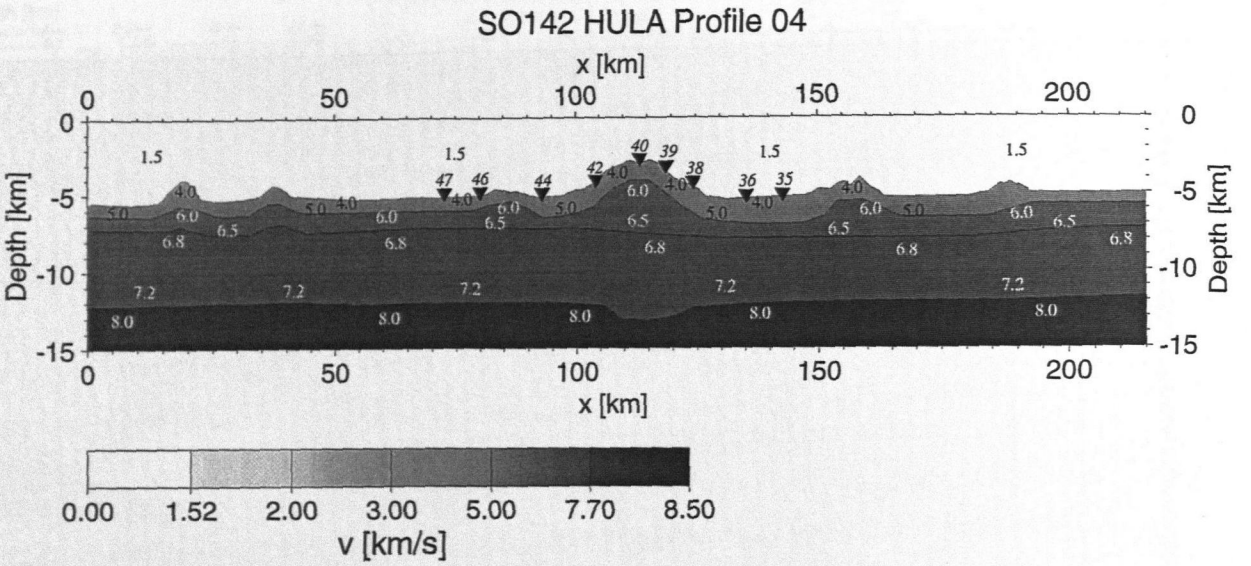

Figure 6.3.4.4.11: 2D preliminary velocity-depth model derived from forward modelling. Velocities are given in km/s. OBH stations are represented by triangles annotated with the station number.

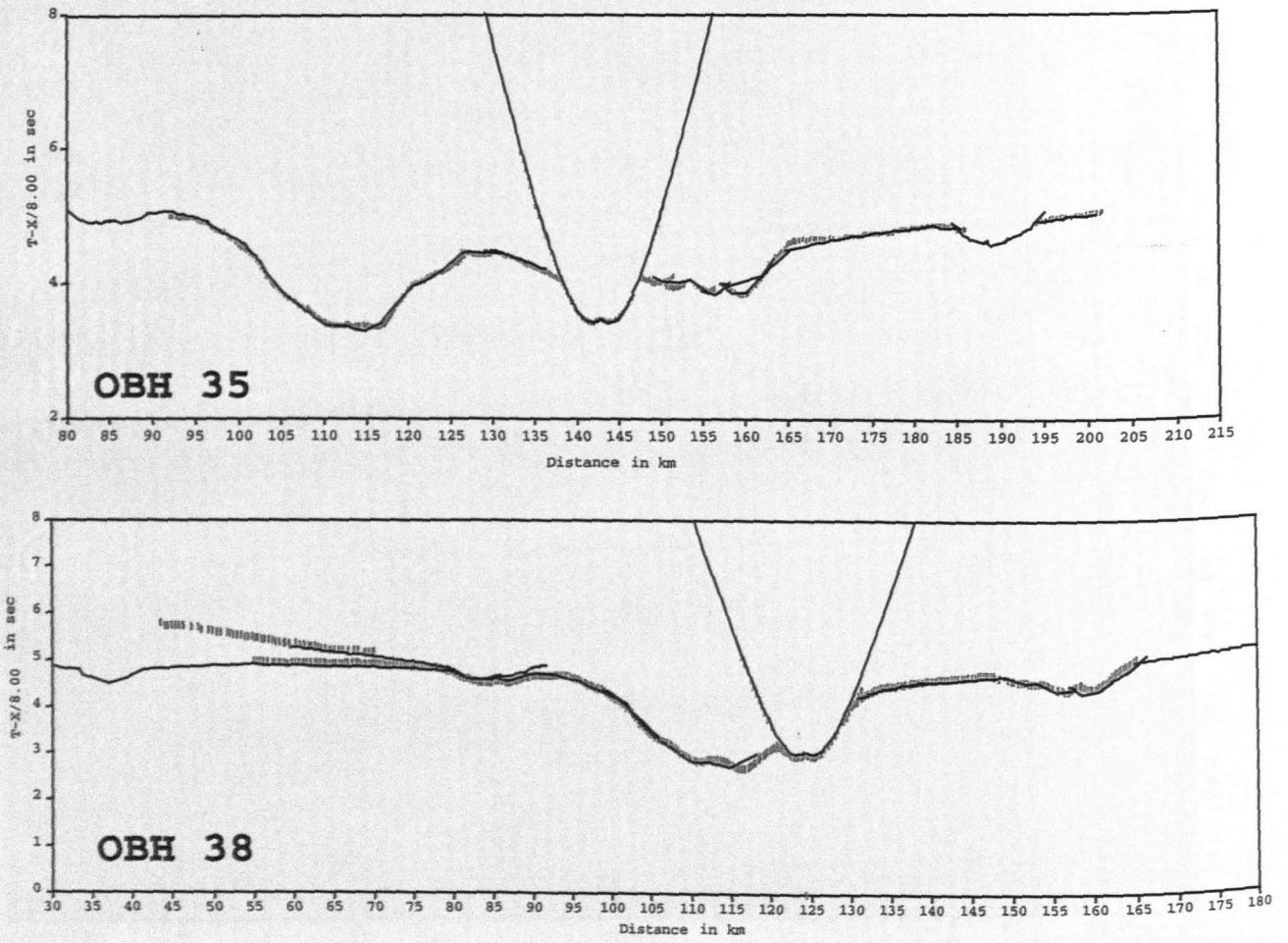

Figure 6.3.4.4.12: Traveltimes and model fit for two OBH positions of profile SO142-04. Arrival times are dominated by the varied seafloor topography.

6.4. MAGNETICS

(C. Kopp and watchkeepers)

Magnetic data across seamounts and ridges show clear anomalies in contrast to the surrounding oceanic cust. In theory, this signature is related to the strength and orientation of the earth's magnetic field at the time of formation, as well as the shape and the size of the seamounts. If the age of a seamount is determined through geological sampling, information about its formation can be gained from the magnetics. On the other hand, assuming a certain geometry and composition of a seamount, it is possible to estimate a 'magnetic age' of the seamount when no rock samples are available. The influence of seafloor spreading anomalies on the SO142 magnetic measurements is expected to be small, as the area around the Musician seamounts is referred to as the Cretaceous magnetic 'quiet zone'.

As on cruise SO141, magnetic data were sampled on every transit- and Hydrosweep profile. In total, 4100 km of magnetic data were recorded on 27 continuous lines. A list of all profiles with starting and ending points is given in Appendix 9.2. Fig. 6.4.1 shows all ship tracks along which magnetic data were recorded as bold lines. The longest profiles are plotted in Figs. 6.4.2 - 6.4.10 together with a Hydrosweep-depth plot along the line. The track of each profile concerned is given below, overlain with the 'predicted bathymetry' dataset of Smith and Sandwell, 1997. Increasing to the north, the total magnetic field ranges between 36500 nT and 40000 nT at the Musician seamounts. The noise level on most of the lines is only a few nT. Against this background, magnetic anomalies across the seamounts are clearly characterised up to 400 nT. Nevertheless, the earth's magnetic field experiences daily variations, so that the data may still contain longer-wavelength disturbances due to interaction of the earth's inner magnetic field with the ionospheric field. For quantification of the daily variations, an experiment was carried out on SO141 of sampling the same profile twice with a time difference of 11 hours. This experiment yielded a very small influence of the magnetic time variations (Cruise Report SO141, in preparation).

There is one substantial difference in the magnetic recordings of SO141 and SO142. Ages of the Hawaiian seamounts that were covered with magnetic measurements on SO141 range between about 45 Ma and 20 Ma (Clague and Dalrymple, 1987, 1989). Changing polarities within this time period are expressed in different polarisations of the sampled seamounts. The Musician Seamounts are, in contrast, built within the cretaceous magnetic quiet zone with normal magnetic field polarization. Hence, magnetic polarisations must all be oriented the same way with a magnetic minimum to the north and a maximum to the south. This behaviour can, for example, be observed clearly on the north-south srtiking lines in Figs. 6.4.3b and 6.4.4b. It is even more obvious in the 2D magnetic maps in Figs. 6.4.5 and 6.4.11: On the northern 'Italian' Ridge and the southern Bach Ridge, short distances of the magnetic recordings allow data interpolation between the profiles. With this 2D information, magnetic maps were created for the northern and the southern research areas. For display purposes, the along-track magnetic data were resampled onto a regular 2D-grid and plotted on a Mercator map, shown in Figs. 6.4.5 and 6.4.11. The correlation between volcanic structures and magnetic anomalies is obvious. The magnetic anomalies near the Musician Seamounts show regional features, like smaller seamounts and elongated ridges, whose magnetic polarisation is oriented in the expected direction.

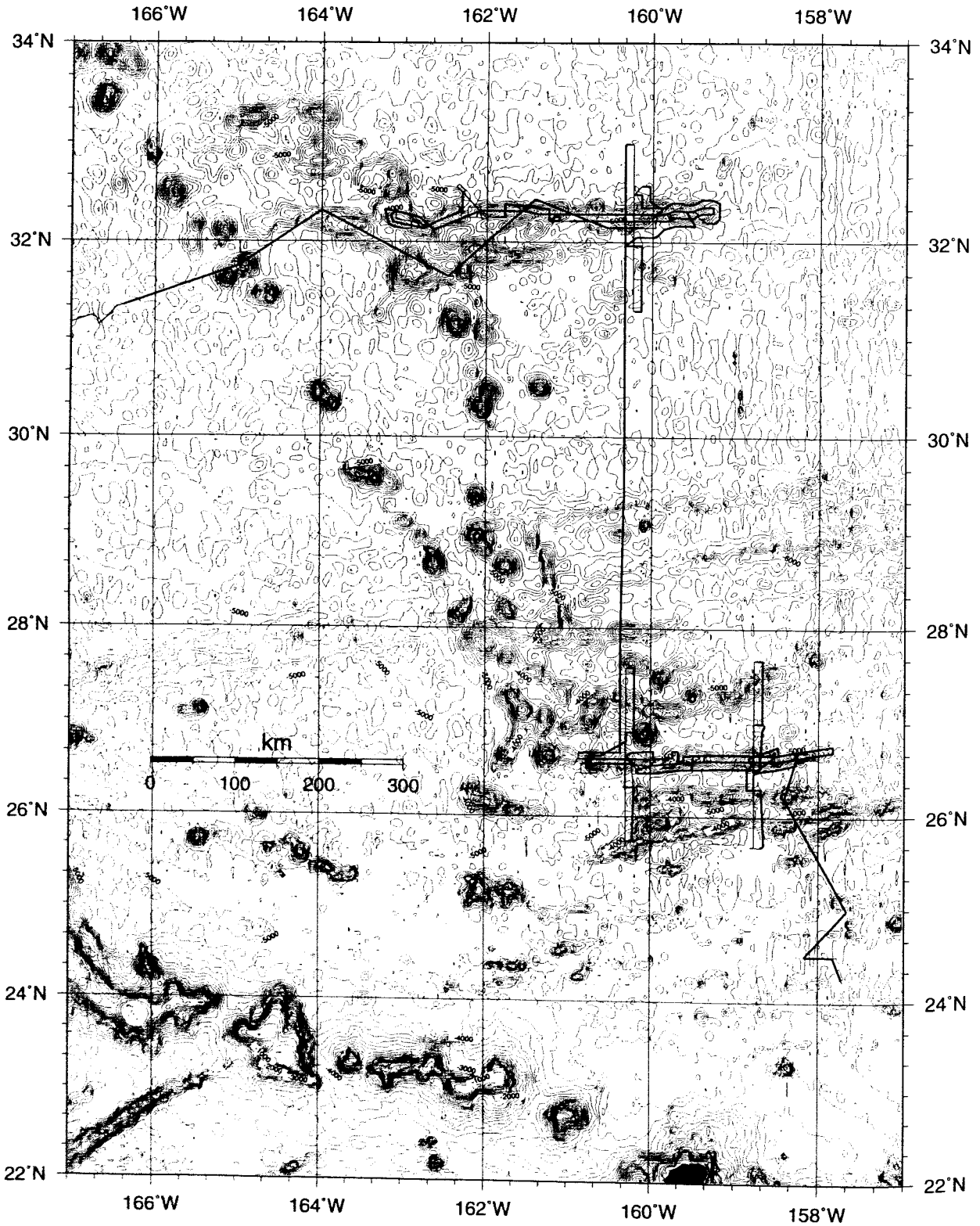

Figure 6.4.1: Ship track across Musician Seamounts on 'predicted bathymetry' map. Magnetic profiles in bold.

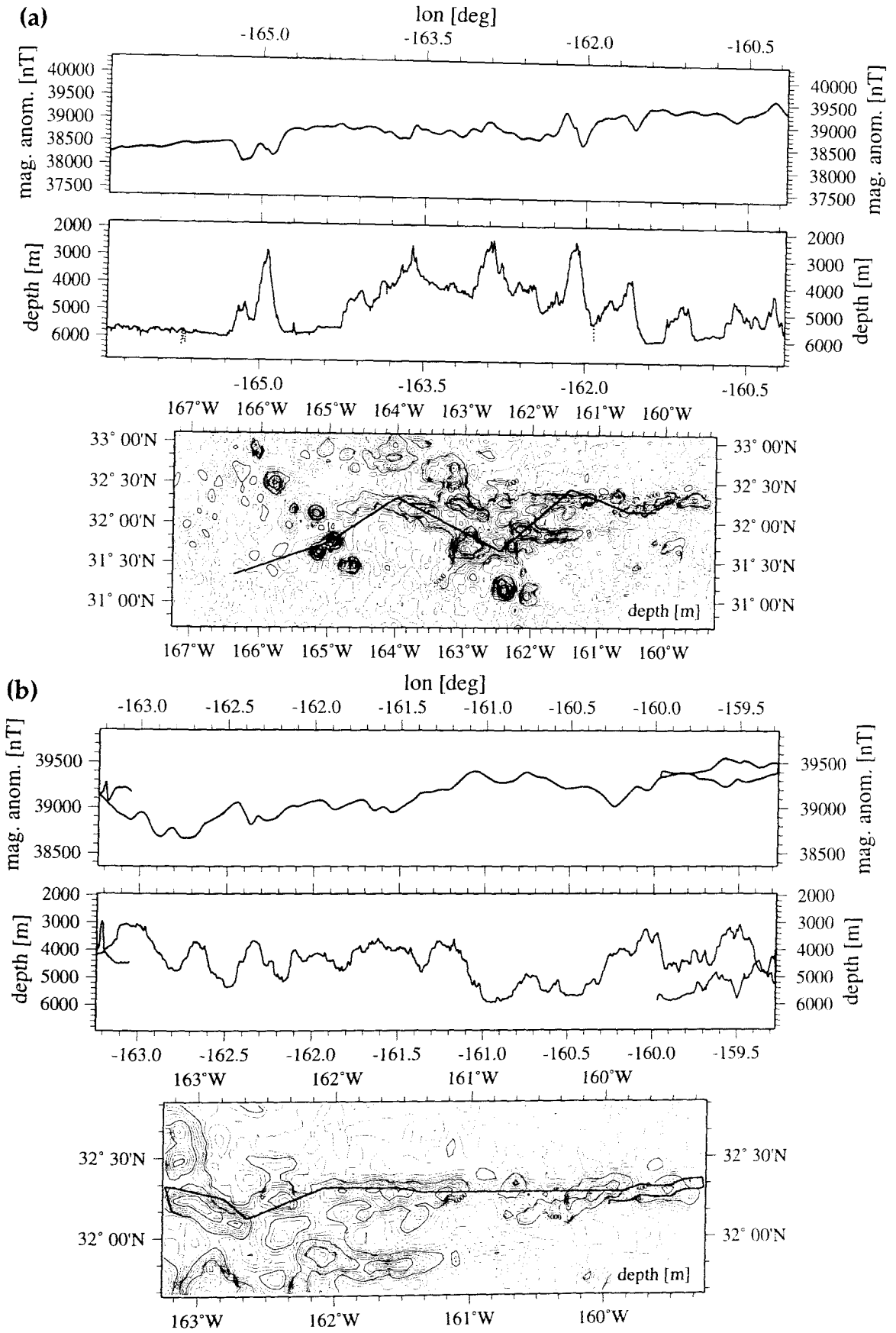

Figure 6.4.2: Magnetic profiles p101 (a) and p107 (b). Lower: track on predicted bathymetry map; middle: depth profile along track; upper: magnetic anomaly.

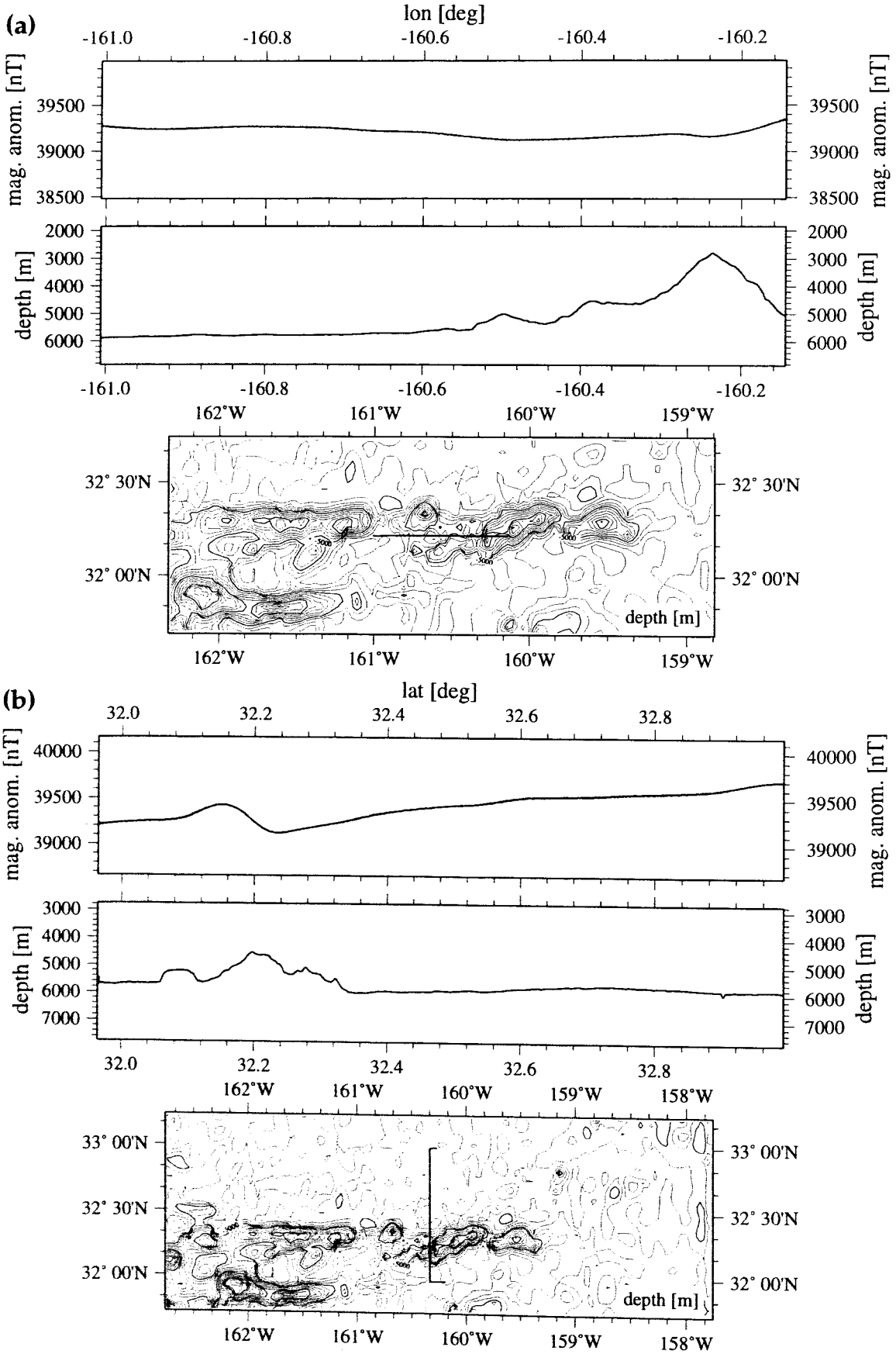

Figure 6.4.3: Magnetic profiles p112 (a) and p115 (b). Lower: track on predicted bathymetry map; middle: depth profile along track; upper: magnetic anomaly.

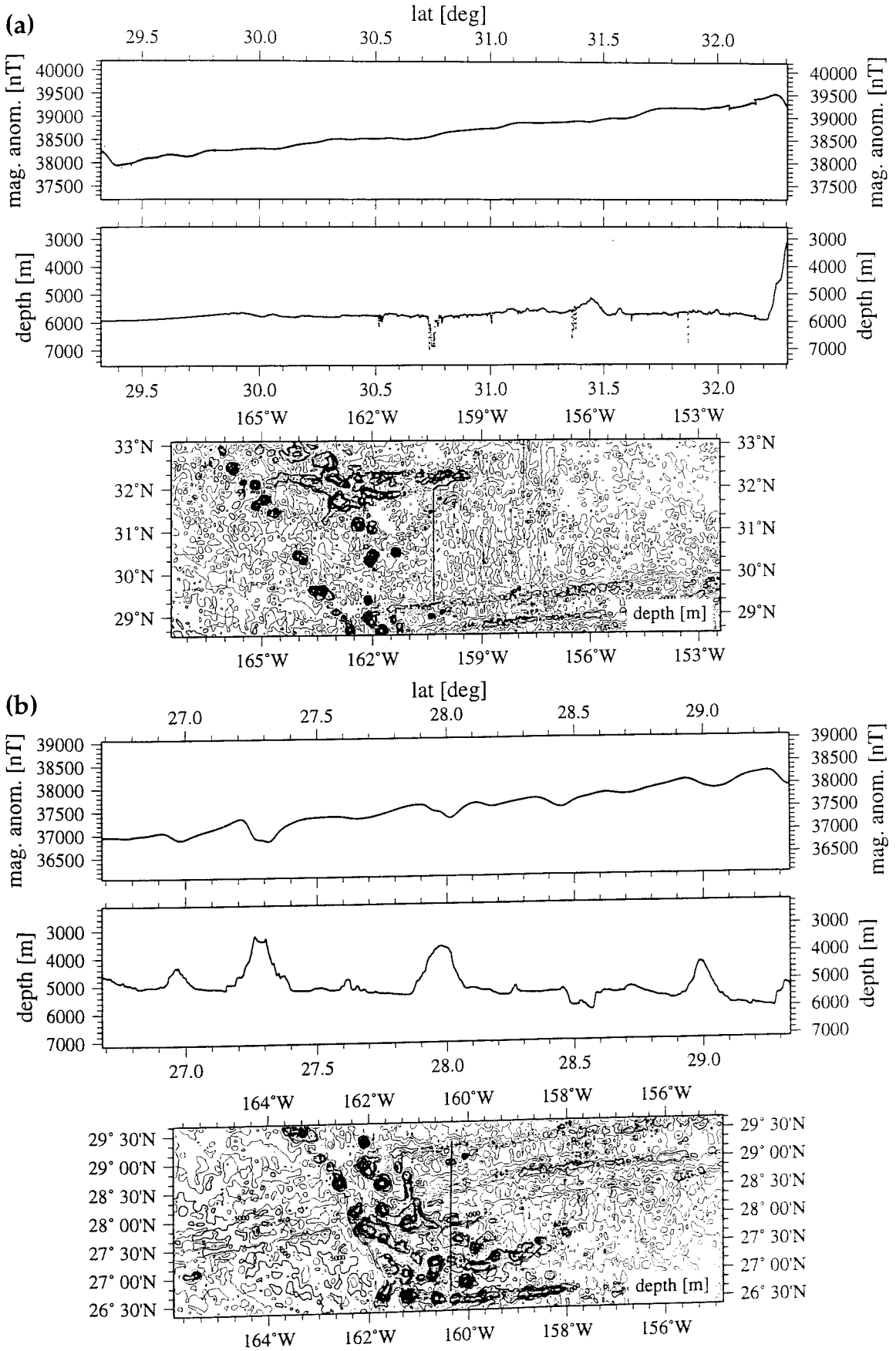

Figure 6.4.4: Magnetic profiles p117 (a) and p118 (b). Lower: track on predicted bathymetry map; middle: depth profile along track; upper: magnetic anomaly.

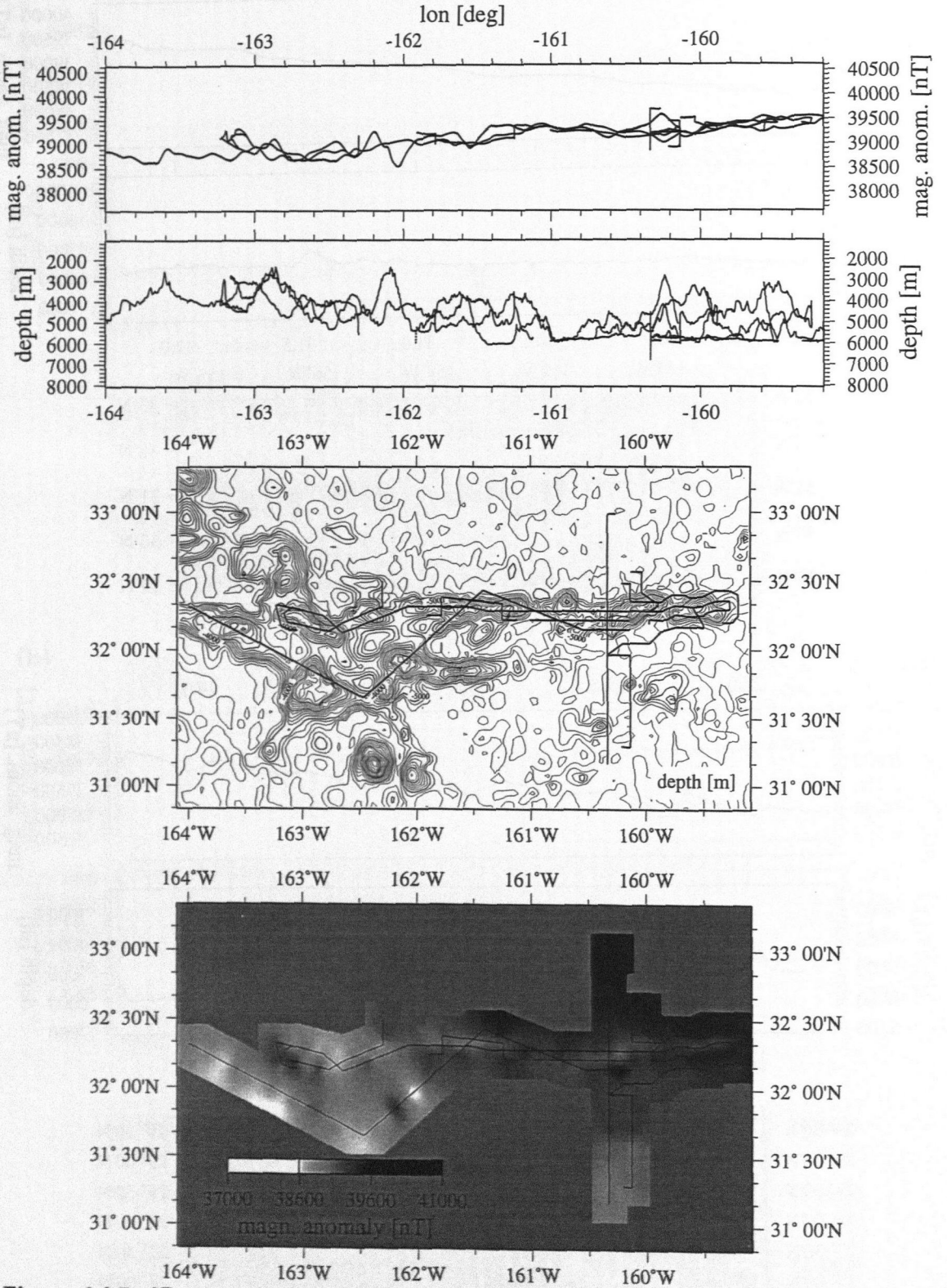

Figure 6.4.5: 2D-magnetic experiment on northern Musician Seamounts. From top to bottom: Magnetic anomaly displayed in horizontal stack; corresponding depth profiles; track on predicted bathymetry map; greyscale coded magnetic anomaly.

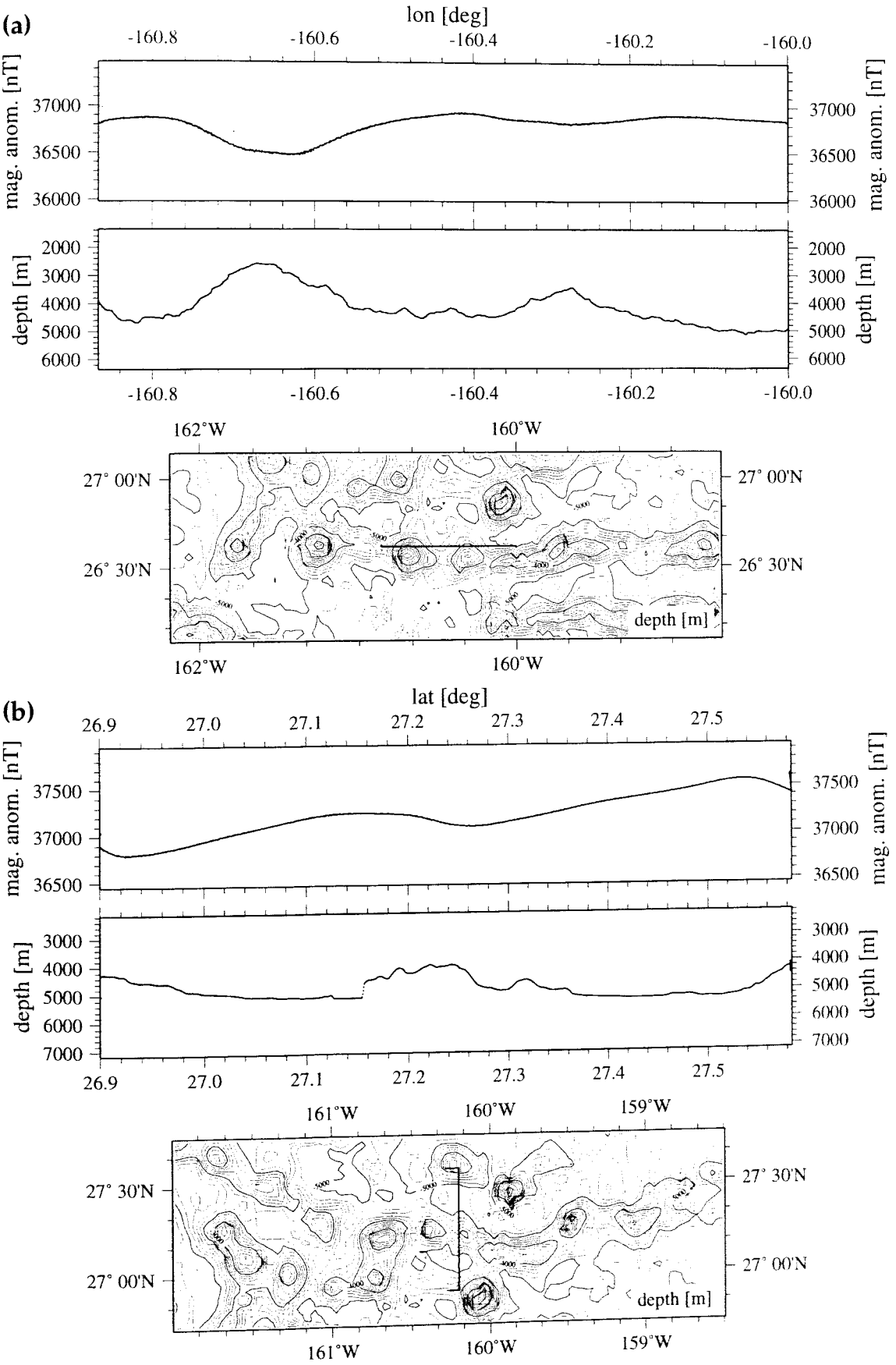

Figure 6.4.6: Magnetic profiles p120 (a) and p122 (b). Lower: track on predicted bathymetry map; middle: depth profile along track; upper: magnetic anomaly.

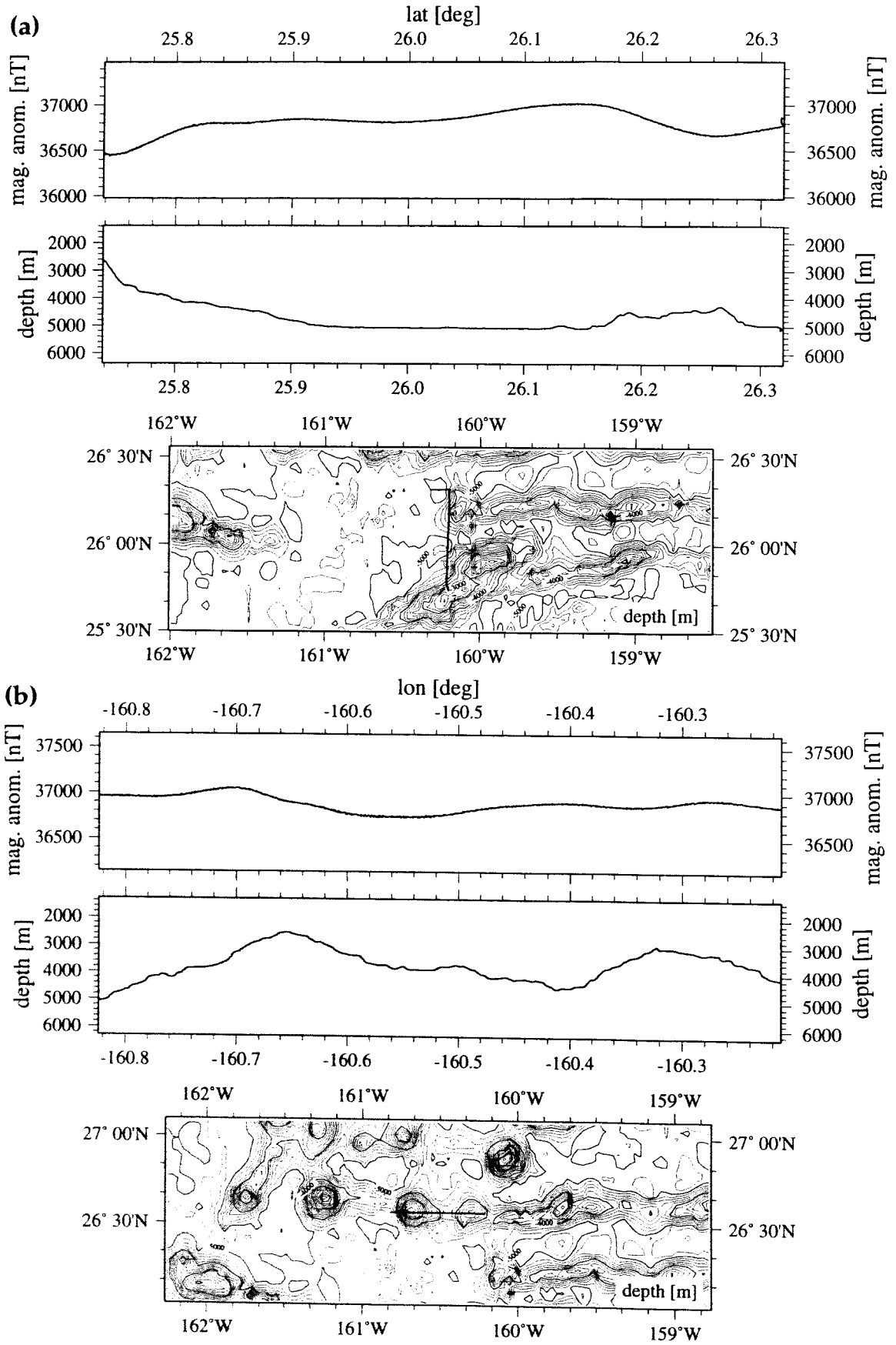

Figure 6.4.7: Magnetic profiles p123 (a) and p125 (b). Lower: track on predicted bathymetry map; middle: depth profile along track; upper: magnetic anomaly.

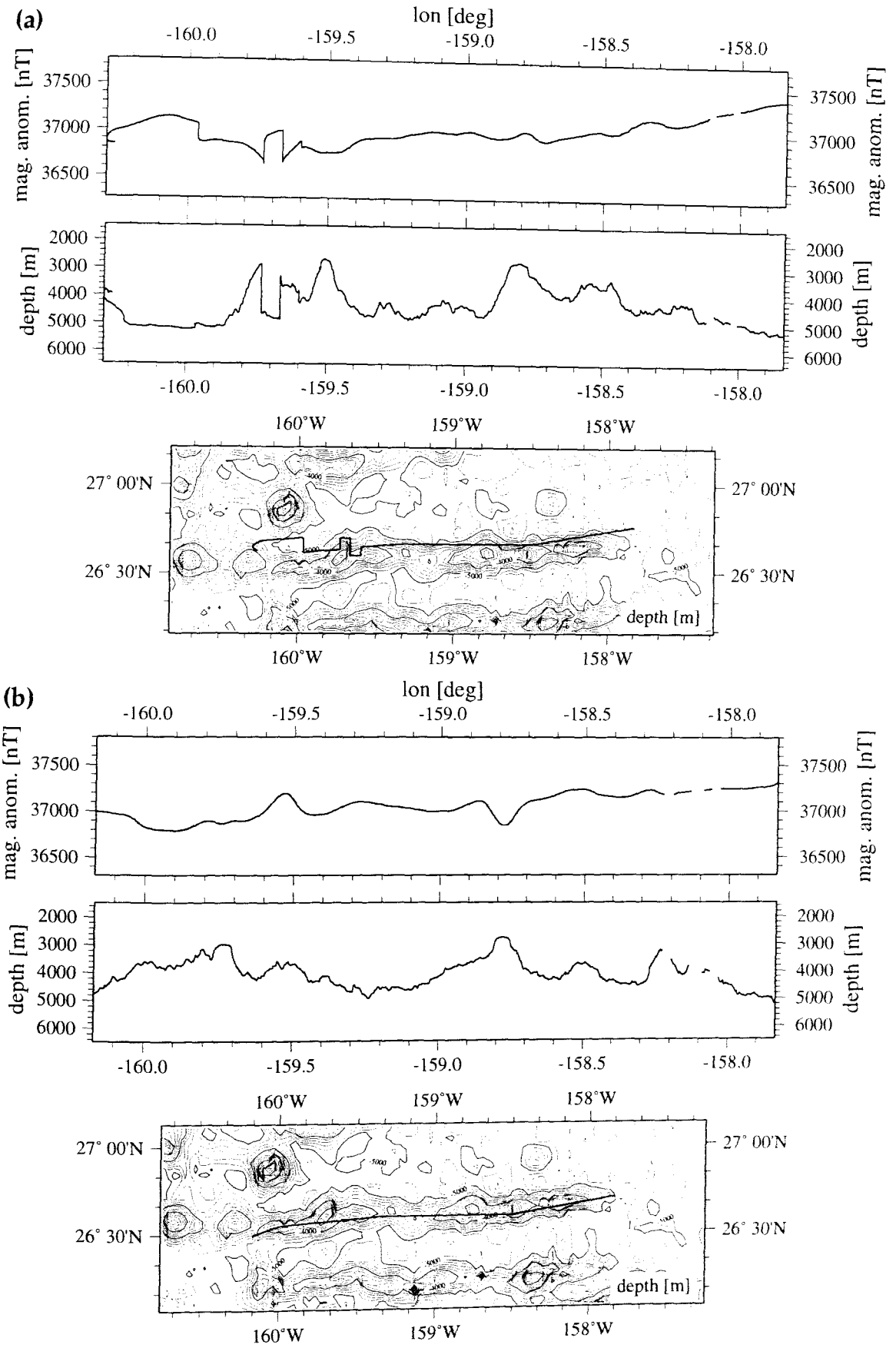

Figure 6.4.8: Magnetic profiles p126.1 (a) and p126.2 (b). Lower: track on predicted bathymetry map; middle: depth profile along track; upper: magnetic anomaly.

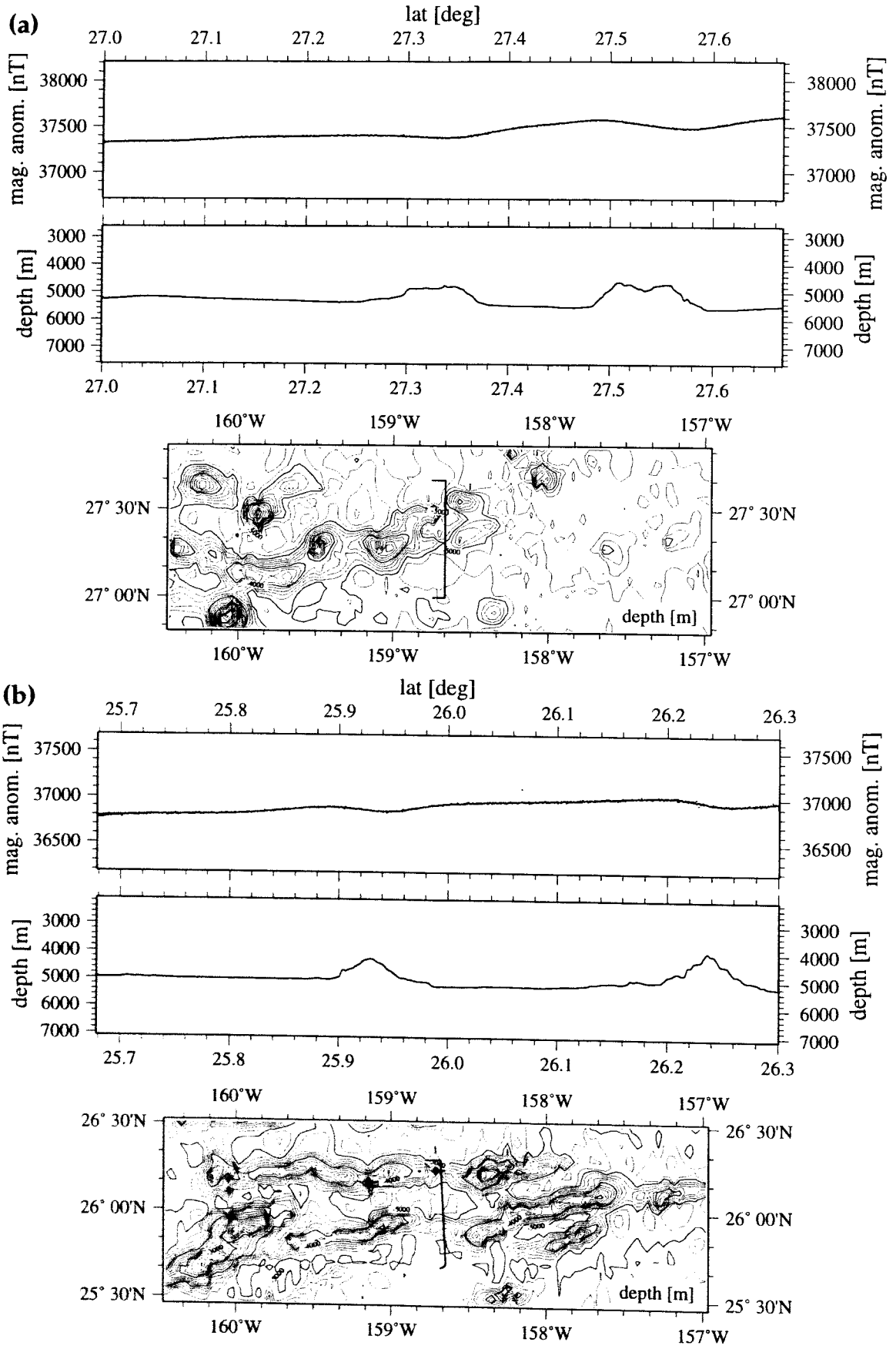

Figure 6.4.9: Magnetic profiles p128 (a) and p129 (b). Lower: track on predicted bathymetry map; middle: depth profile along track; upper: magnetic anomaly.

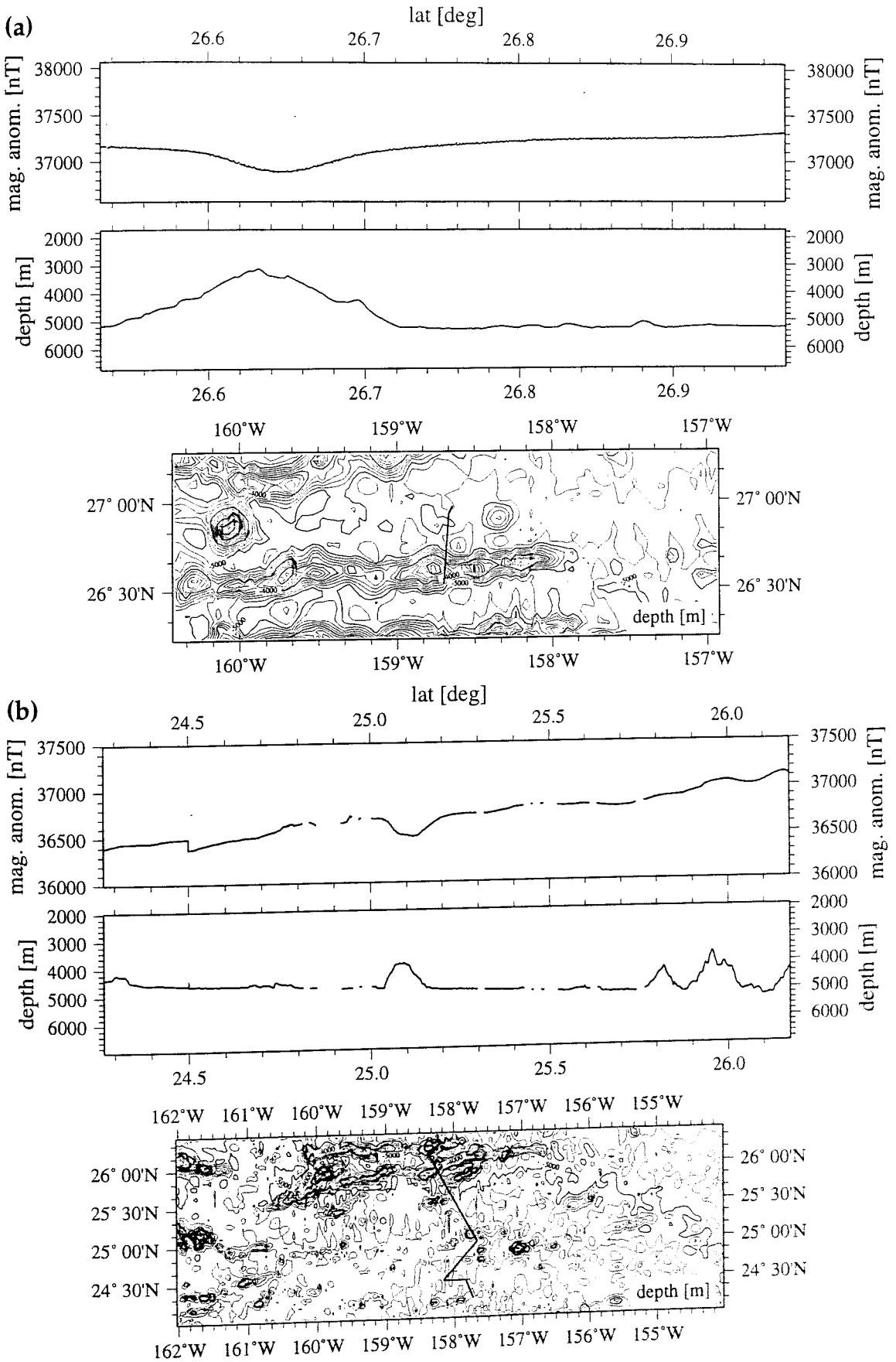

Figure 6.4.10 Magnetic profiles p130 (a) and p135 (b). Lower: track on predicted bathymetry map; middle: depth profile along track; upper: magnetic anomaly.

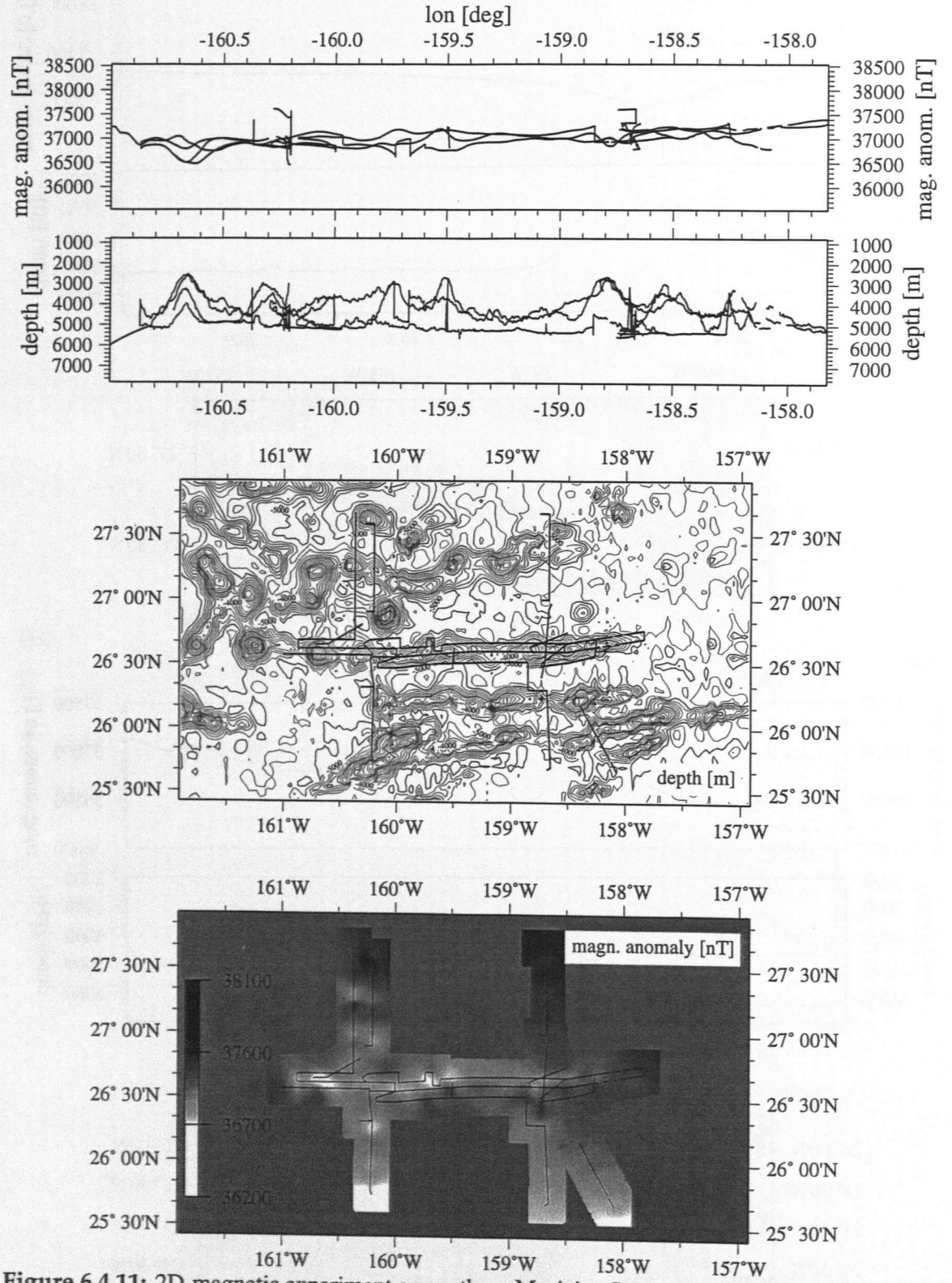

Figure 6.4.11: 2D-magnetic experiment on southern Musician Seamounts. From top to bottom: Magnetic anomaly displayed in horizontal stack; corresponding depth profiles; track on predicted bathymetry map; greyscale coded magnetic anomaly.

6.5 GEOLOGICAL PROVINCES AND ROCK SAMPLES

(R. Hekinian and J. O'Connor)

The Musician Seamount region is located in the North Pacific between two major fracture zones, the Pioneer and the Molakai Fracture Zones (near 23°N-155°W, in the Pacific-Farallon plate), and encompasses several seamounts and ridge provinces. Several East-West trending ridges were observed from the altimetric map and verified by the hydrosweep bathymetric survey carried out during the F.S. SONNE 142 HULA II cruise).

The locations of SO 142 dredge stations are shown in Figure 2.2.2.2.1. Descriptions of samples are in Appendix 9.4.

Of the total of 13 dredge stations attempted during SO-142, all were successful in recovering rock samples. Once onboard, most rocks were cut using a rock saw and cleaned in water. They were then examined with a hand lens, and grouped according to their mineral content and degree of seawater alteration. Samples suitable for the analytical goals of this project were those containing fresh feldspar as a phenocryst or groundmass phase, glass, and those rocks having the most unaltered groundmass. In addition, MnOx and possible hydrothermal crusts were systematically sampled for Prof. Peter Stoffers and colleagues, University of Kiel.

Fresh blocks of representative rock were cut for thin section preparation, microprobe examination, geochemistry, and further processing to extract glass (if applicable). Each of these sub-samples, together with sufficient amount of remaining bulk sample, was sealed in either plastic bags or bubble wrap for transportation to Christian-Albrechts-University of Kiel. Further studies will involve petrographic examination of thin sections, analyses of phenocryst and groundmass phases using the electron microprobe, determination of major and trace element geochemistry by X-ray fluorescence spectrometry or inductively coupled plasma mass spectrometry, and radiometric dating of suitable samples by the $^{40}Ar/^{39}Ar$ incremental heating technique. The key objectives of that work will be to obtain the first definitive age determinations for each seamount and ridge and to assess any changes in geochemistry with time. Theses analyses will allow us to address two basic questions pivotal to achieving the objectives of HULA II, 1) were the Musician elongated ridges created quickly as single lines of volcanism and 2) did their creation involve mixing between plume and spreading-axis material originating from the western and eastern sides if these ridges, respectively.

6.5.1 NORTHERN ELONGATE RIDGES

The northern E-W trending ridges, Rossini, Bizet, and Donizetti, consist of linear en echelon structures. The most northern ridges are discontinuous en echelon structures with a general N280° orientation.

Rossini Ridge

Rossini Ridge has a slightly sigmoidal shape roughly oriented N280° with several volcanic cones. One of these cones, located on the western tip of the ridge, was a dredge target because of the steep steps found on its northern flank. The peak of the seamount is about 3000 m above the surrounding floor (about 6000 m).

Donizetti Ridge

Donizetti Ridge is made up of two segments of 200 km in length. One segment, located between 160°W and 160°30'W (West Donizetti) consists of at least 3 volcanic cones shallower than 3400 m.

The surrounding sea floor is at a depth of about 6000 m. The volcanic cones are easily distinguished at depths shallower than 4500 m. The irregular lobes and indentations on the flanks deeper than 4000 m are probably the result of mass wasting and landslides. There is no evidence of collapsed volcanic summits (craters). To the northeast, the volcanic cones are less prominent and are disrupted by topographic lows near 159°55'W at the 4500 m contour line near the more easterly located ridge segment (East Donizetti). A seismic profile was conducted at about 30 km west of the dredge station (SO142-4DR, 32°14'N-159°56W).

The other segment further to the east of the ridge (East Donizetti), at 159°40'W-159°17'W, consists of an elongated E-W trending feature rising from a depth of about 5600 m to 3000 m. This ridge segment is made up of several (3) coalesced circular volcanic cones. Each of these cones is about 500 to 1500 meters in height and has a base diameter of about 4-7 km.

Bizet Ridge

Bizet Ridge is about 10-15 km wide with three distinct volcanic edifices at depths of about 3000-4000 m. An experimental seismic profile was conducted from north to south across the western tip of the ridge in the vicinity of the dredge station SIO142-2DR near 32°21'N, 162°5'W.

6.5.2 FRACTURE ZONES

The traces of E-W trending linear fracture zones recognized from the satellite altimetric data are criss-crossed by the chain of the Musician Seamounts. The Murray fracture zone near 29°N-160°W. The reason for sampling this fracture zone was to gain insight on the composition of the Cretaceous oceanic crust which formed on an ancient spreading ridge segment of the Farallon plate. The study of these samples will eventually help to determine any existing compositional relationship with the off-axis volcanism that created the various seamounts in the area and might give some indication as to the evolution of volcanism. The basin in the vicinity of the Murray fracture zone is at a depth of about 5900-6000 m and consists of gently rolling hills with a relatively thin (about 20-30 m), transparent sediment cover (parasound sonar) underlain by a thicker, more compacted material (sediment). The site for sampling was picked during the transit south toward the southern E-W trending ridges (Bach and Beethoven). The south-facing slope of the north wall of the transform, with a relief of about 900-1000 m and typical staircase scarps representing normal faults, was sampled successfully.

6.5.3 NORTHERN RIDGES ROCK SAMPLE STATIONS

The previous data from the Bizet Ridge, also called the Musician Horst area by Pringle (1992), consist essentially of alkalic lava (4 analyses) and few (2 analyses) E-MORB types of samples. Most samples collected during SO142 (HULAII cruise) appear old with different degrees of alteration. In addition, they are associated with both manganese crust and Fe-Mn nodules (Figure 2.2.2.2.1).

SO142-1DR, Rossini Ridge. The Rossini Ridge (also called Rossini seamount, Pringle, 1992) dredge haul (SO142-1DR) was conducted along the northern slope of the ridge at the level of the volcanic cone (3147-3840 m). The dredge samples consist of altered aphyric basalt and a slab of volcanoclastic material. The surface texture and the manganese-rich coating of the samples indicates that the material was slumped from local outcrops. The volcanoclastics suggest that reworked outcrops of loose rock fragments may be ejected during submarine explosive events.

SO142-2DR, West Bizet Ridge. The western Bizet Ridge was sampled on its northen flank (SO142-2DR) at a depth of 4179-5273 m. About 90% of the dredge haul consisted of manganese-coated sediment clasts and volcanoclastic material. Only three fragments of plagioclase (<5%) phyric basalts

were collected and four fragments of indurated "silicified" cherty-looking sediment slab. The rocks are abundantly altered (more than in SO142-1DR) and coated with MnOx (1.2 cm thick) crust.

SO142-3DR, East Bizet Ridge. The eastern tip of the Bizet Ridge slope was also dredged (station SO142-3DR). The sampling was carried out along a steep southern slope with about 600 m relief near 32°14.28'N, 161°07.21'W. There does not appear to be a conical feature at 4527-5385 m depth; however a circular volcanic cone occurs at shallower depth (4000-3000 m) along the scarp. The samples from this dredge are rusty light-brown altered plagioclase phyric basalts. Volcanoclastic brecciated material containing palagonatized glassy basalts was also found within the samples.

SO142-4DR, West Donizetti Ridge. This dredge (SO142-4DR) was carried out on the southern part of the western Donizetti Ridge, flanking a circular volcanic edifice which peaks at about 3500 m deph. The dredge was positioned at 4850-3783 m and it is believed that this sampling site is associated with a conical edifice. The dredge was almost full and consisted essentially (75%) of fresher basaltic lava than in SO142-3DR. Preserved glassy chilled margins were apparent. Most of the rocks represent talus material; some are breccias cemented with iron-manganese precipitates. The basalts consist of moderately-altered and aphyric pillow lavas. Their chilled margins are partially palagonatized. However, microprobe analyses will also be performed on the preserved glass chips. Other volcanoclastic breccia with patches of partially altered (palagonatized) glass are set in a yellowish-white colored clay matrix (nontronite-like).

SO142-5DR, East Donizetti Ridge. The dredge haul on the eastern Donizetti Ridge (SO142-5DR) was taken from the southern slope of the ridge at 5177-3790 m depth. This southern slope showed a staircase structure with normal faults of about 900 meters relief. This is comparable to SO142-4DR and consists of many (70%) altered pillow lava fragments mixed with manganese crust, as well as breccias and a few conglomerates of basaltic rocks. Traces of Fe-oxyhydroxide hydrothermal material occur in association with the brecciated and conglomerate material. A very few fragments contain chilled margins that are abundantly altered.

SO142-6DR, Murray Fracture Zone. The dredge haul from the Murray Fracure Zone (SO142-6DR), taken at 29°16'N, 160°24'W between 5537m and 5185m depth, contains essentially old-looking. yellowish, light-brown basaltic fragments and dolerites. The samples are not *in situ* and many show smoothed edges, suggesting avalanche debris. A few fragments show light-greenish impregnation in their fine-grained matrix (sample SO142-6DR-12) as well as veined material suggestive of hydrothermal circulation.

SO142-7DR, West Bach Ridge. The dredge made along the northern slope of a tall volacinc edifice at 3252-4548 m contained only 8 samples: Four Fe-Mn crusts and four highly phyric plagioclase basalts (HPPB) with subrounded pillow lava morphologies.

6.5.4 SOUTHERN E-W TRENDING RIDGES SAMPLES

SO142-8DR, West Bach Ridge. The dredge haul along the western Bach Ridge (SO142-8DR) was carried out on the northern slope of a seamount near 26°37N, 160°15W (2964-3996 m depth). through which a N-S seismic refraction line had been conducted. The seamount has a triangular summit about 3 km wide and culminates at a depth of about 2700 m. The base of the seamount defined by the the 4300 m contour line is about 20 km in diameter. An almost full dredge (about 250 kg.) of altered pillow lavas coated with manganese was recovered. Most samples consist of highly phyric plagioclase basalt (HPPB) due to early accumulation of plagioclase prior to eruption. Some samples have preserved their glassy margins. In addition to the plagioclase phenocrysts.

there are some rounded agglomerates of minerals (mainly plagioclase and some olivine) which are believed to be foriegn inclusions from the host basalt (xenoliths and/xenocryst).

SO142-9DR, East Bach Ridge. The dredge haul from the eastern Bach Ridge (SO142-9DR) was made on the northeastern slope of a seamount located near 26°39.975'N, 159°28.085W (2853-3931 m). This dredge contained essentially altered fragments of pillow lavas representing talus material. The seamount has a conical summit of about 2 km in diameter at about 2000 m depth. There is less manganese coating the surface of the samples and they are more vesicular (>15% vesicles) than the rocks from the previous two dredges. Most of the chilled margins coating the pillows are completely altered (palagonatized). Most samples are aphyric and only a few dark gray fragments are suitable for bulk chemical analyses. However, there are some brecciated rocks containing preserved basaltic glassy chips. Also, a light greenish-yellow hyaloclastite-like material containing altered glassy fragments was collected.

SO142-10DR, East Bach Ridge. The northern slope of a large, flat-topped volcanic edifice - probably a guyot - was sampled near 26°33'N, 158°47'W at 3533-4093 meters (Figure 2.2.2.2.1). All of the samples have a moderately fresh appearance; they are light-gray in color and appear to represent fragments of younger flows than the previous dredges from the same ridge. Some pillow lava fragments contain rounded foreign inclusions (xenoliths) consisting of plagioclase-olivine aggregates. These could be mircrogabbro fragments carried along during extrusion. Few fragments of volcanoclastic material containing small rock debris and altered glass chips in a yellowish hydrothermal matrix occur.

SO142-11DR, East Bach Ridge. The area chosen for dredge station SO142-11DR was on a small adventive cone with a summit crater of about 1 km in diameter and 300 m in depth, located on the northern side of a larger edifice. The summit is at 3500 meters inside the floor of the crater and the peak is elongated in the NW-SE direction (290°). The samples collected on the outer slope of the crater are abundantly altered with a rusty light-brown coloration, and they consist essentially of pillow fragments. These samples are more altered than those from the previous dredges collected along the same ridge. This dredge also contains similar volcanoclastic material as previous hauls, with the material made up of altered glassy chips cemented together with a greenish yellow clay-like material that is believed to be of hydrothermal origin.

SO142-12DR, East Bach Ridge. This station was made near 26°42.34'N, 158°14.64W at 3643-3840 m depth, on the northern slope of a seamount located on one of the E-W trending structures of the Bach Ridge. The seamount appears to be on top of another larger east-west trending topographic feature which extends on both side of the seamount. Steep scarps are seen on the nothern and the southern flanks of the ridge from 4000 m down to about 5000 m depth near the intersection with the abyssal hill province (basin). The dredged seamount peaks at about 3000 m, and its base is at about 3600 m depth according to the available hydrosweep preliminary survey. The samples collected vary between abundantly-altered pillow lava fragments with rusty colorations to moderately-light brownish-gray basalts. Few samples of pillow buds with some preserved glassy margins occur. These samples show a glassy interior which is completely palagonatized. They are coated with a thick manganese crust which might have preserved them from sea water alteration.

SO142-13DR, Beethoven Ridge. A seamount located on another E-W trending ridge was sampled (SO142-13DR) near 26°10'.59N, 158°24.359'W. This drege haul, made along the northern slope of the seamount at a depth of 3765-4905 m, contains altered pillow lava fragments, some of which contain preserved glassy chilled margins. The samples are coated with a Fe-Mn crust of variable thickness and represent talus material due to flow front collapse and/or are slumped material from faulting. The

samples appear less altered than those from the previous dredge (12DR) from the Bach Ridge. Most samples have foreign inclusions (xenoliths and xenocryst) included in their basaltic hosts. These are similar olivine-plagioclase-pyroxene inclusions of microgabbros to those found in SIO142-8DR from a seamount of the Bach Ridge.

6.5.5 STATIONS WITH THE GRABTELEVISION VIDEO BOTTOM (GTVB) CAMERA SYSTEM

Three sites were selected for the use of the grab television camera system in two different geological provinces: the Musician seamount province and the volcanic arch region of the Hawaiian Swell.

Station GTVB 1 occurred on the floor of the Musician basin just south of the Bach E-W trending ridge near the site of OBH 37 (26°28'S-158°46'W) at about 5000 m depth. The aim of this station was to investigate (observe and sample) the nature of an unusual "hard" reflector recognized on the Parasound images. This reflector yields a strong acoustic signal which seems to cover an extensive surface: a few hundred kilometers of the seafloor. Is this an extended manganese crust layer or is it a hard, indurated sediment (chert-like material)? This reflector lies on top of a transparent layer about 20-30 meters thick.

Direct observation with the video showed an abundantly covered sediment floor (100%). The sediment is light in color with no trace of current or the presence of bio-perturbation due to bottom-dwelling organisms. The common occurence (10-15% of the sedimented surface) of small manganese nodules might suggest a low rate of sedimentation. Due to a system failure, we could not close the grab and were thus unable to penetrate the sediment cover.

Station GTVB 2 took place on the Hawaiian Swell, also known as the arch volcanic area, north of the Hawaiian volcanic chain near 24°167S-157°42.8W at 4427 m depth. The aim of this station was to observe and sample an area showing a high reflectivity as detected by the GLORIA side-scan sonar. The TV grab was lowered onto a flat region of seafloor which showed an abundant sediment cover. The recovered sample consists of brown pelagic sediment (red clay).

Station GTVB 3 was also made on the Hawaian Swell (arch region) further to the south of the previous station, near 24°1.63'N-157°42.7'W at 4105 m depth. This area differs from the previous one by the presence of hilly and rugged topography. The TV grab was lowered onto the top of a hill (<100m high) with some moderately steep slopes containing faulted scarps (staircase-type structure) covered with a dark ruggose material. Pockets of brown sediment were also observed. The TV grab brought back semi-indurated brown sediment with a thin (1cm. thick) Fe-Mn crust. No trace of volcanics was seen among the sample recovered. It is likely that the outcrops are partially covered with sediment that is topped with manganese crust.

6.6. THE DEEP SEA FISH TRAWLS

(J. Wagner, R. H. Douglas, P. J. Herring)

During the cruise, our main objective was to collect as many species and specimens as possible and to dissect and preserve them in suitable ways so that the actual analysis of the material could be carried out in the respective laboratories at home. The results of our catches fulfilled all our hopes as regards diversity and abundance of the fauna (see Appendix 9.5). In the following, the outlines of the three main projects are explained, and details of the work carried out on board ship, as well as the remaining work on land, given.

6.6.1 SHORT CHARACTERISATION OF THE PACIFIC FAUNA SAMPLED DURING THIS CRUISE

(P. J. Herring)

The most abundant fishes taken during the cruise were species of *Cyclothone*, with larger gonostomatids, especially *Gonostoma gracile*, and Chauliodontids, (*Chauliodus sloani*, Fig.6.6.1) also numerous. Smaller photichthyids (*Vinciguerria, Ichthyococcus*) were also taken, but relatively infrequently because the sampling focused on the lower mesopelagic zone. Sternoptychids (*Argyropelecus, Sternoptyx* and *Valenciennellus*) were also regularly sampled. Stomiatoid fishes were less common. Numerous *Idiacanthus* were taken, several *Chauliodus* (including one particularly large specimen), *Macrostomias, Rhadinesthes, Echiostoma, Heterophotus, Malacosteus*, and several *Aristostomias* and *Pachystomias*. Other groups of fishes were very well represented, particularly the myctophids (*Diaphus, Lampanyctus, Taaningichthys* and others). Two very large specimens of the tubular-eyed argentinoid *Opisthoproctus* were captured in one haul, with the related but rarer *Winteria*. The tubular eyed *Stylephorus, Benthalbella, Gigantura*, and *Scopelarchus* occurred sporadically, as did *Anoplogaster, Evermanella*, the platytroctid *Sagamichthys* and *Nansenia*. Ceratioid anglerfishes were relatively rare, with just *Ceratias, Gigantactis* and *Chaenophryne* being represented.

Squid were relatively infrequent but of considerable variety. *Pyroteuthis* and *Histioteuthis* were commonest in the shallower samples, while the deeper ones included the cranchiids *Sandalops, Helicocranchia* and *Taonius*, as well as *Octopoteuthis, Discoteuthis, Mastigoteuthis, Bathyteuthis* and *Abraliopsis*. A few small *Ctenopteryx* were also recorded. No ommastrephids were taken in the trawls, though frequently seen at the surface during the night. These squid are too active to be effectively sampled by a slow-moving trawl.

Decapod shrimp comprised the third major nektonic category captured. Of the Oplophoridae the mesopelagic *Acanthephyra quadrispinosa* was commonest, and replaced by the deep *A. indica* in the bathypelagic samples. *Oplophorus* was frequent in the upper 600m and *Meningodora, Hymenodora* and *Notostomus* were regularly taken in the deeper samples. Of the penaeids, species of *Gennadas Sergia* and *Sergestes* were most often encountered.

The gelatinous fauna was most frequently represented by *Pyrosoma* and numerous small medusae. Occasional scyphozoans (*Periphylla, Atolla*) were also taken, but were never numerous.

Many specimens could not be identified on board to species. It is possible that some are new and certainly some of the known species were larger than had previously been recorded. The individual specimens will be preserved for later detailed taxonomic study.

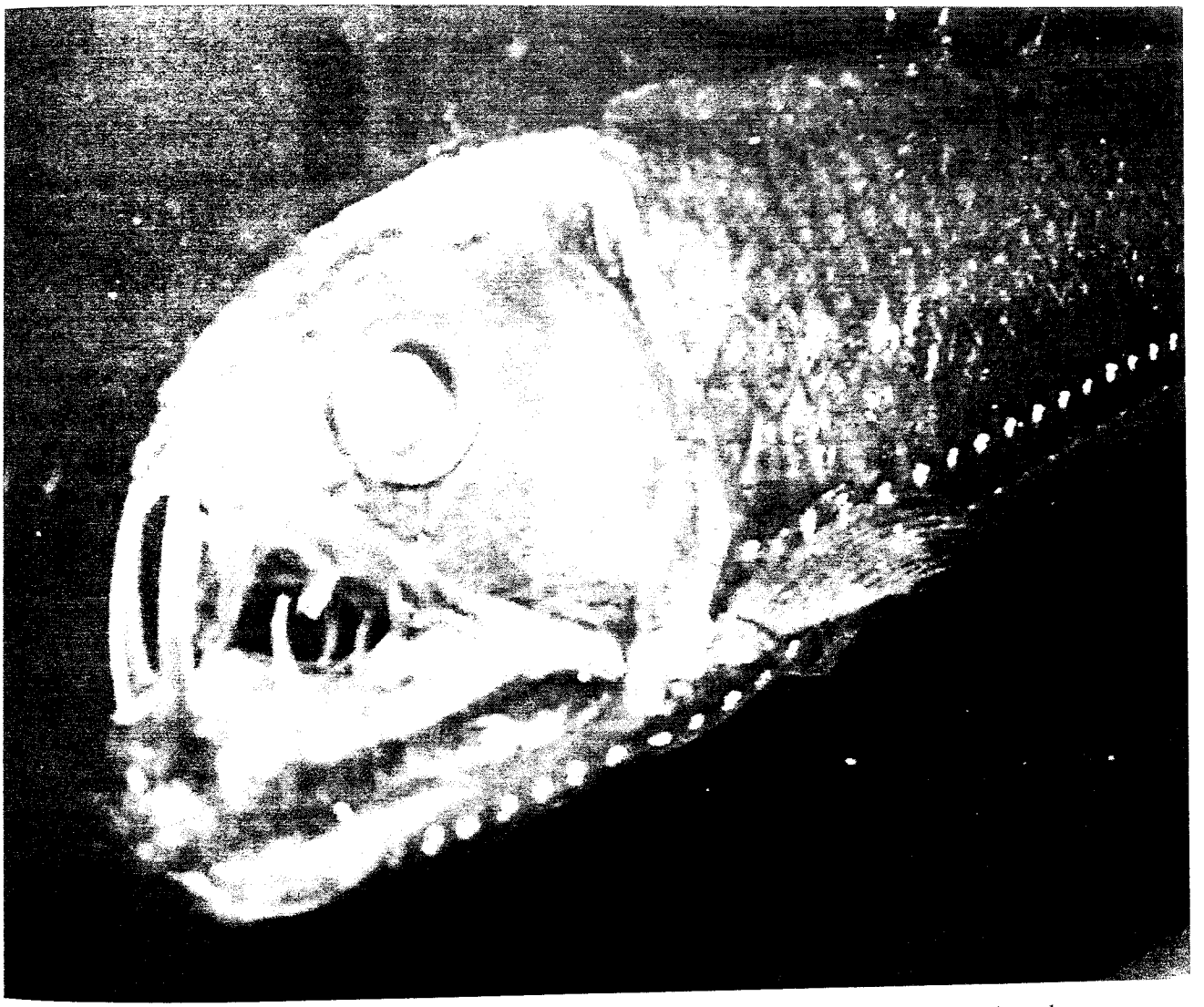

Figure 6.6.1.1: This viperfish *(Chauliodus sloani)* was taken at about 1000m depth. The formidable teeth of this predator are designed to hold and spear the prey. It has rows of light organs on the ventral side. Its large eye is indicative of a well developed visual system adapted to the special photic conditions of the mesopelagic habitat.

6.6.2 BIOLUMINESCENCE AND RELATED STUDIES

(P. J. Herring)

The main objectives of this aspect of the cruise programme were to examine the bioluminescent structures of the midwater fauna, compare them with previous observations on the Atlantic and Indian Ocean fauna and preserve material for spectral (fluorescence) analysis, and for morphological investigation

A particular focus was the comparative study of luminescence in the red-emitting stomiatoids *Pachystomias, Aristostomias* and *Malacosteus.* The last of these is frequently taken in the Atlantic but the other two genera are much rarer there. We have been particularly successful in taking all three genera during Sonne 142, and especially in the number and condition of specimens of *Pachystomias* and *Aristostomias*. Fluorescence spectra of the photocytes, combined with reflectance measurements from the intact photophores will help to determine how these remarkable fishes produce their red emission. Samples from the post-orbital photophores of other stomiatoids have been frozen for later comparison with the red emitters. Additional material from the platytroctid *Sagamichthys* and two ceratioid anglerfishes has been preserved for morphological study.

A second group of interest are the cranchiid squid. In an ongoing comparative study of the ultrastucture of their ocular photophores material from the genus *Sandalops* had been lacking. The samples on Sonne 142 have provided a specimen of this squid, as well as several other cranchiids (*Taonius, Helicocranchia*) and representatives of other families. Frozen material of several of these will be examined ashore. The eyes of representative species have been preserved whole for later study.

In an ongoing study of gill structure in shrimps of several species of Oplophoridae have been preserved for later quantification of gill area and volume in relation to body size. Samples of *Gennadas* and *Sergia* photophores have also been preserved for later detailed examination.

Many species have been photographed for the SOC archives. Images of fresh specimens add considerably to the information garnered from preserved material and help to present the remarkable adaptations of the deep-sea fauna, and their ecological importance, to a wider audience.

6.6.3 ASPECTS OF THE VISUAL SYSTEMS OF DEEP-SEA TELEOST FISH

6.6.3.1 A. LONG-WAVE SENSITIVITY IN STOMIID RETINAE

(R.H. Douglas)

The observation of the different mechanisms conferring longwavelength sensitvity to the three families of dragon fishes have posed a series of questions which we have addressed during the current cruise:

i) We have collected several dark adapted *M. niger* retinae which we have frozen at –80 °C. These will be used on return to land to attempt to detect the triplet state of the photosensitizing pigment using time-resolved electron paramagnetic/spin resonance. This will help us to define the mode of energy transfer during photosensitization.

ii) It is unclear whether the *M. niger* photosensitizer is manufactured de novo by the animals themselves or if it derived from their diet. We therefore plan to analyse *M. niger* gut contents collected during the cruise to see if they contain the photosensitizing pigment. Using molecular biological techniques we will also search for the existence of possible genes that could encode the enzymes required for the synthesis of the photosensitizer.

iii) The retinae of both *A. tittmanni* and *P. microdon* have been shown to contain a so called rhodopsin/porphyropsin visual pigment pair absorbing around 515 and 550nm, as well as an extremely longwave sensitive rhodopsin absorbing at around 588-595nm. Since their retinae already contain the porphyropsin chromophore, 3,4-dehydroretinal, we have suggested that they might, in fact, have an even longer wave absorbing pigment based on the longwave opsin and the A2-based chromophore which we feel we may have missed previously as it may have been bleached by the dim red illumination we used for preparation of the tissue. We have collected several specimens of light adapted *P. microdon*, and *A. scintillans* on this cruise and frozen their retinae at –80 °C. On return to shore we will attempt to regenerate the full complement of these animal's visual pigments under infrared illumination.

iv) Although the opsin gene encoding the *M. niger* visual pigment opsin has been sequenced, this has not yet been done for either *Aristostomias* or *Pachystomias*. The bodies of these two genera we have collected during this cruise will allow such an analysis.

6.6.3.2 SENSITIVITY OF NON-STOMIID TELEOSTS

To date we have examined the spectral characteristics of visual pigments from almost 200 different species of deep-sea fish on which we have based all our ideas about deep-sea visual pigment function. However, these data have been gathered exclusively using animals caught in the Northern Atlantic.

Participation in the Sonne cruise has enable us to sample a completely new (Pacific) fauna. We have frozen retinae from over 40 species of teleost. On return to shore these will be thawed and their visual pigment content will be analysed using extract spectrophotometry. This will enable us to answer several questions:

i) As many of the species we have caught are the same as those we have previously analysed in the Atlantic, we will see if the same species have the same or different visual pigments in the 2 oceans.

ii) We have also caught several species that we have not previously seen in the Atlantic. These will add to our data base of teleost visual pigments.

6.6.3.3 REGENERATION OF VISUAL PIGMENTS

Once a visual pigment molecule has been isomerised during the bleaching process it rapidly regenerates. For several reasons it would be interesting to know the extent and speed of such regeneration in deep-sea fish. Firstly, due to the often high density of deep-sea visual pigments and the relatively low number of photons they are exposed to, it might be argued that the pigments of some deep-sea fish may have no need to regenerate, although calculations show pigment bleaching is probably appreciable even in the deep-ocean. Furthermore, since regeneration involves the retinal pigment epithelium (RPE), it is difficult to see how significant

regeneration could occur in those species with several banks of photoreceptors, most of whose photoreceptors are not in contact with the RPE. In fact it has been suggested that only the most vitread bank of photoreceptors in a multibank retina is functional, the visual pigments in the more sclerad layers having been bleached and not regenerated. Electrophysiological and morphological evidence supports the view that only the most vitread layer of rods is fully functional. Limited in vitro experiments have shown the degree of visual pigment regeneration to vary widely between different deep-sea fish. It would be interesting to know how such variation is related to species' habitat depth and retinal structure.

We will be able to use the retinae we have frozen for visual pigment analysis to ascertain the regenerative capacity of deep-sea fish visual pigments.

6.6.3.4 EFFECT OF PRESSURE ON VISUAL PIGMENT ABSORBANCE

Since the spectral characteristics of a visual pigment depend heavily on the tertiary structure of a protein (opsin), it is possible that the pressure experienced in the deep-sea will affect the absorption characteristics of the pigment. However, all measurements made on visual pigments to date have been performed at atmospheric pressure. We have now built a device for measuring the absorption characteristics of visual pigments at up to 400 atmospheres pressure. Once again, we will be able to use the retinae we have frozen for visual pigment analysis to determine the effect of pressure on visual pigment absorption.

6.6.3.5 VISUAL PIGMENTS OF CRUSTACEANS

Little is known about the visual pigments of deep-sea crustaceans. We have therefore cryoembedded eyes from the genera *Acanthephyra, Oplophorus, Gnathophausia and Notostomus*, which on return to land will be cryosectioned and individual rhabdomes will have their visual pigments analysed by microspectrophotometry.

6.6.3.6 VISUAL OPTICS

Although deep-sea fish appear to have well developed visual systems nothing is know about the quality of the image produced on the retina by the lens. I have previously determined the focal length of such lenses by videoing laser beams passing through lenses suspended in teleost Ringer's solution. I would now like to relate the focal length of the lens to its position within the eye relative to the retina.

To this end I have embedded the heads of species with both tubular and laterally positioned eyes in Tissue Tek which I have then rapidly frozen using cryospray. I will subsequently section these on a cryostat to determine the relative positions of the lens and retina. In this way one should be able to get a good idea of the optical quality of the deep-sea fish eye and hence determine the relative importance of vision to the animal.

6.6.4 MORPHOLOGICAL ASPECTS OF DEEP SEA VISUAL SYSTEMS
6.6.4.1 RETINA
(H.-J. Wagner)

i) In the retinae of terrestrial and surface animals, the photoreceptor outer segments (OS) containing the visual pigments are constantly renewed. This is achieved by adding newly synthesised membrane material (discs) at the OS base and removing "old" discs from the tips for phagocytosis by the RPE cells. In view of the special organisation of the multibank rod retinae found in many deep-sea fish species and the fact that the RPE is in contact only with the outermost bank of rods, it is unclear whether OS renewal takes place in this type of retina, too. We have previously observed electron microscopic evidence or both disc precursor formation as well as RPE phagocytosis. However, direct evidence based on living tissue is still missing. Therefore, I have collected isolated retinae from living specimens and kept thin strips of retinal tissue for 10 h in a culture medium at 4°C in the presence on a fluorescent dye, Lucifer Yellow. This is incorporated into newly formed OS discs and should be detectable after fixation and sectioning. (Appendix 9.5: e.g. 11/1; 13/1)

ii) The incubation in Lucifer Yellow will also stain isolated retinal neurons, such as horizontal, bipolar, amacrine, and ganglion cells revealing their processes in a Golgi-like fashion. This will allow me to obtain a first impression of the detailed retinal circuitry and enable me to get a more realistic estimation of convergence ratios. Previously, such data have been based exclusively on the number of cell bodies without taking into account the diversity of cell types as well as the sizes of dendritic and telodendrial fields.

iii) During the development of vertebrate retinae, typically, cone formation precedes rod formation. It is unclear, whether this is also the case in the pure rod retinae of most deep-sea fishes. Previous observations of the retinal margin of adult specimens (where a proliferation zone with embryonic character is found in teleosts) has revealed no evidence of cone precursors based on immunocytochemical staining with cone visual pigment antisera in deep-sea fishes. It is possible, however, that the proliferation zone is so narrow, that cone precursors were undetected. Therefore, I have collected larval specimens in order to repeat this study. If retinal development bypassing the cone system could be demonstrated in these fish, it would be the first time in vertebrates. (Appendix 9.5: e.g. 1/7, 2/1, 4/4, 10/1)

iv) In the ganglion cell layer of certain deep-sea fish species previous studies (mainly based on cresyl violet stained material) have revealed marked inhomogeneities, and sometimes even specialisations such as area or foveae in the distribution of neurons. Tubular eyes of the pearleyes (Scopelarchids) are of particular interest. I have collected eyes of about 40 different species and used two different methods in order to specifically label the ganglion cells, thereby distinguishing them from the amacrine cells also present in the same layer. In cases where living material was available, dextranes coupled to the fluorescent tetrametylrhodamine were applied to the optic nerve stump and allowed to be transported by retrograde axoplasmic flow towards the perikaryon during a 48 culture period at 4°C. Subsequently isolated retinae turned out to be in very good condition. They were fixed in paraformaldehyde, and will be wholemounted in Tübingen for quantitative analysis. The second labelling technique was applied to dead specimens which were prefixed lightly (4h) in paraformaldehyde. The lipophilic dye DiI applied to the optic nerve stump diffused in the lipophilic phase of the plasma membrane and also reaches the ganglion cell perikarya after several days or weeks depending on the size of the eye.

These preparations will also be evaluated in Tübingen after wholemounting the retinae. (Appendix 9.5: e.g. 1/2; 1/4, 1/6, 10/5, 10/6, 11/6, 11/8)

6.6.4.2. THE VISUAL SYSTEM IN RELATION TO OTHER SENSORY SYSTEMS

It is of major interest to know what role vision plays in relation to the other sensory systems in deep-sea fish. Among the octavolateralis system, (comprising the lateral line, vestibular and auditory apparatus), electroreception, and the chemical senses (gustatory and olfactory), vision may not be as dominant as it may appear from the standpoint of the primarily visually oriented human. During the Sonne cruise, I have collected and prepared material to address this question. In the first place, the relative importance of the visual and the olfactory systems will be studied; later focus will be placed on the octavolateralis and gustatory systems. Two approaches will be used:

i) Quantitative assessment of cranial nerves. In order to evaluate the importance of a particular afferent system to the brain, the most straightforward method is to determine the relative volume in terms of the number of nerve fibres in the respective cranial nerves. For this purpose, I have fixed brains including the cranial nerves in glutaraldehyde, in order to perform an electron microscopic investigation. (Appendix 9.5: e.g. 11/1; 13/1) Interestingly, preliminary observations of olfactory and optic nerves have not only demonstrated myelinated fibres, as would be expected from "normal" afferents, but also revealed a surprisingly high number of unmyelinated axons, clearly outnumbering the myelinated ones. This might indicate that the conduction velocity of sensory impulses is generally slower in deep-sea fishes,- potentially an adaptation to the low temperature environment.

On the other hand, it is conceivable that not all the unmylinated axons constitute afferents to the brain. Rather, in other vertebrates, many unmyelinated fibres in sensory nerves belong to efferent systems providing feedback from the brain to the sense organ. In order to address this problem I have performed the labelling experiments outlined above for the demonstration of retinal ganglion cells also for the olfactory system to visualise the mitral and tufted cells of the olfactory bulbs. The numbers of these projection neurons will be determined and subtracted from the total number of axons in the olfactory tract / optic nerve and will thus reveal the actual number of efferent fibres.

ii) A special kind of efferent system to the eyes is provided by fibres of the "terminal nerve". This is a population of neurons with dendrites in the olfactory mucosa, perkarya in the olfactoretinalis nucleus localised close to the olfactory bulbs, and wide projections throughout the diencephalon, tectum and parts of the rhombencephalon. There are some indications that this system is concerned with the perception of pheromones; therefore it would play a major role in reproduction. Previous studies have shown that terminal nerve fibres are present in the retinae of deep-sea fishes, and thus constitute at least a portion of the efferent fibre complement in the optic nerve. Since the terminal nerve system is readily visualised by immunocytochemical methods using antisera directed against its neuropeptides GnRH and/or FMRFamide, I have prepared suitably fixed brains for this study.

iii) Visualisation of terminal fields: The extent of the terminal fields of the afferent nerves in the various parts of the brain provides a second approach towards the evaluation of the relative importance of the different sensory systems. To this end, I have applied tracers (TRITC-labelled

dextranes and DiI) to the proximal stumps of the olfactory tract and optic nerve. Serial sectioning and 3-D reconstruction will reveal the relative brain volumes occupied by the primary areas for vision and olfaction.

The above attempt to draw conclusion from the organisation of the sensory parts of the CNS regarding the behaviour of the deep-sea fishes constitutes a reverse approach to the established method, where the behaviour of a given species is studied first and then its neural basis is analysed.

Given the large number of species collected (see Appendix 9.5), I propose to place special emphasis on the study of certain species of which more numerous specimens came up in the trawls. Among these are: *Gonostoma gracile, Chauliodus sloani,* and *Sternoptyx pseudoobscura.* All of these may be expected to be visually oriented. These would then be compared with possibly less visually oriented species such as the anglerfish *Ceratias holboelli* and the as yet unidentified mesopelagic rattail. Furthermore, future cruises should allow us to obtain deep demersal species in order to include sensory adaptations to an additional deep-sea environment.

7. ACKNOWLEDGEMENTS

Cruise SO 142 was funded by the German Ministery of Education, Research, Science, and Technology (BMBF) under project No. 03 G 0142 to GEOMAR within the continued and generous most commendable support for marine sciences with an outstanding research vessel such as SONNE. We also gratefully acknowledge the support of TMR to the British scientists of the Bioluminescence project. Unfortunately, the funds pledged have not been made available at the time this cruise ends.

We warmly thank master H. Andresen and his crew for their excellent support in all work done and for the splendid working atmosphere throughout the entire cruise in spite of sometimes adverse weather conditions and the ambitious working program. Fotographs contained in this report were provided by Heiko Buxel.

8. REFERENCES

Ammon, C.J., and J.E. Vidale, 1993: Tomography without rays, *Bull. Seism. Soc., Am.*, 83, 509-528.

Atwater, T., and Severinghaus, J., 1989: The Eastern Pacific Ocean and Hawaii, Tectonic maps of the northeast Pacific. *The Geology of North America, Vol. N.*, The Geological Society of America, 1989, 15-20

Blondel, P. and B.J.Murton, 1997: Handbook of Seafloor Sonar Imagery, John Wiley and Sons, Chichester, 314.

Campbell, J.F, N. Frazer, R. Moberly, W. Sager , J. K. Sinton, and B.H. Wallin, 1980: Musicians Seamount province in the Central Pacific (abstract), *EOS Trans. Am. Geophys.* Un., 61, 989.

Caress, D.W., M.K. McNutt, R.S. Detrick, and J.C. Mutter, 1995: Seismic imaging of hotspot-related crustal underplating beneath the Marquesas islands, *Nature,* 373, 600-603.

Carlson, R.L., 1998: Seismic velocities in the uppermost oceanic crust: age dependence and the fate of layer 2A, *J. Geophys. Res.*, 103, 7069-7077.

Clague, D. A. and Dalrymple, G. B., 1987: The Hawaiian-Emperor Volcanic Chain: Part I. Geologic Evolution. U.S. Geol. Surv. Prof. Paper 1350, chap. 1, part1, 5-54.

Clague, D. A. and Dalrymple, G. B., 1989: The tectonic and geologic setting of the Hawaiian-Emperor volcanic chain. In: The Eastern Pacific Ocean and Hawaii. *The Geology of North America*, The Geological Society of America, 1989, 188-217.

Collin, S.P., Hoskins, R.V. and Partridge, J.C., 1997: Tubular eyes of deep-sea fishes: a comparative study of retinal ganglion cell topography. *Brain Behav.Evol.* 50, 335-357

Dalrymple and Clague 1976: Age of the Hawaiian-Emperor bend, *Earth Planet. Sci. Lett.*, 31, 313-329.

Diament, M., and J. Goslin, 1986: Emplacment of the Marion Dufrense, Lena and Ob Seamounts (south Indian Ocean) from a study of isostasy, *Tectonophysics*, 121, 253-262.

Douglas, R.H., Partridge, J.C. and Hope, A.J, 1995: Visual and lenticular pigments in the eyes of demersal deep-sea fishes. *J. Comp. Physiol. A* 177, 111-122.

Douglas, R.H and Partridge, J.C., 1997: On the visual pigments of deep-sea fish. *J. Fish Biol.* **50**,68-85.

Douglas, R.H., Partridge, J.C. & Marshall, N.J., 1998a: The Eyes of deep-sea fish I: Lens pigmentation, tapeta and visual pigments. *Prog. Ret. Eye Res.* 17(4), 597-636.

Douglas, R.H., Partridge, J.C., Dulai, K., Hunt, D., Mullineaux, C.W., Tauber, A. & Hynninen, P.H.,1998b: Dragon fish see using chlorophyll. *Nature* 393, 423-424.

Flueh, E. R., 1995: Cruise Report SO103, Condor 1B; *Geomar Report* 41, Kiel, 140 pp.

Flueh, E. R. and Bialas, J., 1996: A digital, high data capacity ocean bottom recorder for seismic investigations; *Int. Underwater Sytems Design*, 18(3), 18-20.

Flueh, E. R., Kukowski, N., and Reichert, C., 1997: Cruise Report SO123, Mamut; *Geomar Report* 62, Kiel, 292pp.

Flueh, E.R., I. Grevemeyer, and C. Reichert, 1999a: Investigating the crustal framework at the NERO Hole 1107A, *Joides Journal*, submitted.

Flueh, E.R., I. Grevemeyer, and C. Reichert, 1999b: Ocean site survey reveals anatomy of a hotspot track, *EOS Trans. Am. Geophys.* Un., 80, 77.

Flueh, E. R., Schreckenberger, B., and Bialas, J., 1999c: Cruise Report SO138, GINCO II; *Geomar Report* 81, Kiel, 333pp.

Grevemeyer, I., and W. Weigel, 1996: Seismic velocities of the uppermost igneous crust versus age, *Geophys. J. Int.*, 124, 631-635.

Grevemeyer, I., W. Weigel, and C. Jennrich, 1998: Structure and ageing of oceanic crust at 14°S on the East Pacific Rise, *Geophys. J. Int.*, 135, 573-584.

Grevemeyer, I., N. Kaul, H. Villinger, and W. Weigel, 1999: Hydrothermal activity and the evolution of the seismic properties of upper oceanic crust, *J. Geophys. Res.*, 104, 5069-5079.

Hammer, P.T.C., L.M. Dorman, J.A. Hildebrand, and B.D. Cornuelle, 1994: Jasper seamount: seafloor seismic refraction tomography, *J. Geopys. Res.*, 99, 6731-6752.

Herring, P.J., 1987: Systematic distribution of bioluminescence in living organisms. *Biolum. Chemilum.* 1, 147-163

Herring, P.J., 1996: Light, colour and vision in the ocean. In: Oceonography. An illustrated guide(eds. C.P. Summerhayes and S.A. Thorpe) pp. 212-227. Mason Publ., London

Klein, E.W., 1981: A linear gradient crustal model for south Hawaii, *Bull. Seis. Soc. Am.*, 71, 1503-1510.

Knickmeyer, E.T., 1996: Hochgenaues Differential-GPS, Proc. 11th Annual Meeting of the German Hydrographic Society, Glücksburg, 3.-5.6 1996.

Larson, 1991: Latest pulse of the earth: Evidence from a mid Cretaceous superplume, *Geology*, 19,

Luetgert, J., 1992: Interactive two-dimensional seismic raytracing for the Macintosh, *USGS Open File Report*, 43.

M. Maia, R. Hekinian, D. Ackermand, G. Dehghani, P. Gente, D. Naar, J. O'Connor, K. Perrot, J.Phipps Morgan, G. Ramillien, S. Revillon, A. Sabetian, D. Sandwell, and P. Stoffers, 1998: The Foundation Seamounts: A ridge-hotspot interaction in the South Pacific, *J. Geophys. Res.*,submitted

McKenzie, D.P., and C. Bowin, 1976: The relationship between bathymetry and gravity in the Atlantic Ocean, *J. Geophys. Res.*, 81, 1903-1915.

Morgan, W.J., Rodriguez, Darwin, Amsterdam, ..., a second type of hotspot island, *J. Geophys. Res.*, 83, 5355-5360, 1978

Mueller, D., Roest, W.R., Royer, J.Y., Gahagan, L.M., and Sclater, J.G., 1997: Digital Isochrons of the world's Ocean Floor, *J. Geophys. Res.*, 102, 3211-3214.

Parker, R.L., 1972, The rapid calculation of potential anomalies, *Geophys. J. R. astron. Soc.*, 31, 447-455.

Parson, T., J. McCarthy, W.M. Kohler, mC.J. Ammon, H.M., Genz, J.A. Hole, and E.E. Criley, 1996: Crustal structure of the Colorado Plateau, Arizona: application of a new long-offset seismic data analysis techniques, *J. Geophys. Res.*, 101, 11173-11194.

Partridge, J.C. and Douglas, R.H., 1995: Far-red sensitivity of dragon fish. *Nature* 375, 21-22

Pringle M. S. 1992: Geochronology and petrology of the Musicians Seamounts, and the search for hot spot volcanism in the cretaceous Pacific, Ph.D Thesis, Dissertation, University of Hawaii, 235 p.

Rees, B.A., R.S. Detrick, and B. Coakley, 1993: Seismic stratigraphy of the Hawaiian flexural moat, *Geol. Soc. Am. Bull.*, 105, 189-205.

Schilling, J. -G., 1986: Geochemical and isotopic variation along the Mid-Atlantic Ridge axis from 79°N to 0°N, in *The Geology of North America, Vol. M, The Western North Atlantic Region,* edited by P.R. Vogt, and B.E. Tucholke, pp. 137-156, *Geol. Soc. Am.*, Boulder

Schreiber, R., and H.W. Schencke, 1990: Efficient hydrographic surveying of EEZ with new multibeam echosounder technology for shallow and deep water, *Ocean resources*, 1, 73-87.

Seeber, G., 1996: Stand und Einsatzmöglichkeiten von GPS - ein Überblick, Proc. 11th Annual Meeting of the German Hydrographic Society, Glücksburg, 3.-5.6. 1996.

Smith, W. H. F., Sandwell, D. T. 1997: Global seafloor topography from satellite altimetry and ship depth soundings, *Science*, 277, 1956-1962.

ten Brink, U.S., and T.M. Brocher, 1987: Multichannel seismic evidence for a subcrustal intrusive complex under Oahu and a model for Hawaiian volcanism, *J. Geophys. Res.*, 92, 13687-13707.

Vidale, J.E., 1988: Finite-difference calculation of travel times, *Bull. Seism. Soc. Am.*, 78, 2062-2076

Wagner, H.-J., Fröhlich, E., Negishi, K. and Collin, S.P., 1998: The eyes of deep-sea fish: II. Functional morphology of the retina. *Progress in Retinal and Eye Research,* Vol. 17, pp 637-685

Watts, A.B., 1978: An analysis of isostasy in the world's oceans; 1. Hawaiian-Emperor seamount chain, *J. Geophys. Res.*, 83, 5989-6004.

Weigel, W., and I. Grevemeyer, 1999: The Great Meteor seamount: seismic struture of a submerged intraplate volcanoe, in Oceanic crust and hotspot interaction, P. Charvis and JJ. Danobeitia (eds.), *J. Geodynamics*, 28, 27-40.

Weinrebe, W., 1997: Fahrtbericht SO-112 HIRESBAT, *GEOMAR-Report* 64, GEOMAR-Kiel.

Wessel, P., and W.H.F. Smith, 1991: Free software helps map and display data, *EOS Trans. Am. Geophys. Un.*, 72, 441, 445-446.

Wessel, P. and Smith, W. H. F., 1995: The Generic Mapping Tools (GMT) version 3.0, *Technical Reference and Cookbook*, SOEST/NOAA.

White, R.S., D.M. McKenzie, and R.K. O'Nions, 1992: Oceanic crustal thickness from seismic measurements and rare earth element inversions, *J. Geophys. Res.*, 97, 19683-19715.

Grevemeyer, I., W. Weigel, and C. Jennrich, 1998: Structure and ageing of oceanic crust at 14°S on the East Pacific Rise, *Geophys. J. Int.*, 135, 573-584.

Grevemeyer, I., N. Kaul, H. Villinger, and W. Weigel, 1999: Hydrothermal activity and the evolution of the seismic properties of upper oceanic crust, *J. Geophys. Res.*, 104, 5069-5079.

Hammer, P.T.C., L.M. Dorman, J.A. Hildebrand, and B.D. Cornuelle, 1994: Jasper seamount: seafloor seismic refraction tomography, *J. Geopys. Res.*, 99, 6731-6752.

Herring, P.J., 1987: Systematic distribution of bioluminescence in living organisms. *Biolum. Chemilum.* 1, 147-163

Herring, P.J., 1996: Light, colour and vision in the ocean. In: Oceonography. An illustrated guide(eds. C.P. Summerhayes and S.A. Thorpe) pp. 212-227. Mason Publ., London

Klein, E.W., 1981: A linear gradient crustal model for south Hawaii, *Bull. Seis. Soc. Am.*, 71, 1503-1510.

Knickmeyer, E.T., 1996: Hochgenaues Differential-GPS. Proc. 11th Annual Meeting of the German Hydrographic Society, Glücksburg, 3.-5.6 1996.

Larson, 1991: Latest pulse of the earth: Evidence from a mid Cretaceous superplume, *Geology*, 19,

Luetgert, J., 1992: Interactive two-dimensional seismic raytracing for the Macintosh, *USGS Open File Report*, 43.

M. Maia, R. Hekinian, D. Ackermand, G. Dehghani, P. Gente, D. Naar, J. O'Connor, K. Perrot, J.Phipps Morgan, G. Ramillien, S. Revillon, A. Sabetian, D. Sandwell, and P. Stoffers, 1998: The Foundation Seamounts: A ridge-hotspot interaction in the South Pacific, *J. Geophys. Res.*,submitted

McKenzie, D.P., and C. Bowin, 1976: The relationship between bathymetry and gravity in the Atlantic Ocean, *J. Geophys. Res.*, 81, 1903-1915.

Morgan, W.J., Rodriguez, Darwin, Amsterdam, ..., a second type of hotspot island, *J. Geophys. Res.*, 83, 5355-5360, 1978

Mueller, D., Roest, W.R., Royer, J.Y., Gahagan, L.M., and Sclater, J.G., 1997: Digital Isochrons of the world's Ocean Floor, Journal of Geophysical Research, 102, 3211-3214.

Parker, R.L., 1972, The rapid calculation of potential anomalies, *Geophys. J. R. astron. Soc.*, 31, 447-455.

Parson, T., J. McCarthy, W.M. Kohler, mC.J. Ammon, H.M., Genz, J.A. Hole, and E.E. Criley, 1996: Crustal structure of the Colorado Plateau, Arizona: application of a new long-offset seismic data analysis techniques, *J. Geophys. Res.*, 101, 11173-11194.

Partridge, J.C. and Douglas, R.H., 1995: Far-red sensitivity of dragon fish. *Nature* 375, 21-22

Pringle M. S. 1992: Geochronology and petrology of the Musicians Seamounts, and the search for hot spot volcanism in the cretaceous Pacific, Ph.D Thesis, Dissertation, University of Hawaii, 235 p.

Rees, B.A., R.S. Detrick, and B. Coakley, 1993: Seismic stratigraphy of the Hawaiian flexural moat, *Geol. Soc. Am. Bull.*, 105, 189-205.

Schilling, J. -G., 1986: Geochemical and isotopic variation along the Mid-Atlantic Ridge axis from 79°N to 0°N, in *The Geology of North America, Vol. M, The Western North Atlantic Region,* edited by P.R. Vogt, and B.E. Tucholke, pp. 137-156, *Geol. Soc. Am.*, Boulder

Schreiber, R., and H.W. Schencke, 1990: Efficient hydrographic surveying of EEZ with new multibeam echosounder technology for shallow and deep water, *Ocean resources*, 1, 73-87.

Seeber, G., 1996: Stand und Einsatzmöglichkeiten von GPS - ein Überblick, Proc. 11th Annual Meeting of the German Hydrographic Society, Glücksburg, 3.-5.6. 1996.

Smith, W. H. F., Sandwell, D. T. 1997: Global seafloor topography from satellite altimetry and ship depth soundings, *Science*, 277, 1956-1962.

ten Brink, U.S., and T.M. Brocher, 1987: Multichannel seismic evidence for a subcrustal intrusive complex under Oahu and a model for Hawaiian volcanism, *J. Geophys. Res.*, 92, 13687-13707.

Vidale, J.E., 1988: Finite-difference calculation of travel times, *Bull. Seism. Soc. Am.*, 78, 2062-2076

Wagner, H.-J., Fröhlich, E., Negishi, K. and Collin, S.P., 1998: The eyes of deep-sea fish: II. Functional morphology of the retina. *Progress in Retinal and Eye Research,* Vol. 17, pp 637-685

Watts, A.B., 1978: An analysis of isostasy in the world's oceans; 1. Hawaiian-Emperor seamount chain, *J. Geophys. Res.*, 83, 5989-6004.

Weigel, W., and I. Grevemeyer, 1999: The Great Meteor seamount: seismic struture of a submerged intraplate volcanoe, in Oceanic crust and hotspot interaction, P. Charvis and JJ. Danobeitia (eds.), *J. Geodynamics,* 28, 27-40.

Weinrebe, W., 1997: Fahrtbericht SO-112 HIRESBAT, *GEOMAR-Report* 64, GEOMAR-Kiel.

Wessel, P., and W.H.F. Smith, 1991: Free software helps map and display data, *EOS Trans. Am. Geophys.* Un., 72, 441, 445-446.

Wessel, P. and Smith, W. H. F., 1995: The Generic Mapping Tools (GMT) version 3.0, *Technical Reference and Cookbook*, SOEST/NOAA.

White, R.S., D.M. McKenzie, and R.K. O'Nions, 1992: Oceanic crustal thickness from seismic measurements and rare earth element inversions, *J. Geophys. Res.*, 97, 19683-19715.

Wolfe, C.J., M.K. McNutt, and R.S. Detrick, 1994: The Marquesas archipelagic apron: seismic stratigraphy and implications for volcano growth, mass wasting, and crustal underplating, *J. Geophys. Res.*, 99, 13591-13608.

Zelt, C.A., and R.B. Smith, 1992: Seismic travel time inversion for 2-D crustal velocity structure, *Geophys. J. Int.*, 108, 16-34.

Zindler, A., H. Staudigel and R. Batiza, 1984: Isotope and trace element geochemistry of young Pacific seamounts: implications for the scale of upper mantle heterogeneity, *Earth Planet. Sci. Lett.*, 70, 175-195.

Appendix 9.1.1

HULA2 - SO 142 - Profile 01

INST.	LAT (N)	LON (W)	DIST. TO	DEPTH	REL.	ANT.	REC.	SKEW	REMARKS	FIGURE
	D:M	D:M	NEXT (nm)	(m)	CODE	CH.	NO.	(ms)		
OBH01	32: 30. 040	162: 17. 989	1.0	5307	6A24	C	91.14	?	Battery cut	6.3.4.1.2
OBH02	32: 29. 281	162: 17. 196	5.1	5253	D654	A			test only	
OBH03	32: 25. 600	162: 13. 070	0.7	5594	C679	C	980403	0	DC - shift	
OBH04	32: 25. 110	162: 12. 500	8.0	5610	4949	D	980901	4		6.3.4.1.3
OBH05	32: 19. 301	162: 05. 951	0.8	4031	5929	C	980908	1		6.3.4.1.4
OBH06	32: 18. 738	162: 05. 328		4049	4979	D	980907	0		6.3.4.1.5
Trigger							980906	1		

Appendix 9.1.2

HULA2 - SO 142 - Profile 02

INST.	LAT (N)	LON (W)	DIST. TO	DEPTH	REL.	ANT.	REC.	SKEW	REMARKS	FIGURE
	D:M	D:M	NEXT (nm)	(m)	CODE	CH.	NO.	(ms)		
OBH07	32: 28. 992	160: 14. 003	3.0	5847	4979	E	980907	2		6.3.4.2.2
OBH08	32: 25. 996	160: 13. 991	3.0	5969	5929	B	980908			
OBH09	32: 22. 960	160: 14. 016	3.0	5928	4949	F	980901	13		6.3.4.2.3
OBH10	32: 19. 950	160: 13. 970	3.0	5047	C679	C	980906	9		6.3.4.2.4
OBH11	32: 16. 880	160: 13. 980	2.8	4162	6A24	D	980401	-11		6.3.4.2.5
OBH12	32: 14. 176	160: 14. 000	1.0	3019	D654	C	91.14	-22		
OBH13	32: 13. 190	160: 13. 990	0.6	2855	6969	C	63.96	-29	missing blocks	
OBH14	32: 12. 580	160: 13. 990	2.6	2981	D634	D	02.95	-20		
OBH15	32: 09. 992	160: 13. 970	3.0	4208	5924	B	08.94	-44		
OBH16	32: 06. 919	160: 13. 990	3.0	5339	5934	A	980403	-1		6.3.4.2.6
OBH17	32: 04. 003	160: 13. 986	3.0	5722	D649	A	980903	-2		6.3.4.2.7
OBH18	32: 00. 987	160: 13. 958	3.0	5745	C464	D	980402	-4		6.3.4.2.8
OBH19	31: 57. 963	160: 14. 000		5651	B214	B	92.01		recorder error,data OK	
Trigger							971402	-3		

Appendix 9.1.3

HULA2 - SO 142 - Profile 03

INST.	LAT (N)	LON (W)	DIST. TO	DEPTH	REL.	ANT.	REC.	SKEW	REMARKS	FIGURE
	D:M	D:M	NEXT (nm)	(m)	CODE	CH.	NO.	(ms)		
OBH20	26: 19. 054	160: 17. 988	3.0	5100	D654	C	971202	-7		6.3.4.3.2
OBH21	26: 21. 995	160: 18. 022	3.0	4816	6969	X*	980401	-11		6.3.4.3.3
OBH22	26: 24. 998	160: 18. 049	3.0	4735	D634	B	980908	5		6.3.4.3.4
OBH23	26: 28. 036	160: 17. 996	3.0	4729	5924	D	980906	8		6.3.4.3.5
OBH24	26: 31. 025	160: 17. 988	3.0	3960	5934	C	980901	13		6.3.4.3.6
OBH25	26: 34. 016	160: 18. 005	1.0	3145	C464	D	08.94	-46		
OBH26	26: 35. 031	160: 18. 000	1.0	2814	D649	B	03.96	-26		
OBH27	26: 36. 029	160: 18. 001	3.0	3263	B214	D	02.95	-20		
OBH28	26: 39. 014	160: 18. 011	3.0	4209	4979	C	980903	-1		6.3.4.3.7
OBH29	26: 41. 997	160: 17. 997	3.0	4450	5929	A	980907	3		6.3.4.3.8
OBH30	26: 45. 018	160: 17. 975	3.0	4314	4949	A	980402	-4		6.3.4.3.9
OBH31	26: 48. 000	160: 18. 005	3.0	4907	C679	B	980403	-1	poor signal	6.3.4.3.10
OBH32	26: 51. 001	160: 18. 000	3.0	5053	6A24	D	92.01	-26		
OBH33	26: 53. 994	160: 17. 996		5032	A319	D	980902	7		6.3.4.3.11
Trigger							91.14	-14		

X* = 156.425 Hz

Appendix 9.1.4

HULA2 - SO 142 - Profile 04

INST.	LAT (N)	LON (W)	DIST. TO	DEPTH	REL.	ANT.	REC.	SKEW	REMARKS	FIGURE
	D:M	D:M	NEXT (nm)	(m)	CODE	CH.	NO.	(ms)		
OBH34	26: 17. 979	158: 46. 028	4.0	4766	B214	D	980907	3	DC-shift	
OBH35	26: 21. 958	158: 46. 056	4.0	5290	D649	B	980401	-12		6.3.4.4.2
OBH36	26: 25. 982	158: 46. 053	3.0	5367	C464	C	980908	5		6.3.4.4.3
OBH37	26: 28. 969	158: 46. 038	3.0	5282	5934	A	92.01	-27		
OBH38	26: 31. 968	158: 46. 048	3.0	4481	5924	C	980902	8		6.3.4.4.4
OBH39	26: 34. 986	158: 45. 993	3.0	3456	D634	D	980402	-4		6.3.4.4.5
OBH40	26: 37. 978	158: 45. 987	2.0	2950	6969	D	980403	-1		6.3.4.4.6
OBH41	26: 39. 966	158: 45. 991	3.0	3188	D654	D	08.94	-48		
OBH42	26: 42. 972	158: 45. 993	3.0	4358	4979	X*	980903	-1		6.3.4.4.7
OBH43	26: 46. 003	158: 45. 987	3.0	4984	A319	D	03.96	-23		
OBH44	26: 48. 997	158: 46. 014	3.0	5204	6A24	B	980901	14		6.3.4.4.8
OBH45	26: 51. 992	158: 46. 003	4.0	4850	C679	A	02.95	-21		
OBH46	26: 56. 000	158: 45. 990	4.0	5117	4949	B	980906	8		6.3.4.4.9
OBH47	27: 00. 010	158: 45. 991		5207	5929	C	971202	-6		6.3.4.4.10
Trigger							91.14	-12		

X* = 156.675 Hz

Appendix 9.1.5

HULA2 - SO142 - SEISMIC SOURCES

PROFILE NO.	SHOT NO.	DATE	TIME UTC	LAT (N)	LON (W)	PULSE INT.	GUN POSITION	PROFILE LENGTH	REMARKS
SO142 01	1	06.06.99	20:42	32° 16.491	162° 02.828	60s	STB	45 km	
	354	07.06.99	02:35	32° 33.513	162° 22.031	60s	STB		change of course
	419	07.06.99	03:40	32° 30.856	162° 15.960	60s	STB		
SO 142 02	1	10.06.99	02:42	31° 20.755	160° 14.000	60s	STB	180 km	
	18	10.06.99	02:59	31° 21.968	160° 14.002	60s	STB+PRT		
	1560	11.06.99	06:42	32° 57.591	160° 14.001	60s	STB+PRT		
SO 142 03	1	16.06.99	00:45:48	27° 34.344	160° 17.908	60s	STB	204 km	
	28	16.06.99	01:12:48	27° 32.940	160° 17.997	60s	STB+PRT		
	572	16.06.99	10:16:48	26° 57.433	160° 18.000	60s	PRT		STB gun down
	708	16.06.99	12:32:48	26° 49.887	160° 17.996	60s	STB+PRT		STB operational
	1815	17.06.99	06:59:48	25° 44.400	160° 18.004	60s	STB+PRT		
SO 142 04	1	22.06.99	01:04:50	27° 38.953	158° 45.999	60s	PRT	215 km	
	14	22.06.99	01:17:50	27° 38.186	158° 46.003	60s	PRT+STB		
	1798	23.06.99	06:01:50	25° 42.010	158° 46.012	60s	PRT+STB		

STB: Starboard
PRT: Portside

Appendix 9.2

MAGNETIC PROFILES

Line number	Date UTC	Time UTC	Position [N]	[W]	Depth [m]	Methods
SO142-101	03.06.99 04.06.99	10:42:33 21:33:25	31° 20.85' 32° 08.91'	166° 21.94' 160° 01.83'	5825 5794	M P
SO142-107	05.06.99 05.06.99	00:10:53 23:01:24	32° 11.53' 32° 08.43'	159° 58.04' 163° 03.27'	5841 4435	M P
SO142-109	06.06.99 06.06.99	10:14:42 15:47:35	32° 17.93' 32° 29.57'	163° 06.71' 162° 17.99'	3076 5211	M P
SO142-110	08.06.99 08.06.99	03:06:00 07:48:08	32° 15.00' 32° 13.23'	161° 54.55' 161° 07.54'	5251 5756	M P
SO142-112	08.06.99 09.06.99	21:10:25 00:54:11	32° 12.95' 32° 13.00'	161° 00.40' 160° 08.79'	5885 5051	M P
SO142-113	09.06.99 09.06.99	14:01:40 16:48:54	32° 17.05' 32° 29.09'	159° 57.76' 160° 13.63'	3583 5893	M P
SO142-114	09.06.99 10.06.99	21:32:30 01:35:47	31° 57.87' 31° 17.77'	160° 12.98' 160° 12.43'	5440 5680	M P
SO142-115	11.06.99 11.06.99	05:45:27 11:55:06	32° 59.29' 31° 57.95'	160° 15.90' 160° 11.37'	5869 5715	M P
SO142-116	12.06.99 12.06.99	04:32:56 11:16:57	32° 33.98' 32° 12.00'	160° 07.55' 159° 20.11'	5868 5904	M P
SO142-117	13.06.99 13.06.99	03:05:31 22:05:21	32° 18.24' 29° 15.78'	159° 35.08' 160° 19.61'	3152 5973	M P
SO142-118	14.06.99 15.06.99	14:48:40 14:41:45	29° 20.27' 26° 19.00'	160° 20.35' 160°16.55'	5224 5027	M P
SO142-122	15.06.99 16.06.99	20:11:52 00:23:56	26° 54.05' 27° 35.02'	160° 16.64' 160° 17.14'	5030 4371	M P
SO142-123	17.06.99 17.06.99	11:33:17 15:18:44	25° 44.27' 26° 19.04'	160° 11.99' 160° 19.39'	2625 5021	M P
SO142-124	18.06.99 18.06.99	04:11:09 06:30:52	26° 48.51' 26° 38.80'	160° 17.69' 160°43.94'	5069 4551	M P

Methods used:
M - magnetics
P - Hydrosweep,Parasound

MAGNETIC PROFILES (Continued)

Line number	Date UTC	Time UTC	Position [N]	[W]	Depth [m]	Methods
SO142-125	18.06.99	19:00:13	26° 31.32'	160° 41.69'	3852	M P
	18.06.99	23:58:49	26° 34.02'	160° 12.76'	4141	
SO142-126	19.06.99	17:08:55	26° 36.79'	160° 15.04'	3919	M P
	20.06.99	22:00:52	26° 35.16'	159° 29.75'	3715	
SO142-127	21.06.99	08:09:18	26° 37.93'	159° 29.32'	2681	M P
	21.06.99	13:45:01	26° 18.00'	158° 46.90'	4788	
SO142-129	23.06.99	10:20:38	25° 40.72'	158° 41.15'	4984	M P
	23.06.99	14:22:32	26° 17.98'	158° 46.84'	4794	
SO142-130	24.06.99	05:52:59	26° 58.39'	158° 38.57'	5263	M P
	24.06.99	09:19:12	26° 32.15'	158° 49.01'	4460	
SO142-131	24.06.99	16:33:01	26° 35.20'	158° 48.16'	3378	M P
	24.06.99	18:49:22	26° 45.06'	158° 29.82	5368	
SO142-132	25.06.99	01:56:07	26° 40.17'	158° 29.32'	3643	M P
	25.06.99	03:20:48	26° 30.23'	158° 44.26'	5280	
SO142-133	25.06.99	08:03:39	26° 28.66'	158° 44.71'	5369	M P
	25.06.99	11:29:43	26° 41.44'	158° 14.96'	4045	
SO142-134	25.06.99	17:27:04	26° 40.72'	158° 14.52'	3395	M P
	25.06.99	20:12:08	26° 10.01'	158° 24.99'	4820	
SO142-135	26.06.1999	04:29:57	26° 10.87'	158° 23.43'	4046	M P
	26.06.1999	18:31:01	24° 15.57'	157° 43.74'	4386	

Methods used:
M - magnetics
P - Hydrosweep,Parasound

Appendix 9.3

HULA2-SO142-Hydroacoustic Profiles

Title HS/PS:	Time , Date (UTC)	Coordinats Lat/Lon	Depth
Start Profile F1:	21:04 h, 1.6.1999	30:17.000 N / 169:59.600 W	5527m
End Profile F1:	00:30 h, 2.6.1999	30:18.800 N / 169:50.800 W	5552m
Start Profile F2:	19:45 h, 2.6.1999	31:13.900 N / 166:44.100 W	5778m
End Profile F2:	23:30 h, 2.6.1999	31:08.400 N / 166:40.300 W	5573m
Start Profile 101:	09:52 h, 3.6.1999	31:15.801 N / 166:30.497 W	5692m
End Profile 101:	17:27 h, 3.6.1999	31:44.979 N / 165:00.141 W	4066m
Start Profile 102:	17:27 h, 3.6.1999	31:44.979 N / 165:00.141 W	4066m
End Profile 102:	22:50 h, 3.6.1999	32:19.000 N / 164:00.000 W	5720m
Start Profile 103:	22:50 h, 3.6.1999	32:19.000 N / 164:00.000 W	5720m
End Profile 103:	06:57 h, 4.6.1999	31:39.000 N / 162:28.000 W	4043m
Start Profile 104:	06:57 h, 4.6.1999	31:39.000 N / 162:28.000 W	4043m
End Proofile 104:	13:00 h, 4.6.1999	32:25.516 N / 161:26.695 W	5921m
Start Profile 105:	13:00 h, 4.6.1999	32:25.516 N / 161:26.695 W	5921m
End Profile 105:	17:27 h, 4.6.1999	32:08.823 N / 160:31.185 W	5211m
Start Profile 106:	17:27 h, 4.6.1999	32:08.823 N / 160:31.185 W	5211m
End Profile 106:	19:10 h, 4.6.1999	32:09 000 N / 160:08.000 W	5697m
Start Profile F3:	19:10 h, 4.6.1999	32:09 000 N / 160:08.000 W	5697m
End Profile F3:	00:20 h, 5.6.1999	32:13.264 N / 159:57.667 W	5622m
Start Profile 107:	00:20 h, 5.6.1999	32:13.264 N / 159:57.667 W	5622m
End Profile 107:	03:46 h, 5.6.1999	32:21.574 N / 159:17.459 W	4252m
Start Profile 108:	03:46 h, 5.6.1999	32:21.574 N / 159:17.459 W	4252m
End Profile 108:	23:11 h, 5.6.1999	32:08.358 N / 163:02.731 W	4284m
Start Profile F4:	23:11 h, 5.6.1999	32:08.358 N / 163:02.731 W	4284m
End Profile F4:	02:50 h, 6.6.1999	32:08.200 N / 162.55.000 W	4836m
Start Profile 109:	10:18 h, 6.6.1999	32:17.595 N / 163:07.279 W	3046m
End Profile 109:	03:01 h, 7.6.1999	32:34.900 N / 162:20.400 W	5640m
Start Profile F5:	09:50 h, 7.6.1999	32:18.900 N / 162:05.700 W	3498m
End Profile F5:	12:48 h, 7.6.1999	32:14.934 N / 162:10 492 W	4982m
Start Profile 110:	12:48 h, 7.6.1999	32:14.934 N / 162:10 492 W	4982m
End Profile 110:	14:33 h, 7.6.1999	32:20.865 N / 162:04.981 W	4999m
Start Profile F6:	23:22 h, 7.6.1999	32:17.500 N / 162:02.100 W	4134m
End Profile F6:	03:00 h, 8.6.1999	32:15.013 N / 161:55.102 W	5190m
Start Profile 111:	03:00 h, 8.6.1999	32:15.013 N / 161:55.102 W	5190m
End Profile 111:	07:43 h, 8.6.1999	32:13.005 N / 161:08.028 W	5802m
Start Profile F7:	18:45 h, 8.6.1999	32:13.000 N / 161:07.343 W	5850m
End Profile F7:	23:13 h, 8.6.1999	32:13.000 N / 161:00.000 W	5760m
Start Profile 112:	23:13 h, 8.6.1999	32:13.000 N / 161:00.000 W	5760m
End Profile 112:	01:12 h, 9.6.1999	31:13.000 N / 160:07.600 W	5321m
Start Profile F8:	01:12 h, 9.6.1999	31:13.000 N / 160:07.600 W	5321m
End Profile F8:	05:10 h, 9.6.1999	32:12.900 N / 159:59.600 W	4635m
Start Profile 113:	14:00 h, 9.6.1999	32:17.500 N / 159:57.000 W	4263m
End Profile 113:	16:53 h, 9.6.1999	32:29.000 N / 160:14.000 W	5840m
Start Profile 114:	22:49 h, 9.6.1999	31:47.030 N / 160:08.058 W	5213m
End Profile 114:	01:36 h, 10.6.1999	31:17.773 N / 160:12.426 W	5681m

HULA2-SO142-Hydroacoustic Profiles

Title HS/PS:	Time , Date (UTC)	Coordinats Lat/Lon	Depth
Start Profile S2:	02:19 h, 10.6.1999	31:19.243 N / 160:14.055 W	5592m
End Profile S2:	05:46 h, 11.6.1999	32:59.288 N / 160:16.132 W	5863m
Start Profile 115:	05:46 h, 11.6.1999	32:59.288 N / 160:16.132 W	5863m
End Profile 115:	00:35 h, 12.6.1999	31:57.456 N / 160:11.262 W	5702m
Start Profile F9:	00:35 h, 12.6.1999	31:57.456 N / 160:11.262 W	5702m
End Profile F9	04:22 h, 12.6.1999	32:33.714 N / 160:08.706 W	5888m
Start Profile 116:	04:22 h, 12.6.1999	32:33.714 N / 160:08.706 W	5888m
End Profile 116:	11:23 h, 12.6.1999	32:11.994 N / 159:20.800 W	5906m
Start Profile F10:	11:23 h, 12.6.1999	32:11.994 N / 159:20.800 W	5906m
End Profile F10:	14:43 h, 12.6.1999	32:15.400 N / 159:26.700 W	4539m
Start Profile F11:	23:08 h, 12.6.1999	32:18.500 N / 159:28.600 W	3625m
End Profile F11:	03:04 h, 13.6.1999	32:18.337 N / 159:35.141 W	3159m
Start Profile 117:	03:04 h, 13.6.1999	32:18.337 N / 159:35.141 W	3159m
End Profile 117:	06:05 h, 13.6.1999	23:18.270 N / 159:35.100 W	5722m
Start Profile F12:	00:34 h, 14.6.1999	29:16.500 N / 160:19.600 W	5959m
End Profile F12:	04:09 h, 14.6.1999	29:16.200 N / 160:26.000 W	5986m
Start Profile F13:	11:50 h, 14.6.1999	29:18.100 N / 160:24.600 W	5025m
End Profile F13:	14:36 h, 14.6.1999	29:21.291 N / 160:20.208 W	5241m
Start Profile 118:	14:36 h, 14.6.1999	29:21.291 N / 160:20.208 W	5241m
End Profile 118:	04:51 h, 15.6.1999	26:41.080 N / 160:22.340 W	4597m
Start Profile 119:	04:51 h, 15.6.1999	26:41.080 N / 160:22.340 W	4597m
End Profile 119:	07:08 h, 15.6.1999	26:40.795 N / 160:51.872 W	5060m
Start Profile 120:	07:26 h, 15.6.1999	26:37.260 N / 160:51.842 W	4052m
End Profile120:	11:36 h, 15.6.1999	26:36.898 N / 160:00.000 W	5027m
Start Profile 121:	12:00 h, 15.6.1999	26:33.014 N / 160:00.023 W	3534m
End Profile 121:	14:45 h, 15.6.1999	26:19.013 N / 160:16.912 W	5098m
Start Profile 122:	20:10 h, 15.6.1999	26:54.057 N / 160:16.933 W	5033m
End Profile 122:	00:24 h, 16.6.1999	27:35.022 N / 160:17.221 W	4380m
Start Profile S3:	01:17 h, 16.6.1999	27:32.707 N / 160:18.004 W	5155m
End Profilke S3:	07:00 h, 17.6.1999	25:44.427 N / 160:18.004 W	3786m
Start Profile F14:	07:00 h, 17.6.1999	25:44.427 N / 160:18.004 W	3786m
End Profile F14:	11:36 h, 17.6.1999	25:44.574 N / 160:12.177 W	2828m
Start Profile 123:	11:36 h, 17.6.1999	25:44.574 N / 160:12.177 W	2828m
End Profile 123:	15:18 h, 17.6.1999	26:19.035 N / 160:18.201 W	5020m
Start Profile F15:	00:33 h, 18.6.1999	20:19.232 N / 160:18.201 W	4900m
End Profile F15	04:13 h, 18.6.1999	26:48.350 N / 160:18.070 W	5023m
Start Profile 124:	04:13 h, 18.6.1999	26:48.350 N / 160:18.070 W	5023m
End Profile 124:	06:31 h, 18.6.1999	26:38.800 N / 160:43.940 W	4551m
Start Profile F16:	15:10 h, 18.6.1999	26:37:195 N / 160:42.379 W	3091m
End Profile F16:	19:07 h, 18.6.1999	26:30.757 N / 160:40.753 W	4142m
Start Profile 125:	19:07 h, 18.6.1999	26:30.757 N / 160:40.753 W	4142m
End Profile 125:	23:57 h, 18.6.1999	26:34.007 N / 160:12.963 W	4122m
Start Ptofile F17:	00:46 h, 18.6.1999	26:34.000 N / 160:12.000 W	4160m
End Profile F17:	03:53 h, 19.6.1999	26:31.108 N / 160:07.411 W	2983m
Start Profile F18:	13:20 h, 19.6.1999	26:36.298 N / 160:16.960 W	2983m
End Profile F18:	17:15 h, 19.6.1999	26:37.556 N 7 160:16.111 W	3931m
Start Profile 126:	17:15 h, 19.6.1999	26:37.556 N 7 160:16.111 W	3931m
End Profile 126:	22:00 h, 20.6.1999	26:35.495 N / 159:29.810 W	3648m

HULA2-SO142-Hydroacoustic Profiles

Title HS/PS:	Time , Date (UTC)	Coordinats Lat/Lon	Depth
Start Profile F19:	22:00 h, 20.6.1999	26:35.495 N / 159:29.810 W	3648m
End Profile F19:	01.51 h, 21.6.1999	26:38.400 N / 159:24.251 W	4045m
Start Profile 127:	08:12 h, 21.6.1999	26:37.420 N / 159:29.420 W	2730m
End Profile 127:	13:44 h, 21.6.1999	26:17.996 N / 158:46.966 W	4786m
Start Profile 128:	20:15 h, 21.6.1999	27:00.000 N / 158:45.000 W	5219m
End Profile 128:	00:44 h, 22.6.1999	27:40.000 N / 158:45.640 W	5512m
Start Profile S4:	01:25 h, 22.6.1999	27:37.690 N / 158:46.000 W	5529m
End Profile S4:	06:01 h, 23.6.1999	25:42.066 N / 158:46.011 W	4995m
Start Profile F20:	06:51 h. 23.6.1999	25:40.728 N / 158:48.362 W	4991m
End Profile F20:	10:15 h, 23.6.1999	25:40.491 N / 158:41.658 W	4986m
Start Profile 129:	10:15 h, 23.6.1999	25:40.491 N / 158:41.658 W	4986m
End Profile 129:	14:19 h, 23.6.1999	26:18.000 N / 158:46.530 W	4831m
Start Profile F21:	02:08 h, 24.6.1999	26:59.801 N / 158:45.769 W	5204m
End Profile F21:	05:50 h, 24.6.1999	26:58.128 N / 158:38.770 W	5261m
Start Profile 130:	05:50 h, 24.6.1999	26:58.128 N / 158:38.770 W	5261m
End Profile 130:	09:20 h, 24.6.1999	26:32.256 N / 157:48.913 W	4441m
Start Profile 131:	16:24 h, 24.6.1999	26:34.610 N / 158:47.280 W	3564m
End Profile 131:	18:48 h, 25.6.1999	26:45.010 N / 158:29.942 W	5368m
Start Profile 132:	01:40 h, 25.6.1999	26:40.235 N / 158:28.660 W	3475m
End Profile 132:	03:48 h, 25,6,1999	26:28:034 N / 158:45.651 W	5376m
Start Profile 133:	07:25 h, 25.6.1999	26:28.228 N / 158:45.291 W	5374m
End Profile 133:	11:32 h, 25.6.1999	26:41.630 N / 158:14.938 W	4149m
Start Profile 134:	17:23 h, 25.6.1999	26:41.240 N / 158:14.120 W	3512m
End Profile 134:	20:14 h, 25.6.1999	26:09.683 N / 158:24.990 W	4992m
Start Profile 135:	04:29 h, 26.6.1999	26:10.890 N / 158:23. 430 W	3811m
End Profile 135:	18:51 h, 26.6.1999	24:14.101 N / 157:42.915 W	4453m
Start Profile 136:	22:54 h, 26.6.1999	24:14.250 N / 157:42.390 W	4445m
End Profile 136:	00:13 h, 27.6.1999	24:01.618 N / 157:42.694 W	4117m
Start Profile 137:	03:57 h, 27.6.1999	23:57.042 N / 157:41.934 W	4368m
End Profile 137:	19:43 h, 27.6.1999	21:23.987 N / 157:69.470 W	418m

APPENDIX 9.4: SONNE 142 - Station and sample list

Abbreviations:

DR -	Kettensackdredge	Chain-bag dredge
MS -	Multisonde	CTD + water sampler

Station: No., type and place	**Date, time (UTC), depth and coordinates:** on bottom / stuck (if applicable) / off bottom	**Description:**
01 DR Rossini	06.06.1999 on bottom: 06:34 3828 m 32°19,54 N 163°06,02 W off bottom: 08:57 3142 m 32°18,45' N 163°05,75' W	-1: Size: 13x7x8 cm – Angular, altered and aphyric basalt. Light brown colored with veinlets of FeMn-Hydroxides. Moderately phyric with plagioclase laths and small cavities filled with secondary clay. Coated with MnO_x and yellowish palagonite like product. Useless for bulk chemistry but good for agedating. -2: Extremely altered light yellowish brown basaltic fragment with few laths plagioclase pebble size (4 cm Ø) coated with yellowish brecciated material. Useless for bulk or probe analyses. -3: Small pebble size (4 cm Ø) partially altered basalt with light brown staining. A portion of the sample is dark grey and may be used for analyses. (?) Occasional plagioclase laths (< 1%). -4: Thick manganese crust (4 cm thick) coating extremely altered aphyric basalt debris. Few (< 1%) plagioclase laths occur. -5: Angular pebble size (5 cm Ø) fragment of aphyric basalt. Partially altered with light brown (oxidized) product surrounded by a dark grey fresher material. This dark grey product could be used for bulk or probe analyses. This fragment was detached from a larger volcanoclastic slab. Volcanoclastic slab: (100x35x50 cm) yellowish light green brecciated rock. Unsorted pebble size (> 1cm Ø) altered basaltic fragments cemented by sand and clay size debris of rocks and light greenish yellow "palagonite-like" product (or altered sediment and mineral debris ?). Secondary light grey colored mineral (Zeolite, Halite ?) are observed in cavities and matrix of the slab. Many larger angular basaltic fragments are coated with a dark grey fresher rim wich seems appropriate for bulk and/or microprobe analyses.
02 DR Bizet	07.06.1999 on bottom: 16:31 5227 m 32°21,69' N 162°4,99' W off bottom: 20:59 4179 m 32°19,51 N	About 80-100 kg MnO_x-crust and nodules with few pieces of altered basalts. -1: Altered plagioclase clay phyric basaltic fragment coated with MnO_x (0,5 – 1 cm thick). About 3 to 5 % phenocryst. Size: 11x5x4 cm -2: Altered and angular plagioclase phyric basalt coated with MnO (1 – 2 cm thick) about 3 to 5 % phenocryst. yellowish light brown oxidized zones. Size: 7x4x7 cm

	162°5.03 W	-3: Altered plagioclase phyric basalt coated with MnO_x (3 mm thick) yellowish light brown center and darker, fresher rim. Size: 5 cm Ø -4: Size: 10x12x9 cm MnO_x-coated volcanoclastic breccia. Semi-indurated pelagic sediment clasts, black MnO_x concretions small (0,5 cm Ø) altered basaltic debris (rounded); set in a matrix of MnO_x. Fe-oxyhydroxide and altered sand-clay size material. Manganese crust is 1,5 cm thick. -5: Chunk of "silicified" (gasper-like) material may be pelagic sediment. Size: 9x5x8 cm. Comments: 90 % of the samples consits of MnO_x nodules and MnO_x slabes coating sediment volcanoclastic debris. This dredged material appears more altered than 1DR. Extra: MnO_x-coated volcanoclastics of semi-indurated sediment. Few (2) pieces of indurated (white) sedimented slabs (< 1 cm thick)
03 DR	08.06.1999 on bottom: 10:02 5610 m 32°14,28 N 161°07,21 E off bottom: 14:55 4237 m 32°15,78 N 161°08,90 E	30-40 kg MnO_x-coated material: about 40% of altered rocks and remaining material are sediment and breccia coated with MnO_x-crust. -1: 20x14x10 cm. Boulder of moderately phyric plagioclase basalt with rounded edges and coated by MnO_x (< 5 mm). Pillow lava fragment with altered edges and interior, recognizeable altered chilled margin feature; one part of the surface is coated by cemented breccia. Few vesicles observed (<5%). -2: Size: 9x4x7 cm. Subrounded pillow lava coated with MnO_x (< 5 cm thick). Moderately phyric with altered chilled margin. Plagioclase loths (3-5%) set in a fine grained altered ground mass. Less altered than 2DR. -3: Angular fragment of moderately vesicular basalt with surface "pillow" ridges (radial structure). Vesicles and cavities comprise <5%. Aphyric sample abundantely altered. Size: 10x8x5 cm. -4: Subrounded and altered plagioclase phyric basalt. Small patches of rusty material, probably ghosts of olivine ?, little MnO_x-coating. "Pillow ridges" surface texture. Size: 13x5x6 cm. -5: Subrounded boulder of altered basalts with rusty patches of possibly olivine ghosts. Thin MnO_x-coating and light grey colored silicified material (< 5 mm thick). Size: 5 cm Ø -6: Yellowish light brown volcanoclastic material made of small (3 – 7 mm Ø) volcanic debris set in a yellow clay-like ground mass (cement) of altered sediment and/or hydrothermal precipitates (?). This material looks like nontronite clay (?). Dark grey and rusty colored debris of probably volcanic glass (< 5 mm O) comprise about 10 to 20% of bulk sample. A thin MnO_x-coating on the surface. Size: 15x8x5 cm. -7: Small slab with MnO_x-concretions. Tan colored pelagic sediment. Size: 8x5x3 cm. Extra: Consists of subrounded basaltic cobbles with

		smoothed surface. They are comparable to #1, #2 and #3 samples. Manganese nodules were collected. Comments: Most volcanic from this dredge are less altered than those from the previous dredge (2DR). Also some samples show coatings of yellowish clay (nontronite ?) with altered (pelagonitized glass) chips. Bulk analyses could be done on some samples after cleaning the edges. Also look for glassy chips in hyaloclastic-volcanoclastic material.
04 DR **Donizetti**	09.06.1999 on bottom: 05:39 5120 m 32°14,99 N 159°56,99 W off bottom: 12:24 32°16,54 N 159°58,46 W	-1: Pillow lava "bud" with preserved glassy rim, interior yellowish light brown alteration. Aphyric lava (9*6 cm Ø) Coating of palagonite and thin MnO_x (< 3mm thick) -2: Large altered block of pillow with a thick MnO_x on one side (2 cm thick). A phyric moderatly altered rock with radial jointings. No glass observed. Size: 17x13x12 cm -3: Aphyric pillow lava fragment with smoothed edges and moderatly altered interior (light grey). Small vesicles (< 1mm) filled with yellowish clay. MnO_x (1.5 cm thick) -4: Small slab of crystalline, probably a massive flow or a dyke fragment (?). Plagioclase laths, pyroxene and completly altered olivine (Fe-Oxyde, rusty appearance) abound. Size : 9x4x8 cm. -5: Angular, moderately altered pillow lava fragment with columnar jointings. Thick MnO_x crust (5.5 cm thick) with pockets of tan sediment. Vesicles and cavities (0.5mm Ø) abund (5-10%). The sample is mostly aphyric. -6: Angular fragment with slightly smooth edges. Moderatly crystalline, probably a massive flow with MnO_x patches. Rusty patches speak of possible olivine ghosts. Size: 11x7x4 cm -7: One large (34*12*15cm) slab of volcanic breccia with altered glass fragments(<1cm thick) set in a tan colored, clay-like matrix. -8: Few indurated, tan colored sediments (silicified) occur. -9: One punnice fragment (8x4 cm). -10: Several slabs of breccia material(altered glass) cemented by MnO_x. One sample contains ochre Fe-oxyhydroxide material with chips altered glass and MnO_x. This material is coated by MnO_x. Comments: Many fragments contain preserved and relativly fresh glassy margins. Others are aboundantly palagonatized. Slabs of MnO_x coating pelagic sediment and indunated material occurs throughout the dredge.
05 DR **Donizetti**	12.06.1999 on bottom: 16:58 5177 m 32°16,28' N 159°28,02' W off bottom: 21:18 3790 m	-1: Rounded fragment of moderately altered phyric basalt. Olivine phenocryst (<7%) some altered. Thin (milimetric) MnO_x coating. -2: Subrounded altered basalt with less altered gray zone. Fine grained with light brown altered groundmass. Few vesicles (<1%) and cavities occur. Thin MnO_x coating. No glass, mostly crystalline matrix.

	32°18,20' N 159°28,19' W	-3: Rounded to subrounded (smoothed edges) massive moderately phyric basalt. Mostly crystalline rock made up of plagioclase and clinopyroxene (?) with agglomerate of plagioclase and altered (?) olivine. The whole sample is altered with a light brown colorarion (rusty). Thin coating of MnO_x. Size: 15x11x7 cm. -4: Subrounded columnar moderately phyric basaltic fragment. Size: 15x5x6 cm. Mostly holocrystalline with plagioclase olivine agglomerete. Similar to #3 and altered with rusty coloration. -5: Size: 18x11x8 cm. Subrounded radially jointed altered basalt with altered chilled margin. Occasional minophenocrysts of plagioclase and may be olivine. Few gas cavities occur. The rock is moderately altered with light-brown-gray coloration. Thin MnO_x coating. -6: Size: 18x13x11 cm. Subrounded altered fragment of moderately phyric basalt similar to previous samples with a centraly located cavity due to degasing. No glass observed. Thin MnO_x coating. -7: Size: 13x9x10 cm. Altered fragment of radially jointed pillow lava with a thin altered chilled margin. No preserved glass. Interior contains few large cavities (<0,5 cm ∅) filled by pelagic sediment. MnO_x and sediment coating. -8: Moderately phyric angular columnar basalt with altered chilled margin (palagonatized). Crystalline altered groundmass. The minophenocryst of plagioclase compises less than 5% of the bulk sample. Thin (<0,5 cm) MnO_x coating. Size: 21x8x7 cm. -9: Subrounded altered moderately vesicular pillow lava fragment with a large (3 cm ∅) vesicular inclusion. Probably a gas .... bubbles with some secondary late precipitates (silicate clay?) Thin film of MnO_x coating. Size: 18x5x5 cm. -10: Three fragments of MnO_x crust with some Fe-oxyhydroxide product of hydrothermal origin. -11: Breccia of Fe-Mn and ochreous Fe-oxyhydroxide mixed material. Size: 11x5x6 cm. -12: Similar to #8. Size: 15x8x6 cm. -13: Similar to #8. Size: 17x9x8 cm. -14: Breccia piece. Size: 10x10x9 cm. Comments: This dredge is similar to that previously collected 4DR. Other material recovered consist of large brecciated volcanics and conglomerate (more rounded fragments) cemented by altered fragments (sandsize) of rocks, sediment and manganese.
06 DR Murray FZ	14.06.1999 on bottom: 04:28 5998 m 29°15,51' N 160°24,58' W off bottom: 09:23 5185 m 29°17,56' N 160°24,66' W	-1: Flat slab with laminated texture.The rock has light brown and darker gray horizontal streaks. It could be different cooling unit within a massive flow. Size: 8x11 cm. -2: Radially jointed pillow lava fragment of a metabasalt. This sample appears to be hydrothermally metamorphosed. Successive cooling units going from almost homogeneous aphyric inner zone to a spherulitic intermediate zone and to an altered (chloritized) chilled

		surface. -3: Coasse grained abundantely altered yellowish light brown colored columnar fragment of may be dolerite (dyke unit?). The inner part of the sample is less altered than the outer margin. The block is coated with MnO_x and dusted with pelagic sediment. -4: Subrounded fine grained crystalline basaltic rock with thin MnO_x coating (<1 cm) made up of plagioclase aggregates set in a crystalline groundmass of tiny plagioclase laths and dark mesostasis. Size: 11x10x5 cm. -5: Subrounded fragment of fine grained crystalline basalt coated with thick (3 cm) MnO_x crust. The sample contains tiny plagioclase laths and aggregates of plagioclase. This sample could be used for bulk analyses. Similar to 4DR. Size: 12x10x11 cm. -6: Subrounded massive rock with sherulitic dark brown and dark gray product throughout the whole rock. Size: 10x6x11 cm. -7: Extremely altered, yellowish light brown pillow fragment with radial jointings and altered chilled margin. May be enough glass for probe analyses. Size: 13x5x6 cm. -8: Altered holocrystalline dolertic fragment containing plagioclase, pyroxene and altered olivine (rusty colored). Size: 8x6x9 cm. -9: Columnar fragment with smoothed edges with nodular internal texture of dark greenish gry and light brown material. May be alteration product? Size: 17x14x8 cm. -10: Subrounded columnar fragment of rock with nodular textural feature. Attention to look for pyroxene accumulation (?) need thin section. Size: 10x6x9 cm. -11: Altered poorly crystalline basaltic flow with smoothed surface thin MnO_x coating and chilled margin completely altered. Size: 12x14x10 cm. -12: Altered massive rock fragment with smoothed edges. Secondary hydrothermal veins (green and light brown) occur throughout sample. Need thin section for detail study. -13: Subrounded massive and coasse grained doleritc flow, yellowish light brown colored due to extensive minersl alteration (olivine?). Pyroxene, plagioclase, olivine association. -14: Extremely altered and subrounded basaltic rock with banded texture due to different cooling units. Aphyric sample coated with MnO_x (<1 cm thick). Size: 14x5x6 cm. -15: Subangular altered nodular flow similar to sample #9 and #10. Size: 12x6x4 cm. -16: Extemely altered and angular light olive green rock fragment cemented by a MnO_x material. Look for olivine (thin section needed). The rest of the sample consist essentially of altered basalticflow and one massive columnar doleritic fragment. -17: Altered sherulitic basaltic flow. Light brown groundmass with rounded spherules with darker cores.

		MnO_x coating (<0,5 cm thick) and white pelagic sediment. Size: 10x4x5 cm. -18: Altered spherulitic basalt same as #17 -19: Altered spherulitic basalt same as #17 and #18
07 DR Bach Ridge	18.06.1999 on bottom: 08:30 4548 m 26°38,825' N 160°44,020' W off bottom: 13:17 3258 m 26°34,51' N 160°42,45' W	-1: Highly phyric plagioclase basalt (HPPB) pillow lava. Large and abundant plagioclase (about 1 cm lenght and 20%) Size: 14x10x11 cm. Interior fresh and margin altered. -2: (HPPB) Highly phyric plagioclase basalt with smoothed surface similar to #1, fresh sample for chemistry. Size: 7x6x5 cm. -3: Subrounded highly phyric plagioclase basalt (HPPB) with large and aboundant plagioclase crystals (>15%). The sample is relatively fresh except at the margin. The plagioclase laths show a semi-fluidal texture. Size: 8x4x6 cm. -4: Highly vesicular and porpyristic rock pillow lava fragment (basalt?) with rounded edges. The large crystals are mostly plagioclase (>15%) some crystalline aggregates are rounded and they could be xenoliths (foreign inclusions?). Size: 9x7x4 cm. -5: Extremely altered brecciated rocks with thick (1 cm) Fe-Mn coating. Light yellowish-brown coloration and no glass observed. Size: 5x4x8 cm. -6: Three Fe-Mn slabs with smooth surface. Size: 3x10x7 cm.
08 DR Bach Ridge	19.06.1999 on bottom: 06:24 3996 m 26°37,432' N 160°15,693' W off bottom: 11:25 2964 m 26°36,92' N 160°16,98' W	-1: Highly phyric plagioclase basalt (HPPB) with an altered glassy margin. Aboundant plagioclase (>15%). Some are aggregates probably xenolith. The rock is yellowish light colored. This is a pillow lava fragment. Size: 14x12x11 cm. -2: Fragment of moderately altered pillow lava with plagioclase phenocryst and maybe xenolith (?). Margin more altered than interior. Interior fresh enough for bulk analyses. Maybe some glassy margin occurs. Palagonatized margin. Size: 9x11x12 cm. -3: Highly phyric plagioclase basalt (HPPB) coated with MnO_x (1 cm thick). Plagioclase phyric with relatively fresh groundmass. No preserved glassy margin observed. Size: 21x14x12 cm. -4: HPPB angular fragment with altered veins and more than 10% plagioclase phenocrysts. The veins are filled with MnO_x and Fe-oxyhydroxide. Size: 17x16x12 cm. -5: Pillow lava fragment moderately altered light gray with small vesicles (10-20%). Few (<5%) plagioclase phenocryst are seen. Size: 15x9x12 cm. -6: Fragment of light gray moderately altered pillow lava with few plagioclase phenocrysts and vesicles. Same as #5. Size: 13x8x6 cm. -7: Moderately altered pillow lava fragment same as #5 and #6 with smooth edges and few plagioclase phenocryst (<3%). No glass observed. Size: 15x6xX cm. -8: Aphyric moderately altered basalt with vesicles and few plagioclase phenocryst (<3%). Size: 12x3x9 cm. -9: Moderately phyric plagioclase basalt. Fragment of a

		pillow. Relatively fresh and no glassy margin. Size: 12x11x12 cm. -10: Lobated-pillow lava with a preserved glassy chilled margin. Light brown colored interior. Phyric with plagioclase phenocryst (10-15%). The center of the pillow shows flow differentiation with plagioclase accumulation. Sample appropiate for probe analyses. Size: 16x14x10 cm. -11: Pillow lava bud with MnO_x-crust (<1 cm thick). Moderately phyric with plagioclase phenocryst (<10%). Light brown colored interior. The chilled margin is extremely palagonatized with a light gray margin (<1 cm thick). Not appropriate for bulk analyses. Size: 13x13x8 cm. -12: Vesicular aphyric basalt included in a thick (3 cm thick) Fe-MnO_x crust. The basalt is relatively fresh and may be used for bulk analyses. Size: 23x14x12 cm. -13: A slab of Fe-MnO_x with ochreous hydrothermal material (?) and which indurate sediment patches. Size: 17x16x4 cm. -14: Carbonate coated MnO_x crust. Comments: The dredge consists essantially of pillow lava fragment, brecciated material cemented with MnO_x and semi-indurated pelagic sediment coated with Fe-MnO_x.
09 DR Bach Ridge	21.06.1999 on bottom: 03:47 3931 m 26°39,975' N 159°28,009' W off bottom: 06:50 2855 m 26°39,660' N 159°28,965' W	-1: Angular moderately phyric pillow lava basalt. Few large plagioclase phenocryst (<3%). Patches of MnO_x on the surface. Size: 15x10x15 cm. -2: Vesicular fragment of a pillow, radially jointed. Coating Fe-MnO_x crust (3 mm thick). About 10-15% vesicles (1-2 mm Ø) occur. -3: Vesicular aphyric and angular basaltic fragment. The glassy margin has been completely palagonatized. Light brown chilled margin and a dark gray fresher interior with large cavities (2-3% of bulk rock). MnO_x coating <0,5 cm thick. Radially jointed pillow fragment. Aphyric sample. Size: 13x11x14 cm. -4: Altered vesicular pillow lava fragment with light brownish gray coloration. This sample is fairly altered for bulk chemistry. Occasional plagioclase (<1%) occur. Size: 12x7x7 cm. -5: Light gray aphyric pillow lava fragment with few cavities filled by sediment. Coated with a thin MnO_x crust (<3 mm thick). This sample shows smooth edges. Size: 11x10x5 cm. -6: Rusty colored radially jointed pillow fragment with an altered chilled margin. Thin Fe-MnO_x coating. Size: 18x8x10 cm. -7: Vesicular aphyric altered pillow lava with polygonal outlines and subrounded edge on one side. Palagonatized (rusty) surface . A patch of white pelagic sediment. Size: 13x11x11 cm. -8: Light brownish gray vesicular (15-20%) radially jointed pillow lava. Few (occasional) plagioclase microphenocrysts occur. The sample is mainly aphyric with a thin MnO_x coating. Size: 18x16x11 cm.

		-9: Highly vesicular (>30%) aphyric radially jointed pillow fragment with an altered chilled margin. The whole sample is coated with a film of Fe-MnO_x. Size: 19x14x11 cm. -10: Highly vesicular prismatic pillow fragment. Small vesicles (mm-size) and large ovale shaped cavities (~0,4 mm in Ø) abund. Light brownish gray colored interior and aphyric groundmass. Size: 13x7x7 cm. -11: Highly vesicular subrounded basaltic rock. The sample is aphyric and has a rusty apperance. The large vesicles are concentrated on the surface (one side) of the rock. Lesser amount of large size (0,5-1 cm) occur in the interior. Size: 18x13x8 cm. -12: Altered fragment of radially jointed pillow lava with centrally oriented elongated gas cavities. Altered chilled margin. Light brown coloration in the interior. Size: 18x9x8 cm. -13: Highly vesicular (>50%) with vesicles and cavities, subrounded pillow fragment. Aphyric and strongly altered sample. Size: 8x6x4 cm: -14: Highly vesicular altered fragment of a radially jointed pillow with smooth edges. Strongly altered as sample #13. Size: 19x6x4 cm. -15: Five fragments of "cherty looking" rusty and ochreous (colored) vesicular breccia (?). Some cavities are filled by clear quartz-like crystals in geod like cavities. The fragments have the shape of circular slabs and ovale coated with Fe-MnO_x. The size of the sample do not exceed 10 cm in diameter. -16: Slab of semi-indurated greenish yellow sediment-like material. Coated with Fe-MnO_x. Size: 13 cm in diameter. -17: Ovale shaped block of greenish yellow semi-indurated hyaloclastite like deposit. MnO_x coating on the surface. Rusty fragments of completely altered glass chips comprise about 30-40% of the sample. Size: 18x13x12 cm. -18: Angular block of "spiny" aphyric "aa" like basaltic flow with a thick (1,5 cm) MnO_x crust. Size: 9x8x6 cm. -19: Extremely altered vesicular basalt. Rusty coloration and smoothed edges. White veinlets of probably silicate precipitates. Size: 12x10x5 cm.
10 DR	24.06.1999 on bottom: 09:42 4093 m 26°33,81' N 158°47,50' W off bottom: 14:31 3533 m 26°34,66' N 158°47,31' W	-1: Size: 29x35x20 cm. Large angular fragment of phyric basalt. Moderately altered, light gray aphyric material with about 7-10% of rounded foreign inclusions (xenoliths) of gabbroic-material (plagioclase+olivine+clinopyroxene ?). Large rounded cavities (0,7 mm Ø) occur (7% of bulk sample). No chilled margin. The size of the xenoliths vanies (2-3 mm up to 1 cm Ø). -2: Angular porphyristic moderately altered basalt with xenolith inclusions. This sample is comparable to #1. Also contains large empty cavities. Coated with thin Mn film. Size: 30x23x18 cm. -3: Vesicular angular porphyristic basalt. The sample is moderately altered and could be used for bulk rock

		chemistry. This is a radially jointed pillow fragment containing large (1-2 mm to 1 cm Ø) inclusions of plagioclase olivine associations. -4: Moderately fresh aphyric angular basaltic fragment coated with MnO_x crust (up to 4 cm thick). No glass seen, fair amount (~10%) of small vesicles occur. Good for bulk rock analyses. Size: 15x8x8 cm. -5: Moderately altered light gray angular basalt with very few (<1%) plagioclase phenocrysts. Similar to #4. Good for bulk rock analyses. Size: 10x8x7 cm. -6: Subangular radially jointed pillow fragment with an altered glassy rim. A chilled margin surroundded by palagonite. The rock is weakly porphyristic with some plagioclase phenocrysts. Size: 23x9x10 cm. -7: Small subrounded light brown highly vesicular basalt with an altered chilled margin. Size: 7x7x2 cm. -8: Moderately fresh aphyric basalt coated with MnO_x (max. 2 cm thick). Occasional small (<1%) plagioclase laths are seen . Good for bulk chemistry. This is radially jointed pillow fragment. Size: 12x14x9 cm. -9: Moderately altered pillow lava fragment with a chilled rim and radial jointing coated with palagonite. Maybe some preserved glass occur. Size: 15x12x10 cm. -10: Moderatly fresh pillow lava fragment with a chilled margin and a palgonatized surface. Similar to #9. Few plagioclase (<3%) phenocryst are seen. The sample is coated with MnO_x (2cm thick). Size 14 x 15 x 6 cm. -11: Volcanoclastic breccia, yellowish light green groundmass with fragments of altered glass. -12: Manganese crust.
11 DR	24.6.1999 on bottom: 20:53 4482 m 26°41,59' N 158°28,01' W off bottom: 00:01 3390 m 26°40,39' N 158°28,30' W	-1: Moderately altered fragment of a radially jointed pillow with smooth edges. Aphyric with rusty patches of maybe ghosts of olivine (5-6%). Thin film of MnO_x coating and traces of pelagic sediment. Size 10 x 7 x 8 cm. -2: Altered blocky fragment of a pillow similar to # 1. veinlets of carbonate and Fe-oxyhydroxide. Size 10 x 5 x 6 cm. -3: Altered pillow lava fragment with extremely altered rusty colored rim (2cm thick). Palagonite replacing glass. White veinlets and rusty patches; some appear to be vesicles filled with Fe-hydroxide products, others could be alterations of olivine. Size 10 x 8 x 7 cm. -4: Altered pillow lava fragment comparable to #1, 2 and 3. The MnO_x coating is less than 0.3mm thick. Size 2 x 6 x 10 cm. -5: Moderately altered and angular pillow lava fragment with an altered (palagonatized) margin. MnO_x coating of about 1cm thick. Size 11 x 7 x 6 cm. -6: Subrounded (smooth edges) aphyric pillow fragment with MnO_x coating (0.5cm thick). Vesicles and patches of rusty Fe-oxyhydroxide filling material. Size 11 x 10 x 8 cm. -7: Massive altered fragment with smooth surface. Concentric rim of alteration within an aphyric groundmass. Size 10 x 4 x 7 cm.

		-8: Altered pillow lava with a preserved glassy margin. The interior is rusty colored and abundantly altered. Ovale shaped sample coated with MnO_x (0.7mm thick). Size 8 x 7 x 7 cm.
12 DR	25.6.1999 on bottom: 11:53 4466 m 26°42,34' N 158°14,64' W off bottom: 15:50 3643 m 26°41,64' N 158°14,11' W	-1: Subrounded moderately altered basaltic fragment; vesicles and cavities, comprising about 10 –15 % of the rock are filled with rusty colored fe-hydroxide material. No phenocryst seen, light gray-green groundmass. Thin MnO_x and pelagic sediment coating. Size 9 x 10 x 5 cm. -2: Altered subrounded aphyric basalt fragment similar to #1. Size 10 x 7 x 5 cm. -3: Angular, altered basalt fragment. No glass, holocrystalline without phenocrysts. -4: Holocrystalline angular and moderately altered fragment basalt. Size 3cm in diameter. -5: Moderately altered holocrystalline basalt abundantely veined with claylike product. Similar as #4. Size 4cm in diameter. -6: Subrounded holocrystalline basaltic fragment with veinlets of Fe-oxyhydroxide coated with MnO_x. About 7cm in diameter. -7: Altered pillow bud with chilled glassy margin. The core of the sample is rusty; abundantely altered (fe-hydroxide). Thin MnO_x coating. Ovale shaped, about 7x 6 cm. -8: Brecciated rock cemented and coated by MnO_x. The breccia fragments consist of altered, rusty colored and aphyric subrounded fragments (sand to pebble size). Few chips of palagonatized fragments of glass occur. Size 15 x 12 x 18 cm. -9: Fragment of a pillow bud imbedded in a greenish yellow clay-like matrix. Chips of altered glassy fragment abound (40% of bulk sample). Fresh glass occur in the rims of the rounded buds. The all brecciated rock is coated with MnO_x. Size = 24 x 20 x 12 cm. -10: A ball shaped (rounded) pyroclastic brecciated material consisting essentially of large (0.2 – 1 cm Ø) shard –like glass fragments with palgonatized edges. Size = 8cm in diameter. -11: Angular and altered rock imbedded in MnO_x nodule of about 16 x 14 x 15 cm. -12: Indurated white chalk with a thin MnO_x film.
13 DR Beethoven Ridge	25.6.1999 on bottom: 22:08 4905 m 26°09,81' N 158°25,00' W off bottom: 02:47 3765 m 26°11,55' N 158°23,98' W	-1: Large fragment of highly phyric pillow lava with inclusion of probably xenoliths. Rounded agglomerate of equigranular rock fragments included in host of basaltic flow. The samples are angular and moderately altered with reddish brown-gray groundmass. The inclusions are about 1cm in diameter. Size 55 x 30 x 30cm. -2: Large xenolith bearing pillow lava fragment with altered chilled margins. Rusty brown palagonite rim. Maybe some preserved glass occur. The interior appears fresher with dark gray matrix. Some of the inclusions have angular edges, others are corroded (rounded). Size 50 x 30 x 20 cm.

		-3: Angular xenolith bearing pillow lava, same as #1 with thin MnO_x coating. Size 40 x 20 x 20 cm. -4: Phyric pillow lave fragment with plagioclase and rounded xenoliths (plagioclase – pyroxene association). Palagonatized chilled margin coated with MnO_x occurs. Size 11 x 12 x 10 cm. -5: Small aphyric and moderately altered pillow lava fragment of basalt. No glass and no phenocrysts. Fe-oxide coating. Size 7 x 3 x 4 cm. -6: Similar to #3, Size 10 x 8 x 7 cm.

Appendix 9.5

Species-List of
RV SONNE cruise 142
30. 5. 1999 - 27. 6. 1999
Midway to Honolulu
with excursion to the
Musician Seamounts

Station F1: 1.6. 1999, 9.45-12.45, local time
Location: 30° 17,66' N, 169° 54,642'W
Rope length: 1,000m; Speed in water: 2Kn; water depth: 5554m

1/1	*Stylephorus chordatus*	16.5cm TL	left eye: isol. retina: GA right eye: isol. retina: PA
1/2	*Chauliodus sloani*	10.5cm TL	left eye intact: PA right eye: DEXTRITC; culture 3d, 4°, PA
1/3	*Benthalbella infans*, juv.	8.1cm TL	entire head: PA
1/4	*Chauliodus sloani*	9.5cm TL	head and brain: PA; optic nerve: GA both eyes: DEXTRITC; culture 3d, 4°, PA
1/5	*Macrostomias longibarbatus*	35cm TL	head and brain: PA; optic nerve: GA left eye: DEXTRITC; culture 3d, 4°, PA right eyecup: GA
1/6	*Chauliodus sloani*	9.8cm TL	head and brain: PA; optic nerve: GA left eye: DEXTRITC; cult. 3d, 4°, PA; nsg right eyecup: GA
1/7	*Scopelarchid*, larval		total: PA

Station F2: 2.6. 1999, 8.35-11.35, local time
Location: 31° 13,160' N, 166° 42,912'W
Rope length: 1,200m; Speed in water: 2Kn; water depth: 5718m

2/1	Larva	2,5cm TL	total: PA
2/2	*Chauliodus sloani*	21.5cm TL	left eye: PA; optic nerve: GA right eye: DEXTRITC; culture 2d, 4°, PA brain: nn. I & II DEXTRITC; c 2d, 4°, PA
2/3	*Winteria*	12cm TL	left eye intact: GA (Ron has other eye)
2/4	*Pachystomias microdon.*	7cm TL	right eye: PA; optic nerve: GA left eye: DEXTRITC; cult 2d, 4°, PA, nsg brain: nn. I & II DEXTRITC; c 2d, 4°, PA
2/5	*Chauliodus sloani*	20.5cm TL	brain: nn. I & II DEXTRITC; c 2d, 4°, PA both eyes: DEXTRITC; c. 3d, 4°, PA, nsg

			optic nerves: GA
2/5	*Macrostomias longibarbatus*	35cm TL	head and brain: PA; optic nerve: GA left eye: DEXTRITC; culture 3d, 4°, PA right eyecup: GA
2/6	*Photostomias guernei*	8.3cm TL	right eye: GA left eye: DEXTRITC; cult 2d, 4°, PA, nsg brain: nn. I & II DEXTRITC; c 2d, 4°, PA
2/7	*Chauliodus sloani*	21.5cm TL	right eye: PA; left opt. nerve: GA left eye: DEXTRITC; culture 3d, 4°, PA brain:?
2/8	*Echiostoma barbatum*	28 cm TL	right eye: PA; 2optic nerves: GA left eye: DEXTRITC; cult. 3d, 4°, PA, g brain kaputt

Station F3: 4.6. 1999, 8.20-11.20, local time
Location: 32° 8,91' N, 160° 2,01'W
Rope length: 1,400m; Speed in water: 2Kn; water depth: 5795m

3/1	*Gonostoma gracile*	13cm TL	left eye: PA right eye: DEXTRITC; cult 3d, 4°, PA brain: nn. I & II DEXTRITC; c 3d, 4°, PA
3/2	*Gonostoma gracile*	11.1cm TL	left eye: GA right eye: DEXTRITC; cult 3d, 4°, PA brain: nn. I & II DEXTRITC; c 3d, 4°, PA
3/3	"rattail", juv	13.5cm TL	left eye: PA; right eye: GA totally pickled in PA for ID
3/4	*Porometra crassiceps*	13cm TL	right eye: DEXTRITC; cult 3d, 4°, PA
3/5	*Sternoptyx diaphana*		three specimens fixed total
3/6	*Cyclothone pallida*		several specimens fixed total GA
3/7	*Cyclothone pallida*		several specimens fixed total PA

Station F4: 5.6. 1999, 12.15-15.15 local time
Location: 32° 8,19' N, 163° 0,79'W
Rope length: 1,000m; Speed in water: 2Kn; water depth: 3960m

4/1	*Chauliodus sloani*	14cm TL	left eye: DEXTRITC, cult 2.5d 4°, PA brain GA, right eye PA
4/2	*Aristostomias tittmanni*	10cm TL	eyes: Ron, brain
4/3	*Stylephorus chordatus*	18cm TL	r eye, brain DEXTRITC, cult 2.5d 4°, PA left eye: PA
4/4	*Idiocanthus* larvae		total: PA
4/5	*Stylephorus chordatus*	11cm TL	l eye, brain I, II DEXTRITC, 2.5d 4°, PA right eye: PA
4/6	*Evermanella indica*	6cm TL	l eye, brain I, II DEXTRITC, 2.5d 4°, PA right tube eye: PA; o.n. GA

4/7	*Opisthoproctus soleatus*	12.5cm TL	brain I, II DEXTRITC, 3.5d 4°, PA; eyes: Ron; opt. nerve: GA
4/8	*Opisthoptoctus soleatus*	12.5cm TL	r eye, brain I, II DEXTRITC, 3.5d 4°, PA left tube eye: PA; 2 opt. n. GA
4/9	*Scopelarchus analis, juv.*	4.5cm TL	r eye, brain I, II DEXTRITC, 2.5d 4°, PA left eye: PA; opt. nerve:GA
4/10	rattail, juv.	5.5cm TL	total PA; eyes bashed>Nigel for ID
4/11	*Gonostoma gracile*	15.5cm TL	2 eyes, brain I,II DEXTRITC, 2.5d 4°, PA
4/12	*Lampanyctus macropterus*	13.5cm TL	2 eyes, brain I,II DEXTRITC, 2.5d 4°, PA optic nerve: GA
4/13	*Lampanyctus macropterus*	11.0cm TL	left eye:PA; right eye: GA; brain: PA

Station F5: 6./7.6. 1999, 22.45-1.45 local time
Location: 32° 18.751' N, 162° 5.806'W
Rope length: 500m; Speed in water: 2Kn

Only four fish caught; all processed by Ron Douglas for visual pigments.

Station F6: 7.6. 1999, 12.15-15.15 local time
GPS latitude: 32° 17.33' N, longitude 162° 1.82'W
Rope length: 1,200m; Speed in water: 2Kn; water depth: 4145m

6/1	*Chauliodus sloani*	11.5cm TL	2 eyes, brain I,II DEXTRITC, 2.5d 4°, PA
6/2	*Aristostomias scintillans*	4.7cm TL	r eye, brain I, II DEXTRITC, 2.5d 4°, PA left eye: GA
6/3	*Aristostomias scintillans*	4.7cm TL	r eye, brain I, II DEXTRITC, 2.5d 4°, PA left eye:
6/4	*Gonostoma gracile*	12.3cm TL	l eye, brain I DEXTRITC, 2.5d 4°, PA right eye: PA
6/5	*Chauliodus sloani*	27.5cm TL	brain I, II DEXTRITC, 2.5d 4°, PA both eyes: Ron
6/6	*Nemighthys curvirostris*	28cm TL	head total: PA
6/7	*Nemighthys curvirostris*	28cm TL	head total: GA (NB. asymmetrical eyes!!)
6/8	*Idiocanthus fasciola*	21cm TL	l eye, brain I DEXTRITC, 2.5d 4°, PA right eye: PA
6/9	*Idiocanthus fasciola*	20.5cm TL	2 eyes, brain I DEXTRITC, 2.5d 4°, PA
6/10	*Idiocanthus fasciola*	11.9cm TL	l eye, brain: PA; r. eye & barbel: GA
6/11	*Cerateas holboelli* (angler)	7.5cm TL	l eye, brain: PA; r. eye: GA
6/12	rattail	16cm TL	total: PA
6/13	*Idiocanthus fasciola*	17.5 TL	head total: PA

6/14	*Melanostomias tentaculatus*	8.5cm TL	head total: PA
6/15	*Melanostomias tentaculatus*	7.0cm TL	head total: GA

Station F7: 8.6. 1999, 6.05-9.05 local time
Location: 32° 13,05' N, longitude 161° 3,94'W
Rope length: 1,500m; Speed in water: 2Kn; water depth: 5865m

7/1	*Gonostoma gracile*	14.cm TL	l eye, brain I DEXTRITC, 1d 4°, PA right eye: PA
7/2	*Pseudoscopelus altipinnis*	14cm TL	l eye, brain I DEXTRITC, 2.5d 4°, PA right eye: PA
7/3	*Anoplogaster cornuta*	18cm TL	l eye, brain I DEXTRITC, 2.5d 4°, PA right eye: PA; left N. o. GA
7/4	*Nemichthys curvirostris*	74cm TL	r eye, brain I DEXTRITC, 2.5d 4°, PA left eye: PA
7/5	*Gonostoma gracile*	12.5.cm TL	r eye, brain I DEXTRITC, 1d 4°, PA left eye: PA
7/6	*Gonostoma gracile*	12.5cm TL	head total: GA
7/7	*Gonostoma gracile*	12.5cm TL	head total: GA
7/8	*Gonostoma gracile*	12.5cm TL	head total: GA
7/9	*Gonostoma gracile*	12.5cm TL	head total: GA
7/10	*Gonostoma gracile*	12.5cm TL	head total: GA
7/11	*Gonostoma gracile*	12.5cm TL	head total: GA
7/12	*Gonostoma gracile*	12.5cm TL	head total: GA
7/13	*Gonostoma gracile*	12.5cm TL	head total: GA
7/14	*Gonostoma gracile*	12.5cm TL	head total: PA
7/15	*Gonostoma gracile*	12.5cm TL	head total: PA
7/16	*Gonostoma gracile*	12.5cm TL	head total: PA
7/17	*Gonostoma gracile*	12.5cm TL	head total: PA
7/18	*Gonostoma gracile*	12.5cm TL	head total: PA
7/19	*Gonostoma gracile*	12.5cm TL	head total: PA
7/20	*Gonostoma gracile*	12.5cm TL	head total: PA
7/21	*Gonostoma gracile*	12.5cm TL	head total: PA
7/22	*Gonostoma gracile*	12.5cm TL	head total: PA
7/23	*Gonostoma gracile*	12.5cm TL	head total: PA
7/24	*Gonostoma gracile*	12.5cm TL	head total: PA
7/25	*Gonostoma gracile*	12.5cm TL	head total: PA
7/26	*Gonostoma gracile*	12.5cm TL	head total: PA
7/27	*Gonostoma gracile*	12.5cm TL	head total: PA
7/28	*Gonostoma gracile*	12.5cm TL	head total: PA
7/29	*Gonostoma gracile*	12.5cm TL	head total: PA
7/30	*Gonostoma gracile*	12.5cm TL	head total: PA
7/31	*Poromitra megalops*	10cm TL	left eye GA: brain GA; r eye: PA
7/32	*Poromitra megalops*	10cm TL	2 eyes, brain DEXTRITC, 2d ,4°, PA
7/33	*Poromitra megalops*	10cm TL	head total: PA

Station F8: 8.6. 1999, 6.05-9.05 local time
Location: 32° 12.94' N, 160° 2.96'W
Rope length: 1,300m; Speed in water: 2Kn; water depth: 5390m

8/1	*Scopelarchus michaelsarsi*	14.2cm SL	l eye, brain I DEXTRITC, 2.5d 4°, PA right eye: PA; 2 opt. nerves: GA
8/2	*Benthalbella infans*	15.3cm SL	l eye, brain I DEXTRITC, 2.5d 4°, PA right eye: PA; 2 opt. nerves: GA
8/3	*Anoplogaster cornuta*	11.5cm TL	l eye, brain I DEXTRITC, 2.5d 4°, PA right eye: PA; 2 opt. nerves: GA
8/4	*Gonostoma gracile*	13.5cm TL	l eye, brain I DEXTRITC, 2.5d 4°, PA right eye: PA, dorsal incision
8/5	rattail	17cm TL	l eye, brain I DEXTRITC, 2.5d 4°, PA right eye: PA; 2 opt. nerves: GA
8/6	*Sternoptyx pseudodiaphana*	7.3cm SL	l eye: PA; r eye: GA; brain: GA
8/7	rattail	16cm TL	right eye: PA: left eye kaputt; brain: PA
8/8	rattail	16cm TL	right eye: PA: left eye: GA; brain: GA
8/9	rattail	9cm TL	head total: PA
8/10	*Poromitra megalops*	11cm TL	right eye: PA; left eye: GA: brain: GA

Station F9: 11.6. 1999, 13.30-16.30 local time
Location: 32° 29,92' N, 160° 12,75'W
Rope length: 1,300m; Speed in water: 2Kn; water depth: 5900m

9/1	*Gonostoma gracile*	12.5cm SL	3 eyecups & 3 isol. ret. strips LY 15h PA
9/2	*Sternoptyx pseudodiaphana*	2.4cm SL	r eye, brain I: DEXTRITC, 2d, 4°, PA, l eye: PA
9/3	*Sternoptyx pseudodiaphana*	2.5cm SL	whole head: GA
9/4	*Sternoptyx pseudodiaphana*	5.5cm SL	l eye: PA, DiI; r eye: PA,dors; brain: PA; l opt. nerve, GA; r. opt. n. GA after cult.
9/5	*Idiocanthus fasciola*	41cm SL	r eye, brain I: DEXTRITC, 2d, 4°, PA l eye: PA, dors. nick
9/6	*Anoplogaster cornuta*	16cm TL	r eye, brain I: DEXTRITC, 2d, 4°, PA l eye: PA, dors. nick: r. opt. n.: GA
9/7	*Lampanyctus macropterus*	11.7cm SL	l eye, brain I: DEXTRITC, 2d, 4°, PA r eye: PA, dors. nick
9/8	*Poromitra megalops*	8cm SL	r eye, dors.nick PA; l eye dors. nick PA; brain:PA
9/9	*Poromitra megalops*	7.5cm SL	total head: GA

Station F10: 12.6. 1999, 0.30-3.30 local time
Location: 32° 15,09' N, 159° 26.13'W
Rope length: 300m; Speed in water: 2Kn; water depth: 5900m

10/1	*Leptocephalus* larva	61cm SL	total head: PA, developing tube eyes!

10/2	*Vincinguerria nimbaria*	3.2cm TL	total head: PA
10/3	*Vincinguerria nimbaria*	3.4cm TL	total head: GA
10/4	*Vincinguerria nimbaria*	3.3cm TL	total head: PA
10/5	*Vincinguerria nimbaria*	3.5cm TL	total head: PA; r eye, brain I, II: DiI
10/6	*Benthalbella infans*	4.8cm SL	total head GA
10/7	*Benthalbella infans*	5.4cm SL	total head PA; r eye, brain I, II: DiI

Station F11: 12.6. 1999, 12.05-15.05 local time
Location: 32° 18,50' N, 159° 28,67'W
Rope length: 1200m; Speed in water: 2Kn; water depth: 3546m

11/1	*Gonostoma gracile*	13cm SL	4 isol. ret strips LY 15h, 15h cult med, PA
11/2	*Malacosteus niger*	13.4cm SL	brain PA; eyes: Ron
11/3	*Heterophotus sp.*	26.5cm SL	l eye, brain I: DEXTRITC, 2d, 4°, PA, r eye: PA; dors. inc.
11/4	*Lampanyctus macropterus*	10cm SL	2 isol. ret strips LY 15h, 15h cult med, PA
11/5	rattail	14.3cm TL	r eye, brain I: DEXTRITC, 2d, 4°, PA, l eye: PA
11/6	*Gonostoma gracile*	12.5cm SL	r.eye, l.eye, brain I, II PA-DiI
11/7	rattail	8.3cm TL	total head: GA
11/8	*Sternoptyx pseudodiaphana*	3.8cm SL	r.eye, l.eye (dors.inc.), brain, I, II PA-DiI
11/9	*Sternoptyx pseudodiaphana*	2.6cm SL	whole head: GA
11/10	*Sternoptyx pseudodiaphana*	2.5cm SL	whol head PA
11/11	rattail	10cm TL	whole head PA
11/12	*Gonostoma gracile*	12.5cm SL	r.eye, l.eye, (dors.inc.) brain.I: DiI
11/13	*Poromitra megalops*	5cm SL	total head: PA
11/14	*Poromitra megalops*	5cm SL	total head: GA

Station F12: 13.6. 1999, 12.35-15.35 local time
location: 29° 16,37' N, 160° 21,62'W
Rope length: 1000m; Speed in water: 2Kn; water depth: 5952m

12/1	*Chauliodus sloani*	10.2cm SL	head total: PA; n.I,II: DiI eyes and brain in situ
12/2	*Chauliodus sloani*	12.0cm SL	head total: PA; n.I: DiI
12/3	*Chauliodus sloani*	11.1cm SL	head total: PA
12/4	*Chauliodus sloani*	13.5cm SL	brain, II; r eye, l eye: DiI
12/5	*Chauliodus sloani*	10.0cm SL	brain, II; r eye, l eye: DiI
12/6	*Chauliodus sloani*	8.2cm SL	head total: PA

12/7	*Gonostoma gracile*	11.6cm SL	head: brain, n.I.:DiI
12/8	*Gonostoma gracile*	11.1cm SL	brain, II; r eye, l eye: DiI
12/9	*Nemichthyes curvirostris*	62.8cm TL	brain, n.II DiI, eyes: Ron
12/10	*Nemichthyes curvirostris*	40.28cm TL	brain, n.I&II, r eye, DiI
12/11	*Eustomias sp.*	4.2cm TL	total head PA
12/12	*Scopelarchus michaelsarsi*	4.5cm SL	brain, II; r eye, l eye: DiI
12/13	*Sternoptyx pseudodiaphana*	2.7cm SL	total head: PA
12/13	*Sternoptyx pseudodiaphana*	2.0cm SL	total head: PA
12/14	*Sternoptyx pseudodiaphana*	2.0cm SL	total head: PA

Station F13: 14.6. 1999, 1.20-4.20 local time
location: 29° 20,73' N, 160° 20,70'W
Rope length: 200m; Speed in water: 2Kn; water depth: 5237m

13/1	*Myctophid sp.*	4.3cm SL	4 isol. rets. Strips, LY cultured
13/2	*Pteraclis carolinus*	2.9cm SL	total PA
13/3	*Vincinguerria nimbaria*	3.4cm SL	head, PA
13/4	*Vincinguerria nimbaria*	3.5cm SL	head, PA
13/5	*Vincinguerria nimbaria*	2.8cm SL	head, PA
13/6	*Bregmacerops sp.*	2.6cm SL	total, PA
13/7	*Vincinguerria nimbaria*	3.7cm SL	head, PA
13/8	*Astronesthes sp.*	3.8cm SL	total PA

Station F14: 16. 6. 1999, 21.45-0.45 local time
location: 25° 44,02' N, 160° 17,52'W
Rope length: 1000m; Speed in water: 2Kn; water depth: 3592m

14/1	*Opisthoproctus soleatus*	9.7cm SL	right eye: PA: brain, l.eye in situ, I, II DiI
14/2	Leptocephalus larva; speckled,	10cm SL	head total ,PA
14/3	*Avocetina infans* (?)	68cm SL	brain, PA: DiI: eyes: Ron
14/4	*Pachystomias microdon*	23.5cm SL(!)	brain PA: DiI: eyes: Ron: o.n. GA
14/5	*Ceratoscopelus warmingii*	5.3cm SL	head total
14/6	exocoetid	4.8cm SL	total

14/7	assorted larvae RMT1	5mmSL	total

Station F15: 17. 6. 1999, 14.20-17.20 local time
location: 26° 54,157' N, 160° 17,53'W
Rope length: 2000m; Speed in water: 2Kn; water depth: 5032m

15/1	*Ceratoscopelus warmingii* (myctophid)	4.2cm SL	head total, PA, DiI I II, l eye isol DiI, ventr. inc.; opt. n.GA
15/2	*Ceratoscopelus warmingii*	4.6cm SL	4 isol ret strips; LY
15/3	*Ceratoscopelus warmingii*	4.2cm SL	head total PA; DiI, I.II l eye isol, dors. inc.; opt. n.GA
15/4	*Ceratoscopelus warmingii*	4.5cm SL	head total PA
15/5	*Chauliodus sloani*	19.6cm	head PA; DiI, I, II l eye isol DiI, dors. inc.; opt. n.GA
15/6	*Gonostoma gracile*	12.1cm SL	head PA; DiI, I, II l eye isol, dors. inc.; opt. n.GA
15/7	*Cyema atrum*	19.8cm SL	head PA; DiI, I, II l eye isol, dors. inc.; opt. n.GA
15/8	*Paralepis sp.*	4.8cm SL	total PA
15/9	*Bregmaceros sp.*	3.9cm SL	total PA
15/10	*Bathyphilus sp.*	7.8cm SL	head total PA

Station F16: 18. 6. 1999, 5.00-8.00 local time
location: 26° 34,06' N, 160° 42,42'W
Rope length: 1200m; Speed in water: 2Kn; water depth: 3495m

16/1	*Poromitra megalops*	10.6cm SL	2 isol ret. strips LY; brain PA; I, II DiI
16/2	*Poromitra megalops*	9.6cm SL	brain PA; I, II DiI; l eye GA
16/3	*Dolipichthys sp.*, angler	1.8cm SL	total PA
16/4	*Canthigaster rostrata* (?) puffer	1.5cm SL	total PA
16/5	*Sternoptyx pseudodiaphana*	3.7cm SL	head total: GA; photophores: GA
16/6	*Sternoptyx pseudodiaphana*	2.6cm SL	head total: GA
16/7	*Sternoptyx pseudodiaphana*	1.8cm SL	head total: GA; photophores:GA
16/8	*Sternoptyx pseudodiaphana*	3.6cm SL	head total: PA; DiI; l.eye, d.n. PA
6/9	*Sternoptyx pseudodiaphana*	3.4cm SL	head total: PA
16/10	*Eustomias sp.*	14.9cm SL	head total, PA
16/11	*Ceratoscopelus warmingii*	4.5cm SL	head total GA
16/12	*Ceratoscopelus warmingii*	4.1cm SL	head total GA
16/13	*Ceratoscopelus warmingii*	3.8cm SL	head total PA
16/14	*Ceratoscopelus warmingii*	3.9cm SL	head total PA
16/15	*Alepisaurus ferox* (no deep-sea)	8.2cm SL	total

Station F17: 18. 6. 1999, 14.05-17.05 local time
location: 26° 33.69' N, 160° 10.44'W
Rope length: 1000m; Speed in water: 2Kn; water depth: 4274m

17/1	rattail	ca. 20cmTL	total head PA; eyes bashed
17/2	*Gigantura vorax* (!!)	8.8cm SL	head PA; DiI: I, II; r.eye: Ron
17/3	*Ceratias holboelli* (angler)	8.1cm TL	head PA; DiI II, V!!
17/4	*Sternoptyx pseudodiaphana*	2-12mm TL	various sizes; 10 specs; 3 vials PA
17/5	*Evermanella indica*	4.1cm SL	head total PA; l.eye DiI, brain I.II DiI; l.n.o. GA, tiny
17/6	*Evermanella indica*	2.6cm SL	total PA
17/7	*Serrivomer beani* (?)	32.6cm SL	head total PA, no brain; nn I & II ok
17/8	*Gonostoma gracile*	11.8cm SL	l.eye, d.n. DiI: brain I, II DiI, l.o.n. GA
17/9	*Howella sherboni*	2.0cm SL	total PA
17/10	*Bathophilus metallicus*	7.8cm SL	l. eye, brain, I, II: DiI, PA
17/11	*Thysanactis deutex*	8.3cm SL	l. eye, brain I, II DiI; PA
17/12	*Thysanactis deutex*	5.9cm SL	head total PA
17/13	*Idiocanthus fasciola*	16.8cm SL	r. eye, brain, I.II DiI; PA
17/14	*Idiocanthus fasciola*	12.1cm SL	head total PA

Station F18: 19. 6. 1999, 3.15-6.15 local time
location: 26° 34,26' N, 160° 11,92'W
Rope length: 800m; Speed in water: 2Kn; water depth: 4277m

18/1	*Opisthoproctus soleatus* baby,	1.2cm SL	total PA
18/2	*Scopelarchus analis*	3.9cm SL	total PA
18/3	*Ceratoscopelus warmingii*	4.8cm SL	head total PA
18/4	*Eustomias braueri* (?)	5.5cm SL	head total PA

Station F19: 20. 6. 1999, 12.15-15.15 local time
location: 26° 35.60' N, 159° 29.84'W
Rope length: 1200m; Speed in water: 2Kn; water depth: 4277m

19/1	*Sternoptyx pseudodiaphana*	5.4cm SL	2 retinae isol. LY cult.10h; PA, nsg?

19/2	*Stylephorus chordatus*	10.2cm SL	brain. I. II: DiI; eyes gone. PA
19/3	*Gonostoma gracile*	13cm SL	2 eyes. brain I.II DEXTRITC isol.rets. ok; 2 n. opt. GA
19/4	*Idocanthus fasciola*	22.2cm SL	l. eye. brain I.II DiI. PA
19/5	*Bregmacerops sp*	4.8cm SL	total, PA
19/6	*Bregmacerops sp*	4.6 cm SL	total, PA
19/7	*Bregmacerops sp*	4.5 cm SL	total, PA
19/8	*Bregmacerops sp*	4.7 cm SL	total, PA
19/9	Chiasmodont	4.1cm SL	total, PA
19/10	Leptocephalus angustifol.	14cm SL	head, PA
19/11	*Serrivomer beani*	25.2cm SL	head total PA
19/12	*Serrivomer beani*	34cm SL	l. eye. brain I. II DiI
19/13	*Valencinellus tripunctulatus*	2.9cm SL	total PA
19/14	*Sternoptyx pseudodiaphana*	4.2cm SL	l. eye. brain I, II DiI PA
19/15	*Sternoptyx pseudodiaphana*	4.0cm SL	head total PA

Station F20: 22. 6. 1999, 21.45-23.45 local time
location: 25° 40,75' N, 158° 48,32'W
Rope length: 600m; Speed in water: 2Kn; water depth: 4996m

20/1	*Gonostoma elongatum*	24.5cm SL	l.eye: LY, 7h cult. R. opt n. GA r.eye; brain I. II DEXTRITC, PA
20/2	*Gonostoma elongatum*	16.8cm SL	r. eye, brain, I, II DiI, PA
20/3	*Argyropelecus olfersi*	4.5cm SL	r. eye, brain, I II, DiI, PA
20/4	Leptocephalus	>7cm SL	total; develop. Tube eyes?
20/5	*Gonostoma ebelingli*	15.5cm SL	r. eye. brain I. II. DiI. PA
20/6	*Valencinellus tripunctulatus*	3.1cm SL	total PA
20/7	*Gonostoma ebelingli*	15.2cm SL	r. eye. brain, I, II, DiI. GA, olf.!!
20/8	*Bathylagus bericoides*	14.2cm SL	l eye, ventr.nick. DiI; brain: I, II DiI. PA retina with 2 vis. pigments: cones???

Station F21: 23. 6. 1999, 16.00-19.00 local time
location: 26° 59,82' N, 158° 45,61'W
Rope length: 1100m; Speed in water: 2Kn; water depth: 5205m

21/1	*Gigantura vorax*	9.7cm TL	left eye. brain I. II DiI. PA

21/2	*Stylephorus chordatus*	31.9cm SL	r ret. isol; l. eye& brain I, II, DiI, in situ
21/3	*Gonostoma elongatum*	21.2cm SL	r.eye LY; l.eye, brain PA
21/4	*Gonostoma elongatum*	19.8cm SL	l. eye, brain, I, II: DiI PA
21/5	*Gonostoma ebelingli*	11.2cm SL	r. eye, brain, I, II DiI PA
21/6	*Echiostoma barbatum*	25.5cm SL	brain: I, II DiI, PA; eyes: Ron
21/7	*Serrivomer beani*	38.7cm SL	l.eye, brain, I, II: DiI PA in situ
21/8	*Serrivomer beani*	32.6cm SL	head PA
21/9	*Serrivomer beani*	31.9cm SL	head GA
21/10	*Idiocanthus fasciola*	12.3cm SL	head: GA
21/11	*Eustomias braueri* (?)	7.0cm SL	head GA
21/12	*Eustomias obscura*	11.1cm SL	head PA
21/13	*Photostomias guerni*	7.3cm SL	l. eye, brain, I, II: DiI PA
21/14	*Photostomias guerni*	7.2cm SL	head GA
21/15	*Photostomias guerni*	8.4cm SL	head PA
21/16	*Photostomias guerni*	7.6cm SL	head PA
21/17	larval angler	2.7cm SL	total PA

The identification of several of the above specimens is tentative and subject to confirmation by Dr. Nigel Merret (Brit. Museum of Natural History, London) through reference specimens taken by Dr. Ron Douglas

Paraformaldehyde (PA)-fixed retinae: Immunochytochemistry of terminal nerve system (GnRH); wholemount and cresyl violet stain

1. Labelling of primary afferents with Rhodamine-coupled dextranes (DEXTRITC)
All DEXTRITC retinae to be wholemounted in Tübingen; possibly remove opt. nerve for electron microscopic (EM) axon counts after glutaraldehyde (GA) fixation before mounting.

Brains: DEXTRITC material: first study olfactory system: localise olf. bulb and mucosa. isolate bulb for count of projection neurons (labelled); isolate olf. nerves (where possible) and olf. tract for EM axon counts; ID of remaining cranial nerves: octavolateral; gustatory for isolation, osmication plastic embedding, sectioning and EM analysis (Shaun?)

2. Labelling of primary afferents with DiI
DiI applied to freshly PA-fixed olfactory and optic nerves. Transport by diffusion in lipophilic membranes over weeks in formaldehyde. Wholemount retinae; section olf. bulb to count projection neurons.

The number of efferent fibres in the olfactory (nerve) tract and optic nerve is determined by subtracting the number of labelled projection neurons in each case (mitral and tufted cells, ret. ganglion cells) from the total axon count in each nerve.

Appendix 9.6

Captains Report

RF Reedereigemeinschaft
Forschungsschiffahrt GmbH

FS SONNE
SO 142

Stationsprotokoll F.S. "S O N N E" Reise SO 142

Gebrauchtes Instrumentarium		Anzahl der Einsätze
RMT	Rectangular Midwater Trawl	21
CTD	Kranzwasserschöpfer mit CTD-Sensoren	1
DR	Dredge (Kettensack)	13
OBH	Ocean Bottom Hydrophon	47
GTVA	Fernsehgreifer (Typ A)	3
HS/PS/MAG		2432 sm
HS/PS		32
Seismik/HS/PS		373 sm

Eingesetzte Winden:

Winde			RF-Nr.	SO 142 Einsatz	Gesamt Einsatz	SO 142 S`länge	gefierte max.Sl	Gesamt S`länge	Zust
W 1	LWL	18,2	816233	011 h	0011 h	013907 m	5370 m	013907	2
W 2	LWL	18,2	865017	000 h	1327 h	000000 m	6390 m	834249	4
W 4	NSW	11,0	817141	005 h	0103 h	005000 m	5000 m	092449	3
W 5	NSW	11,0	817164	000 h	0000 h	000000 m	0000 m	217297	1
W 6	Drako	18,2	814150	182 h	0444 h	103418 m	6350 m	343408	2

Geräteverluste : keine

Abkürzungen im Stationsprotokoll:

z.W.	zu Wasser
a.D.	an Deck
Boko	Bodenkontakt
Bosi	Bodensicht
Slmax.	Seillänge
LT	Lottiefe nach Hydrosweep
W x	eingesetzte Winde
HS	Hydrosweep
PS	Parasound

Zeit : UTC - 11 Stunden

31.05.1999

Teststation W6

1300	Beginn Station	LT = 5300 m	29-15.62N 173-21.48W
1301	Rosette m. 8 Releaser z/W		
1306	SL 10 m Rosette m. 4 Releaser z/W		
1424	Slmax 5100 m		
1425	Release Comm.; keine Antwort		
1447	Hydrophon z/W		
1702	Rosetten m. Releaser a/D; Ende Station		

01.06.1999

Station F1 RMT W6

0948	Beginn Station	LT = 5525 m	30-16.99N 169-56.57W

0958	RMT z/W	LT = 5528 m	30-17.02N 169-56.85W
	V = 2.0Kn Kurs 071°		
1032	SLmax 1000 m		
1327	RMT a/D		30-19.13N 169-49.46W
1328	Ende Station		

Teststation W6

1345	Beginn Station	LT = 5523 m	30-19.13N 169-49.46W
1347	Rosette m. 8 Releaser z/W		
1350	SL 10 m Rosette m. 4 Releaser z/W		
1508	Sl 5300 m		
1510	Release Comm., keine Antwort		
1533	Slmax 5400 m		
1739	Rosetten m. Releaser a/D; Ende Station		

02.06.1999

Station F2 RMT W6

0842	Beginn Station	LT = 5776 m	31-13.89N 166-44.19W
0845	RMT z/W	LT = 5773 m	31-13.89N 166-44.14W
	V = 2.0Kn Kurs 160°		
0923	SLmax 1200 m		
1217	RMT a/D		31-08.36N 166-40.25W
1218	Ende Station		

Teststation W6

1322	Beginn Station	LT = 5663 m	31-15.53N 166-30.26W
1324	Rosette m. 8 Releaser z/W		
1327	SL 10 m Rosette m. 3 Releaser und Pinger z/W		
1327	Hydrophon z/W		
1444	SL 5500 m		
1445	Release Comm.		
1505	Slmax 5568 m		
1715	Rosette m. Releaser a/D; Ende Station		

Station CTD 1 W4

1726	Beginn Station	LT = 5623 m	31-14.35N 166-30.98W
1729	CTD/ROS z/W		
1937	SLmax 5000 m	LT = 5638 m	31-14.41N 166-31.25W
2231	CTD a/D		
2232	Ende Station		

2240	Magnetometer z/W		

Profil 101 (HS/PS/MAG)

2246	Beginn Profil		31-15.44N 166-30.69W

03.06.1999

0626	Ende Profil	71 sm	31-45.00N 165-00.00W

RF Reedereigemeinschaft
Forschungsschiffahrt GmbH

FS SONNE
SO 142

Profil 102 (HS/PS/MAG)			
0626	Beginn Profil		31-45.00N 165-00.00W
1150	Ende Profil	61 sm	32-19.00N 164-00.00W
Profil 103 (HS/PS/MAG)			
1150	Beginn Profil		32-19.00N 164-00.00W
1957	Ende Profil	86 sm	31-39.00N 162-28.00W
Profil 104 (HS/PS/MAG)			
1957	Beginn Profil		31-39-00N 162-28.00W
04.06.1999			
0203	Ende Profil	92 sm	32-26.00N 161-25.00W
Profil 105 (HS/PS/MAG)			
0203	Beginn Profil		32-26.00N 161-25.00W
0626	Ende Profil	49 sm	32-08.90N 160-32.40W
Profil 106 (HS/PS/MAG)			
0626	Beginn Profil		32-08.90N 160-32.40W
0808	Ende Profil	20 sm	32-08.90N 160-08.20W
0818	Magnetometer a/D		
Station F3 RMT W6			
0823	Beginn Station	LT = 5684 m	32-08.81N 160-06.87W
0829	RMT z/W	LT = 5685 m	32-08.79N 160-06.71W
	V = 2.0Kn Kurs 090°		
0912	SLmax 1400 m		
1214	RMT a/D		32-08.94N 159-58.10W
1215	Ende Station		
Teststation W6			
1232	Beginn Station	LT = 5821 m	32-10.45N 159-58.00W
1233	Rosette m. 8 Releaser z/W		
1242	SLmax 500 m		
1257	Rosette a/D, Ende Station		
1300	Magnetometer z/W		
Profil 107 (HS/PS/MAG)			
1318	Beginn Profil		32-13.23N 159-57.55W
1645	Ende Profil	42 sm	32-21.55N 159-17.21W
Profil 108 (HS/PS/MAG)			
1645	Beginn Profil		32-21.55N 159-17.21W

05.06.1999

1200	Ende Profil 224 sm		32-08.44N 163-03.46W
1208	Magnetometer a/D		
Station F4 RMT W6			
1213	Beginn Station	LT = 4534 m	32-08.34N 163-02.67W
1218	RMT z/W	LT = 4530 m	32-08.30N 163-02.58W
	V = 2.0 Kn Kurs 090°		
1249	SLmax 1000 m		
1546	RMT a/D		32-08.16N 162-55.00W
1547	Ende Station		
Teststation W6			
1611	Beginn Station	LT = 2795 m	32-10.44N 162-54.76W
1612	Rosette m. 7 Relaeser z/W		
1621	SLmax 500 m		
1637	Rosette a/D, Ende Station		
Station G1 DR W6			
1815	Beginn Station	LT = 3836 m	32-19.56N 163-06.03W
1816	DR z/W		
1932	Boko SL 3850 m	LT = 3827 m	32-19.54N 163-06.01W
2020	Slmax 4100 m	LT = 3593 m	32-18.91N 163-05.87W
2258	DR a/D		
2301	Ende Station		
2314	Magnetometer z/W		
Profil 109 (HS/PS/MAG)			
2315	Beginn Profil		32-17.67N 163-07.14W

06.06.1999

0445	Ende Profil 64 sm		32-29.44N 162-17.99W
0457	Magnetometer a/D		
0509	OBH # 1 abgetaucht	LT = 5307 m	32-30.04N 162-17.98W
0532	OBH # 2 abgetaucht	LT = 5252 m	32-29.28N 162-17.19W
0609	OBH # 3 abgetaucht	LT = 5594 m	32-25.60N 162-13 07W
0625	OBH # 4 abgetaucht	LT = 5601 m	32-25.11N 162-12.50W
0719	OBH # 5 abgetaucht	LT = 4027 m	32-19.29N 162-06.00W
0730	OBH # 6 abgetaucht	LT = 4032 m	32-18.73N 162-05.35W
0819	Stb-Airgun z/W		
0829	Versorgungsleitungen z/W		

RF Reedereigemeinschaft
Forschungsschiffahrt GmbH

FS SONNE
SO 142

Profil S 1 (Seismik/HS/PS)

0902	Beginn Profil		32-14.72N 162-00.55W
1554	Ende Profil	26 sm	32-33.95N 162-21.88W
1559	Stb-Airgun/Versorgungsleitungen a/D		
1649	Release Command OBH #1/#2		
1720	OBH # 2 gesichtet		
1747	OBH # 2 a/D		32-29.11N 162-17 01W
1733	OBH #1 gesichtet		
1813	OBH # 1 a/D		32-29.75N 162-17.85W
1854	Release Command OBH #3/#4		
1946	OBH # 3 gesichtet		
2009	OBH # 3 a/D		32-25.68N 162-13.36W
1946	OBH # 4 gesichtet		
2030	OBH # 4 a/D		32-25.28N 162-12.85W
2105/2116	Release Command OBH #5/#6		
2157	OBH # 5/OBH #6 gesichtet		
2214	OBH # 5 a/D		32-19.42N 162-06.08W
2232	OBH # 6 a/D		32-19.05N 162-05.50W

Station F5 RMT W6

2240	Beginn Station	LT = 3973 m	32-18.97N 162-05.62W
2245	RMT z/W	LT = 3970 m	32-18.90N 162-05.69W
	V = 2.0Kn Kurs 210°		
2310	SLmax 500 m		

07.06.1999

0141	RMT a/D		32-14.91N 162-08.08W
0142	Ende Station		

Profil 110 (HS/PS)

0141	Beginn Profil		32-14.91N 162-08.08W
0330	Ende Profil	19 sm	32-20.86N 162-04.97W

Station G2 DR W6

0351	Beginn Station	LT = 5274 m	32-21.88N 162-05.00W
0353	DR z/W		
0530	Boko SL 5263 m	LT = 4221 m	32-21.68N 162-04.99W
0737	Slmax 5400 m	LT = 4857 m	32-20.55N 162-04.96W
1130	DR a/D		
1132	Ende Station		

Station F6 RMT W6

1213	Beginn Station	LT = 4900 m	32-17.52N 162-02.14W
1220	RMT z/W	LT = 4895 m	32-17.50N 162-02.08W
	V = 2.0Kn Kurs 130°/090°		
1259	Slmax 1200 m		
1555	RMT a/D		32-15.00N 161-55.39W

1556	Ende Station		
1559	Magnetometer z/W		
Profil 111 (HS/PS/MAG)			
1559	Beginn Profil		32-15.01N 161-55.15W
2043	Ende Profil 51 sm		32-13.00N 161-08.00W
2057	Magnetometer a/D		
Station G3 DR W6			
2106	Beginn Station	LT = 5586 m	32-14.24N 161-07.25W
2114	DR z/W		
2303	Boko SL 5627 m	LT = 5610 m	32-14.28N 161-07.21W
2351	Slmax 5900 m	LT = 5431 m	32-14.68N 161-07.56W

08.06.1999

0536	DR a/D		
0538	Ende Station		
Station F7 RMT W6			
0607	Beginn Station	LT = 5587 m	32-14.59N 161-06.96W
0613	RMT z/W	LT = 5595 m	32-14.55N 161-07.00W
	V = 2.0Kn Kurs 238°/090°		
0701	Slmax 1500 m		
0955	RMT a/D		32-12.99N 161-01.65W
0956	Ende Station		
1009	Magnetometer z/W		
Profil 112 (HS/PS/MAG)			
1009	Beginn Profil		32-12.95N 161-00.38W
1356	Ende Profil 46 sm		32-13.00N 160-08.97W
1405	Magnetometer a/D		
Station F8 RMT W6			
1407	Beginn Station	LT = 5125.m	32-12.00N 160-07.73W
1415	RMT z/W	LT = 5120 m	32-11.99N 160-07.71W
	V = 2.0Kn Kurs 090°		
1456	Slmax 1300 m		
1758	RMT a/D		32-12.94N 159-59.65W
1759	Ende Station		
Station G4 DR W6			
1836	Beginn Station	LT = 5169 m	32-15.00N 159-57.00W
1838	DR z/W		
2012	Boko SL 5129 m	LT = 5158 m	32-14.99N 159-56.99W
2037	Slmax 5450 m	LT = 5040 m	32-15.21N 159-57.19W

RF Reedereigemeinschaft
Forschungsschiffahrt GmbH

FS SONNE
SO 142

09.06.1999

0240	DR a/D		
0252	Ende Station		
0256	Magnetometer z/W		
Profil 113 (HS/PS/MAG)			
0300	Beginn Profil		32-17.06N 159-57.73W
0538	Ende Profil	30 sm	32-29.08N 160-12.78W
0548	Magnetometer a/D		
0556	OBH # 7 abgetaucht	LT = 5937 m	32-28.99N 160-14.00W
0619	OBH # 8 abgetaucht	LT = 5965 m	32-26.02N 160-13.99W
0640	OBH # 9 abgetaucht	LT = 5929 m	32-22.98N 160-14.00W
0702	OBH # 10 abgetaucht	LT = 5072 m	32-19.98N 160-13.98W
0723	OBH # 11 abgetaucht	LT = 4170 m	32-16.98N 160-13.99W
0744	OBH # 12 abgetaucht	LT = 3029 m	32-14.20N 160-14.00W
0758	OBH # 13 abgetaucht	LT = 2866 m	32-13.21N 160-13.99W
0809	OBH # 14 abgetaucht	LT = 2976 m	32-12.57N 160-13.98W
0834	OBH # 15 abgetaucht	LT = 4215 m	32-09.99N 160-13.97W
0903	OBH # 16 abgetaucht	LT = 5339 m	32-06.91N 160-13.99W
0931	OBH # 17 abgetaucht	LT = 5722 m	32-04.00N 160-13.99W
0958	OBH # 18 abgetaucht	LT = 5738 m	32-00.98N 160-13.97W
1020	OBH # 19 abgetaucht	LT = 5654 m	31-57.99N 160-14.00W
1025	Magnetometer z/W		
Profil 114 (HS/PS/MAG)			
1031	Beginn Profil		31-57.87N 160-13.00W
1436	Ende Profil	48 sm	31-17.77N 160-12.48W
1443	Magnetometer a/D		
1453	Stb-Airgun z/W (SL 150 m)		
1455	Versorgungsleitungen z/W		
1509	Bb-Airgun z/W (SL 150 m)		
1513	Versorgungsleitungen z/W		
Profil S 2 (Seismik/HS/PS)			
1606	Beginn Profil		31-21.67N 160-14.00W

10.06.1999

1800	Ende Profil	97 sm	32-59.00N 160-14.00W
1814	Bb-Airgun/Versorgungsl. a/D		
1829	Stb-Airgun/Versorgungsl. a/D		

RF Reedereigemeinschaft Forschungsschiffahrt GmbH

FS SONNE
SO 142

1832 Magnetometer z/W

Profil 115 (HS/PS/MAG)

1844 Beginn Profil 32-59.29N 160-15.94W

11.06.1999

0013 Release Command OBH # 19

0054 Ende Profil 72 sm 31-57.95N 160-11.58W

0104 Magnetometer a/D

0114 OBH # 19 gesichtet
0134 OBH # 19 a/D 31-57.64N 160-13.83W
0143 Release Command OBH # 18 (div. Commands, keine Antwort)
0320 Release Command OBH # 17
0428 OBH # 17 gesichtet
0445 OBH # 17 a/D 32-03.74N 160-13.96W
0502 OBH # 18 gesichtet
0529 OBH # 18 a/D 31-59.77N 160-13.81W
0556 Release Command OBH # 16
0624 Release Command OBH # 15
0654 OBH # 16 gesichtet
0704 OBH # 16 a/D 32-06.75N 160-13.86W
0732 OBH # 15 gesichtet
0737 Release Command OBH # 14
0748 OBH # 15 a/D 32-09.67N 160-13.81W
0803 Release Command OBH # 13
0813 OBH # 14 gesichtet
0822 OBH # 14 a/D 32-12.36N 160-13.84W
0823 Release Command OBH # 12
0842 OBH # 13 a/D gesichtet
0858 OBH # 13 a/D 32-12.94N 160-13.81W
0858 Release Command OBH # 11
0903 OBH # 12 gesichtet
0915 OBH # 12 a/D 32-13.91N 160-13.83W
0950 OBH # 11 gesichtet
0950 Release Command OBH # 10
0958 OBH # 11 a/D 32-16.67N 160-13.72W
1020 Release Command OBH # 9
1050 OBH # 10 gesichtet
1059 OBH # 10 a/D 32-19.75N 160-13.77W
1125 Release Command OBH # 8
1139 OBH # 9 gesichtet
1149 OBH # 9 a/D 32-22.68N 160-13.63W
1214 Release Command OBH # 7
1248 OBH # 8 gesichtet
1258 OBH # 8 a/D 32-25.83N 160-13.64W
1321 OBH # 7 gesichtet

RF Reedereigemeinschaft
Forschungsschiffahrt GmbH

FS SONNE
SO 142

1329	OBH # 7 a/D		32-28.68N 160-13.77W
Station F9 RMT W6			
1335	Beginn Station	LT = 5907 m	32-28.62N 160-13.67W
1339	RMT z/W	LT = 5910 m	32-28.66N 160-13.64W
	V = 2.0Kn Kurs 350°		
1422	Slmax 1300 m		
1712	RMT a/D		32-33.39N 160-08.99W
1713	Ende Station		
1721	Magnetometer z/W		
Profil 116 (HS/PS/MAG)			
1727	Beginn Profil		32-33.92N 160-08.22W

12.06.1999

0021	Ende Profil	79 sm	32-12.00N 159-21.00W
0030	Magnetometer a/D		
Station F10 RMT W6			
0038	Beginn Station	LT = 5901 m	32-12.19N 159-21.30W
0041	RMT z/W	LT = 5900 m	32-12.20N 159-21.29W
	V = 2.0Kn Kurs 305°		
0049	Slmax 300 m		
0343	RMT a/D		32-15.44N 159-26.67W
0344	Ende Station		
Station G5 DR W6			
0419	Begin Station	LT = 5223 m	32-16.22N 159-27.94W
0422	DR z/W		
0558	Boko 5199 m	LT = 5177 m	32-16.27N 159-28.02W
0626	Slmax 5500 m	LT = 4950 m	32-16.61N 159-28.06W
1136	DR a/D		
1140	Ende Station		
Station F11 RMT W6			
1208	Beginn Station	LT = 3585 m	32-18.48N 159-28.42W
1212	RMT z/W	LT = 3580 m	32-18.49N 159-28.41W
	V = 2.0Kn Kurs 310°		
1252	Slmax 1200 m		
1550	RMT a/D		32-19.02N 159-35.72W
1551	Ende Station		
1558	Magnetometer z/W		
Profil 117 (HS/PS/MAG)			
1605	Beginn Profil		32-18.27N 159-35.10W

Zeit : UTC – 10 Stunden

13.06.1999

1200	Ende Profil	216 sm	29-16.60N 160-20.00W
1215	Magnetometer a/D		
Station F12 RMT W6			
1233	Beginn Station	LT = 5981 m	29-16.49N 160-19.58W
1236	RMT z/W	LT = 5979 m	29-16.47N 160-19.57W
	V = 2.0 Kn Kurs 260°		
1308	Slmax 1000 m		
1609	RMT a/D		29-16.25N 160-25.96W
1610	Ende Station		
Station G6 DR W6			
1630	Beginn Station	LT = 5991 m	29-15.54N 160-24.58W
1633	DR z/W		
1826	Boko SL 6008 m	LT = 5993 m	29-15.56N 160-24.58W
1917	Slmax 6350 m	LT = 5832 m	29-16.08N 160-24.58W

14.06.1999

0118	DR a/D		
0120	Ende Station		
Station F13 RMT W6			
0147	Beginn Station	LT = 5024 m	29-18.06N 160-24.61W
0154	RMT z/W	LT = 5020 m	29-18.08N 160-24.50W
	V = 2.0Kn Kurs 060°		
0159	Slmax 200 m		
0433	RMT a/D		
0434	Ende Station		
0443	Magnetometer z/W		
Profil 118 (HS/PS/MAG)			
0448	Beginn Profil		29-20.32N 160-20.34W
1847	Ende Profil	159 sm	26-41.00N 160-22.00W
Profil 119 (HS/PS/MAG)			
1847	Beginn Profil		26-41.00N 160-22.00W
2106	Ende Profil	27 sm	26-41.00N 160-52.00W
Profil 120 (HS/PS/MAG)			
2125	Beginn Profil		26-37.00N 160-52.00W

15.06.1999

0136	Ende Profil	47 sm	26-37.00N 160-00.00W

Profil 121 (HS/PS/MAG)

0159	Beginn Profil		26-33.00N 160-00.00W
0444	Ende Profil	31 sm	26-19.00N 160-16.92W
0456	Magnetometer a/D		
0502	OBH # 20 abgetaucht	LT = 5109 m	26-19.04N 160-17.98W
0525	OBH # 21 abgetaucht	LT = 4825 m	26-21.98N 160-18.01W
0549	OBH # 22 abgetaucht	LT = 4738 m	26-24.98N 160-18.04W
0611	OBH # 23 abgetaucht	LT = 4720 m	26-28.02N 160-17.99W
0636	OBH # 24 abgetaucht	LT = 3955 m	26-31.01N 160-17.98W
0659	OBH # 25 abgetaucht	LT = 3146 m	26-33.99N 160-18.00W
0712	OBH # 26 abgetaucht	LT = 2802 m	26-35.01N 160-18.00W
0725	OBH # 27 abgetaucht	LT = 3262 m	26-36.00N 160-18.00W
0748	OBH # 28 abgetaucht	LT = 4209 m	26-38.99N 160-18.01W
0814	OBH # 29 abgetaucht	LT = 4447 m	26-41.99N 160-17.99W
0841	OBH # 30 abgetaucht	LT = 4308 m	26-45.01N 160-17.98W
0906	OBH # 31 abgetaucht	LT = 4907 m	26-47.99N 160-18.00W
0932	OBH # 32 abgetaucht	LT = 5051 m	26-50.99N 160-18.00W
0958	OBH # 33 abgetaucht	LT = 5033 m	26-53.99N 160-17.99W
1003	Magnetometer z/W		

Profil 122 (HS/PS/MAG)

1008	Beginn Profil		26-54.05N 160-17.07W
1424	Ende Profil	49 sm	27-34.97N 160-17.11W
1437	Stb-Airgun z/W		
1440	Versorgungsleitungen z/W		
1503	Bb-Airgun z/W		
1506	Versorgungsleitungen z/W		
1512	Stb/Bb-Airgun ausgesteckt jeweils SL 150 m		

Profil S 3 (Seismik/HS/PS)

1512	Beginn Profil		27-33.02N 160-17.99W

16.06.1999

0032	Stb-Airgun/Versorgungsleitungen a/D (Reperatur)		
0130	Stb-Airgun/Versorgungsleitungen z/W		
0134	Stb-Airgun/Versorgungsleitungen a/D (Reperatur)		
0224	Stb-Airgun/Versorgungsleitungen z/W		
2100	Ende Profil	132 sm	25-44.43N 160-18.00W

2111	Bb-Airgun/Versorgungsleitungen a/D		
2122	Stb-Airgun/Versorgungsleitungen a/D		
Station F14 RMT W6			
2137	Beginn Station	LT = 3464 m	25-43.68N 160-17.94W
2142	RMT z/W	LT = 3460 m	25-43.70N 160-17.93W
	V = 2.0Kn Kurs 080°		
2214	Slmax 1000m		
17.06.1999			
0120	RMT a/D		25-43.59N 160-11.63W
0121	Ende Station		
0127	Magnetometer z/W		
Profil 123 (HS/PS/MAG)			
0133	Beginn Profil		25-44.30N 160-12.01W
0445	Release Command OBH # 20		
0518	Ende Profil	31 sm	26-19.03N 160-19.35W
0526	Magnetometer a/D		
0532	Release Command OBH # 21		
0544	OBH # 20 gesichtet		
0552	OBH # 20 a/D		26-19.18N 160-18.22W
0609	Release Command OBH # 22		
0637	OBH # 21 gesichtet		
0648	OBH # 21 a/D		26-22.15N 160-18.34W
0707	Release Command OBH # 23		
0714	OBH # 22 gesichtet		
0724	OBH # 22 a/D		26-25.19N 160-18.30W
0745	Release Command OBH # 24		
0759	OBH # 23 gesichtet		
0808	OBH # 23 a/D		28-28.29N 160-18.25W
0824	Release Command OBH # 25		
0837	OBH # 24 gesichtet		
0845	OBH # 24 a/D		26-31.44N 160-18.35W
0900	Release Command OBH # 26		
0912	OBH # 25 gesichtet		
0920	OBH # 25 a/D		26-34.46N 160-18.23W
0920	Release Command OBH # 27		
0936	OBH # 26 gesichtet		
0947	OBH # 26 a/D		26-35.37N 160-18.19W
0954	OBH # 27 gesichtet		
0955	Release Command OBH # 28		
1021	OBH # 27 a/D		26-36.60N 160-18.23W
1040	Release Command OBH # 29		

1041	OBH # 28 gesichtet		
1055	OBH # 28 a/D		26-39.39N 160-18.09W
1113	Release Command OBH # 30		
1146	OBH # 29 a/D		26-42.41N 160-18.09W
1201	Release Command OBH # 31		
1208	OBH # 30 gesichtet		
1217	OBH # 30 a/D		26-45.33N 160-17.95W
1236	Release Command OBH # 32		
1258	OBH # 31 gesichtet		
1302	Release Command OBH # 33		
1307	OBH # 31 a/D		26-48.30N 160-17.95W
1338	OBH # 32 gesichtet		
1346	OBH # 32 a/D		26-51.27N 160-17.92W
1359	OBH # 33 gesichtet		
1414	OBH # 33 a/D		26-54.34N 160-17.87W
Station F15 RMT W6			
1424	Beginn Station	LT = 5031 m	26-54.33N 160-17.73W
1428	RMT z/W	LT = 5030 m	26-54.32N 160-17.72W
	V = 2.0Kn Kurs 180°		
1534	Slmax 2000 m		
1759	RMT a/D		26-49.00N 160-17.13W
1800	Ende Profil		
1804	Magnetometer z/W		
Profil 124 (HS/PS/MAG)			
1810	Beginn Profil		26-48.51N 160-17.67W
2029	Ende Profil 26 sm		26-38.80N 160-44.00W
2034	Magnetometer a/D		
Station G7 DR W6			
2054	Beginn Station	LT = 4555 m	26-38.80N 160-44.06W
2056	DR z/W		
2229	Boko SL 4585 m	LT = 4557 m	26-38.82N 160-44.02W
18.06.1999			
0027	Slmax 4600 m	LT = 4068 m	26-38.19N 160-43.31W
0432	DR a/D		
0433	Ende Station		
Station F16 RMT W6			
0504	Beginn Station	LT = 3213 m	26-37.40N 160-42.45W
0510	RMT z/W	LT = 3210 m	26-37.39N 160-42.44W
	V = 2.0Kn Kurs 180°		
0548	Slmax 1200 m		
0846	RMT a/D		26-32.11N 160-42.37W
0847	Ende Station		

0852	Magnetometer z/W		
Profil 125 (HS/PS/MAG)			
0859	Beginn Profil		26-31.39N 160-41.75W
1357	Ende Profil 57 sm		26-34.00N 160-13.00W
1407	Magnetometer a/D		
Station F17 RMT W6			
1410	Beginn Station		26-34.05N 160-12.24W
1414	RMT z/W		26-34.04N 160-12.23W
	V = 2.0Kn Kurs 180°		
1445	Slmax 1000 m		
1750	RMT a/d		26-31.15N 160-07.43W
1751	Ende Station		
Station G8 DR W6			
1858	Beginn Station	LT = 4031 m	26-37.49N 160-15.72W
1859	DR z/W		
2024	Boko SL 4009 m	LT = 3999 m	26-37.43N 160-15.69W
2054	Slmax 4300 m	LT = 3791 m	26-37.19N 160-15.97W

19.06.1999

0240	DR a/D		
0255	Ende Station		
Station F18 RMT W6			
0315	Beginn Station	LT = 2980 m	26-36.28N 160-16.80W
0321	RMT z/W	LT = 2985 m	26-36.26N 160-16.82W
	V = 2.0Kn Kurs 120°		
0347	Slmax 800 m		
0637	RMT a/D		26-34.35N 160-11.54W
0639	Ende Station		
0646	Magnetometer z/W		
Profil 126 (HS/PS/MAG)			
0655	Beginn Profil		26-35.26N 160-12.96W

20.06.1999

1200	Ende Profil 308 sm		26-34.87N 159-29.73W
1207	Magnetometer a/D		
Station F19 RMT W6			
1210	Beginn Station	LT = 3643 m	26-35.64N 159-29.83W
1218	RMT z/W	LT = 3640 m	26-35.66N 159-29.82W
	V = 2.0Kn Kurs 070°		

RF Reedereigemeinschaft
Forschungsschiffahrt GmbH

FS SONNE
SO 142

1257	Slmax 1200 m		
1554	RMT a/D		26-38.42N 159-24.21W
1555	Ende Station		

Station G9 DR W6

1629	Beginn Station	LT = 3921 m	26-40.00N 159-28.06W
1633	DR z/W		
1747	Boko SL 3934 m	LT = 3935 m	26-39.98N 159-27.99W
1843	Slmax 4000 m	LT = 3401 m	29-39.54N 159-28.46W
2153	DR a/D		
2155	Ende Station		
2201	Magnetometer z/W		

Profil 127 (HS/PS/MAG)

2207	Beginn Profil		26-37.90N 159-29.33W

21.06.1999

0344	Ende Profil 57 sm		26-17.99N 158-46.92W
0353	Magnetometer a/D		
0404	OBH # 34 abgetaucht	LT = 4766 m	26-17.98N 158-46.02W
0435	OBH # 35 abgetaucht	LT = 5291 m	26-21.94N 158-46.06W
0506	OBH # 36 abgetaucht	LT = 5365 m	26-25.97N 158-46.03W
0530	OBH # 37 abgetaucht	LT = 5285 m	26-28.97N 158-46.04W
0554	OBH # 38 abgetaucht	LT = 4481 m	26-31.96N 158-46.04W
0618	OBH # 39 abgetaucht	LT = 3460 m	26-34.98N 158-45.98W
0642	OBH # 40 abgetaucht	LT = 2951 m	26-37.98N 158-45.99W
0705	OBH # 41 abgetaucht	LT = 3180 m	26-39.97N 158-45.99W
0730	OBH # 42 abgetaucht	LT = 4371 m	26-42.98N 158-45.99W
0756	OBH # 43 abgetaucht	LT = 4975 m	26-46.00N 158-45.98W
0825	OBH # 44 abgetaucht	LT = 5203 m	26-48.99N 158-46.00W
0855	OBH # 45 abgetaucht	LT = 4869 m	26-51.99N 158-46.00W
0930	OBH # 46 abgetaucht	LT = 5117 m	26-56.00N 158-45.99W
1001	OBH # 47 abgetaucht	LT = 5207 m	27-00.00N 158-45.99W
1006	Magnetometer z/W		

Profil 128 (HS/PS/MAG)

1012	Beginn Profil	26-59.98N 158-45.06W
1440	Ende Profil 50 sm	27-40.00N 158-24.21W
1447	Magnetometer a/D	
1454	Bb-Airgun z/W	
1459	Versorgungsleitungen z/W	
1508	Stb-Airgun z/W	
1510	Versorgungsleitungen z/W	

Profil S 4 (Seismik/HS/PS)

1516	Beginn Profil		27-38.70N 158-46.00W

22.06.1999

2000	Ende Profil	118 sm	25-42.03N 158-46.01W
2014	Bb-Airgun/Versorgungsleitungen a/D		
2025	Stb-Airgun/Versorgungsleitungen a/D		

Station F20 RMT W6

2050	Beginn Station	LT = 4992 m	25-40.73N 158-45.35W
2051	RMT z/W	LT = 4991 m	25-40.73N 158-45.35W
	V = 2.0Kn Kurs 075°		
2114	SImax 600 m		

23.06.1999

0009	RMT a/D		25-40.39N 158-41.84W
0010	Ende Station		
0015	Magnetometer z/W		

Profil 129 (HS/PS/MAG)

0020	Beginn Profil		25-40.69N 158-41.10W
0419	Ende Profil	43 sm	26-17.99N 158-46.59W
0355	Release Command OBH # 34		
0420	Release Command OBH # 35		
0433	Magnetometer a/D		
0448	OBH # 34 gesichtet		
0515	OBH # 34 a/D		26-17.75N 158-46.40W
0535	OBH # 35 gesichtet		
0543	Release Command OBH # 36		
0551	OBH # 35 a/D		26-21.72N 158-46.51W
0622	Release Command OBH # 37		
0701	OBH # 36 gesichtet		
0714	Release Command OBH # 38		
0714	OBH # 36 a/D		26-25.83N 158-46.33W
0720	OBH # 37 gesichtet		
0745	OBH # 37 a/D		26-28.70N 158-46.48W
0806	Release Command OBH # 39		
0807-0825	Div. Release Command OBH # 38		
0836	OBH # 38 gesichtet		
0843	OBH # 38 a/D		26-31.83N 158-46.30W
0902	OBH # 39 gesichtet		
0905	Release Command OBH # 40		
0918	OBH # 39 a/D		26-34.61N 158-46.73W

0938	Release Command OBH # 41		
0949	OBH # 40 gesichtet		
0955	OBH # 40 a/D		26-37.69N 158-46.31W
1010	Release Command OBH # 42		
1036	OBH # 41 gesichtet		
1049	OBH # 41 a/D		26-39.43N 158-46.63W
1122	OBH # 42 gesichtet		
1128	Release Command OBH # 43		
1132	OBH # 42 a/D		26-42.54N 158-46.53W
1206	Release Command OBH # 44		
1225	OBH # 43 gesichtet		
1240	OBH # 43 a/D		26-45.73N 158-46.15W
1301	Release Command OBH # 45		
1311	OBH # 44 gesichtet		
1323	OBH # 44 a/D		26-48.78N 158-46.06W
1348	Release Command OBH # 46		
1406	OBH # 45 gesichtet		
1416	OBH # 45 a/D		26-51.78N 158-46.00W
1445	Release Command OBH # 47		
1451	OBH # 46 gesichtet		
1500	OBH # 46 a/D		26-55.78N 158-45.96W
1548	OBH # 47 gesichtet		
1558	OBH # 47 a/D		26-59.85N 158-45.95W

Station F21 RMT W6

1604	Beginn Station	LT = 5203 m	26-59.78N 158-45.87W
1609	RMT z/W	LT = 5200 m	26-59.79N 158-45.87W
	V = 2.0Kn Kurs 075°		
1644	Slmax 1100 m		
1939	RMT a/D		26-59.29N 158-38.18W
1940	Ende Station		
1946	Magnetometer z/W		

Profil 130 (HS/PS/MAG)

1955	Beginn Profil		26-57.92N 158-38.88W
2320	Ende Profil	37 sm	26-32.30N 158-48.86W
2326	Magnetometer a/D		

Station G10 DR W6

2341	Beginn Station	LT = 4105 m	26-33.75N 158-47.57W
2342	DR z/W		

24.06.1999

0102	Boko SL 4101 m	LT = 4078 m	26-33.80N 158-47.50W
0134	Slmax 4250 m	LT = 3709 m	26-34.41N 158-47.36W
0355	Haker		
0435	DR frei		

0618	DR a/D		
0620	Ende Station		
0625	Magnetometer z/W		
Progil 131 (HS/PS/MAG)			
0627	Beginn Profil		26-35.19N 158-48.18W
0847	Ende Profil	23 sm	26-44.99N 158-30.00E
0856	Magnetometer a/D		
Station G11 DR W6			
0925	Beginn Station	LT = 4460 m	26-41.51N 158-28.06W
0927	DR z/W		
1052	Boko SL 4510 m	LT = 4478 m	26-41.58N 158-28.01W
1155	Slmax 4650 m	LT = 4097 m	26-41.11N 158-28.12W
1536	DR a/D		
1544	Ende Station		
1547	Magnetometer z/W		
Profil 132 (HS/PS/MAG)			
1553	Beginn Profil		26-40.17N 158-29.21W
1721	Ende Profil	17 sm	26-30.22N 158-44.28W
1727	Magnetometer a/D		
Station TV1 GTVA W1			
1747	Beginn Station	LT = 5370 m	26-28.03N 158-45.65W
1749	GTVA z/W		
1926	Bosi SL 5362 m	LT = 5370 m	26-28.03N 158-45.71W
1937	Bildausfall (Keine Datenübertragung)		
	Slmax 5370 m	LT = 5368 m	26-28.04N 158-45.66W
2128	GTVA a/D		
2130	Ende Station		
2156	Magnetometer z/W		
Profil 133 (HS/PS/MAG)			
2203	Beginn Profil		26-28.60N 158-44.78W
25.06.1999			
0131	Ende Profil	35 sm	26-41.68N 158-14.93W
0138	Magnetometer a/D		
Station G12 DR W6			
0147	Beginn Station	LT = 4584 m	26-42.59N 158-14.85W
0151	DR z/W		

RF Reedereigemeinschaft
Forschungsschiffahrt GmbH

FS SONNE
SO 142

0316	Boko SL 4491 m	LT = 4492 m	26-42.51N 158-14.76W
0335	Slmax 4800 m	LT = 4240 m	26-42.29N 158-14.60W
0710	DR a/D		
0715	Ende Station		
0720	Magnetometer z/W		

Profil 134 (HS/PS/MAG)

0726	Beginn Profil		26-40.84N 158-14.42W
1011	Ende Profil	33 sm	26-10.00N 158-25.00W
1021	Magnetometer a/D		

Station G13 DR W6

1032	Beginn Station	LT = 4945 m	26-09.88N 158-25.05W
1033	DR z/W		
1208	Boko SL 4920 m	LT = 4905 m	26-09.85N 158-25.00W
1240	Slmax 5350 m	LT = 4708 m	26-10.11N 158-24.70W
1814	DR a/D		
1820	Ende Station		
1822	Magnetometer z/W		

Profil 135 (HS/PS/MAG)

1828	Beginn Profil		26-10.89N 158-23.43W

26.06.1999

0832	Ende Profil	151 sm	24-15.28N 157-43.60W

Station TV2 GTVA W1

0847	Beginn Station	LT = 4468 m	24-14.07N 157-42.96W
	(Keine Datenübertragung)		
0944	GTVA z/W		
1047	Bosi SL 4427	LT = 4458 m	24-14.07N 157-42.77W
1119	1.Griff Slmax 4450 m	LT = 4454 m	24-14.14N 157-42.59W
1254	GTVA a/D		
1255	Ende Station		

Profil 136 (HS/PS)

1254	Beginn Profil		24-14.25N 157-42.39W
1440	Ende Profil	13 sm	24-01.67N 157-42.48W

Station TV3 GTVA W1

1412	Beginn Station	LT = 4115 m	24-01.61N 157-42.66W
1418	GTVA z/W		
1524	Bosi SL 4064 m	LT = 4112 m	24-01.58N 157-42.72W
1526	1.Griff Slmax 4079 m	LT = 4111 m	24-01.58N 157-42.72W
1530	2.Griff SL 4078 m	LT = 4099 m	24-01.57N 157-42.73W
1542	3.Griff SL 4079 m	LT = 4100 m	24-01.58N 157-42.71W

RF Reedereigemeinschaft
Forschungsschiffahrt GmbH

FS SONNE
SO 142

1706 GTVA a/D
1708 Ende Station

MS SONNE KAPITÄN